Leveraging a polycycloether structure into functional biomaterials

Jean-Baptiste Masclef

Submitted in fulfilment of the requirements for the
Degree of Doctor of Philosophy

School of Chemistry
College of Science and Engineering
University of Glasgow

October 2024

Abstract

Polysaccharides are ubiquitous in nature: cellulose is the main structural component of plants, glycogen is an important energy reserve for animals and fungi, starch is an essential part of human diet. In comparison, poly(ethylene glycol) (PEG) is a synthetic polyether that has found an ever-increasing amount of use-cases: medical tools and devices, laxatives, shampoos, shower gels, ceramic binders, plastic bags, rocket fuel and many more.

Inspired by nature's polysaccharides and the commercial success of PEG, this thesis reports the synthesis of various novel polycycloethers sharing structural elements from the two aforementioned polymers. The singular polycyclic structure obtained was leveraged into materials with unique properties.

PEGose-*b*-PLA, an amphiphilic block copolymer was synthesised and used for the preparation of highly stable nanoparticles, capable of encapsulating and steadily releasing both hydrophilic and hydrophobic cargoes. The high biocompatibility and cell permeation suggests that it might be used as an efficient PEG-free drug delivery system. The morphology of the nanoparticles could be tuned by controlling the tacticity of the PEGose block, from nanospheres to cubic particles depending on the buffer used. A series of polycycloether-*b*-PEG was synthesised, mimicking the structure of commonly used Poloxamers. The block copolymer proved to be a highly effective surfactant, with high-internal phase emulsions obtained at low concentration, irrespective of the oil/water ratio used. Finally, polycyclic cationic homopolymers were synthesised with a various amount of cationic charges through different post-polymerisation functionalisation strategies, with potential use as gene vectors.

Author's declaration

The work described in this thesis is of my own unless I have acknowledged help from a named person or referenced a published source. Chapter 2 and Chapter 4 of this thesis have been adapted with permission from self-written articles.[1,2] This thesis has not been submitted, in whole or in part, for any other degree.

May 10th 2024

Acknowledgements

I would like to thank my supervisors Dr. Joëlle Prunet and Dr. Bernhard Schmidt for the opportunity to do my PhD in their group. Thank you for your help, your enthusiasm and your trust. Thank you Joëlle for the abundance of snacks throughout the PhD. Bernhard you were also a great supervisor and a *decent* Magic The Gathering opponent.

Huge thanks to the Schmidt group. Thank you Alex for being my espresso buddy. Thank you Steve for the frogs, the bread, the shromps and being a ~~terrible~~ terrific person. Thank you Iona for the squid-dancing, the drawings and your chaotic *(but appreciated)* energy. Thank you all for the memories that I will hold dear.

Many thanks as well to the people who work or worked in the Henderson lab. Big thank you to the Maltese falcon Justin Spitteri, the prettiest boy. Thank you Hollie for putting up with me, I could not have thought of a better person to *work* with. Thank you Temi for the good energy, thank you Emily for the opposite.

Thanks as well to the people who worked with me in the Louden lab. Especially Stuart, Alex and bachata expert Brendan. Thank you Patrick for the fashion comments and not breaking my legs at football, very nice.

Finally, thanks to everyone else working at the Joseph Black Building, it has been a real pleasure spending these years with you all.

:)

Contents

List of Tables

List of Figures

List of Acronyms

ABC Accelerated Blood Clearance.

AROP Anionic Ring-Opening Polymerization.

ATPS Aqueous Two-Phase System.

BSA Bovine Serum Albumin.

CAC Critical Aggregate Concentration.

CD Circular Dichroism.

CLSM Confocal Laser Scanning Microscopy.

CM Cross-Metathesis.

CMC Critical Micelle Concentration.

CROP Cationic Ring-Opening Polymerization.

cryoEM Cryogenic Electron Microscopy.

CuAAC Copper catalyzed azide/alkyne cycloaddition.

DCE 1,2-Dichloroethane.

DCM Dichloromethane.

DH Dihydroxylation.

DHBC Double Hydrophilic Block Copolymer.

DLS Dynamic Light Scattering.

DMF Dimethylformamide.

DMSO Dimethylsulfoxide.

DNA Deoxyribonucleic Acid.

DOSY Diffusion-Ordered Spectroscopy.

DSC Differential Scanning Calorimetry.

EG Ethylene Glycol.

EPR Enhanced Permeability and Retention.

ESI-MS Electrospray Ionisation Mass Spectrometry.

FBS Fetal Bovine Serum.

FITC Fluorescein Isothiocyanate.

GPC Gel Permeation Chromatography.

HIPE High-Internal Phase Emulsion.

HLB Hydrophilic-Lipophilic Balance.

HPLC High-Performance Liquid Chromatography.

HRMS High-Resolution Mass Spectrometry.

ICP-MS Inductively Coupled Plasma Mass Spectrometry.

MADLS Multi-Angle Dynamic Light Scattering.

Me Methyl.

MEM Minimum Essential Medium.

mPEG Poly(ethylene glycol) monomethyl ether.

mRNA Messenger Ribonucleic Acid.

MWCO Molecular Weight Cut-Off.

NHC *N*-Heterocyclic Carbene.

NMMO *N*-Methylmorpholine *N*-oxide.

NMP *N*-Methyl-2-pyrrolidone.

NMR Nuclear Magnetic Resonance.

NP Nanoparticle.

O/W Oil in Water.

PAGE Poly(allyl glycidyl ether).

PBS Phosphate-Buffered Saline.

PCE Poly(cycloether).

PCGE Poly(crotyl glycidyl ether).

PCL Poly(caprolactone).

PDLA Poly(D-lactic acid).

PEB Poly(epoxybutene).

PEG Poly(ethylene glycol).

PEI Polyethylenimine.

PEO Poly(ethylene oxide).

PLA Poly(lactic acid).

PLLA Poly(L-lactic acid).

PMAGE Poly(methallyl glycidyl ether).

POEGMA Poly(oligo(ethylene glycol) methyl ether methacrylate).

POM Poly(oxymethylene).

POX Poly(oxazoline).

PPG Poly(propylene glycol).

PPGE Poly(prenyl glycidyl ether).

PPO Poly(propylene oxide).

PVA Poly(vinyl alcohol).

PVP Poly(vinylpyrrolidone).

PXRD Powder X-Ray Diffraction.

RCM Ring-Closing Metathesis.

Red-Al Sodium *bis*(2-methoxyethoxy)aluminium hydride.

ROM Ring-Opening Metathesis.

ROMP Ring-Opening Metathesis Polymerization.

ROP Ring-Opening Polymerization.

RSD Relative Standard Deviation.

SAXS Small-Angle X-ray Scattering.

SEC Size-Exclusion Chromatography.

SEM Scanning Electron Microscopy.

SLS Static Light Scattering.

SPCE Saturated Poly(cycloether).

TEM Transmission Electron Microscopy.

THF Tetrahydrofuran.

TMS Tetramethylsilane.

TPPAlCl Tetraphenylporphyrin Aluminium Chloride.

$TPPH_2$ Tetraphenylporphyrin.

Tris Tris(hydroxymethyl)aminomethane.

Publications

Advanced Science

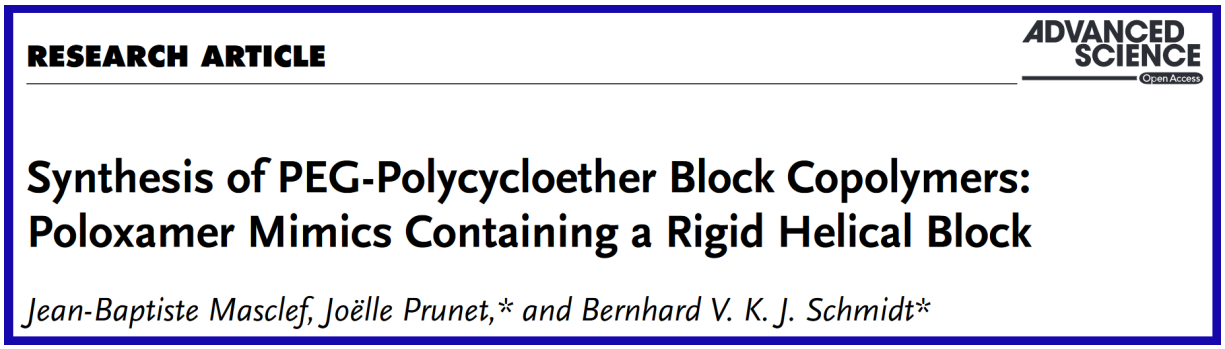
RESEARCH ARTICLE

ADVANCED SCIENCE Open Access

Synthesis of PEG-Polycycloether Block Copolymers: Poloxamer Mimics Containing a Rigid Helical Block

Jean-Baptiste Masclef, Joëlle Prunet, and Bernhard V. K. J. Schmidt**

DOI: 10.1002/advs.202310277

Macromolecules

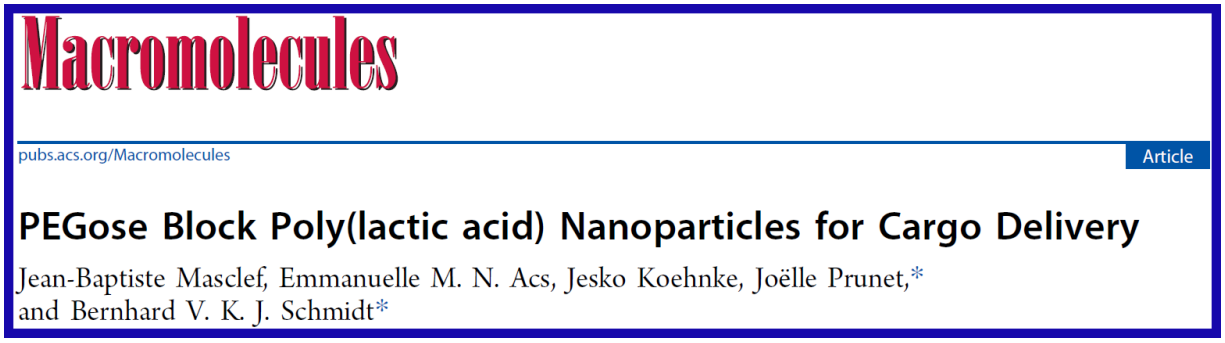
Macromolecules

pubs.acs.org/Macromolecules Article

PEGose Block Poly(lactic acid) Nanoparticles for Cargo Delivery

Jean-Baptiste Masclef, Emmanuelle M. N. Acs, Jesko Koehnke, Joëlle Prunet,* and Bernhard V. K. J. Schmidt*

DOI: 10.1021/acs.macromol.4c00528

Chapter 1

Introduction

Polymers are ubiquitous in our everyday life, but the general mental representation of a polymer is plastic: a cheap material to produce bags and junk. While it is true that poly(ethylene), poly(propylene) and poly(styrene) are some of the most mass-produced polymers in the world, polymers are also increasingly needed for specific applications that require high-value materials. Biomedical applications in particular: cell culture,[3] wound healing,[4] drug delivery,[5–7] tissue engineering,[8] 3D bioprinting[9] to cite a few, have all seen a tremendous surge of interest for hydrophilic polymers.[10] Poly(ethylene glycol) (PEG) is one of these hydrophilic polymers; for half a century it was considered and still is considered the golden standard for nanomedicines.[11] A notable recent application is the Pfizer COVID-19 vaccine, where PEG homopolymer chains are used to stabilise the liposomes that contain the mRNA.[12]

Another layer of sophistication that can be added to a polymer is simply another polymer. Indeed, a so-called block copolymer consists of at least two polymers or 'blocks' covalently bound together. The main attraction for polymers with blocks of different solubility comes from a phenomenon known as self-assembly. Self-assembly is omnipresent in nature, from the phospholipids that form our cell membranes to the surface-active agents in soap bubbles. In biomedical applications, it is mainly used for drug delivery,[13] gene therapy[14–17] and imaging.[18] The self-assembly of a block copolymer into nanoscopic particles is the basis for the encapsulation and release of various drugs, drastically enhancing their efficiency and reducing their side-effects.[11]

In view of the recent growth of polymeric biomaterials in medicine, this thesis focuses on the expansion of the current library of polymers that can be used for biomedical applications. More specifically, an unusual polycycloether structure was leveraged into materials with unique properties.

1.1 Polyethers

1.1.1 Synthesis of polyethers

Polyethers are a particular class of polymer whose repeating units are connected by an ether linkage (an oxygen atom bound to two carbon atoms). A broad range of polyethers are manufactured everyday, whether hydrophilic or hydrophobic polymers, that can be used as low-cost plastics or high-end materials.[19,20] While the structure of different polyethers may vary significantly, they all share the same ether linkage pattern. This ether linkage usually leads to flexible polymers in the case of acyclic polymers.[19] The simplest and most common polyether is poly(ethylene glycol) (PEG). PEG is an aliphatic linear polyether, with two carbon between each oxygen atoms $(CH_2CH_2O\text{-})_n$. If the mass of the polymer exceeds 20,000 Daltons, the polymer is traditionally referred to as poly(ethylene oxide) (PEO). Another common polyether is poly(propylene glycol) (PPG), which can similarly be referred to as poly(propylene oxide) (PPO) $(CH_2CH(CH_3)O\text{-})_n$. The difference between poly(propylene glycol) and poly(ethylene glycol) is that PPG contains an additional methyl group on its repeating unit, turning the polymer hydrophobic, whereas PEG is highly hydrophilic. Other prevalent polyethers include polyoxymethylene (POM) (also referred to as polyacetal or polyformaldehyde) $(CH_2O\text{-})_n$ and polytetrahydrofuran (polyTHF), also called poly(tetramethylene oxide) or poly(tetramethylene glycol) $(CH_2CH_2CH_2CH_2O\text{-})_n$ (See Figure 1.1).[21–24] These polyethers are commercially available as viscous solids, waxy solids or dry pellets, depending on their molecular weight.

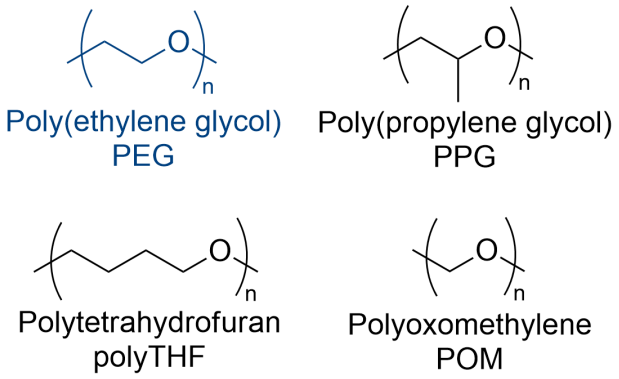

Figure 1.1: Chemical structure of most common polyethers, from which only poly(ethylene glycol) is hydrophilic.

The synthesis of poly(ethylene glycol) was first reported in 1859 by C. A. Wurtz and A. V. Lourenço.[22] The polymerisation of ethylene oxide can by catalysed either by an acid, leading to a cationic ring-opening polymerisation (CROP) or a base, leading to an anionic ring-opening polymerisation (AROP).[25] Ethylene oxide is used as a monomer and water or ethylene glycol can be used as an initiator. Nowadays, ethylene glycol and its oligomers are used preferentially instead of water as it leads to polymer with a lower dispersity (Đ). Similarly, base-catalysed

ring-opening polymerisation also leads to a lower dispersity. It is worth noting that if a multi-functional initiator like glycerol is used (three hydroxyl groups), a branched polyether will be obtained instead of a linear polymer. The base typically used is potassium hydroxide (KOH). Poly(propylene glycol) can be obtained in a similar fashion, using propylene oxide as a monomer instead. During the propagation step of the polymerisation, the anionic active chain will preferentially attack the non-substituted carbon, leading to a regioselective ROP and head-to-tail linkages only (See Figure 1.2).

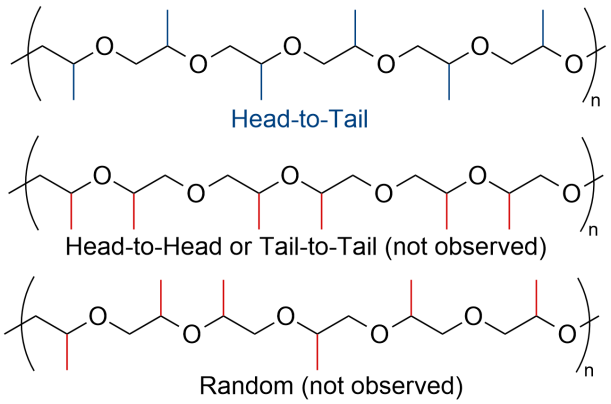

Figure 1.2: Structures of Head-to-Tail, Head-to-Head, Tail-to-Tail and random linkages for poly(propylene glycol).

Using base-catalysed ring-opening polymerisation techniques, atactic PPG is obtained if a racemic mixture of propylene oxide is used. However, optically active propylene oxide can be produced, using for example the Jacobsen hydrolytic kinetic resolution of propylene oxide using a chiral salen cobalt ligand.[26] If the enantiopure monomer is used, the stereoconfiguration of the substituted carbon is preserved during the AROP and an isotactic polymer can be obtained. In a similar fashion, coordination polymerisation can be used; a salen cobalt catalyst has been reported to catalyse the isospecific polymerisation of racemic propylene oxide (See Figure 1.3).

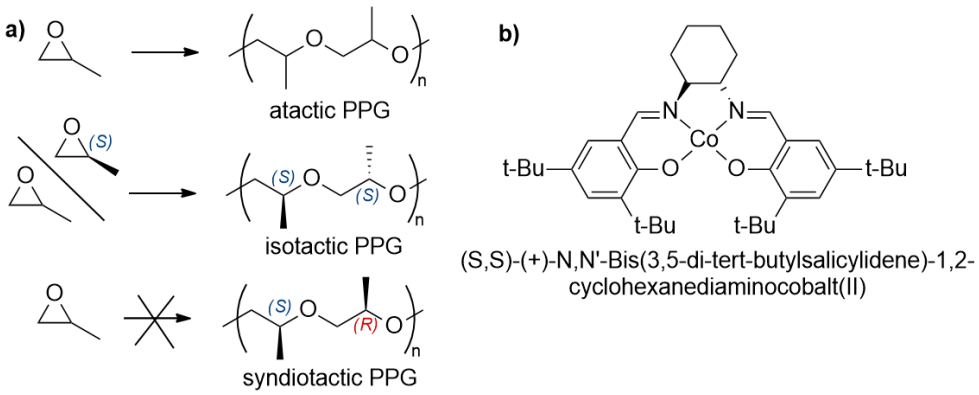

Figure 1.3: a) Scheme of the different tacticity that can be obtained with PPG: atactic PPG using AROP catalysed by potassium hydroxide or isotactic PPG using enantiopure propylene oxide and KOH or racemic propylene oxide and **b)** a cobalt salen catalyst. The synthesis of syndiotactic PPG has not been reported yet.

Poly(propylene glycol) can then be synthesised using any of the three main ring-opening polymerisation methods used to produce polyethers: cationic ROP, anionic ROP and coordination polymerisation (See Figure 1.4).

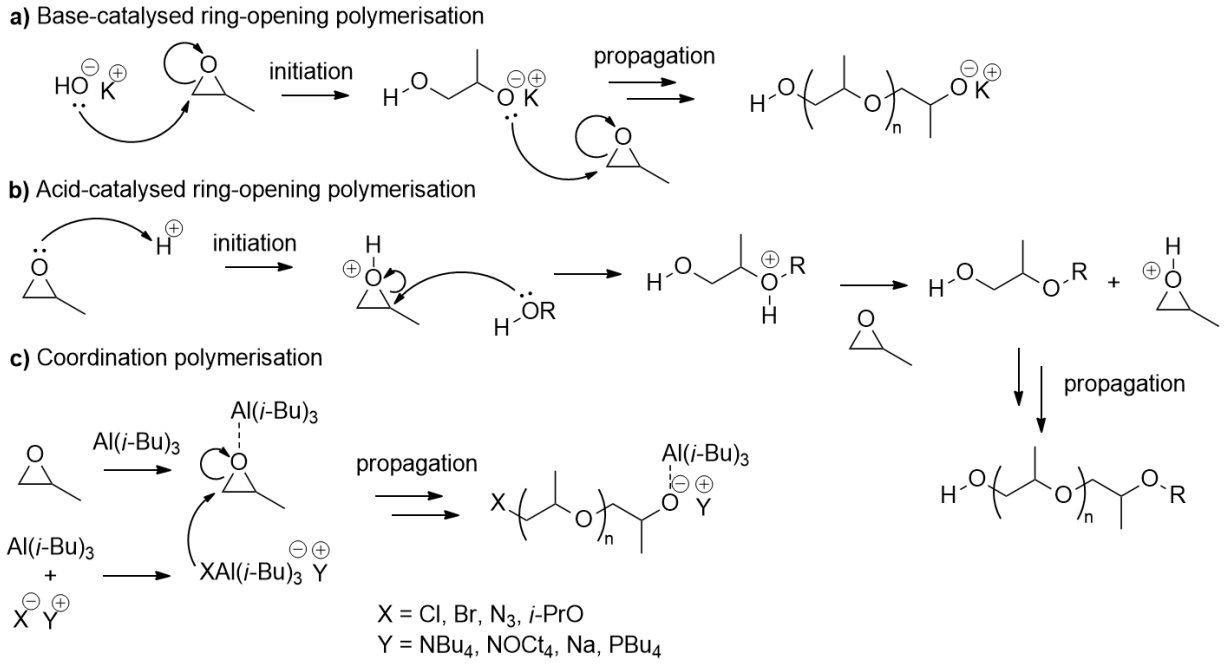

Figure 1.4: Scheme of the different ring-opening polymerisation mechanisms that can be used on propylene oxide: **a)** anionic ROP, **b)** cationic ROP and **c)** coordination polymerisation.

Unlike the synthesis of PEG or PPG, polyTHF can only be obtained through a cationic ring-opening polymerisation. The acid catalysis is achieved using protic acids (e.g. perchloric acid) and oxonium salts (e.g. triethyloxonium tetrafluoroborate $(C_2H_5)_3O(BF_4)$). Polyoxomethylene is not obtained through the strain release of an epoxide or a cycloether but rather through the addition polymerisation of anhydrous formaldehyde or 1,3,5-trioxane (See Figure 1.5).

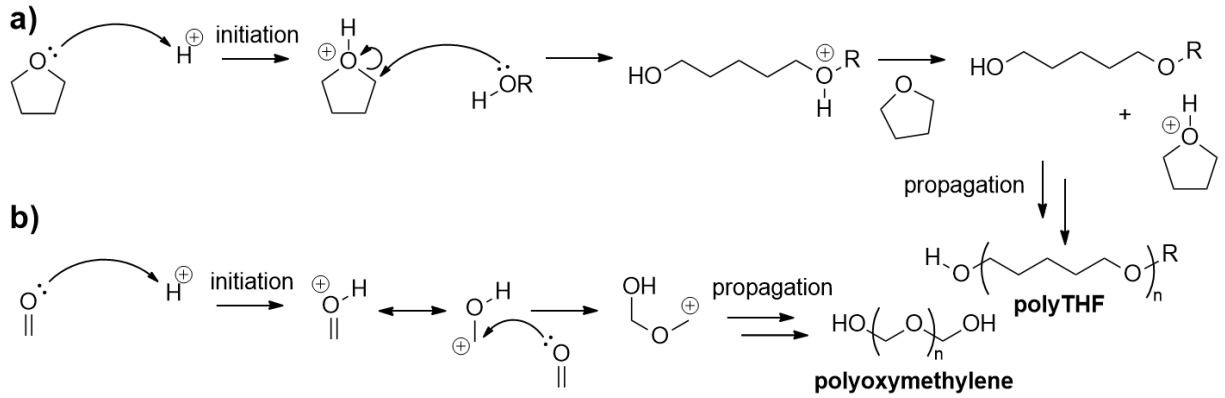

Figure 1.5: Mechanism for **a)** the cationic ring-opening polymerisation of tetrahydrofuran and **b)** the addition polymerisation of formaldehyde.

The polyethers mentioned (PEG, PPG, polyTHF, POM) will usually have two hydroxyl end-groups (hence the use of the term glycol, another word for diol) but methyl-capped polymers are also commercially available. For example, methoxy-PEG (mPEG) is a poly(ethylene glycol) with one hydroxyl group and one methoxy end-group.

1.1.2 Poly(ethylene glycol) (PEG)

Among all the polyethers mass-produced everyday, PEG is by far the most used.[22] One major difference between PEG and the other polyethers mentioned so far is that PEG is soluble in water (and most organic solvents). The hydrophilicity of PEG is non-trivial: it has two carbons for each oxygen atom whereas POM has one carbon for each oxygen. Based on these carbon/oxygen ratios one could expect POM to be more hydrophilic than PEG. It turns out that POM is completly insoluble in water, unlike PEG. The reason behind this counter-intuitive result has been a subject of discussion for many years. In 1969, Blandamer et al. suggested that water molecules can form an efficient hydrogen-bond network, due to the anti-gauche-anti conformation of PEG backbone.[27] The good fit of this hydrogen-bond network was the implied reason for PEG solubility. Fifty years later, in 2019, Ensing et al. refuted these claims.[27] Using spectroscopic experiments in combination with *ab initio* calculations and molecular dynamics simulations, they showed that the reason for PEG solubility is the partial charges on oxygen atoms (due to the induction effects of neighboring carbons). In conclusion, despite the apparent simplicity of PEG structure, its hydrophilicity is quite unique, as it is the only water-soluble polyether that does not bear any additional functional groups. PEG hydrophilicity coupled to its low-cost, ease of manufacturing and broad range of molecular weights available, led PEG to be considered as the gold standard of hydrophilic polymers. On top of that, PEG was generally considered to be a polymer exhibiting a very low immunogenicity, antigenicity and toxicity.[28] Consequently, PEG inertness allowed it to be used extensively in food, cosmetics and medicine.[29] In particular, PEG is commonly used in the field of drug delivery.[30] For example, one frequent issue found in the field of cancer therapy is the poor water solubility of anti-cancer drugs. SN-38 is a potent anticancer drug but its solubility in water is 7.2 µg/mL only. This water solubility can be improved by a PEGylation strategy, consisting of attaching a PEG chain to the drug. Zhao et al. reported that by connecting SN-38 to a 40 kDa PEG chain, they increased the water solubility of the compound from 7.2 µg/mL to 6.7 mg/mL, a 1000-fold increase (See Figure 1.6).[31]

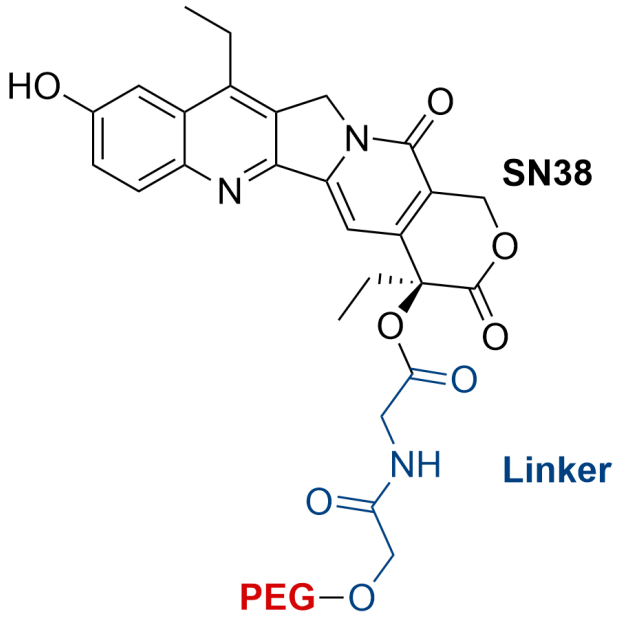

Figure 1.6: Structure of the PEGylated anti-cancer drug SN-38.[31]

A PEGylation strategy can be employed on small molecules as previously shown but also on liposomes or other nanoparticles. Another advantage of the PEGylation of a molecule or a nanoparticle is the "stealth effect" PEG confers. This "stealth effect" describes the fact that when a nanoparticle has been PEGylated, it is less susceptible to be detected by the immune system, leading to a longer blood circulation time, a more sustained release, fewer side effects and an improved efficiency. To give a recent example of PEG's ubiquitous use in nanomedicine formulations: the Pfizer mRNA COVID-19 vaccine contains PEG chains to stabilise the liposome that encapsulates the mRNA.[32,33] However, it was recently reported that PEG is not as non-immunogenic as initially assumed.[34] It has been found that the administration of PEGylated drugs or nanoparticles can induce the formation of anti-PEG antibodies.[35] In addition, the exponentially increased use of PEG in food, cosmetics and drugs means that these anti-PEG antibodies are found in an increasing share of the population. In 2021, flow cytometry studies showed that anti-PEG antibodies were present in 65% of healthy donors' analysed plasma, which can lead to adverse effects and a decreased therapeutic efficiency of PEG-containing drugs.[36] It was also demonstrated that following the administration of PEGylated drugs or PEG nanoparticles, these antibodies led to an immunogenic response known as the "accelerated blood clearance (ABC) phenomenon", drastically decreasing drug/nanoparticle blood circulation time. In the case of the COVID-19 vaccine, it was proposed that PEG was responsible for the anaphylactic reactions of some individuals to the vaccine.[11] This reaction would be due to the weak interaction between anti-PEG antibodies on the surface of the solid lipid nanoparticles, which would lead to the complement activation pathway of the immune system (See Figure 1.7).[12]

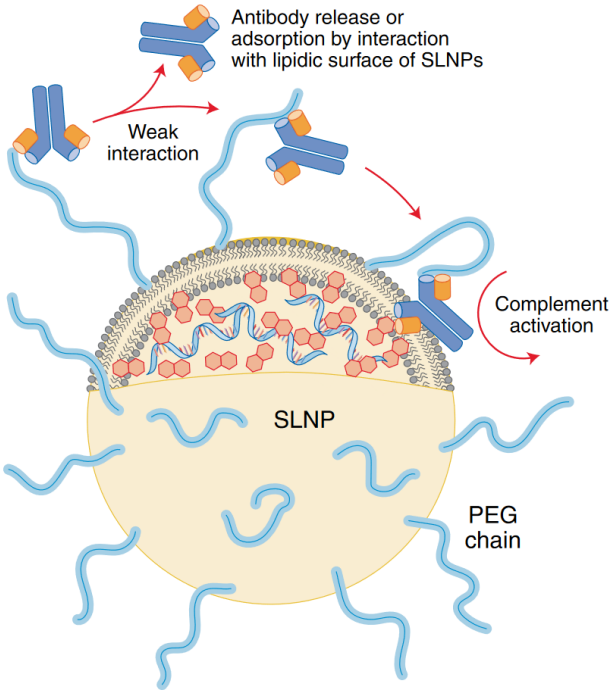

Figure 1.7: Schematic representation of the interaction between anti-PEG antibodies and the mRNA COVID-19 vaccine (solid lipid nanoparticle (SLNP)). Adapted with permission.[12] Copyright © 2021, Springer Nature Limited.

1.1.3 PEG alternatives

Due to the discovery of PEG immunogenicity, the search for PEG alternatives has intensified in the past few years.[37] To be considered a potential PEG alternative, a polymer needs to fulfil an extensive number of criteria. It needs to have an adequate molecular weight, to be easily synthesised at a low cost, to be biocompatible, to be non-immunogenic, to confer stealth properties to a molecule or nanoparticle, to be biodegradable and to be sufficiently hydrophilic. Suffice to say that to this day, no polymer meets all of these criteria at once.[35] Then, each PEG alternative represents a trade-off between cost, biocompatibility, degradability and efficiency. PEG alternatives can be non-ionic synthetic polymers (e.g. poly(glycerol)s), zwitterionic polymers (e.g. poly(sulfobetaine)s) or natural polymers (polysaccharides or poly(amino acid)s) (See Figure 1.8).[24]

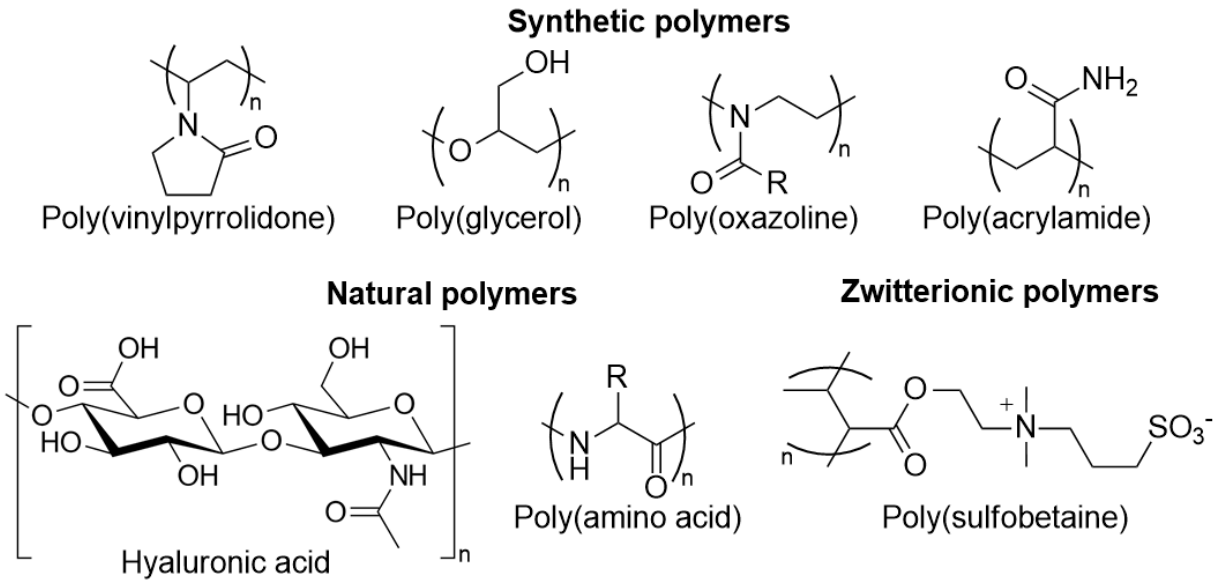

Figure 1.8: Structure of different hydrophilic polymers that are discussed as PEG alternatives.

Poly(vinylpyrrolidone) (PVP) is a hydrophilic polymer that is synthesised via the free radical polymerisation of *N*-vinylpyrrolidone, using a radical initiator such as azo*bis*isobutyronitrile (AIBN). PVP has been widely used in the cosmetic, food, and pharmaceutical industry, demonstrating its low toxicity. It has the advantage over PEG to be more stable with regard to UV irradiation or ultrasound. However, the carbon-carbon backbone of the polymer as well as the 5-membered ring of the repeating unit makes PVP more rigid than PEG. This lack of flexibility translated to less steric hindrance and a less efficient stealth effect compared to PEG.[38] It has also been reported that the biocompatibility of PVP decreases as its molecular weight increases, as its elimination through the kidneys is compromised (especially above 70 kDa).[39]

Poly(glycerol)s are polyethers bearing hydroxyl groups on their repeating unit. They are traditionally hyperbranched polymers synthesised through the polycondensation of glycerol on itself. A catalytic amount of acid is used, and the reaction is generally heated under reduced pressure to remove the water by-product, thus driving the polymerisation towards full conversion. Linear poly(glycerol) can also be obtained through the anionic ring-opening polymerisation of ethoxyethyl glycidyl ether (EEGE) as an acetal-protected glycidol derivative, followed by the acidic deprotection of the acetal protecting group.[20] Unlike PVP and PEG, poly(glycerol)s can be easily functionalised through their hydroxyl-groups, leading to tuned properties. Poly(glycerol)-based drug delivery systems have been reported to increase the blood circulation time without inducing any accelerated blood clearance (ABC) phenomenon.[40] Despite their non-immunogenicity, the use of poly(glycerol)-based nanomedicine formulations can lead to a high accumulation of poly(glycerol) in tissues. This issue is worsened by the non-biodegradability of the polymer.[41–43]

Poly(oxazoline)s (POXs) showed promising results for biomedical applications. The most

commonly used POX is poly(2-ethyl-2-oxazoline) (PEtOx), synthesised via cationic ring-opening polymerisation.[44] Iodomethane can be used as an initiator, the reaction is performed using acetonitrile as solvent and can be terminated using methanol or a primary amine.[45] The polymerisation conditions are close to living polymerisation, the polymer can be obtained easily with different conditions/substrates, leading to tunable properties.[46,47] Unlike the previously mentioned polymers, POXs are biodegradable.[48] They are also highly biocompatible with a good renal clearance.[49] While POX are biocompatible, they can sometime contain residual impurities from the polymerisation. On top of that, their high cost has been hindering their translation into clinical trials.[50–53] To this day, only PEtOx has been approved by the United States Food and Drug Administration (FDA) as indirect food additive.

Poly(acrylamide) is a linear polymer bearing amide groups. It is not a polyamide since the amide group is not part of the polymer backbone. The carbon bearing the amide group is a stereocenter, thus, poly(acrylamide) can be synthesised as an atactic, isotactic or syndiotactic polymer. Atactic poly(acrylamide) is generally obtained due to the non-specificity of the radical polymerisation of the acrylamide monomer.[21] Thioglycolic acid is often used as the initiator and the reaction is run at moderate temperature (40°C). The popularity of poly(acrylamide) comes from the excellent biocompatibility of the polymer, as well as its protein antifouling ability.[54] Yet, the acrylamide monomer used for its synthesis are highly toxic. The polymer is also not biodegradable and activation of the immune system has been reported to be more severe than for PEG.[21]

Zwitterionic polymers represent a relatively new class of hydrophilic polymers that gained a lot of attention in recent years.[55] Numerous zwitterionic polymers can be synthesised but poly(sulfobetaine)s are one of the most discussed.[56–59] **Poly(sulfobetaine)s** are linear polymers bearing a positively charged quaternary ammonium and a negatively charged sulfonate group on each repeating unit. Many poly(sulfobetaine)s feature an upper critical solution temperature (UCST), leading to interesting thermo-responsive properties that could be used for drug delivery.[60] It has been noted that the zwitterionic repeating unit is the cause of a tighly bound hydration layer, inducing excellent anti-fouling capabilities.[61,62] Poly(sulfobetaine)s are also biocompatible. They are synthesised through radical polymerisation, even though only a limited amount of monomer are compatible with this type of polymerisation, due to their lack of solubility in most organic solvents.[60]

Natural polymers are a class of hydrophilic polymers composed mainly or polysaccharides or poly(amino acid)s. **Polysaccharides** are high molecular weight polymers of carbohydrates, each monosaccharide unit being bound by glycosidic linkages. Polysaccharides can be amorphous or crystalline, linear or highly branched, and contain a broad range of functional groups (e.g. carboxylic acids, alcohols, amines, amides).[63] It should be noted that not every polysaccharide is soluble in water (e.g. cellulose). They can react with water through different mechanisms, generally leading to a high biodegradability.[64] Polysaccharide cost of production

can be low due to their abundance in nature. Since they are endogenously found within the body, they do not induce immune responses, and are highly biocompatible.[65] They also provide a shielding effect similar to PEG.[66] In some circumstances, they even have targeting capabilities.[67] For all that, they are still rarely used as delivery vehicles in clinical settings. Their isolation and purification into monodisperse and highly-defined polymers is highly challenging and has been impeding their use in biomedical applications.[68–70]

Poly(amino acid)s can be synthetically produced or naturally occurring polymers. They are composed of α-amino acids linked by peptide bonds whereas pseudo-poly(amino acid)s are linked by ester, carbonate or urethane linkages. Poly(amino acid)s can be prepared with a wide variety of functional groups.[71] Due to their peptide linkages, poly(amino acid)s are highly biodegradable.[21] They have been shown to increase the blood circulation time of nanoparticles and to decrease their interaction with blood components (e.g. antibodies).[72] Their solubility however can be low or pH-dependent. They also have poor mechanical properties and complement activation of the immune system has been reported in some cases.[48] Still, various funtionalisations have been reported taking advantage of the variety of functional groups on the main chain: aminolysis, ester exchange, condensation reactions or even the introduction of polymer blocks.[73] These modifications might be able to overcome poly(amino acid)s current limitations, even though some poly(amino acid)s are already being tested in clinical trials.[24]

1.1.4 PEGose

It is clear that PEG alternatives are needed, but as previously mentioned, the library of hydrophilic polymers that could replace PEG is still limited. For that reason, the Prunet group in collaboration with the Shaver group developed a new hydrophilic polymer coined PEGose.[74] PEGose is a water-soluble polycycloether (PCE) whose structure resembles that of PEG and a polysaccharide like amylose. Its backbone is the same as PEG, with each oxygen atom separated by two carbons. This polyether structure differs from the acetals found in a polysaccharide, in a way that PEGose backbone cannot be hydrolysed unlike most polysaccharides. The similarity to amylose comes from the polycyclic structure as well as the presence of hydroxyl groups. Morever, it was found that if PEGose is isotactic, it adopts a helical structure like amylose.[74] To be able to synthesise this polymer, Alkattan et al. performed the coordination anionic ring-opening polymerisation of butadiene monoxide, using tetraphenylporphyrin aluminium chloride as a catalyst and initiator. The key step of the synthesis is the use of a ring-closing metathesis to go from the poly(epoxybutene) (PEB) to a polycycloether (PCE). Lastly, the polycyclic polymer is submitted to a diastereoselective dihydroxylation to afford PEGose (See Figure 1.9).

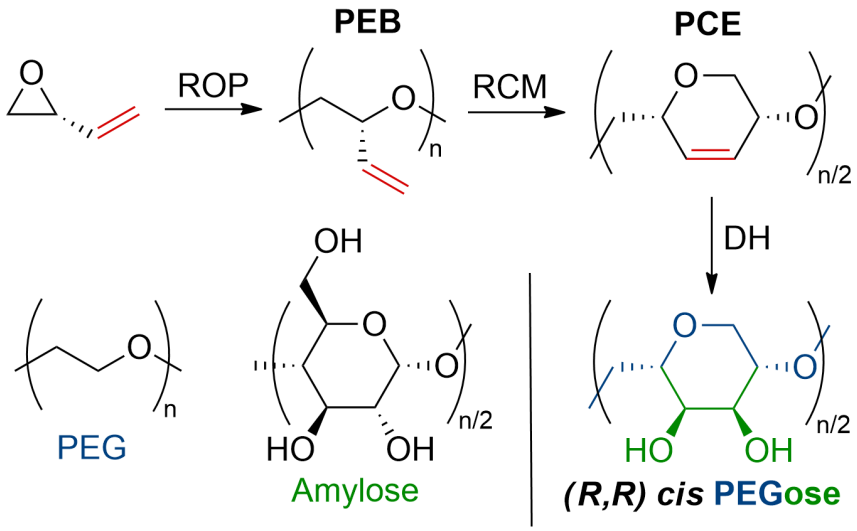

Figure 1.9: Scheme for the synthesis of isotactic PEGose: ring-opening polymerisation (ROP) of enantiopure butadiene monoxide, followed by ring-closing metathesis (RCM) and subsequent dihydroxylation (DH).

The synthesis of PEGose has been reported for the first time in 2018. Consequently, none of its properties are known except that it becomes water soluble once 90% of the polycycloether has been dihydroxylated. However, one could hope that due to its unique structure, PEGose might have some of the benefits from being a synthetic polymer similar to PEG: controlled polymerisation, low amount of impurities, accurate molecular weight with low dispersity, hydrophilic, stealth effect. Similarly, PEGose might have some advantages that polysaccharides and natural polymers have: ease of functionalisation, biocompatibility, biodegradability, stereocontrolled structure.

1.2 Block copolymers

1.2.1 Block copolymers and their use drug in delivery systems

A block copolymer is one of the multiple types of copolymer that can be synthesised (See Figure 1.10). A copolymer is a polymer comprising at least two different repeating units. A block copolymer will be defined as two or more homopolymers linked together via covalent bonding. These blocks can be connected by the use of a linker or they can directly react on each other. One strategy is to use one block or homopolymer as a macroinitiator for the polymerisation of the second block. A block copolymer can also be made in one-step if the reactivity of the two different monomers are sufficiently different, so that the active chain keeps reacting on the same monomer during the propagation step. Living polymerisation techniques are extremely useful to produce block copolymers. A polymerisation is considered "living" when chain-transfer and termination reactions are eliminated. Living polymerisations can then be used to synthesise a homopolymer with an active chain-end then add another monomer after the conversion of the

first one, to synthesise a block copolymer. A diblock copolymer will generally be obtained when the initiator bears one active group, whereas a triblock copolymer will be obtained if the initiator is bifunctional. Other common copolymers include alternating copolymers, whose polymer contains two monomeric units in an alternating sequence. Statistical copolymers, or random copolymers, are called so when the monomeric units are distributed randomly, sometimes unevenly. Gradient copolymers are copolymers whose monomeric units are distributed gradually along the chain. Graft copolymers are non linear copolymers. Their backbone is composed of a single monomeric unit, with side-chains composed of a different monomeric unit (See Figure 1.10). Other branched copolymers include brush copolymers, comb copolymers, or star copolymers.

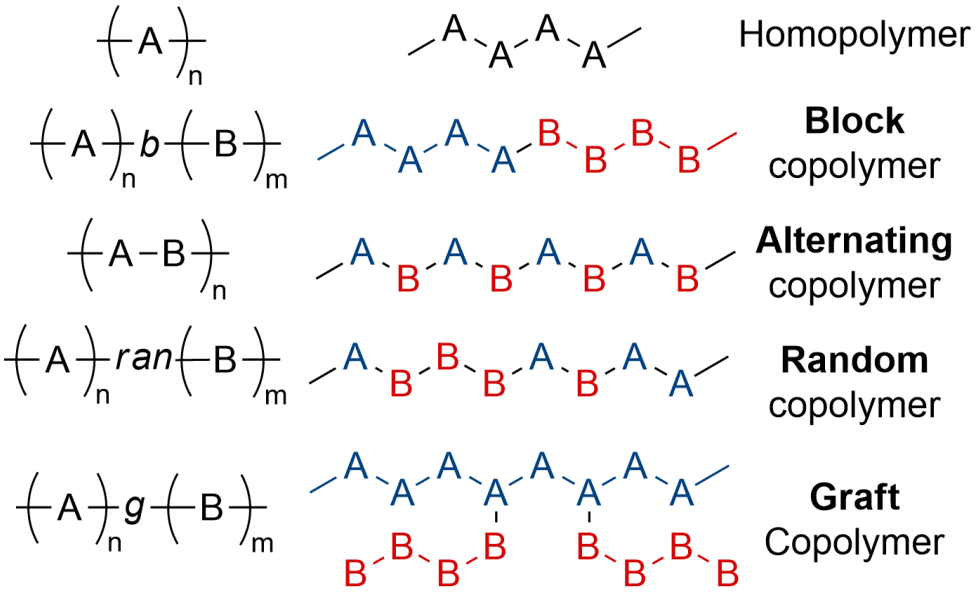

Figure 1.10: Different structures of copolymer consisting of two monomeric units A and B.

One common design choice when synthesising a block copolymer is to have a hydrophilic block and a hydrophobic block. The amphiphilicity of the two blocks is the driving force of the block copolymer self-assembly in water.[75] During the self-assembly process into micelles or vesicles, a hydrophobic drug can be encapsulated in a micelle core or a vesicle membrane. This type of drug delivery system represents a simple and convenient way to achieve drug shielding, controlled release and enhanced solubility.[13] Block copolymers are then a typical pathway towards nanoparticles formation and nanomedicine formulation. One of the most common block copolymer used for drug delivery is PEG-*b*-poly(lactic acid).[76] Poly(lactic acid) (PLA) is used as a hydrophobic block because it is an aliphatic polyester. The presence of hydrolysable linkages allows PLA to be biodegradable. Moreover, PLA is biocompatible and is already used in the medical field, from tissue engineering templates (Resolut®) to dental (Antrisorb®) or orthopedic fixation devices (Biofix®).[77] Lastly, PLA synthesis, degradation profiles, physical and crystalline properties have been extensively studied in the literature.[78] PLA and other aliphatic

polyesters can be synthesised via polycondensation or ring-opening polymerisation. Polycondensation tends to yield polymers with a lower mass; indeed, removing the residual water is difficult, which will prevent the formation of long polymer chains.[79] On the other hand, ring-opening polymerisation has proven to be successful for the synthesis of long polymer chains with a low molecular dispersity. The degradation profile of PLA will dictate its efficiency as a nanocarrier, as it forms the hydrophobic core that contains the drug.[80] This degradation profile depends on many factors, notably the PLA molar mass, distribution and crystallinity. It is also worth noting that three distinct mechanisms can be described to explain the degradation of PLA:

1. Enzymatic degradation
2. Microbial degradation
3. Hydrolytic degradation

The enzymatic degradation of PLA can be performed with the help of several enzymes. Proteinase K has been reported as highly efficient for the acceleration of the degradation of PLA.[81] The first step of this degradation mechanism consists of the adsorption of the enzyme on the polymer, followed by the cleavage of the chain. The microbial degradation is the reason why PLA is degraded after being buried in the soil; it has been reported that *Tritirachium album* is a fungus capable of cleaving PLA macromolecular chains.[82] Lastly, the hydrolytical degradation of PLA can happen through the cleavage of the ester bond, catalysed by an acid or a base. While some authors affirmed that the degradation happens only on the surface of the polymer, other declared that it can only happen in the bulk. More recently, it has been proven that a heterogeneous degradation happens, autocatalysed by the acidic degradation product and the diffusion-reaction phenomenon.[82] Finally, it is worth bearing in mind that the PLA monomer contains a stereogenic center. Three different lactides can be used as a monomer (L-lactide, D-lactide, DL-lactide); accordingly, PLA with different chain stereochemistry can be made (See Figure 1.11). It has been reported that physical interactions (namely stereocomplexation) exist between PLLA and PDLA, and can then influence the morphology and properties of the nanocarriers composed of such stereocomplexed hydrophobic core.[83]

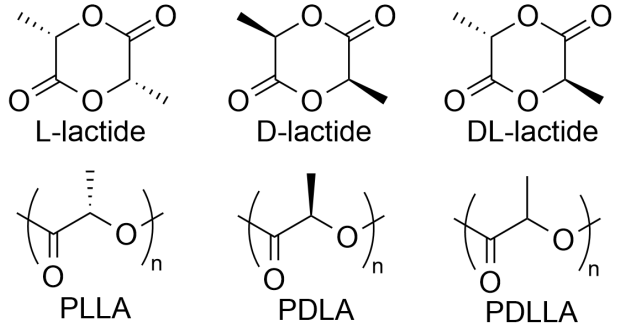

Figure 1.11: Lactide stereoisomers and their corresponding polymer.

The amount of literature on nanomicelles self-assembled from PEG-*block*-PLA copolymers is quite large.[77,84–86] This abundance of papers stems from the fact that changing a single parameter can have a large impact on the properties of the nanocarrier and its release profile. Despite this abundance of papers, the relation between the structure of a copolymer and its pharmacokinetics is not easy to predict. There are various properties that can be studied to evaluate the performance of a drug carrier,[87] namely:

- The stability, which is correlated to the CMC (Critical Micellar Concentration) and K_d (dissociation constant)
- The size of the nanocarrier
- The surface properties, in particular the hydrophilicity
- The release profile or kinetics
- The loading efficiency
- The morphology

So far, an extensive amount of factors have been reported having an impact on these properties,[88] especially:

- M_W the weight average molecular weight
- c the concentration of nanocarriers in a solution
- HLB the Hydrophilic-Lipophilic Balance
- The molecular dispersity (Đ)
- The length of the core block
- The length of the corona block
- δ_{ph}, δ_{pl}, δ_d, the solubility parameters of hydrophobic, hydrophilic block, and drug
- T_g the glass transition temperature
- The biodegradability of the core block
- The biocompatibility of the corona block
- The molar volume of the drug molecules
- The concentration of the drug
- The method for the preparation of the nanocarriers

Among all these properties, the size of the nanocarrier is of the utmost importance and should be finely tuned and be as monodisperse as possible.[89] To be successful, a nanomedicine should be able to circulate in the blood vessels while avoiding any interaction with blood components and the reticuloendothelial systems (RES), then extravasate at the diseased site, be uptaken by cells, and release the drug in an intracellular fashion.[90] If the size distribution is high enough, nanoparticles will not be able to extravasate in healthy tissues. The size of the drug delivery system will not only allow a selective extravasation in damaged tissues but will also affect the renal clearance of drug, as the threshold for glomerular filtration in kidney is approximately 50 kDa, or 6 nm.[7] The PEG layer is essential to avoid interaction with opsonins proteins and further elimination by the liver and the spleen.[91] Since PEG is a neutral hydrophilic layer, it is less susceptible to elimination by the liver and spleen compared to positively charged nanocarriers.[92] Over the years, to further improve the performance of self-assembled nanoparticles, different chemical functionalisations have been performed to make these nanocarriers able to respond to certain stimuli. This stimulus must be exacerbated in the damaged tissue so that the release of the incorporated drug happens exclusively at the target site. For example, the pH of cancerous tissues is lower than that of healthy tissues.[75] Authors explained this phenomenon by the aerobic glycolysis and lactate production, overexpression of particular biomolecules, extracellular reactive oxygen species (ROS), and altered redox potential.[93,94] External stimuli such as ultrasound or light irradiation can also be used to target tissues in pinpoint therapies.[95] The various stimuli that have been used over the years are outlined in Figure 1.12.

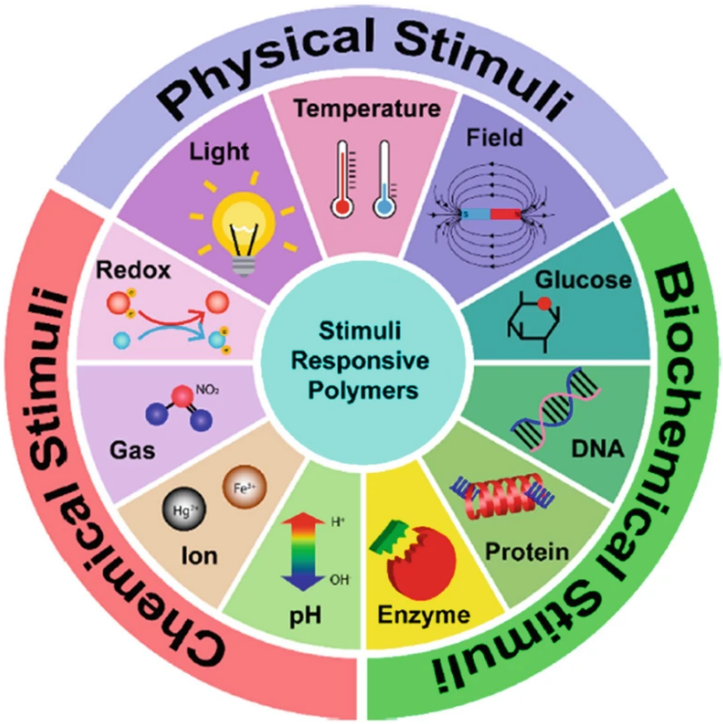

Figure 1.12: Various stimuli that can be used to enhance nanomedicines specificity. Adapted with permission.[96] Copyright © 2021 American Chemical Society.

Lastly, nanocarrier selectivity can be enhanced by attaching a ligand molecule at the end of the hydrophilic chain.[97] While PEG is very effective for shielding drugs from blood components, it has been proven that it also limits the internalisation of such nanomedicines.[87] This is known as the "PEG dilemma", although it has been observed for other shell-forming chains. The end-group functionalisation of these chains have been able to circumvent this issue. This so-called "pilot" molecule, located at the surface of the nanomedicine, can be an antibody, a peptide, a sugar, or another small molecule such as folic acid.[98] Folate receptor are over-expressed in tumors, folic acid end groups have then been able to increase the selectivity of anticancer nanomedicines. Folate-drug conjugates have even been able to reach phase III clinical trials.[99] Reports mentioned that nanomedicines represent a several billion-dollars market; however, only a very few drug delivery systems have been clinically approved. The most common obstacle to a market approval is the intricacy of these formulations, which hampers scaling-up a laboratory procedure.[99]

1.2.2 Block copolymer self-assembly and cubosomes

As previously mentioned, various types of nanoparticles have been developed over the years with the goal of encapsulating and releasing compounds in a controlled fashion. Organic nanoparticles are either composed of lipids, polymers, or a mixture of the two.[100] The self-assembly of these lipids or polymers into nanoparticles is driven by their amphiphilicity. Three main types of nanoparticle morphology are frequently encountered: micelles, worm-like micelles and vesicles. All these mophologies can be obtained by using either lipids or polymers, and the morphology achieved depends mainly on the chemical structure of the lipid or polymer used.[101] The concept of critical packing parameter (See Equation 1.1) has been introduced to explain or even predict the morphology adopted by an amphiphilic compound.[102]

$$p = \frac{v}{a * l} \tag{1.1}$$

p is the critical packing parameter, **v** is the volume of the hydrophobic chain, **l** is the length of the hydrophobic chain, **a** is the optimum surface area of the hydrophilic part at the hydrophilic-hydrophobic interface. A particular value of the packing parameter can be translated into an aggregate shape:

- For $p < 1/3$, micelles are obtained
- For $1/3 < p < 1/2$, worm-like micelles are obtained
- For $1/2 < p < 1$, vesicles are obtained

The way the critical packing parameter is computed has been debated over the years, for example, R. Nagarajan mentioned that the role of the surfactant tail is usually neglected.[102] However, a common consensus is that altering the relative volume of the hydrophilic part over the

hydrophobic part gives rise to different morphologies.[103] The interest in the morphology of the nanoparticles comes from the different properties of each individual morphology. Indeed, micelles have been shown to have a better cellular uptake than worms or vesicles.[13] Worm-like micelles have the highest surface area. Vesicles have the unique advantage to be able to encapsulate both hydrophilic and hydrophobic compounds.[104] But while different morphologies have specific advantages, they also have their own limitations. For instance, vesicles are able to encapsulate hydrophilic compounds thanks to their hollow-core structure; nevertheless, that same hollow-core structure renders them unstable against osmotic pressure, making them unable to perform efficient drug delivery in certain parts of the human body, such as the gastrointestinal tract.[105–107] In this regard, efforts have been made to access different morphologies with unique sets of properties. One of these morphologies that got some newfound interest are cubosomes.[108] Cubosomes are usually defined as colloids with inverted liquid crystal phases as internal structure. Liquid crystals have some properties similar to both liquid and solid crystals, they can flow like a liquid while still having molecules oriented in the same direction. Like micelles and vesicles, cubosomes can be composed of polymers or lipids. They consist of a regular network of water channels and lipid or polymer membranes.[109] Due to this unique structure, cubosomes have numerous advantages over traditional morphologies: similarly to worm-like micelles they have a large specific surface area, akin to spherical micelles they have a high chemical and mechanical stability, and similarly to vesicles they have the ability to encapsulate both hydrophilic and hydrophobic compounds.[110] It has been known for a long time that lipids are able to self-assemble into liquid crystal phases, including micellar cubic phases.[111] This phenomenon is driven by the same hydrophobic effect as the self-assembly into micelles: molecules organise themselves to minimise the contact area between the hydrophobic part and water, thus minimising the free energy of the system. Interestingly, the critical packing parameter can be used one more time to explain the transition from traditional morphologies to cubosomes.[112] By increasing the critical packing parameter even more, a transition from vesicles to cubosomes can be observed. Various articles reported that by using block copolymers with longer hydrophobic blocks, the critical packing parameter would increase and a vesicle morphology could be obtained. To increase the packing parameter even more and obtain cubosomes, a common strategy is to use AB_n star polymers with two or more arms to have an even higher hydrophobic volume.[113] It should be noted that further increase of the critical packing parameter can induce a transition from cubosomes to hexosomes.[110] A summary of the nanostructures achievable by varying the structure of a block copolymer is represented in Figure 1.13.

In light of the previously listed advantages of cubosomes, recent reviews presented lipid cubosomes as the next generation of smart lipid nanoparticles.[109] However, using lipids presents some limitations such as the incapacity to control the pore and channel size. This limitation comes from the short alkyl chain of the lipid. The small size of the hydrophobic tail also means

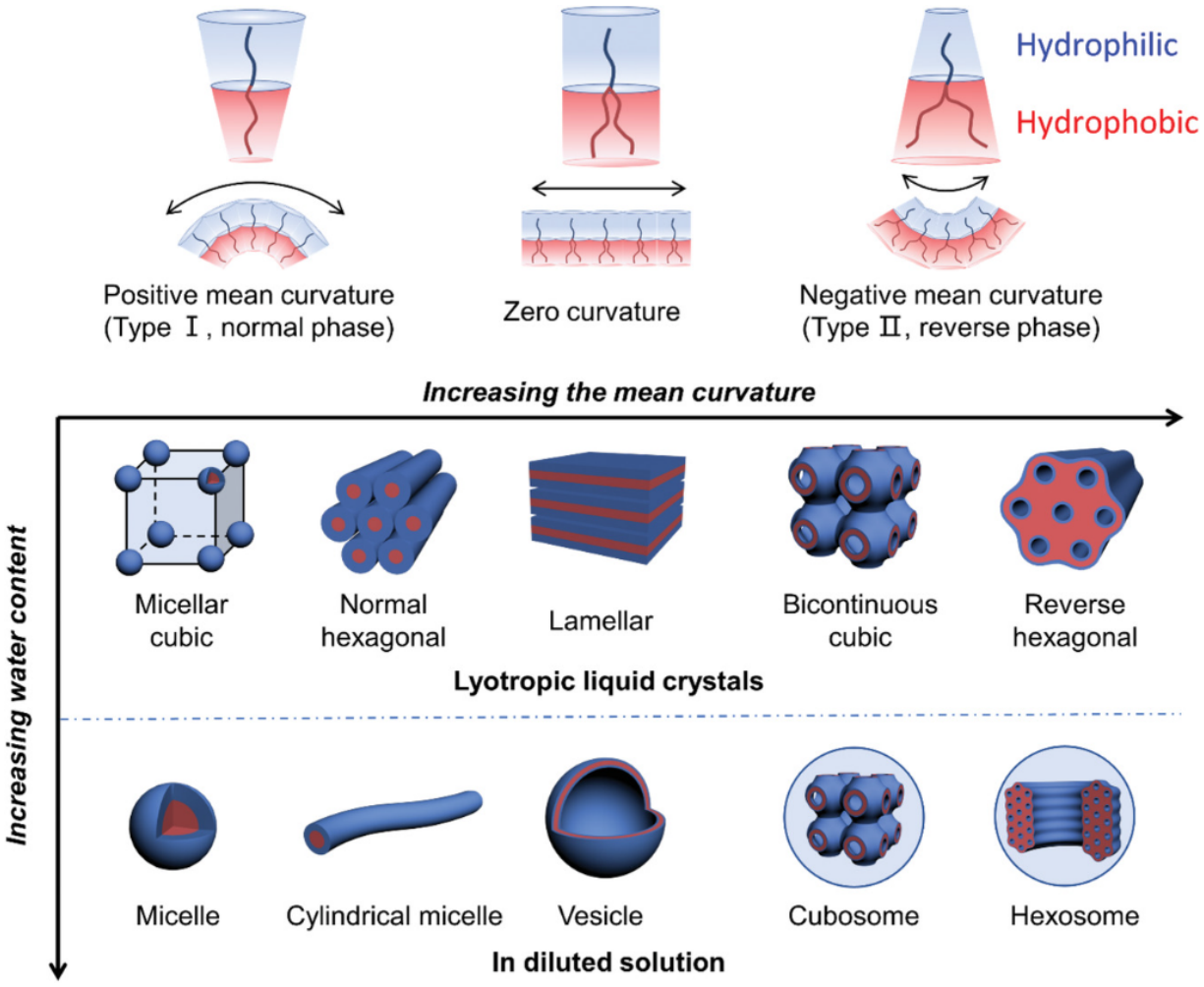

Figure 1.13: Schematic representation of the different morphologies that can be obtained by varying the mean curvature of an amphiphilic block copolymer. Adapted with permission.[113]

that mesopores are obtained, consequently limiting the range of compounds that can be encapsulated to sub-5 nm molecules. In addition, a stabilising agent is often needed to obtain lipid cubosome formulations.[114] This stabiliser is usually an amphiphilic block copolymer: Pluronic™ F127 is often used, which consists of the triblock polymer poly(ethylene glycol)-poly(propylene glycol)-poly(ethylene glycol) (PEG-PPG-PEG). Thus, using amphiphilic block copolymers instead of lipids to prepare cubosomes have seen increasing interest over the recent years.[115] The use of polymers for cubosomes circumvent the need for stabilising agents. Because of their increased molecular weight, they display an increased chemical and mechanical stability. Lastly, the extensive tools offered by polymer chemistry could potentially allow for precisely engineered cubosomes, with stimuli-responsivity and a functionality tailored for a specific application.[116] Unfortunately, the diversity of polymer building blocks used for such systems is low and needs to be addressed.

1.2.3 Double hydrophilic block copolymers

All of the block copolymers mentioned so far are amphiphilic block copolymers, composed of one hydrophilic block and one hydrophobic block. This amphiphilicity usually induces self-assembly at very low concentration. However, double hydrophilic block copolymers (DHBC)s have gained considerable attention in the recent years.[10] DHBCs, as the name suggests, are block copolymers composed of two water-soluble polymers. In this instance, it is the hydrophilicity difference between the two blocks that drives the self-assembly in water. The hydrophilicity difference needs to be quite large for nanoassemblies to form.[117] The self-assembly of DHBCs can seem counter-intuitive at first but can be understood through a more commonly observed phenomenon: aqueous two-phase systems (ATPS). An ATPS can form when two homopolymers are mixed in water at high concentration. Even though only one solvent is used (water), two phases can be observed, one phase will contain predominantly one homopolymer, while the other phase the other one.[118] This phenomenon was first observed in 1896, when M. W. Beijerinck noticed that an agar solution (water-soluble) was immiscible with gelatin or starch water solutions. These days, the most studied biphasic system is PEG-Dextran.[119] In this system, PEG is less hydrophilic and less dense than dextran and will then form the upper layer (See Figure 1.14). This can be exploited by covalently binding these two polymers to form a DHBC capable of self-assembly in water. Compared to amphiphilic block copolymers, DHBCs can have an increased biocompatibility and biodegradability.[119,120] It should also be noted that these DHBCs assemblies can have an increased permeability compared to traditional liposomes, which might prove useful for the preparation of artificial cells.[121] Similarly to amphiphilic block copolymers, DHBCs can form nanoparticles with a broad range of morphologies: micelles, worm-like micelles, capsules or particles (See Figure 1.14).[119,122–124] These morphologies can be affected by numerous factors: polymer molecular weight, block lengths ratio, polymer concentration or polymer architecture.[119,124–129]

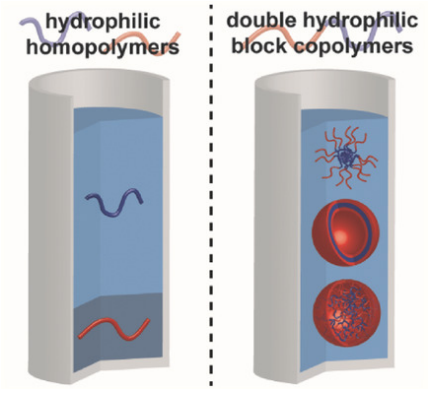

Figure 1.14: Schematic representation of an aqueous two-phases system (ATPS) using two hydrophilic homopolymers, and the corresponding double hydrophilic block copolymer (DHBC) self-assemblies in water. Adapted with permission.[117] Copyright © 2021 John Wiley and Sons.

1.3 Post-polymerisation functionalisation

1.3.1 General functionalisation of polymers

The use of polymers in everyday life has increased tremendously over the last few decades. The most produced polymers are simple polyolefins like polyethylene (PE) or polypropylene (PP) that are used as cheap materials or packaging.[130] However, there is an increased demand for high-value functional polymers with tailored properties, especially for biomedical applications: cancer therapy, regenerative medicine, drug delivery, bioimaging, biosensing, immune therapy, tissue engineering, implants, wound dressings, the list goes on.[131] This demand for functional materials was supported by progress in polymerisation methods: reversible deactivation radical polymerisation, cationic/anionic ring-opening polymerisation, stereospecific catalytic polymerisation, olefin metathesis polymerisation, enzymatic polymerisation, supramolecular polymerisation and metal catalyst for olefin insertion polymerisation. Despite this abundance of synthetic methods, some functional groups are extremely challenging to obtain. For example, hydroxyl or amino groups are incompatible with anionic ring-opening polymerisation since their nucleophilicity can lead to unwanted ring-opening side-reactions. Their properties to act as a ligand can also be a drawback for polymerisation catalysed by late-transition metals or other Lewis acids. One way to circumvent this issue is the use of post-polymerisation reactions.[132] This strategy consists of using a monomer that is not bearing the desired functional group, but instead an inert functional group that can be modified into the desired functional group after the polymerisation. One of the most common examples is the synthesis of poly(vinyl alcohol) (PVA). The free radical polymerisation of vinyl alcohol is extremely challenging under normal conditions since it tautomerises into acetaldehyde at room temperature. Poly(vinyl acetate) is polymerised instead using radical polymerisation, the resulting polymer is then subjected to a post-polymerisation hydrolysis to finally afford the desired polymer bearing the hydroxyl group (See Figure 1.15).[133]

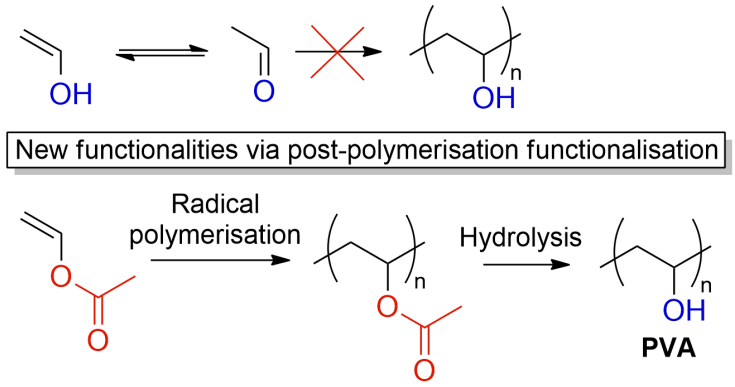

Figure 1.15: Scheme of the synthesis of poly(vinyl alcohol) (PVA) via the post-polymerisation functionalisation of poly(vinyl acetate).

For a reaction to be used as a post-polymerisation functionalisation it needs to fulfil certain criteria. It ideally needs to be a single-step reaction, with a high yield and quantitative conversion, and with a sufficiently high chemoselectivity and orthogonality so that it can be done on polymers bearing various functional groups. Additionally, due to the occasional difficulties to purify polymers, it should require a low catalytic loading (or no catalyst at all) and produce low amounts of side-products. For these reasons, click chemistry has been increasingly used for the addition of functional groups to polymer chains.[47] The **Diels-Alder** cycloaddition is one example of a reaction that produces no side-products and is compatible with a broad range of functional groups. The reaction consists of a diene reacting with a dieneophile. Usually, furan is used as a diene and maleimide is used as a dienophile to form an oxabicycle. On top of that, the reaction is reversible: the diene and dienophile can be obtained back by heating, thus paving the way for the synthesis of thermoresponsive materials. Recently, H. Muljana et al. reported a cross-linked polypropylene through a Diels-Alder post-polymerisation reaction (See Figure 1.16).[134]

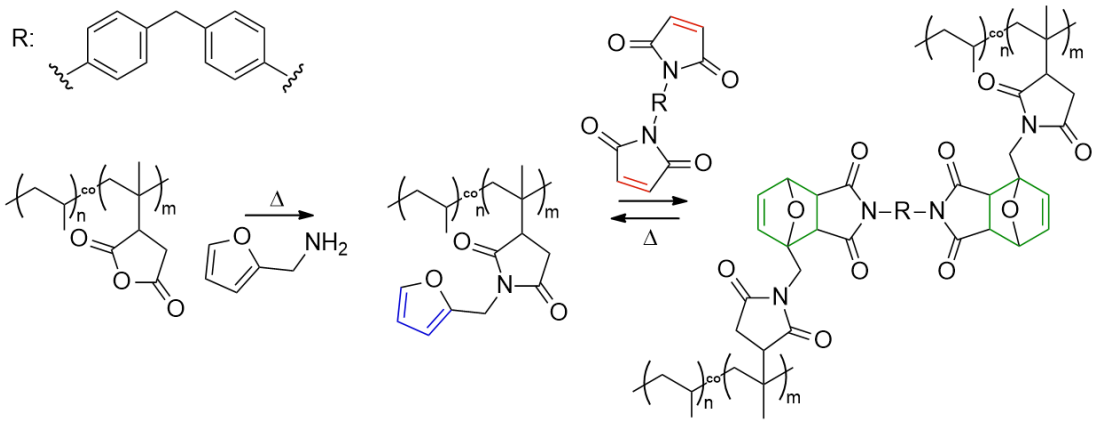

Figure 1.16: Scheme for the synthesis of reversibly cross-linked polypropylene via post-polymerisation Diels-Alder.[134]

The **Copper-catalysed azide alkyne cycloaddition (CuAAC)** is another commonly used click reaction. It has been increasingly used in recent years as a post-polymerisation functionalisation tool as both azide and alkyne are generally inert towards most polymerisation techniques. Additionally, the reaction can be undertaken in organic solvents or water under mild conditions. Hasegawa et al. were able to use CuAAC click chemistry to functionalise natural polysaccharide with various functional appendages (See Figure 1.17).[135]

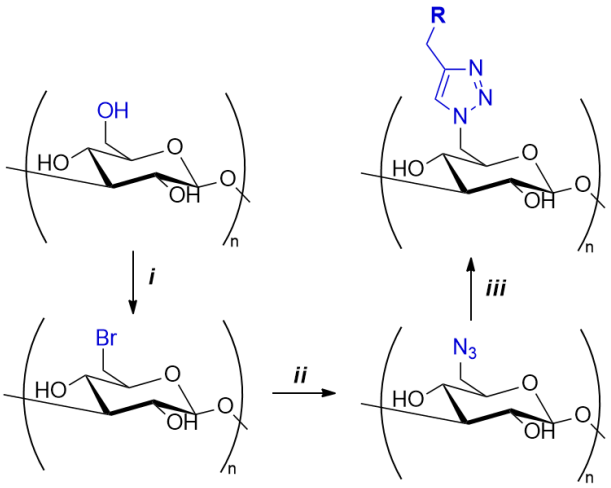

Figure 1.17: Copper catalysed azide/alkyne cycloaddition (CuAAC) between 6-azido-6-deoxycurdlan and alkyne-terminated functional modules. Reagents and conditions: (i) PPh_3, DMF, LiCl, RT, 3 h, then CBr_4, 60°C, 24 h; (ii) NaN_3, DMSO, 80°C, 36 h; (iii) alkyne-terminated functional modules, $CuBr_2$, ascorbic acid, propylamine, RT, 12 h, DMSO or NMP. Adapted from.[135]

One last example of click reactions that have been used are **Michael type addition** reactions. Michael type reactions between thiols and activated alkenes can proceed in aqueous medium, at low temperature, and give good yields.[136] Having an acrylate side-chain is challenging if a free radical polymerisation is employed but can be achieved through the ring-opening polymerisation of a lactone. Rieger et al. demonstrated the ease of functionalisation of a poly(caprolactone) (PCL) bearing an acrylate side-chain via the addition of various thiols.[136] Poly(caprolactone)s are biodegradable and biocompatible but their functionalisation is challenging due to the susceptibility of the ester linkage towards nucleophiles. Using Michael-type thiol-ene addition a PEG chain was grafted on the poly(caprolactone) and an amphiphilic polymer was synthesised via post-polymerisation functionalisation (See Figure 1.18).

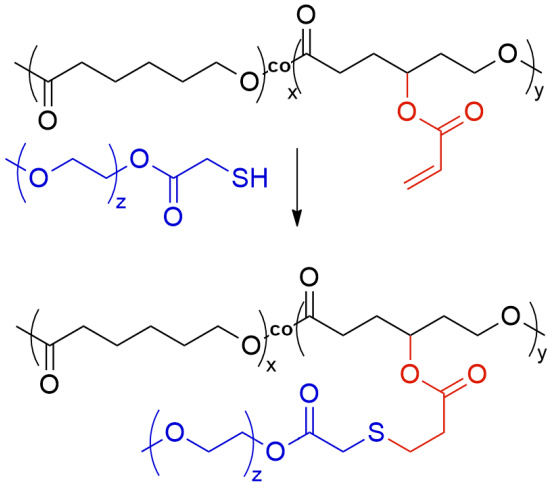

Figure 1.18: Scheme of the synthesis of PCL-*g*-PEG via a Michael type thiol-ene addition on an acrylate-bearing PCL. The reaction was performed in THF, using pyridine as a catalyst.[136]

1.3.2 Functionalisation of unsaturated polyethers

PEG has found many uses in a broad range of industries but its lack of functional groups can be detrimental. To remediate this issue, an olefin-bearing polyether poly(allyl glycidyl ether) (PAGE) has been synthesised via ring-opening polymerisation. Olefins are incompatible with radical polymerisation methods but are generally inerts with techniques like anionic ring-opening polymerisation.[137] Olefin-bearing polymers can then be modified through post-polymerisation reactions on alkenes to access a broad range of different functionalities. For example, PAGE has been reported to undergo cross-metathesis reactions (See next section), isomerisation, dihydroxylation, hydroformylation, reductive amination or thiol-ene reactions under different conditions (See Figure 1.19).[138] Dihydroxylation of the double bond was performed using osmium tetroxide OsO_4 and *N*-methylmorpholine *N*-oxide (NMMO) and produced a hydrophilic polymer. Isomerisation allowed the subsequent cleavage of the side chain to obtain a linear polyglycidol. This is a structure of interest as the polymerisation of glycerols traditionally yields hyperbranched polyglycerols. The hydroformylation followed by reductive amination is a powerful functionalisation as it allows a broad range of R-groups to be added, on top of an amino group increasing the polarity of the polymer. Thiol-ene radical additions have also been used to functionalise PAGE, yielding a polyampholyte polymer capable of protecting living cells during their cryopreservation.[137] It was proposed that this polymer increases the post-thaw cell survival by stabilising the cell membrane and inhibiting ice grain coarsening during freezing and thawing. Finally, the addition of cysteamine hydrochloride promotes the formation of cationic polymers that could be potentially complex DNA and be used in gene therapy.[16]

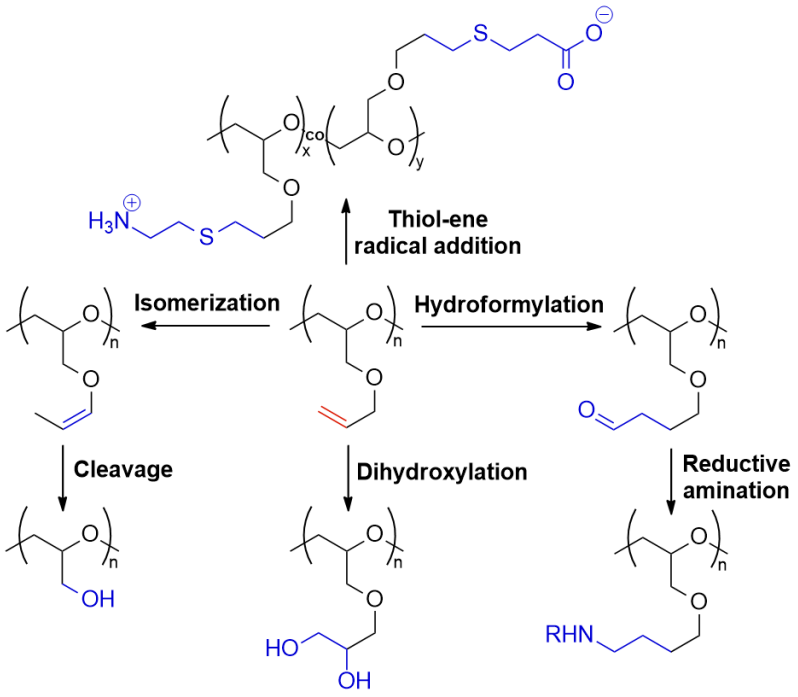

Figure 1.19: Scheme of different olefin post-polymerisation functionalisations of PAGE that have been reported.[138]

1.3.3 Olefin metathesis as a post-polymerisation functionalisation tool

Olefin metathesis is a very powerful reaction used in the field of organic chemistry to generate new carbon-carbon bonds. The elucidation of the reaction mechanism and the discovery of efficient catalysts resulted in Yves Chauvin, Robert H. Grubbs and Richard R. Schrock being awarded the 2005 Nobel prize in chemistry. Olefin metathesis can generally be classified into three categories: cross-metathesis (CM), ring-closing metathesis (RCM) and ring-opening metathesis (ROM) (See Figure 1.20).

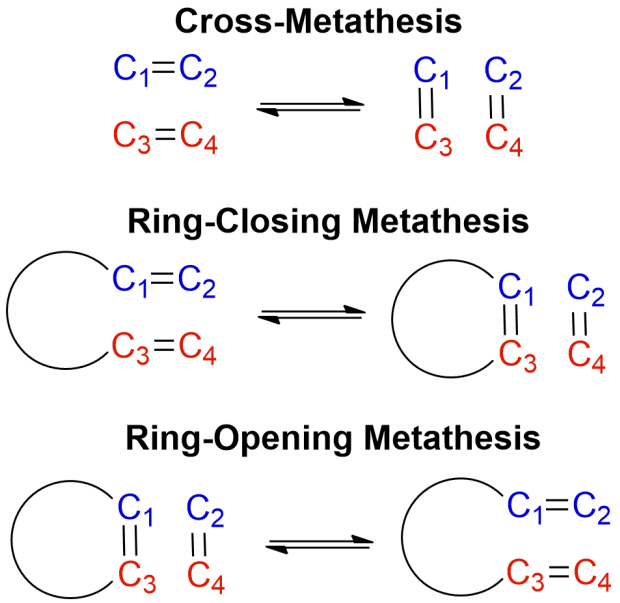

Figure 1.20: Scheme of the different categories of olefin metathesis: cross-metathesis, ring-closing metathesis and ring-opening metathesis.

During a cross-metathesis, two acyclic olefins react to form new olefins with transposed substituting groups. Controlling this reaction can be challenging since a large number of side-products can be obtained, including homodimers. Ring-closing metathesis occurs when two olefins react to form a cyclic olefin and a smaller acyclic olefin. This reaction is more or less favored depending on the size of the cyclic olefin formed, with 6-membered rings being generally thermodynamically favored. Another driving force of the reaction is the release of ethylene when the two olefins reacting together are terminal alkenes. Finally, ring-opening metathesis consists of the reaction between a cyclic olefin and an acyclic one to form an acyclic diene. The driving force of this reaction is the release of ring stain.[139] Olefins can be classified into different types based on their reactivity. Electron-rich and sterically unhindered alkenes are considered type I olefins; they are very reactive and can homodimerise quickly. Electron-poor and sterically hindered alkenes are considered Type IV olefins, they cannot homodimerise and generally will not react with any other olefin. Type II and type III olefins have an intermediate reactivity; type II can still homodimerise, although slowly, while type III will not homodimerise (See Figure 1.21).

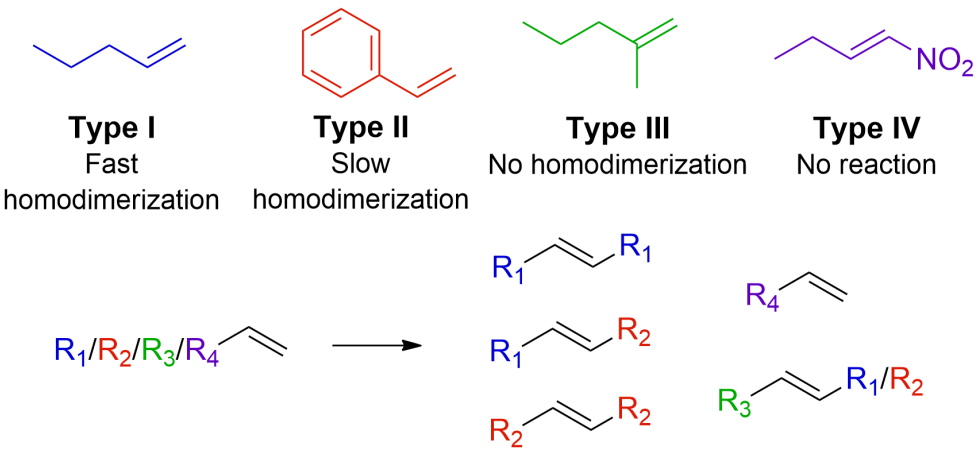

Figure 1.21: Structure of different olefin types and scheme of the different metathesis products based on the olefin type.

Olefin metathesis reactions are catalysed by a metal. The first catalysts used for olefin metathesis were based on rhenium, tungsten and osmium but were poorly reactive and quite unstable. Nowadays, molybdenum and ruthenium systems are mostly used, especially Grubbs I, Grubbs II and Hoveyda-Grubbs II complexes. First-generation Grubbs catalyst is synthesised from $RuCl_2(PPh_3)_3$, phenyldiazomethane, and tricyclohexylphosphine in a one-pot procedure. Second-generation Grubbs catalyst has the same uses as Grubbs I but with a generally higher activity, on top of being stable to air, moisture and various functional groups. It has the same structure as Grubbs I with a phosphine ligand replaced with an *N*-heterocyclic carbene (NHC). Hoveyda-Grubbs catalyst has the same *N*-heterocyclic carbene, but the second phosphine ligand has been replaced by a chelating *ortho*-benzylidene ligand attached to the benzene rings. The catalyst has an improved stability compared to the previous two. Its reactivity can be further tuned by modifying the steric and electronic properties of the added chelate.[140–142] All three catalyst structures are represented in Figure 1.22.

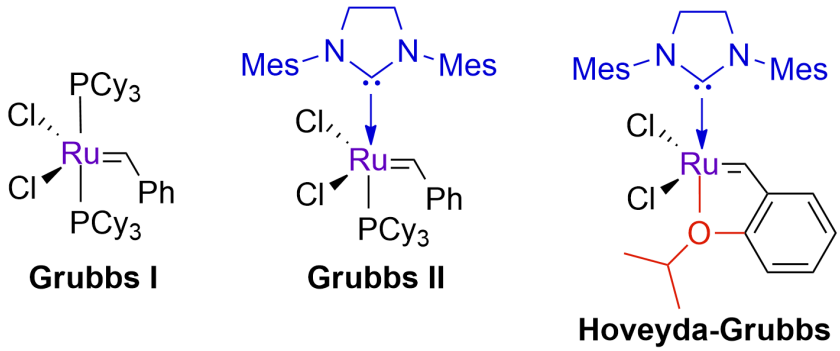

Figure 1.22: Structure of first-generation Grubbs catalyst, second-generation Grubbs catalyst and second-generation Hoveyda-Grubbs II catalyst.

While olefin metathesis has been used extensively for the polymerisation of cyclic olefins (for example the ring-opening metathesis polymerisation (ROMP) of 1,5-cyclooctadiene),[143]

it can also be used for the post-polymerisation functionalisation of alkene-bearing polymers. Olefin cross-metathesis was used by Stephen Morrison with the Prunet group to functionalise different PAGE derivatives (See Figure 1.23).[138]

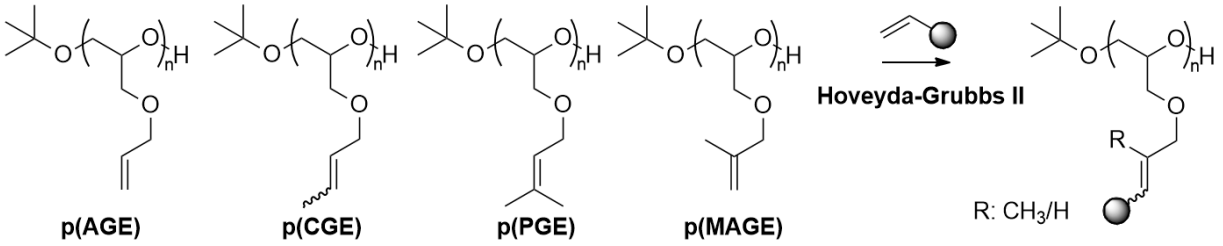

Figure 1.23: Scheme for the post-polymerisation functionalisation of poly(allyl glycidyl ether) PAGE, poly(crotyl glycidyl ether) PCGE, poly(prenyl glycidyl ether) PPGE and poly(methallyl glycidyl ether) PMAGE by cross-metathesis using Hoveyda-Grubbs II catalyst.[138]

It was shown that poly(methallyl glycidyl ether) would not undergo self metathesis pathway, preventing any cross-linking between polymer chains. It was also demonstrated that various functional groups could be installed, as well as a cell signalling peptide. The use of ring-closing metathesis as a post-polymerisation functionalisation tool is less intuitive since it does not introduce any new functionalities. However, introducing cycles in a polymer backbone can modify a wide range of properties like the glass transition temperature T_g. It was used for the first time by Grubbs and Coates, for the cyclisation of vinyl substituents in 1,2-polydienes using first-generation Grubbs catalyst.[139] The reaction was shown to be highly selective and quantitative. One remarkable phenomenon was that no isolated and unreacted olefin could be detected. The kinetic profile of the reaction showed that a 90% conversion was quickly achieved, with a second slower phase up to 100%. This suggests that the catalyst randomly closes adjacent olefins, then the catalyst migrates through the polymer backbone to scavenge any remaining unreacted vinyl group by ring-rearrangement metathesis (See Figure 1.24).

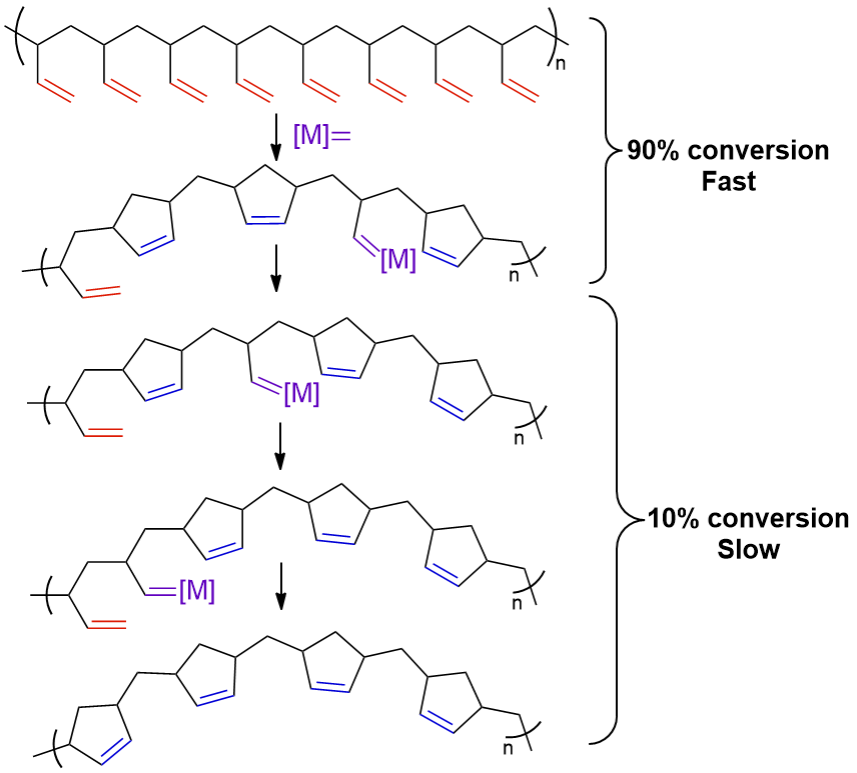

Figure 1.24: Mechanism of the ring-closing metathesis of poly(1,2-butadiene) using first generation-Grubbs catalyst.[139]

1.3.4 Post-polymerisation functionalisation towards cationic polymers

The science behind nucleic acids has seen tremendous progress. Using again the COVID-19 vaccine as example, the delivery of precisely engineered messenger RNA was proven essential to allow the production of antibodies capable of fighting the virus.[144] Nonetheless, the use of nucleic acids for therapeutic applications remains limited. The main bottleneck towards the development of nucleic acid based medicines is the delivery of the gene towards the desired cellular site of action. The main obstacle towards an effective gene delivery is the increased size of the nucleic acids compared to a traditional drug. This large size prevents any diffusion through the lipid membrane, thus limiting therapeutic benefits.[15] Another handicap is the low biological stability of these compounds. To solve these limitations, different solutions have been explored, notably:

- The chemical modification of the oligonucleotide backbone, as well as synthesising smaller oligonucleotides
- Conjugating the oligonucleotide to carriers such as membrane translocating compounds
- Nanoparticles and supramolecular self-assembly

Regardless of numerous chemical modifications of small oligonucleotides, diffusion through the cell membrane remains far less efficient compared to small drugs. This led to the development

of nanosized gene carriers that could enhance membrane permeation.[16] Liposomes or polymer micelle formulations that are already used to encapsulate small drugs could be used to transport nucleic acids as well. Yet, what is mostly used are cationic polymers that can complex the negatively charged nucleotides. These complexes have been coined polyplexes.[145] Still, both extracellular and intracellular delivery is not straightforward. Various limitations need to be overcome by the polyplex to achieve its therapeutic effect. Firstly, the polyplex needs to be able to shield the nucleic acids from nucleases that would otherwise clear free nucleic acids from the bloodstream.[146] Secondly, the polyplex must have suitable pharmacokinetics and biodistribution.[14] An important factor that governs the pharmacokinetics and biodistribution of a nanoparticle is its size. For example, nanoparticles with a size of 5 nm or less will likely be cleared by the kidneys.[147] Unlike traditional polymer micelles, the size of a polyplex will mainly depend on the cargo, as a single polymer complexed with a small oligonucleotide will assemble into smaller nanoparticles than a polyplex made of a long plasmid DNA. One limitation of polyplexes is that the cationic charges needed to complex nucleic acids is also responsible for unwanted side reactions with blood components, consequently activating the immune system.[148] One way to remedy to this problem is to use a block copolymer composed of one cationic block and one non-ionic hydrophilic block such as PEG, to shield these cationic charges from blood components.[149] Another way to improve a polyplex efficiency is to introduce ligands, improving cell binding and consequent cellular internalisation. Without these ligands, polyplexes usually struggle to cross some tissue barriers such as the extremely tight blood-brain-barrier, which cannot be crossed by passive diffusion.[150] All of these diverse limitations concern only extracellular delivery; intracellular delivery comes with numerous additional limitations. The polyplex should be able cross the cell membrane while preserving the membrane integrity. Thus, a fine balance should be found between cell permeability and biocompatibility.[151] Secondly, polyplexes are usually internalised by being engulfed into intracellular vesicles; escaping this vesicle has been the biggest challenge so far towards an efficient transfection. Finally, after reaching its target site, which can be the cytosol or the nucleus, the polyplex and its polycationic core should be able to release the nucleic acid.[152] Such fine balance between cell permeation versus biocompatibility, gene protection versus gene release, blood components shielding versus cell binding, calls for highly tuned polymers, hence the need for post-polymerisation functionalisation techniques.[153]

One of the first cationic polymer used for transfection is poly(ethylenimine) (PEI). Previously, cationic polymers were able to complex with nucleic acids but failed to perform the endosomal escape needed for an efficient transfection. PEI takes advantage of the difference between the extracellular and the endosomal pH. The neutral extracellular pH leads to a moderately protonated PEI able to complex with nucleic acids, which gets increasingly protonated in the acidic endosome. The increase of the protonation and charge density leads to two effects. Firstly, it will generate an osmotic pressure that causes the endosome to swell, and destabilise its mem-

brane. Secondly, the higher cationisation will induce lytic effects to the membrane (See Figure 1.25).[154]

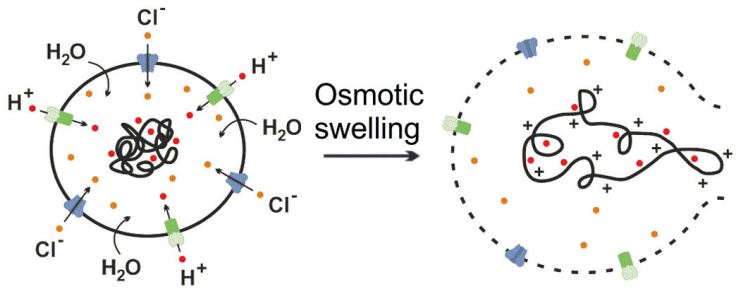

Figure 1.25: Representation of the swelling effect of PEI due to its higher charge density in an acidic endosome. The income of water and ions leads to the membrane destabilisation and consequently the endosomal escape. Adapted with permission.[152] Copyright © 2015 American Chemical Society.

The molar mass and architecture (branched versus linear) of PEI can then be tuned to achieve a somewhat balance between polyplex stability and gene release. The main limitation of using PEI as a homopolymer are its nondegradability, high toxicity, and a low variety of functional groups for further tunability.[132] The high toxicity comes from the cationic charges; these can interact and destabilise the cell surface and trigger cellular death. The cationic charges are also responsible for activating the complement system, leading to immunological responses.[155] More complex formulations have then been developed, using PEG to mask these cationic charges, ligands to target specific body area, and sometimes stimuli-responsive crosslinkers to improve the endosomal release. An example of such polymer can be found in Figure 1.26.[152]

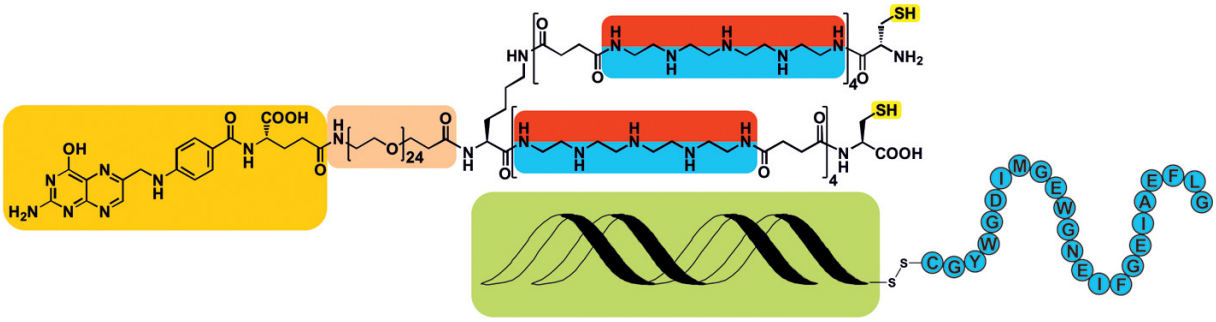

Figure 1.26: Structure of an oligomer used for multifunctional gene delivery using PEG, folic-acid targeting, and cross-linking cysteines in combination with an endosomolytic siRNA-Inf7 conjugate. Adapted with permission.[152] Copyright © 2015 American Chemical Society.

More recently, efforts were made to replace PEI with nature-derived polymers that have the advantage of being biodegradable and less toxic. These nature-derived polymers such as the polysaccharide chitosan have also issues of their own, such as a high dispersity and poorly controlled structure.[156] Polymers bearing functionalisable groups might be the solution to PEI dilemma. Indeed, compared to traditional polyamines such as PEI, a functionalisation strategy

has the advantage of precisely tailoring the charge density of the polymer. Charge density tunability is highly sought, as cationic polymers need to be able to complex the nucleotide but also release it when needed. A functionalisation with different amino groups could yield a polymer with a pH dependent protonation, in such a way that the polymer would get increasingly protonated in an acidic endosome, which might trigger an endosomal escape and efficient delivery of a gene.[157] Furthermore, functional groups might allow cross-linking or the attachment of stimuli-responsive groups, which could further enhance the shift of polyplex properties when going from the bloodstream to the endosome. One of the first application of this approach was based on polymers with a polyacrylate main chain, more specifically poly(*N*-methacryloxysuccinimide). The functional side-chains could be substituted by primary/secondary/tertiary amines with varying hydrophobicity and cationic charges (See Figure 1.27).[132,133]

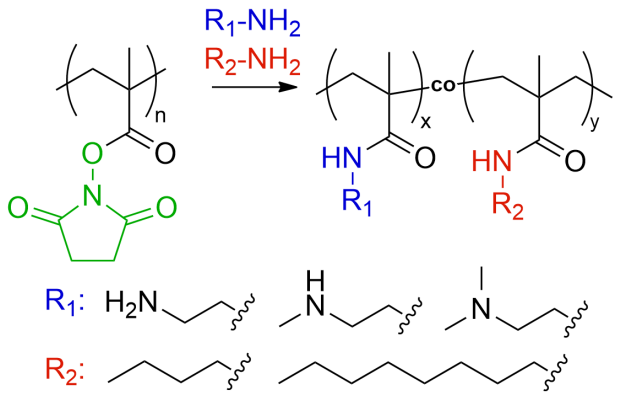

Figure 1.27: Scheme for the synthesis of polycationic polymers to be used for transfection. A library a polymer can be synthesised via a post-polymerisation functionalisation approach using poly(*N*-methacryloxysuccinimide) as a polymer precursor. NH_2-R_1 are examples of cationic hydrophilic side-chains while NH_2-R_2 are hydrophobic side-chains.

1.4 Project aims

Polycyclic compounds are ubiquitous in nature, mainly as polysaccharides. However, a limited number of synthetic polycyclic polymers have been produced so far.[158,159] This is unfortunate, as the presence of rings on a polymer backbone could affect its conformation, further affecting its properties towards a wide range of applications. The main goal of this project is to use ring-closing metathesis as a post-polymerisation functionalisation method to access a polycycloether structure, then to functionalise it to obtain novel polymers:

- Non-ionic hydrophilic polyethers (PEG alternative).
- Cationic polymers (PEI alternative).
- Hydrophobic polyethers (PPG alternative).
- Amphiphilic block copolymers (PEG-*b*-PLA alternative, poloxamer alternative).

- Double hydrophilic block copolymers.

The second goal of this project will be to study the self-assembly of all these different polymeric systems in water to discover the role/importance of a polycyclic backbone. Finally, the third goal of this work will be to leverage these novel polycyclic structures into functional materials for biomedical applications (See Figure 1.28).

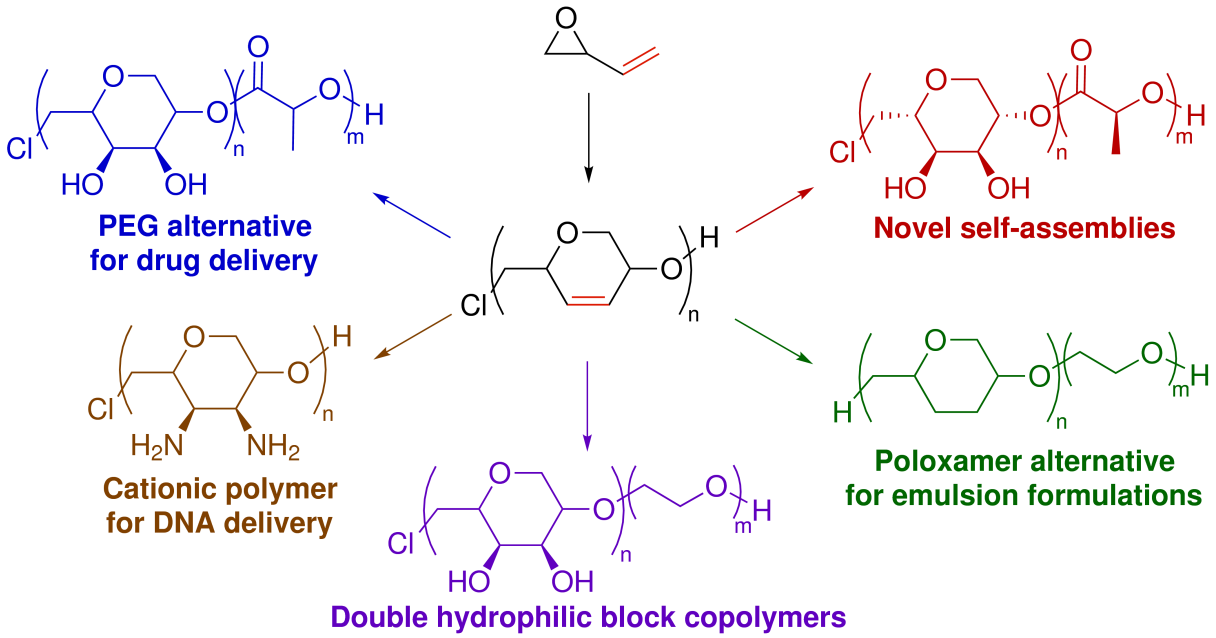

Figure 1.28: Overview of the different projects of the thesis with examples of structure synthesised.

Chapter 2

PEGose-PLA nanoparticles for drug delivery

Parts of this Chapter have been submitted for publication.[1]

2.1 Introduction

It has been emphasised in chapter 1 that the need for PEG alternatives for biomedical applications is increasing steadily.[7,158] The Prunet group recently reported in collaboration with the Shaver group the synthesis of a water-soluble amylose mimic coined PEGose.[74] PEGose has a unique structure: it has both a polyether backbone like PEG and a polycyclic chain like amylose. The PEGose structure might be a convenient middle ground between synthetic polymers such as PEG or poly(glycerol)s, and natural polymers such as polysaccharides. It combines some advantages of these structures without some of their drawbacks. For example, PEG chains cannot be functionalised but end-groups are easily tuned. Polysaccharide chains can be conveniently functionalised but it is difficult to only modify end-groups.[64] The PEGose precursor on the other hand is a functionalisable polycycloether that allows for a convenient modification of both the polymer backbone and its end-groups. Unlike common natural polysaccharides, the PEGose mass and purity are easily controlled. A major difference between PEG and a polysaccharide is that PEG is a flexible polymer while most polysaccharides, due to their polycyclic structure and their well-defined stereochemistry, are highly rigid. PEGose's rigidity, however, can be determined by tuning its tacticity: atactic PEGose is amorphous and flexible, isotactic PEGose is helical and rigid. It is worth mentioning that unlike amylose, both helical handedness can be readily obtained by monomer choice. Being stiffer than PEG, PEGose could form nanoparticles with a higher packing number, which may yield more stable nanoparticles and a better cargo retention.[160] Consequently, in this chapter the aim was to synthesise amphiphilic block copolymers PEGose-*b*-PLA that would self-assemble into core-shell nanoparticles. The nanoparticles would then be tested to see if dyes could be encapsulated then released, to mimic

drug delivery. Biological in vitro assays were planned to assess the biocompatibility and cell permeation of the prepared nanoparticles (See Figure 2.1).

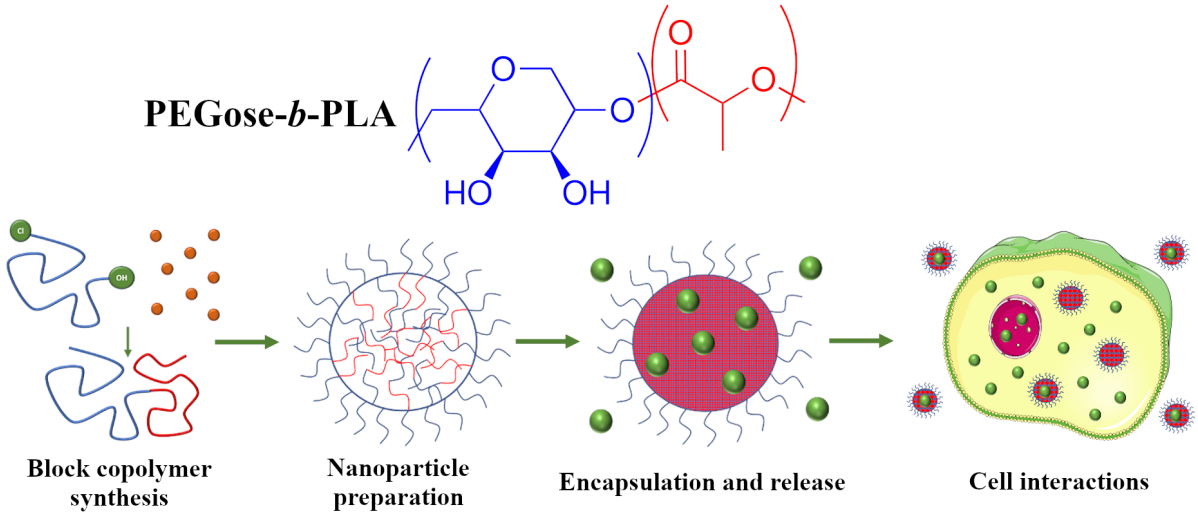

Figure 2.1: PEGose-*b*-PLA structure and schematic representation of its use as a drug carrier.

2.2 Synthesis of PEGose-*b*-poly(lactic acid) block copolymers

2.2.1 PEB synthesis

Poly(epoxybutene) (PEB) was synthesised by ring-opening polymerisation of commercially available butadiene monoxide (Figure 2.2a). The reaction was performed in a Schlenk tube, under inert atmosphere and at ambient temperature employing tetraphenylporphyrin aluminium chloride (TPPAlCl) as a catalyst and initiator, which was synthesised according to literature in a 2-step procedure.[74] A 1:50 ratio of butadiene monoxide/TPPAlCl was used to obtain a polymer with approximately 50 repeating units, yielding a mass of 3.5 kDa after 3 days, with a low dispersity (Đ < 1.20) according to SEC (See Table 2.2). The polymer structure was analysed by ^{1}H NMR, the two terminal protons from the vinyl group displayed a peak around 5.2 ppm, the remaining alkene proton showed up at 5.7 ppm, the proton from the carbon bearing the vinyl group showed up at 3.9 ppm and the two remaining protons showed up as a multiplet between 3.6 and 3.4 ppm (See Figure 2.2b). Before using the PCE as a macroinitiator, the structure of the end-groups were confirmed using electrospray ionisation mass spectrometry (ESI-MS) on a low molecular weight atactic PEB (See Figure 2.3). Each peak of the mass spectrum are separated by 70.04 Da which is the molecular weight of the repeating unit. Chlorine-35 and chlorine-37 isotopes can be observed. The polymer mainly formed sodium adducts, each peak masses can then be calculated using:

$$Peak\ mass\ =\ n * M_{butadiene\ monoxide} + M_H + M_{Cl} + M_{Na} \tag{2.1}$$

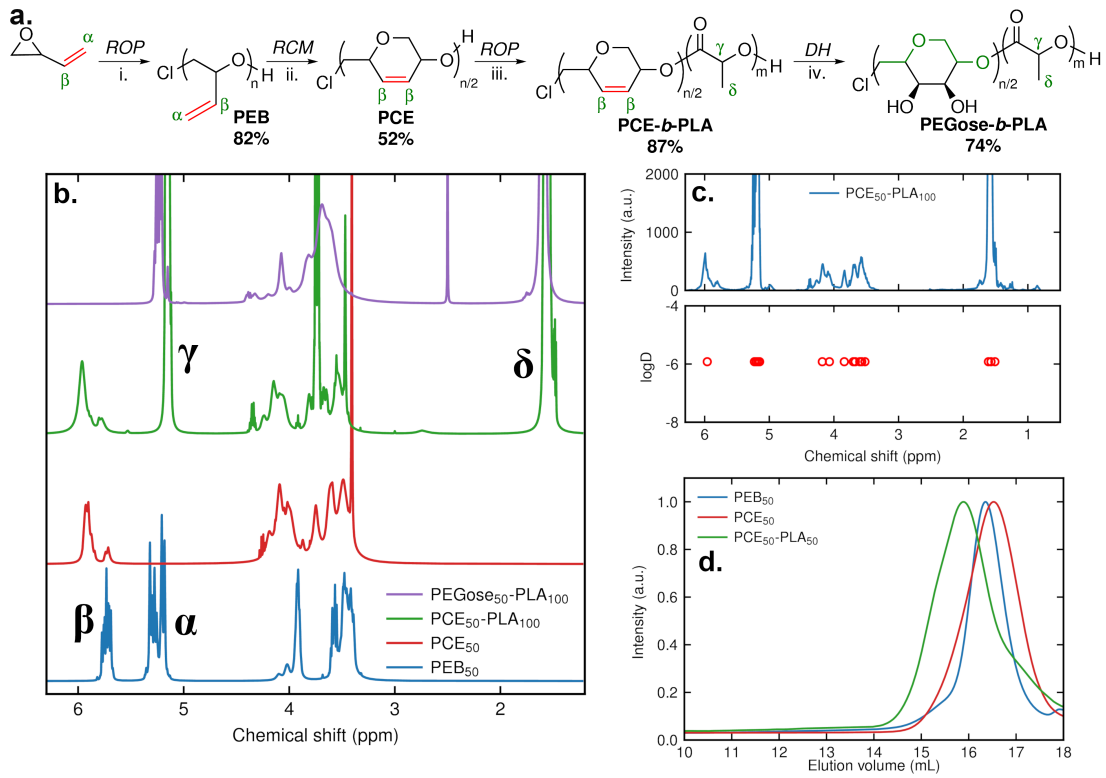

Figure 2.2: **a)** Scheme of the synthesis of the PEGose-PLA block copolymer starting from butadiene monoxide. **i.** Tetraphenylporphyrin aluminium chloride, **ii.** Grubbs II catalyst in dichloroethane, **iii.** DL-lactide and stannous octoate in toluene, **iv.** osmium tetroxide and NMMO in an acetone/water mixture. **b)** ^{1}H NMR of the synthesised polymers in $CDCl_3$ for PEB_{50}, PCE_{50} and PCE_{50}-PLA_{100} or DMSO-d_6 for $PEGose_{50}$-PLA_{100}. Remaining NMR spectra and integrals can be found in the appendix (See Figure 7.3 and 7.4) **c)** ^{1}H DOSY NMR of the block copolymer PCE_{50}-PLA_{100}. **d)** SEC traces of PEB_{50}, PCE_{50} and all synthesised PCE-PLA block copolymers measured in THF.

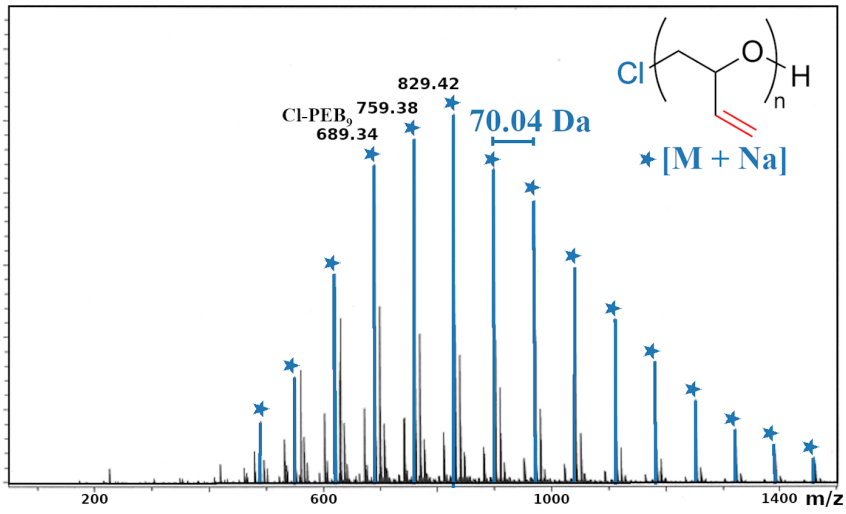

Figure 2.3: Electrospray ionisation mass spectra of atactic poly(epoxy butene). The masses of PEB_9, PEB_{10} and PEB_{11} are shown.

2.2.2 Ring-closing metathesis towards a polycycloether structure

In the next step, a polycycloether (PCE) was synthesised by performing a ring-closing metathesis reaction on PEB (See Figure 2.2a). Compared to the previous PCE synthesis described in the literature[74] (Hoveyda-Grubbs II 5.0 mol%), Grubbs II catalyst was used with a decreased amount of 2.5 mol%. The conversion of PEB to PCE was monitored by integrating the terminal alkene protons peak at 5.3 ppm (α proton, See Figure 2.2b) corresponding to PEB starting material with the internal alkene proton peak at 5.7 ppm (β proton, See Figure 2.2b). Even though a conversion of 80% could be achieved in an hour, nearly full conversion (>99%) could only be achieved after 5 days. The mass of the resulting polymer was 2.9 kDa according to SEC, which supports the elimination of ethylene during the ring-closing metathesis reaction. Since the synthesised polymer is meant to be used for drug delivery, the main challenge of the block copolymer synthesis was to avoid any residual metals to achieve a high biocompatibility. Thus, residual ruthenium was removed employing an oxidative procedure described previously.[161] Ruthenium content before and after various purification methods was quantitatively evaluated by ICP-MS. Results showed that 99.5% of the ruthenium were removed successfully with the oxidative procedure with H_2O_2, with only 32 ppm of ruthenium left. (See Table 2.1). For indication, the European Medicines Agency established a permitted daily exposure of 10 µg of ruthenium via parenteral administration. If 10.0 mg of the polymer is injected in the context of a biomedical application, 32 ppm ruthenium content would represent only 0.32 µg of ruthenium.

Table 2.1: Residual ruthenium content and relative standard deviation (RSD) determined by ICP-MS after various purification methods: addition of DMSO followed by filtration, gel permeation chromatography with Sephadex LH-20, CupriSorb heavy metals resin, oxidative procedure with H_2O_2.

Purification procedure	Purification efficiency (%)	Ruthenium content (ppm)	RSD (%)
Unpurified	0	5941	0.79
DMSO, filtration	74	1544	0.89
DMSO, filtration, GPC	79	1231	1.31
DMSO, filtration, GPC, CupriSorb	92	475	1.24
Oxidative procedure	99.5	32	2.39

2.2.3 PCE-*b*-PLA block copolymer synthesis

The diblock copolymer PCE-*b*-PLA was synthesised by ring-opening polymerisation of DL-lactide using PCE as an initiator and stannous octoate as a catalyst. The reaction was performed under inert atmosphere using a Schlenk line, in toluene under reflux for 3 h. Four block copolymers were synthesised comprising four different PLA lengths (15, 25, 50, 100 repeating units)

with a fixed PCE length of 50/2 repeating units (50 ether linkages, 25 6-membered rings). PCE-*b*-PLA block copolymer structure was confirmed by ^{1}H NMR, DOSY-NMR and SEC. ^{1}H-NMR showed peaks corresponding to both blocks, e.g. 5.2 and 1.2 ppm for the PLA block and 5.8 and 4.0-3.5 ppm for the PCE block (Figure 2.2b). Furthermore, DOSY-NMR showed that PCE and PLA peaks had the same diffusion coefficient whatever the PCE/lactide ratio used for the ring-opening polymerisation (Figure 2.2c), thus confirming the block copolymer structure. SEC derived masses of the block copolymers were slightly lower than expected for PCE_{50}-PLA_{50} and PCE_{50}-PLA_{100} (See Table 2.2) which might be due to the structural difference between the two blocks and the polystyrene standards used for the calibration curve. Nevertheless, the shift of the peak after polymerisation with decreasing PCE/lactide ratios confirmed the chain-extension of the polymer. Looking at the SEC elution trace, a single peak could be observed, suggesting that no PLA homopolymers were formed or that the Sephadex purification step successfully removed any PLA homopolymers (See Figure 2.2d). The mass of the block copolymers was also calculated by integrating ^{1}H NMR peaks from PLA repeating units against PCE peaks. This method yielded masses similar to the theoretical ones calculated from the PCE/lactide ratio (See Table 2.2). While the block copolymer dispersities were quite high considering the polymerisation type ($Đ$ = 1.32 for PCE_{50}-PLA_{25} up to $Đ$ = 1.52 for PCE_{50}-PLA_{100}), a recent study showed that a high polymer size dispersity might be advantageous to obtain nanoparticles with a narrow size distribution.[162]

Table 2.2: Theoretical polymer masses and experimental polymer masses measured by SEC and ^{1}H NMR.

Polymer	M_n **SEC**[a)] (kDa)	M_n **NMR**[b)] (kDa)	M_n **Thr**[c)] (kDa)	**Đ**[a)]
PEB_{50}	3.5	-	3.6	1.27
PCE_{50}	2.9	-	2.8	1.37
PCE_{50}-PLA_{15}	4.7	3.7	3.9	1.34
PCE_{50}-PLA_{25}	5.0	4.8	4.6	1.32
PCE_{50}-PLA_{50}	5.6	6.3	6.4	1.37
PCE_{50}-PLA_{100}	7.1	10.9	10.0	1.52

a) measured via SEC in THF with a 1 mL/min flow rate, **b)** measured via ^{1}H NMR in $CDCl_3$, **c)** calculated from starting material equivalents.

2.2.4 PEGose-*b*-PLA synthesis

The dihydroxylation of the PCE alkene was achieved by using osmium tetroxide and *N*-methylmorpholine *N*-oxide at ambient temperature in a water/acetone solvent mixture. The conversion was monitored by ^{1}H NMR in DMSO-d_6 by integrating the alkene peak at 5.7 ppm.

Full conversion was achieved overnight. Fully converted PEGose-PLA was found to be only soluble in DMSO. Due to the insolubility of PEGose-PLA in most organic solvents, the mass of the block copolymer was calculated from the mass of PCE-PLA. In order to achieve a high biocompatibility, another route was developed to avoid the use of osmium. First, the diboration of PCE with *bis*(pinacolato)diboron was performed, followed by the addition of hydrogen peroxide and sodium hydroxide to obtain an osmium-free PEGose. However, this method gave a lower yield and conversion, while not significantly improving the biocompatibility of the polymer, since osmium-free PEGose showed roughly the same biocompatibility as PEGose-PLA nanoparticles containing traces of osmium (See Figure 2.9).

2.3 Self-assembly of PEGose-*b*-PLA in water

2.3.1 Nanoparticle preparation

In order to form nanoparticles, the solvent-switch method was used.[90,163–166] The average diameter of the nanoparticles was determined by using Multi-Angle Dynamic Light Scattering (MADLS). The hydrodynamic diameter size ranged between 150 nm and 200 nm. No clear correlation could be observed between the size of the nanoparticles and the length of the PLA chain (See Table 2.3).

Table 2.3: Hydrodynamic diameter of the nanoparticles in deionised water (0.5 mg/mL) at 25°C prepared from $PEGose_{50}$-PLA_{100}, $PEGose_{50}$-PLA_{50}, $PEGose_{50}$-PLA_{25} (same sample for all three angle measurements), $PEGose_{50}$-PLA_{15}, measured by MADLS using intensity weighting.

PLA units	Hydrodynamic diameter	PDI	Measurement angle
25	149 nm	0.25	15°
25	156 nm	0.03	90°
25	164 nm	0.20	175°
100	190 nm	0.21	175°
50	192 nm	0.16	175°
15	192 nm	0.22	175°

A manual slow addition (1 mL/min) of water in the copolymer DMSO solution allowed for reproducible results with a low dispersity. The size of the nanoparticles tended to increase over time, presumably due to aggregation or ripening. Thus, zeta potential measurements were performed on $PEGose_{50}$-*b*-PLA_{50} and $PEGose_{50}$-*b*-PLA_{100}. $PEGose_{50}$-*b*-PLA_{100} nanoparticles solution had a zeta potential of -5.86 mV while $PEGose_{50}$-*b*-PLA_{50} had a zeta potential of -4.20 mV. These values are similar to the zeta potential values reported for PEG-*b*-PLA nanoparticles, usually ranging between -2.0 mV and -11.0 mV.[84,167] The low absolute value of the zeta po-

tential (less than 30 mV) might be a reason for the aggregation over time of the nanoparticles. While TEM confirmed the spherical structure of the nanoparticles and their size (See Figure 2.4a), it did not give any insight on the internal structure of the nanoparticles. Based on the low molecular weight of the block copolymers (between 5 and 11 kDa) and its contour length, the nanoparticles cannot be traditional polymer micelles. Moreover, both negative staining with uranyl acetate and the absence of any staining supplied images that did not indicate any hollow architecture, meaning they are probably not vesicles either (See Figure 2.4).

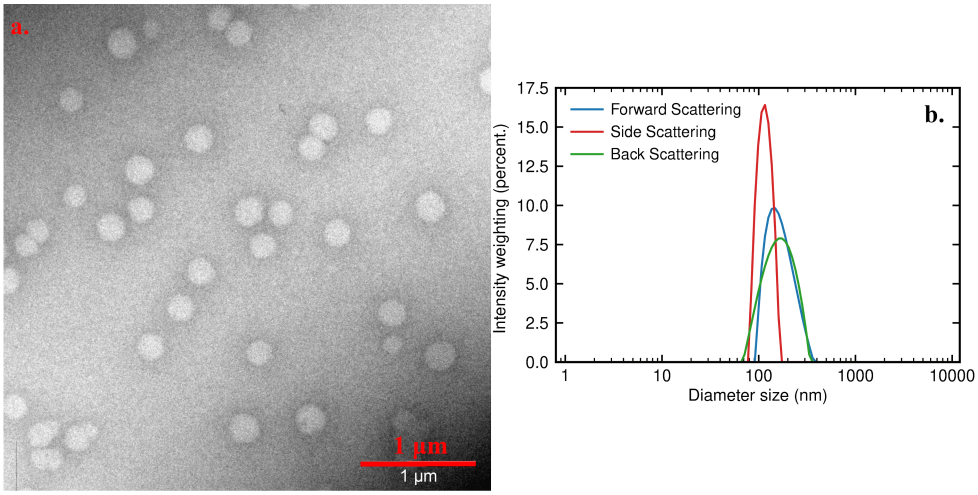

Figure 2.4: **a)** TEM image of $PEGose_{50}$-PLA_{25} nanoparticles without using any stain. **b)** MADLS size measurements of $PEGose_{50}$-PLA_{25} nanoparticles solution in deionised water (0.5 mg/mL, 25°C) at 15°, 90° and 175°.

To further prove the absence of a core-shell/hollow structure, the nanoparticles response towards an osmotic shock were studied. Nanoparticles were formed in deionised water, with a hydrophobic dye (Nile Red) encapsulated (with insoluble residues filtered out) and then added to a 100 mg/mL NaCl in water solution. While the size of the nanoparticles increased, it did not lead to any cargo release, which would be expected for vesicles (See Figure 2.5).[168] However, one possibility could be that some vesicles did burst but that the Nile Red dye stayed inside the membrane of the ruptured nanoparticle.

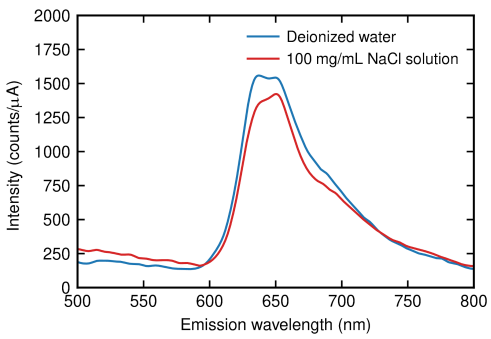

Figure 2.5: Fluorescence trace of $PEGose_{50}$-PLA_{50} nanoparticles loaded with Nile Red in deionised water and in a 100 mg/mL NaCl solution.

Another argument invalidating the traditional polymer micelle structure is the ability of PEGose-PLA NPs to encapsulate hydrophilic compounds such as the hydrophilic dye Rhodamine B (See Figure 2.7a). As PEGose is less hydrophilic than PEG, a stronger interaction between the chains is expected, which probably led to these highly dense nanoparticles. As these nanoparticles are neither micelles nor vesicles/polymersomes, we hypothesized that complex aggregates are formed with a PEGose corona and a mixed core composed of PEGose-PLA aggregates. The chain packing parameter theory could also explain why no micelles were obtained; PEGose is more rigid than PEG, a decreased chain mobility leads to a decreased hydrophilic volume/surface, thus a higher packing parameter, leading to more complex structures.

2.3.2 Nanoparticle stability tests

The nanoparticles have a hypothetically highly packed structure, we then envisaged an increased stability compared to regular micelles and vesicles. To investigate the stability of these particles in different media, their size was monitored over several days by using DLS (See Figure 2.6).

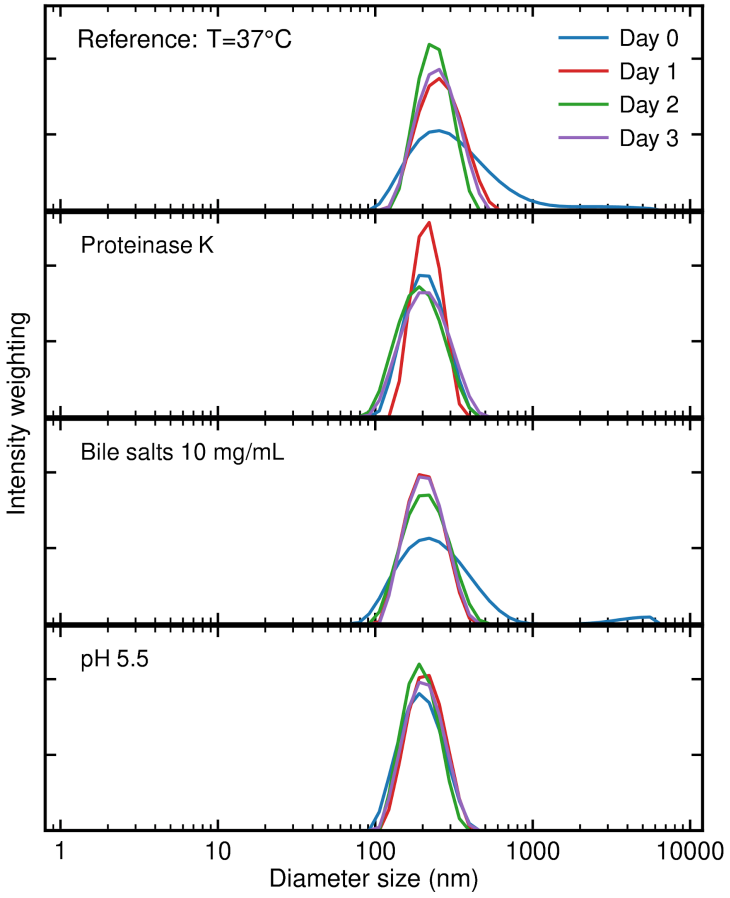

Figure 2.6: Back-scattering DLS size distribution with intensity weighting of a $PEGose_{50}$-PLA_{50} nanoparticle dispersion (0.5 mg/mL) over 4 days at 37°C, under different conditions: **a)** deionised water, **b)** 0.1 M Tris with 0.17 mg/mL proteinase K from *Tritirachium Album*, **c)** 10 mg/mL sodium cholate hydrate in deionised water and **d)** pH 5.5 solution prepared from diluted HCl.

The nanoparticles size remained stable over 3 days at 20°C or 37°C, with even a decrease in dispersity that we were not able to explain. The nanoparticles even continued to be stable over 1 year when stored at 4°C then extruded through a 0.2 µm filter (some large aggregates may also have been removed but after drying the solution, no significant mass loss was observed). The PEGose corona proved to be able to prevent the degradation of PLA by the Proteinase K enzyme, which has been employed to degrade PLA before.[169] Additionally, a *p*-hydroxydiphenyl test was realised to detect the presence of lactic acid or PLA oligomers but the presence of neither species could be found. A bile salt concentration of 10 mg/mL and a pH of 5.5 that can be found in the gastrointestinal tract of the human body[107] did not have any impact on the size of the nanoparticles as well. The ability of the PEGose-PLA nanoparticles to withstand enzymes, bile salts, low pH at 37°C could be useful for oral delivery, where highly stable drug delivery systems are needed. Targeting the gastrointestinal tract could lead to promising results, as traditional vesicular structures such as liposomes or polymersomes cannot resist this harsh environment.[170]

2.4 Encapsulation and release of hydrophilic and hydrophobic dyes

2.4.1 Encapsulation

To provide an alternative to vesicle formulations, a drug delivery system should be able to encapsulate both hydrophobic and hydrophilic compounds. Here, the encapsulation and release of two different dyes were studied using four different PEGose-PLA block copolymers (method described in Chapter 7.2). While the length of the PLA chain did not have an impact on the size of the nanoparticles (See Table 2.3), it had an impact on the encapsulation of both the hydrophobic dye Nile Red and the hydrophilic dye Rhodamine B (See Table 2.4).

Table 2.4: Encapsulation efficiency of Rhodamine B and Nile Red for all four copolymers synthesised: $PEGose_{50}$-PLA_{100}, $PEGose_{50}$-PLA_{50}, $PEGose_{50}$-PLA_{25} and $PEGose_{50}$-PLA_{15}.

PLA units	Rhodamine B encapsulation	Nile Red encapsulation
100	49%	14%
50	68%	52%
25	34%	49%
15	14%	41%

Encapsulation efficiency values are approximative since the experiments were not performed in triplicates. The highest encapsulation efficiency for both Rhodamine B and Nile Red was achieved using $PEGose_{50}$-PLA_{50}. For Rhodamine B, 68% of the dye was successfully encap-

sulated, 52% in the case of Nile Red. Interestingly, for Nile Red, there was a sharp decrease in the encapsulation efficiency when increasing the PLA length from 50 units to 100 units. Similarly, for Rhodamine B, the encapsulation efficiency declined to 14% for PEGose$_{50}$-PLA$_{15}$. These results illustrate the fact that a longer hydrophobic chain does not systematically lead to a better encapsulation of hydrophobic compounds. A similar phenomenon was described by Gianneschi and coworkers,[171] who deduced the mismatch between chain length and encapsulation efficiency of hydrophobic compounds to the lower mobility of longer hydrophobic blocks in the micelle core and during micelle formation. In this chapter, the opposite effect was found for correlation of hydrophobic chain length and encapsulation hydrophilic compounds, as elongation of the hydrophobic block led to an increase of hydrophilic dye encapsulation. This can potentially be explained with the hypothesised decreasing mobility of hydrophilic PEGose chains at the interface of particles and even more so for internalised PEGose chains anchored to longer PLA with increasing hydrophobicity. Both PEGose and PLA blocks play an important role for the encapsulation of hydrophobic and hydrophilic dyes.

2.4.2 Release

The release of both dyes was measured by fluorescence or UV-Vis spectroscopy for Nile Red and Rhodamine B, respectively (method described in Chapter 7.2). In most cases, nanoparticles released some of their cargo on the first few days then the release slowed, with still roughly half of the cargo still encapsulated after one week (See Figure 2.7).

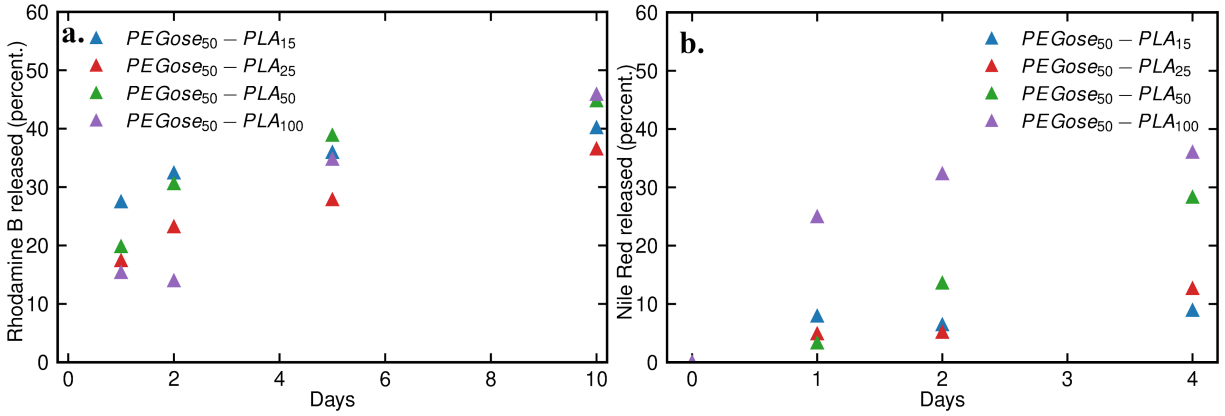

Figure 2.7: a) Amount of Rhodamine B released over 10 days measured by UV-Vis spectroscopy. **b)** Amount of Nile Red released over 4 days measured by fluorescence spectroscopy.

While the encapsulation efficiency of Rhodamine B depends on the length of the PLA chain, the release profile is similar for all block copolymers. The release profile of Nile Red, however, highly depends on the PLA chain length. PEGose$_{50}$-PLA$_{100}$ had a burst release the first day, PEGose$_{50}$-PLA$_{50}$ had a linear sustained release, PEGose$_{50}$-PLA$_{25}$ and PEGose$_{50}$-PLA$_{15}$ only released around 10% of their cargo. PEGose$_{50}$-PLA$_{50}$ nanoparticles seem like the most efficient drug carriers, with the best encapsulation efficiency of both dyes and the most sustained

release. The low leakage of $PEGose_{50}$-PLA_{25} and $PEGose_{50}$-PLA_{15} could also be promising if stimuli-responsiveness is added to the drug delivery system. The slower release of hydrophobic compounds supports the core-shell structure theory, with hydrophobic compounds in the core and hydrophilic compounds predominantly in the shell. Additional functionalisation of $PEGose_{50}$-PLA_{50} such as disulfide bonds between the two blocks could be introduced to speed up the release of hydrophobic compounds. Alternatively, poly(lactic-*co*-glycolic acid) could be used instead of PLA as a more easily degradable alternative.[172]

2.5 Cell interactions

2.5.1 Protein aggregation

One of the most important attributes of PEG in drug delivery is its so-called stealth effect. Indeed, attaching PEG chains to a drug or a nanoparticle will shield it from blood components and increase its blood circulation time. For PEGose to be a suitable alternative to PEG, it should be able to replicate this phenomenon. To evaluate PEGose capability of preventing blood components adsorption, an in vitro test was realised by incubating FITC-labelled BSA protein with PEGose-PLA nanoparticles and PLA nanoparticles for one hour at 37°C. The dispersion of FITC-BSA proteins and nanoparticles was then centrifugated at 10,000 RPM for 15 minutes to separate the nanoparticles with proteins adsorbed and the free proteins. The fluorescence intensity of the supernatant was then compared to a FITC-BSA water solution of the same concentration that was not incubated with any nanoparticles. The amount of FITC-BSA proteins that were adsorbed on the nanoparticles can then be calculated using the maximum intensity of each spectrum:

$$BSA_{adsorbed}\,(\%) = \frac{I_{reference} - I_{supernatant}}{I_{reference}} * 100 \tag{2.2}$$

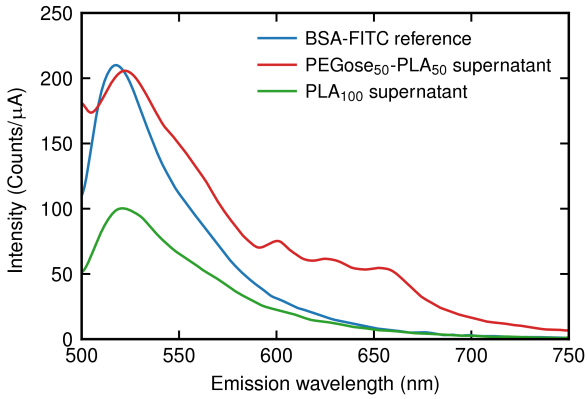

Figure 2.8: Fluorescence emission spectra of a FITC-BSA solution in water (0.02 mg/mL), incubated with $PEGose_{50}$-PLA_{50} (5 mg/mL), or incubated with PLA_{100} nanoparticles.

The experiment showed that only 2% of FITC-BSA proteins were adsorbed on PEGose-PLA nanoparticles, whereas 52% were adsorbed on PLA nanoparticles (See Figure 2.8). The absence of protein aggregation on $PEGose_{50}$-PLA_{50} nanoparticles confirms the potential of PEGose for increasing the blood circulation time of drug delivery systems. However, the presence of unexpected peaks around 600-650 nm casts doubts on the actual intensity at 520 nm, since traces of an impurity could artificially increase the fluorescein peak. Considering that PEGose is able to protect PLA from being degraded by the proteinase K enzyme, the lack of BSA protein aggregation was not unexpected.

2.5.2 Cytotoxicity

To assess the capacity of PEGose-PLA nanoparticles to be used in drug delivery, their cytotoxicity was evaluated. The cytotoxicity experiments were performed by Emmanuelle Acs in the group of Jesko Koenke. Cells from a human hepatocellular carcinoma cell line were cultured, then incubated with PEGose-PLA nanoparticles or PEGose homopolymers for 24 h at 37°C. AlamarBlue™ Cell Viability Reagent was then added as a cell health indicator. The fluorescence of cells incubated with nanoparticles or homopolymers were compared to a control without polymer to obtain a cell viability percentage (See Figure 2.9). Given that PEG and amylose are biocompatible, it was expected that PEGose, which shares a similar structure, would be nontoxic to cells. In vitro cytotoxicity assays confirmed this hypothesis. Even with the highest concentration of 500 µg/mL the cell viability remained above 80% for PEGose and the nanoparticles. Interestingly, the cell viability with PEGose-PLA nanoparticles was higher than the PEGose homopolymer for the highest concentration tested. The PEGose-PLA block copolymer was synthesised through the osmium dihydroxylation route, but the very low amount of OsO_4 used and the intensive dialysis steps seemed to have prevented any undesirable cytotoxicity. The cell viability when using the PEGose homopolymer decreased when increasing the concentration from 50 µg/mL to 500 µg/mL while the standard deviation considerably increased. Synthesising the PEGose homopolymer through the osmium-free pathway did not seem to avert the drop in cell viability (See Figure 2.9).

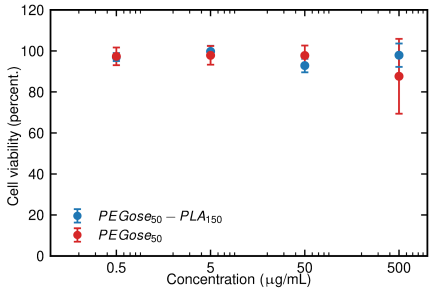

Figure 2.9: Human hepatocellular carcinoma cell viability after incubation with osmium-free $PEGose_{50}$ or $PEGose_{50}$-PLA_{150} nanoparticles prepared using an OsO_4 dihydroxylation with a concentration of 0.5, 5, 50 or 500 µg/mL in a humidified incubator at 37°C under 5% CO_2.

2.5.3 Cell permeability

To further explore the potential of PEGose-PLA nanoparticles as drug delivery systems, their cell permeability was studied. Fluorescein isothiocyanate (FITC) was chosen as a fluorescent label to react with PEGose hydroxyl groups (the reaction to covalently attach the label was performed before the preparation of nanoparticles). A calibration curve with different solutions of FITC was prepared to determine the degree of substitution of the PEGose chains by fluorescence spectroscopy (See Figure 2.10). The degree of substitution was very low (d.s. ≈ 0.0005 FITC units per PEGose repeating unit), so roughly 2.5% of $PEGose_{50}$ chains had a FITC tag (d.s. multiplied by the the number of repeating units), which suggests that the modification of the polymer structure was small enough to not affect the polymer cell permeability properties.

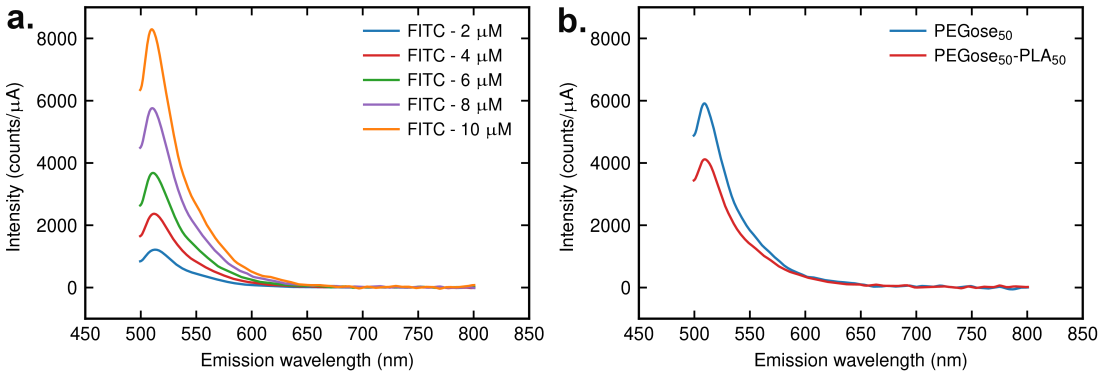

Figure 2.10: a) Fluorescence trace of FITC solutions in a Tris buffer with concentration ranging from 2 μM to 10 μM. **b)** Fluorescence trace of FITC-labelled $PEGose_{50}$ and $PEGose_{50}$-PLA_{50}.

After being incubated for 24 h at 37°C, the cells from human hepatocellular carcinoma cell line and the polymers were observed under a confocal microscope under two different channels: one to inspect the fluorescence from the homopolymers or nanoparticles, and the other one to obtain bright-field images of the cells. Merging the images from the two channels shows that the fluorescent spots from the PEGose homopolymer and PEGose-PLA nanoparticles superimposed with the cells observed through the bright field channel (See Figure 2.11). These results indicate that both the homopolymer and the nanoparticles were either able to penetrate the cell membrane or to attach themselves to the cell surface. An additional experiment with nuclear staining could confirm that the nanoparticles seem to accumulate in the nucleus. The negligible cytotoxicity of the nanoparticles as well as their capability to cross the cell membrane exhibit their potential for intracellular drug delivery and further studies in the future.

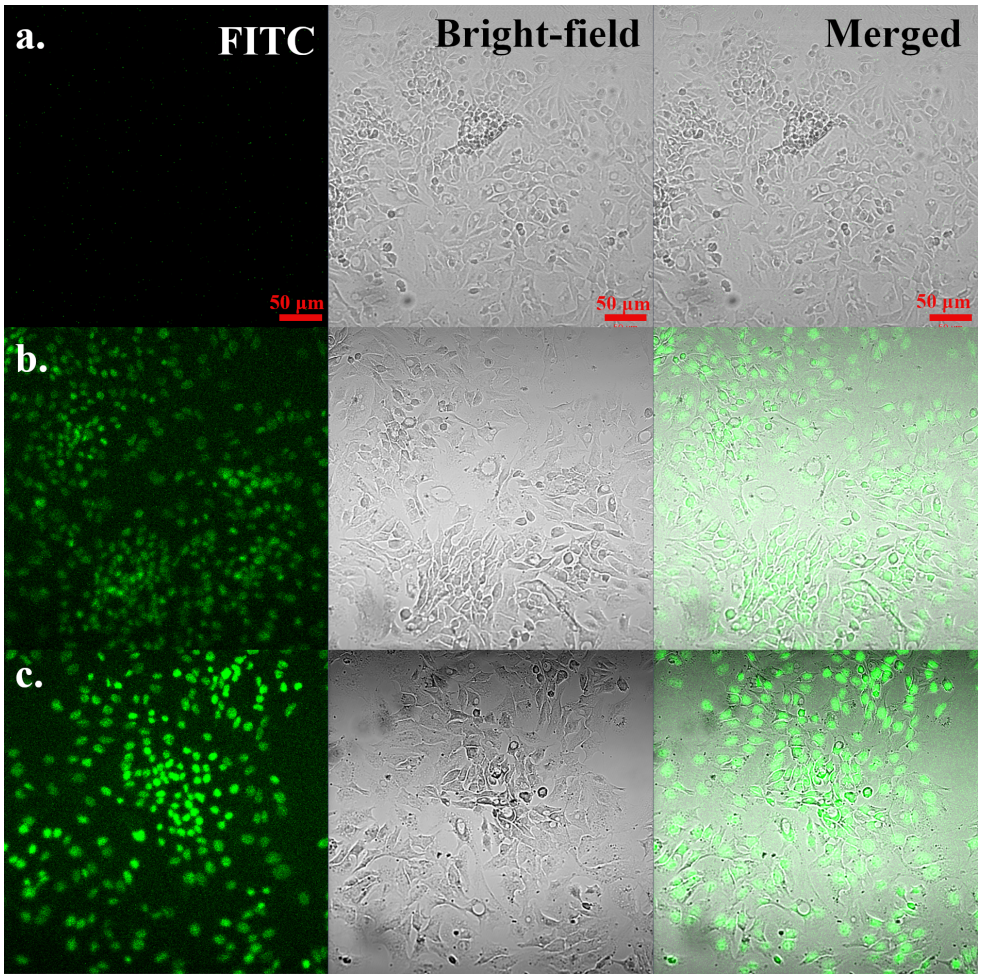

Figure 2.11: Confocal microscope images of **a)** control (cells incubated without any polymer), **b)** cells incubated with PEGose homopolymer and **c)** cells incubated with $PEGose_{50}$-PLA_{50} nanoparticles. For each sample, the fluorescence, bright-field and merged images are shown. Human hepatocellular carcinoma cells ($2{\cdot}10^4$ cells per well) were incubated at 37°C in a 5% CO_2 atmosphere for 24 h, with a polymer or nanoparticle concentration of 50 µg/mL. The images were obtained with the help of Emmanuelle Acs, Alexander Plucinski and Jesko Koehnke.

2.6 Conclusion

PEGose, a polymer that shares structural similarities with amylose and PEG, has been used to form a novel diblock copolymer with PLA. The polymer self-assembled into nanoparticles that were capable of encapsulating both hydrophilic and hydrophobic dyes. The low cytotoxicity, high cell permeability, and high stability of these drug carriers could lead to an efficient cargo delivery in previously problematic harsh environments, such as the gastrointestinal tract. While additional in vivo biological tests need to be realised, the nanoparticles developed herein appear as a potential alternative to PEG-based drug delivery systems (See Figure 2.12). This work might become increasingly relevant as adverse effects of PEG are more and more observed.

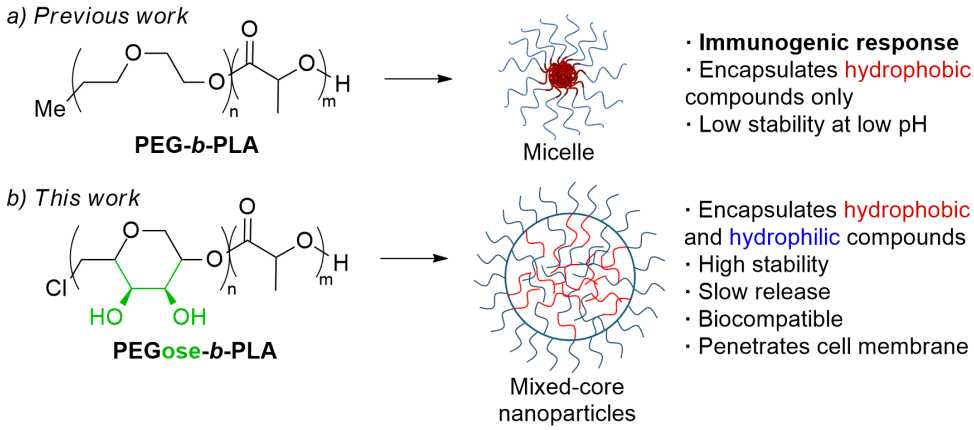

Figure 2.12: Comparison of PEG-*b*-PLA and PEGose-*b*-PLA structures and their self-assemblies (hypothesised morphology in the case of PEGose-*b*-PLA).

Chapter 3

Self-assembly of i-PEGose-*b*-PLA into polymeric microcubes

3.1 Introduction

It has been mentioned in Chapter 1 of this thesis that by using amphiphilic block copolymers with longer hydrophobic chains, a transition from micelles to worms then vesicles could be obtained.[13] By using star polymers with multiple hydrophobic arms, the critical packing parameter can be even more increased and cubosomes can be observed.[173] To obtain a negative mean curvature between the hydrophilic and the hydrophobic part, we hypothesised that instead of increasing the hydrophobic volume we could decrease the hydrophilic volume. To obtain a block copolymer with a reduced hydrophilic volume, the goal was to once again use PEGose-*b*-PLA block copolymers but with an isotactic PEGose block. We assumed that because of the rigid polycyclic structure and helicity of PEGose, we would obtain more complex nanoparticle morphologies compared to PEG-*b*-PLA systems where PEG is highly flexible.

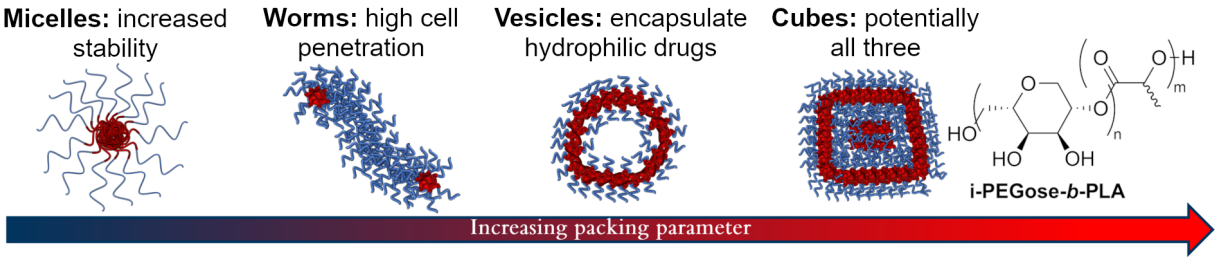

Figure 3.1: Schematic representation of different nanoparticle morphologies in relation to their packing parameter.

3.2 Synthesis of the block copolymers

The synthesis of the block copolymers used to prepare anisotropic nanoparticles closely resembles the general scheme applied in Chapter 2 to synthesise atactic PEGose-PLA block copolymers. The main new step is the Jacobsen hydrolytic kinetic resolution of racemic butadiene monoxide to give enantiopure butadiene monoxide. This enantiopure monomer is then polymerised to obtain isotactic poly(epoxybutene) (PEB). The ring-closing metathesis of PEB preserved the isotacticity of the polymer and gave an isotactic polycycloether (PCE). Another difference with the previous chapter is that the tacticity of the poly(lactic acid) (PLA) block was also investigated. For this reason, i-PCE was used as a macroiniator for the polymerisation of DL-lactide and L-lactide. The resulting i-PCE-*b*-PLA was then subjected to a dihydroxylation to obtain i-PEGose-*b*-PLA (See Figure 3.2).

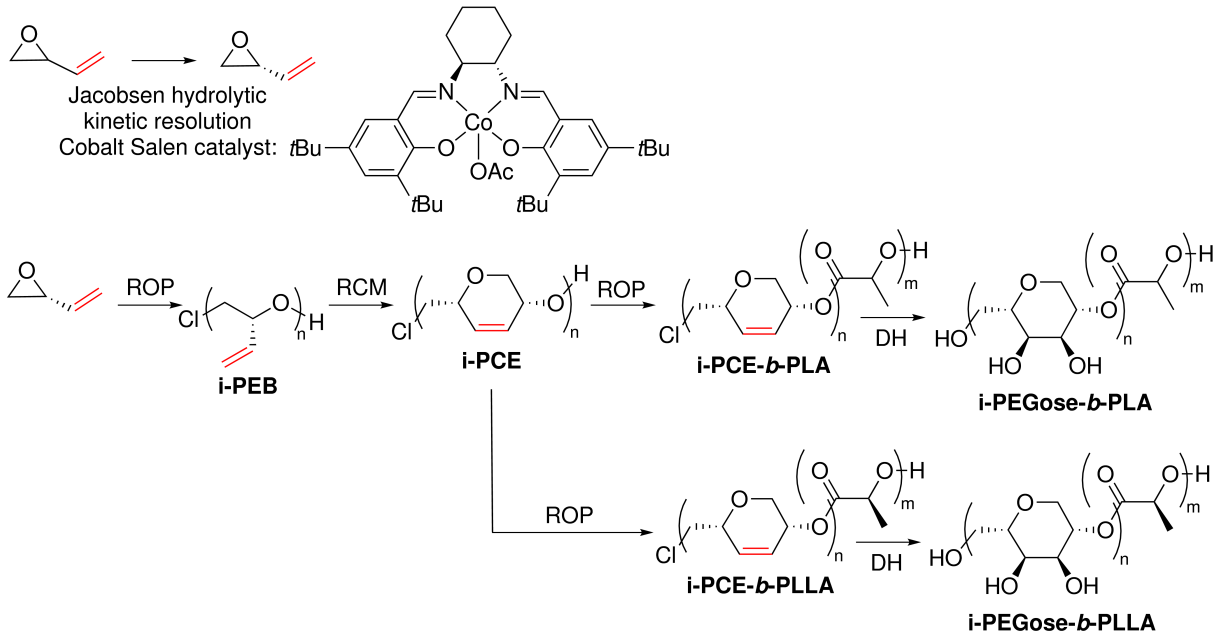

Figure 3.2: Scheme for the synthesis of i-PEGose-*b*-PLA. Conditions used were the same as for Chapter 2

The obtention of enantiopure butadiene monoxide was previously reported in the Prunet group by Alkattan et al.[74] The reported enantiomeric excess (ee) was measured via the chiral HPLC analysis of the 2-naphthylsulfide derivative. This derivative was obtained through the ring-opening of the enantiopure butadiene monoxide with 2-naphtalenethiol. Analysis of the two enantiomer peaks showed a 95% ee. In the case of the synthesis of i-PEGose-*b*-PLA block copolymers, the success of the kinetic hydrolytic resolution of butadiene monoxide was assessed by measuring the specific optical rotation of the enantiopure monomer. The optical rotation was found in good agreement with values reported in the literature (See Chapter 7.5).[26] The monomer was then used to obtain i-PEB. The tacticity of isotactic poly(epoxy butene) was also confirmed using ^{13}C NMR (See Figure 3.3), as the spectrum for atactic PEB shows two peaks

at 81 ppm whereas the spectrum for isotactic PEB only shows a single peak (See Figure 3.3).

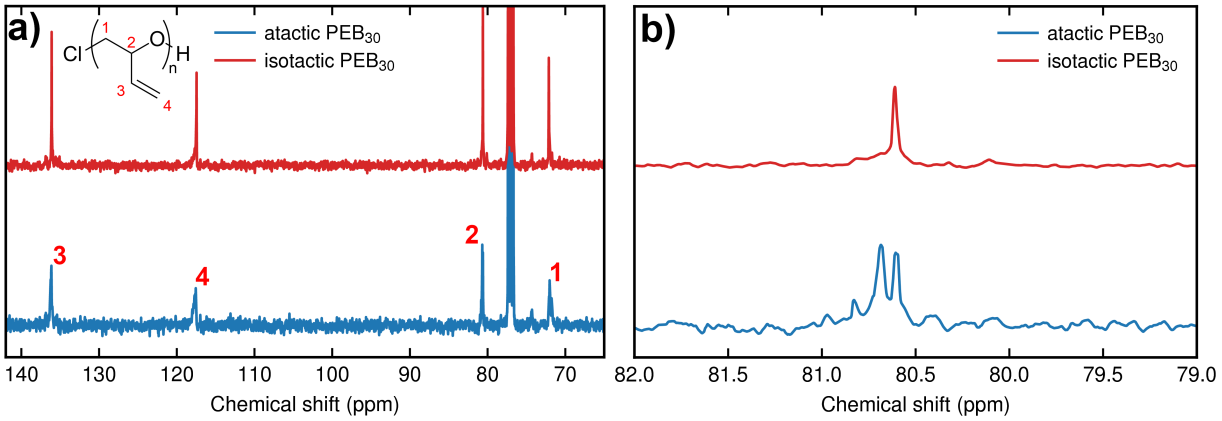

Figure 3.3: ^{13}C NMR of atactic PEB_{30} and isotactic PEB_{30} in $CDCl_3$. **a)** Shows the full spectrum while **b)** focuses on PEB stereogenic carbon.

The isotactic PEB was subjected to a ring-closing metathesis to furnish an isotactic polycycloether (PCE). Both i-PEB and i-PCE were analysed using NMR (See Figure 7.8), SEC (See Figure 3.4) and circular dichroism spectroscopy.

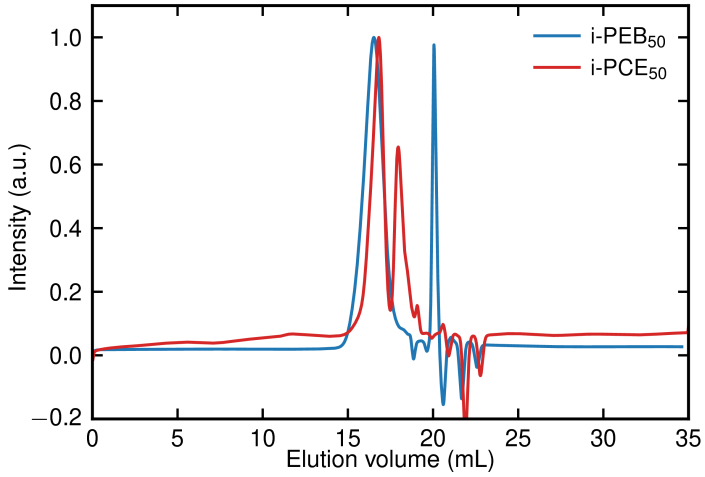

Figure 3.4: SEC traces of i-PEB_{50} and i-PCE_{50} measured in THF with a 1 mL/min flow rate.

The circular dichroism spectrum of i-PEB showed a flat baseline, indicating the absence of any chiral secondary structures. Atactic PCE also showed a flat baseline. However, the circular dichroism spectrum of i-PCE showed a peak at 198 nm, indicating a positive Cotton effect (the optical rotation first increases as the wavelength decreases) hinting towards a helical structure (See Figure 3.5).

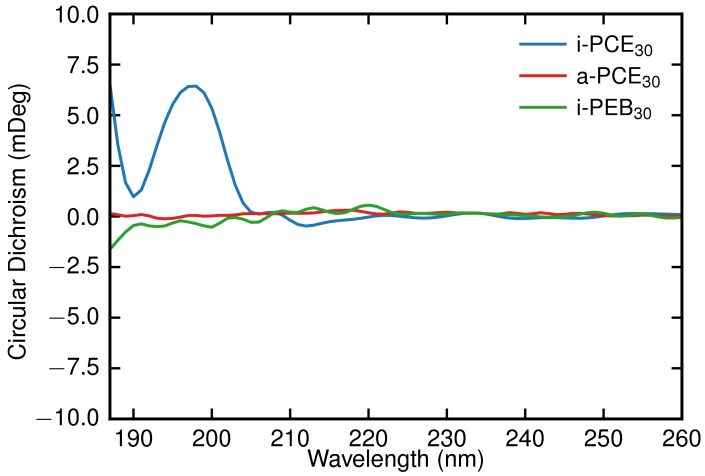

Figure 3.5: Circular dichroism spectra of i-PCE_{30}, a-PCE_{30} and i-PEB_{30} as a 0.1 mg/mL solution in methanol.

In conclusion, the optical rotation, ^{13}C NMR and circular dichroism results all validate the isotactic structure of the synthesised polycycloether. The isotactic polycycloether was then used as a macroinitiator for the ring-opening polymerisation of commercially available DL-lactide to obtain i-$PEGose_{50}$-PLA_{50}. L-lactide was used to obtain i-$PEGose_{50}$-$PLLA_{50}$ (See Figure 3.2). Atactic PCE was also synthesised to further obtain a-$PEGose_{50}$-PLA_{50} and a-$PEGose_{50}$-$PLLA_{500}$. Two issues arised when using an isotactic PCE for the ring-opening polymerisation of DL-lactide. Firstly, PLA homopolymers impurities were obtained, likely due to traces of water from the monomer or air in the reaction mixture. These homopolymers were removed after the dihydroxylation reaction, leading to a lower NMR integration of the PLA peaks after the dihydroxylation compared to after the ring-closing metathesis (See Figure 7.13). Secondly, full conversion was harder to achieve using an isotactic PCE leading to traces of PCE in one of the i-$PEGose_{50}$-PLA_{50} block copolymers (See Figure 7.13d). Additionally, using PLLA as a hydrophobic block, the block copolymers were dispersible but insoluble in DMSO, leading to poor NMR spectra (See Figure 7.10c and 7.10d). The size of the PLLA block was then determined using the NMR spectrum of the PCE-PLLA precursor, via the relative integration of the PCE and PLLA blocks (See Figure 7.10).

3.3 Self-assembly of the block copolymers

3.3.1 Self-assembly in deionised water

First, a block copolymer that contained an isotactic PEGose block was used with the same goal as for the previous chapter: cargo delivery. The objective was to study the influence of PEGose tacticity as part of a block copolymer. For this reason, i-$PEGose_{50}$-*b*-PLA_{50} was synthesised. Nanoparticles were prepared and characterised by transmission electron microscopy (TEM) and

dynamic light scattering (DLS). DLS indicated that the nanoparticles formed using an isotactic PEGose block had a slightly increased size compared to their atactic counter part (See Table 3.1). Moreover, images obtained from TEM also showed nanoparticles of similar size and morphology (See Figure 3.6).

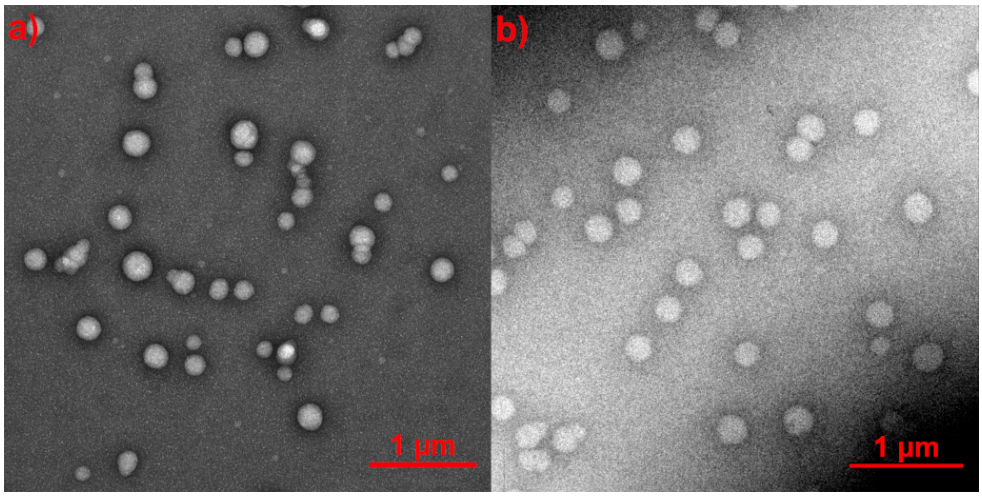

Figure 3.6: Transmission electron microscopy images of unstained **a)** i-PEGose$_{50}$-PLA$_{50}$ and **b)** a-PEGose$_{50}$-PLA$_{50}$ in deionised water. Scale bars represent 1 µm. See Figure 7.14 for the corresponding size analyses.

Table 3.1: Hydrodynamic size of PEGose-*b*-PLA self-assemblies in deionised water, measured by dynamic light scattering at an angle of 175°.

Block copolymer	Hydrodynamic size (nm)
a-PEGose$_{50}$-PLA$_{50}$	169
i-PEGose$_{50}$-PLA$_{50}$	226

While the tacticity of the PEGose block did not have an important influence on the size and morphology of the nanoparticles produced, it could still impact the encapsulation efficiency of hydrophobic or hydrophilic cargo. i-PEGose$_{50}$-*b*-PLA$_{50}$ have then been used to encapsulate a hydrophilic and hydrophobic dye: Rhodamine B and Nile Red respectively. Unfortunately, the encapsulation efficiency of the block copolymer containing an isotactic PEGose block was lower than that of the atactic counterpart (See Table 3.2).

Table 3.2: Encapsulation efficiency of Rhodamine B and Nile Red for atactic and isotactic PEGose-PLA block copolymers, determined by UV-vis and fluorescence spectroscopy.

Polymer	Rhodamine B encapsulation	Nile Red encapsulation
a-PEGose$_{50}$-PLA$_{50}$	43 %	25 %
i-PEGose$_{50}$-PLA$_{50}$	28 %	11 %

While these results did not seem to encourage the use an isotactic PEGose block over an atactic one, the biocompatibility and cellular uptake of the isotactic PEGose homopolymer and the i-PEGose-PLA block copolymer was still assessed (See Figure 3.8 and 3.7).

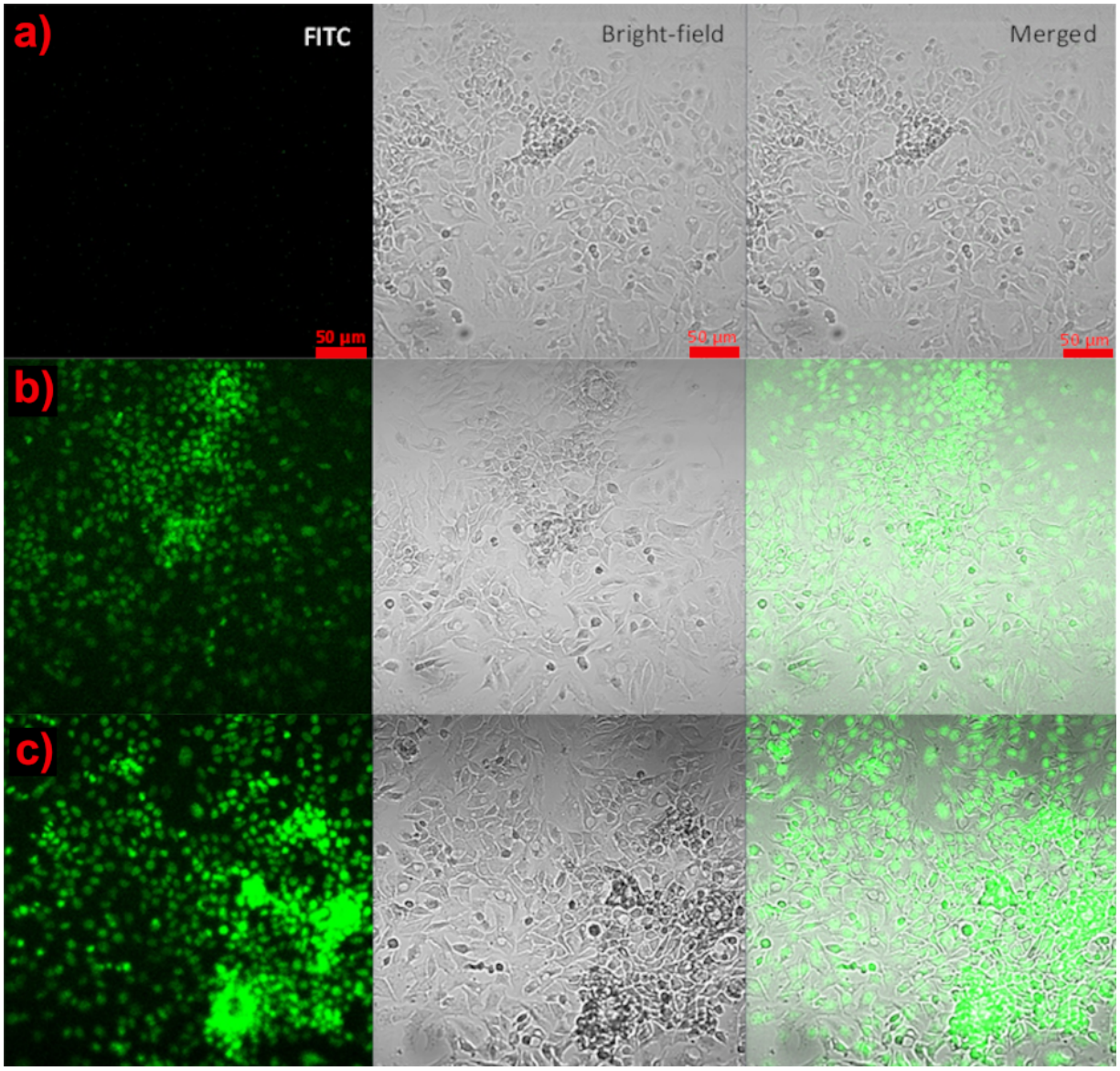

Figure 3.7: Confocal microscope images of **a)** control (cells incubated without any polymer), **b)** cells incubated with isotactic $PEGose_{50}$-*b*-PLA_{50} nanoparticles and **c)** cells incubated with isotactic $PEGose_{50}$ homopolymer. For each sample, the fluorescence, bright-field and merged images are shown. Human hepatocellular carcinoma cells ($2{\cdot}10^4$ cells per well) were incubated at 37°C in a 5% CO_2 atmosphere for 24 h, with a polymer or nanoparticle concentration of 50 µg/mL.

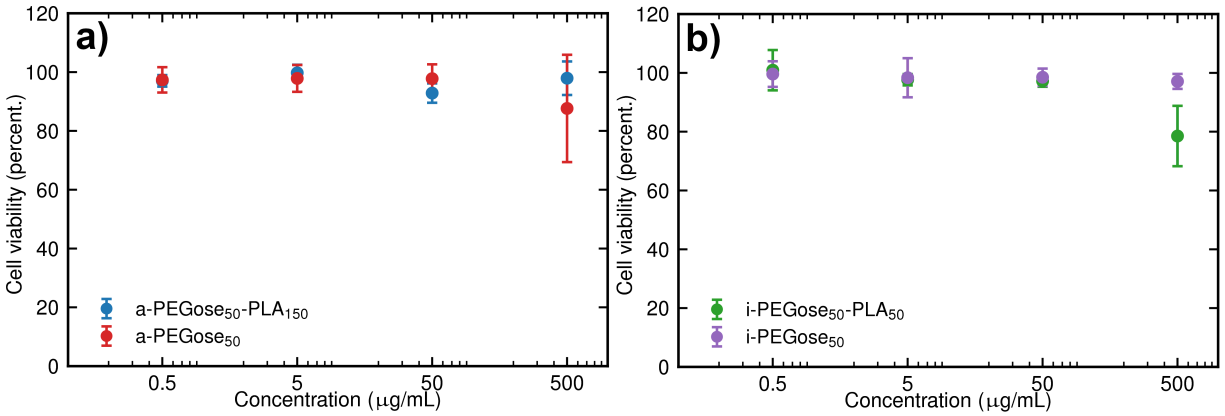

Figure 3.8: Human hepatocellular carcinoma cell viability after incubation with **a)** a-PEGose$_{50}$ or a-PEGose$_{50}$-PLA$_{150}$ nanoparticles or **b)** i-PEGose$_{50}$, i-PEGose$_{50}$-PLA$_{50}$ nanoparticles with a concentration of 0.5, 5, 50 or 500 µg/mL in a humidified incubator at 37°C under 5% CO_2. The images were obtained with the help of Emmanuelle Acs, Alexander Plucinski and Jesko Koehnke.

The number of cells alive was close to 100% for both atactic and isotactic homopolymers and nanoparticles up to a concentration of 50 µg/mL. Usually, a polymer will be considered biocompatible if the cell viability is above 80%. The cell viability only decreases at a concentration of 500 µg/mL for the i-PEGose$_{50}$-*b*-PLA$_{50}$ nanoparticles but this very high concentration will likely never occur in a drug delivery context. Isotactic PEGose and i-PEGose$_{50}$-*b*-PLA$_{50}$ were stained using fluorescein isothiocyanate (FITC) and incubated with cells to assess their cellular uptake. By superimposing the FITC channel and the bright field image, it becomes apparent that both PEGose homopolymers and nanoparticles are accumulating in cells or on the cell surface. This means that both the polymer and the nanoparticles could cross the cell membrane and can potentially partake in intracellular drug delivery. However, these results obtained with isotactic PEGose do not differ significantly from the atactic PEGose results, and do not particularly warrant the use of isotactic PEGose for this application, considering the extra step needed to synthesise the isotactic polymer.

3.3.2 Self-assembly in a sodium chloride solution

In deionised water, the block copolymer composed of an isotactic PEGose block had similar properties to the atactic counterpart. However, in a sodium chloride solution, new nanoparticle morphologies could be obtained. Such behaviour was first observed when evaluating the stability of nanoparticles in different buffers. It was noticed that using a 100 mg/mL sodium chloride solution the size of the nanoparticles increased. More interestingly, the correlation function obtained from the intensity trace could not be fitted into a single exponential decay function (See Figure 3.9).

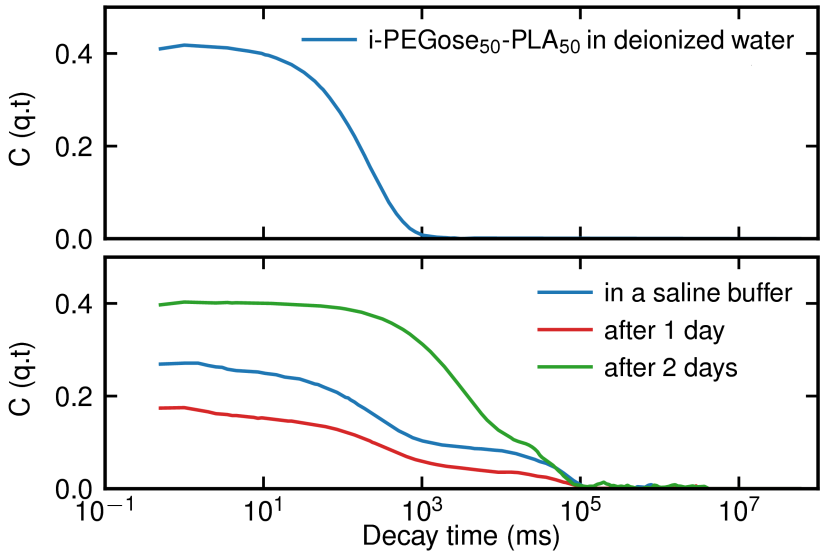

Figure 3.9: Correlation function obtained from the DLS intensity trace of i-PEGose$_{50}$-*b*-PLA$_{50}$ nanoparticles in water and in a 100 mg/mL sodium chloride solution.

Therefore, Stokes law cannot be used to obtain the particle size because the nanoparticles are not spherical. This was the first time that non-spherical nanoparticles were obtained using a PEGose-*b*-PLA system. To confirm this first observation, TEM was used to compare nanoparticles made from a-PEGose$_{50}$-PLA$_{50}$ and i-PEGose$_{50}$-PLA$_{50}$ nanoparticles in deionized water and in a 100 mg/mL sodium chloride solution (See Figure 3.10).

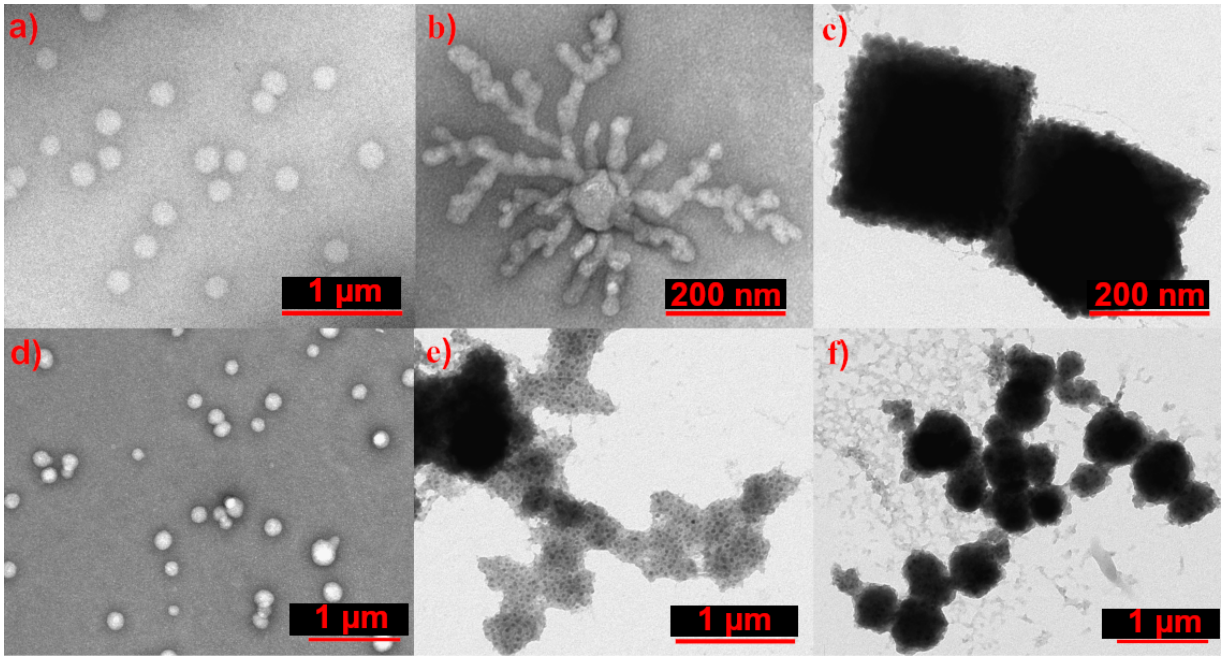

Figure 3.10: Unstained TEM images of isotactic **(a, b, c)** and atactic **(d, e, f)** PEGose$_{50}$-PLA$_{50}$ in deionised water **(a, d)** or a 100 mg/mL NaCl solution after 1 hour **(b, e)** or 3 days **(c, f)**. See Figure 7.17 for additional TEM images.

The TEM images indicate that the saline buffer had an influence on both a-PEGose$_{50}$-*b*-PLA$_{50}$ and i-PEGose$_{50}$-*b*-PLA$_{50}$ nanoparticles, but that it led to different morphologies depending on the tacticity of PEGose block. Nanoparticles made from an atactic PEGose block started forming aggregates when added to the NaCl solution. The high contrast spots could indicate two different phases: a PEGose-rich phase and a PLA-rich phase. After 3 days, spherical nanoparticles were obtained with a different aspect than the ones formed in deionised water, with seemingly more compartmentalised cores. The nanoparticles composed of an isotactic PEGose block formed 'octopus-like' nanoparticles 1 hour after being added to a NaCl solution. It should be noted that the similarity to a lightning strike could be an artefact resulting from the high-voltage used by the TEM electron beam. Nevertheless, after 3 days, cube-shaped nanoparticles with an uneven surface could be obtained. To further confirm the influence of sodium chloride on PEGose conformation, circular dichroism experiments were performed on i-PEGose$_{50}$ in deionised water and a sodium chloride solution. The wavelength shift of PEGose Cotton effect confirmed that the helicity of the polymer is indeed impacted by the salinity of the buffer, potentially due to salting out effects (See Figure 3.11).

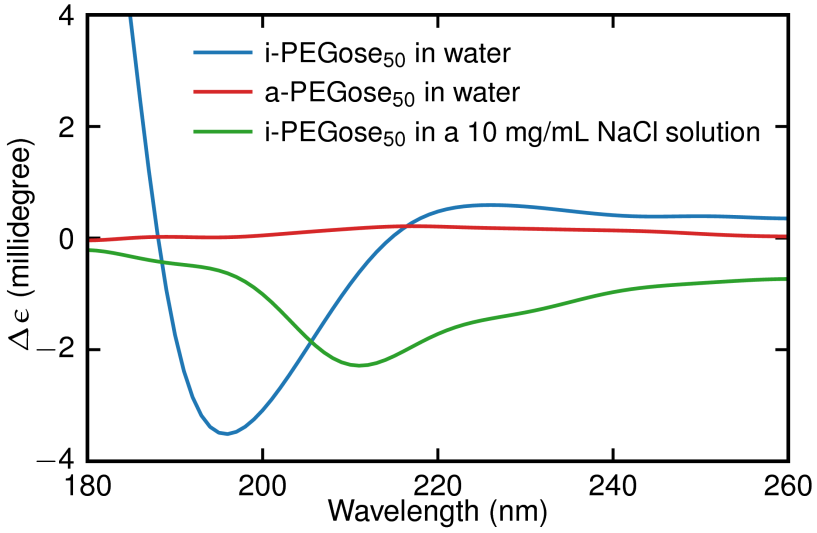

Figure 3.11: Circular dichroism spectrum of a-PEGose$_{50}$ and i-PEGose$_{50}$ in deionised water and i-PEGose$_{50}$ in a 10 mg/mL sodium chloride solution.

3.3.3 Influence of the nanoparticle preparation method

After witnessing the formation of cube-shaped polymeric particles in a saline buffer, the objective was to reproduce these results and find out which parameters can affect this phenomenon. It was then decided to study if preparing the nanoparticles in deionised water then adding solid sodium chloride would produce similar results to preparing the nanoparticles directly in a sodium chloride solution. Moreover, the influence of the salt concentration and the polymer concentration was also considered (See Figure 3.13). The order of addition of sodium chlo-

ride did not seem to have a drastic influence on the morphology of the nanoparticles, meaning that cube-shaped nanoparticles were obtained in both cases. However, adding sodium chloride after preparing the nanoparticles in deionised water first produced a more homogeneous population of nanoparticles, with a roughly five times smaller size (See Figure 3.12). Using a solution with a smaller polymer concentration (from 10 mg/mL to 1.0 mg/mL) yielded homogeneous cube-shaped nanoparticles, with the only noticeable difference being a smaller number of nanoparticles (See Figure 3.13a and 3.13b). Decreasing the salt concentration from 100 mg/mL to 10 mg/mL while keeping the polymer concentration at 10 mg/mL led to a less homogeneous population of nanoparticles, with some spherical aggregates that could be observed (See Figure 3.13a and 3.13c).

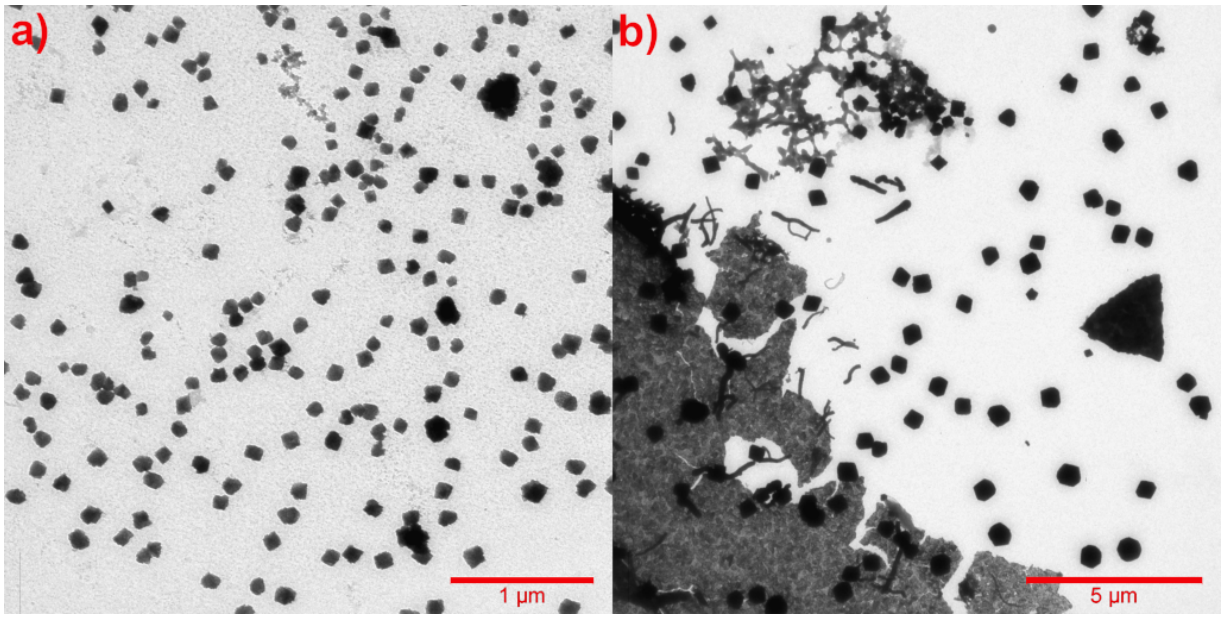

Figure 3.12: TEM images of i-PEGose$_{50}$-*b*-PLA$_{50}$ nanoparticles prepared in **a)** deionised water then salt was added to make a 100 mg/mL solution (1 µm scale bar). TEM images of nanoparticles prepared in **b)** a 100 mg/mL sodium chloride solution (5 µm scale bar). See Figure 7.15 for the corresponding size analysis.

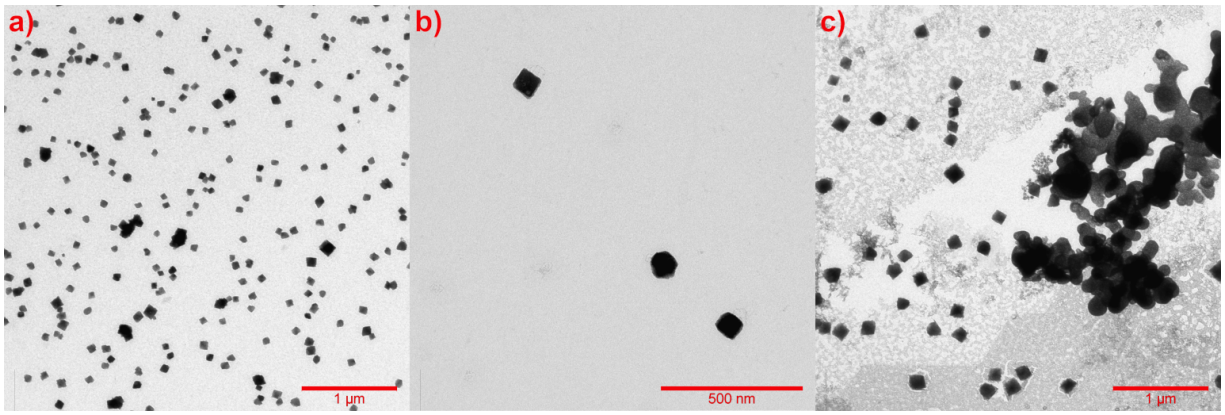

Figure 3.13: TEM images of i-PEGose$_{50}$-*b*-PLA$_{50}$ nanoparticles in **a)** a 100 mg/mL NaCl solution at a 10 mg/mL polymer concentration, **b)** a 100 mg/mL NaCl solution at a 1 mg/mL polymer concentration, **c)** a 10 mg/mL NaCl solution at a 10 mg/mL polymer concentration. See Figure 7.18 for additional TEM images.

3.3.4 Elemental analysis

As the morphology of the nanoparticles in solution and after drying on the TEM grid might be different, investigation was undertaken to determine if the cube-shaped particles could be some residual salt crystals. The TEM instrument used is not equipped with an energy-dispersive X-ray spectroscopy (EDX) system, scanning electron microscopy (SEM) was then used. The first scanning electron microscope used did not have a sufficient resolution to confirm the morphology of the nanoparticles produced but the EDX system confirmed that the sample was more than 95% organic (See Figure 3.14).

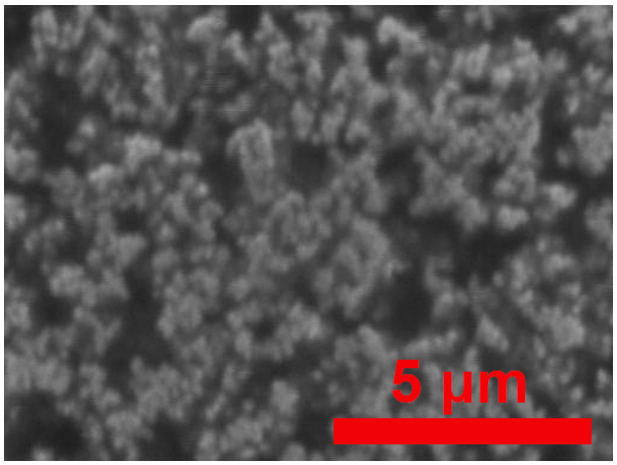

Element	Wt%
C	83.2
O	12.1
Na	2.1
Cl	1.4
S	0.5
Os	0.5
Ca	0.1

Figure 3.14: Scanning electron microscopy images of a drop of a 10 mg/mL i-PEGose$_{50}$-*b*-PLA$_{50}$ solution in a 100 mg/mL NaCl solution, further washed by deionised water then dried again. Table indicating the relative weight of each element in the imaged sample.

Additional imaging was then performed on a SEM allowing for a higher resolution. While TEM mostly showed images of cube-shaped nanoparticles, SEM also showed sherical particles

and sheet-like structures (See Figure 3.15). These results could be explained by the drying rate of the sample droplet. Indeed, Waymouth and coworkers reported that a triblock copolymer containing a central PEG block and terminal poly(trimethylene carbonate/dithiolane) (PTM-CDT) blocks could form cube-shaped nanoparticles but only if dried in a vacuum dessicator (100 mbar), as opposed to a slower air drying.[174]

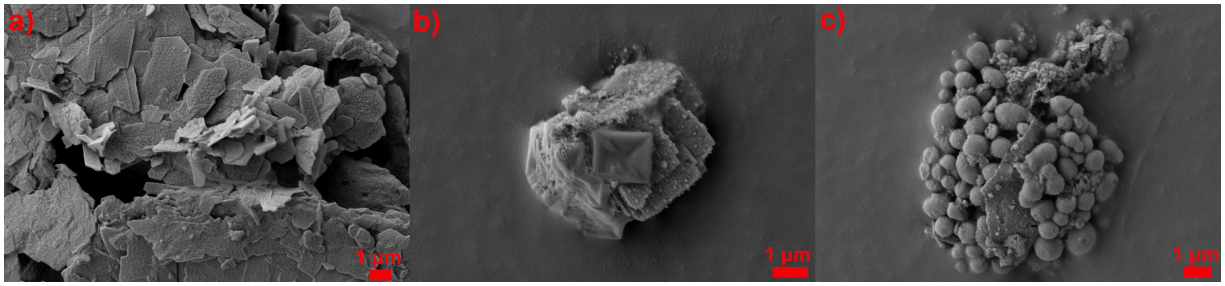

Figure 3.15: Scanning electron microscopy images of a drop of a 10 mg/mL i-PEGose$_{50}$-*b*-PLA$_{50}$ solution in a 100 mg/mL NaCl solution, further washed by deionised water then dried again slowly under atmospheric pressure. Morphologies that can be observed are **a)** sheet-like porous structures, **b)** aggregated cubes or **c)** aggregated spherical particles. All scale bars are 1 µm

3.3.5 Influence of the nature of the salt

After studying the influence of the salt addition order, the salt concentration and the polymer concentration, the influence of the nature of the salt was studied. A phosphate-buffered saline (PBS) was used as well as potassium chloride (KCl) to change the nature of the cation or the anion. The size of i-PEGose$_{50}$-*b*-PLA$_{50}$ self-assemblies in deionised water were compared to the nanoparticles obtained in a PBS buffer by DLS. A single exponential decay was obtained for the DLS correlation function, indicating a single population of spherical nanoparticles. The size roughly tripled from 113 nm for nanoparticles in deionised water to 297 nm for nanoparticles in a PBS buffer. The dispersity also increased when a PBS buffer was used (See Figure 3.16). TEM confirmed the results obtained from MADLS, showing bigger spherical aggregates when a PBS buffer was used (See Figure 3.17a). Surprisingly, no cube-shaped nanoparticles could be obtained when potassium chloride was used instead of sodium chloride (See Figure 3.17b). The nature of the salt thus plays a major role for the obtention of cube-shaped nanoparticles; more salts could be tested like lithium chloride (smaller cation), sodium fluoride (smaller anion) or sodium bromide (larger anion).

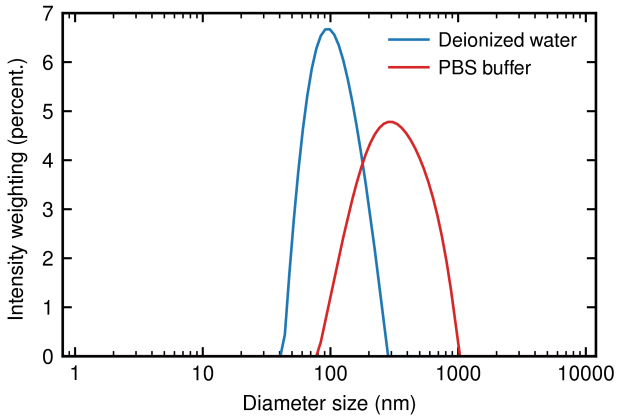

Figure 3.16: DLS size distribution of i-PEGose$_{50}$-*b*-PLA$_{50}$ nanoparticles prepared in deionised water and a PBS buffer. Measured with a 175° angle using intensity weighting.

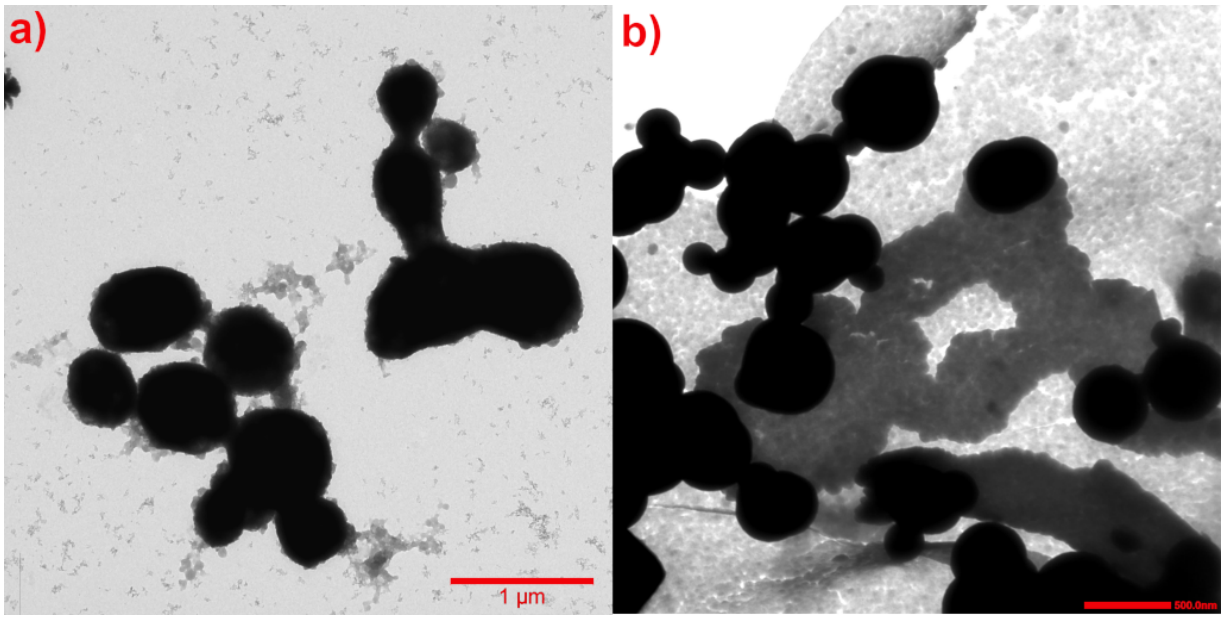

Figure 3.17: TEM images of nanoparticles obtained from the self-assembly of i-PEGose$_{50}$-*b*-PLA$_{50}$ in **a)** a PBS buffer (1 µm scale bar) and **b)** a 100 mg/mL KCl solution (500 nm scale bar).

3.3.6 Influence of the dihydroxylation conversion

It has been mentioned previously that the dihydroxylation of the isotactic PCE was harder to achieve than for the atactic counterpart. For this reason, i-PEGose$_{50}$-*b*-PLA$_{50}$ with still 15% of PCE units was once obtained (See Figure 7.13d). The block copolymer self-assemblies in a saline buffer were imaged by TEM: only spheres or spherical aggregate/network could be seen (See Figure 3.18) confirming the necessity of a fully converted PEGose chain to obtain cube-shaped nanoparticles.

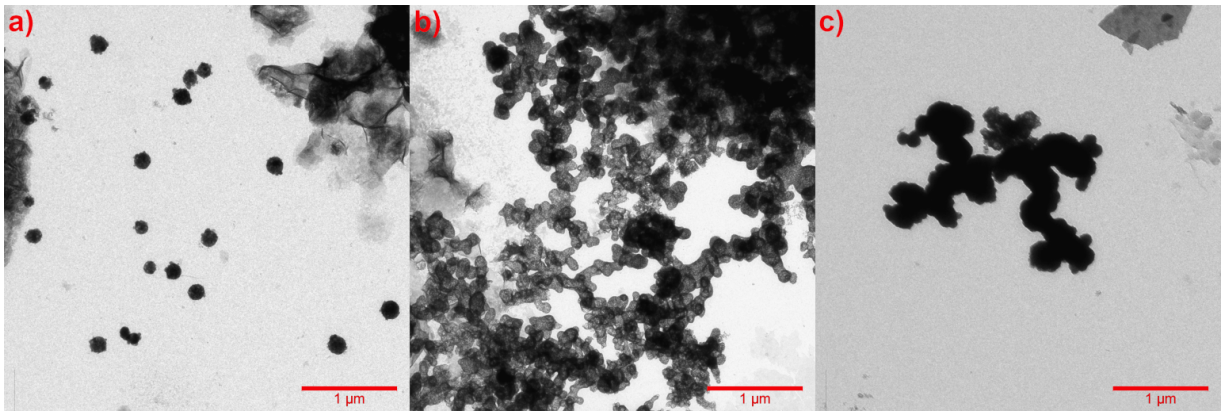

Figure 3.18: TEM images of a 10 mg/mL 85% converted i-PEGose$_{50}$-*b*-PLA$_{50}$ solution in a 100 mg/mL NaCl solution showing **a)** spherical particles, **b)** a worm network, **c)** an aggregate of spherical particles. All scale bars represent 1 µm.

3.3.7 Influence of PLA tacticity

Next, i-PEGose$_{50}$-*b*-PLLA$_{50}$ was synthesised to study the influence of the tacticity of the PLA block. Interestingly, anisotropic nanoparticles could still be obtained but they differed from the nanoparticles obtained with i-PEGose$_{50}$-*b*-PLA$_{50}$. Indeed, cubes could be observed but also hexagon-shaped or multicompartmentalised nanoparticles (See Figure 3.19). Finally, a-PEGose$_{50}$-*b*-PLLA$_{500}$ was synthesised to see if having only an isotactic PLA but an atactic PEGose block could result in anisotropic nanoparticles. The longer PLLA block prevents a direct comparison of the two block copolymer but TEM indicated that for a-PEGose$_{50}$-*b*-PLLA$_{500}$ no particles could be observed except for disordered aggregates (See Figure 3.20).

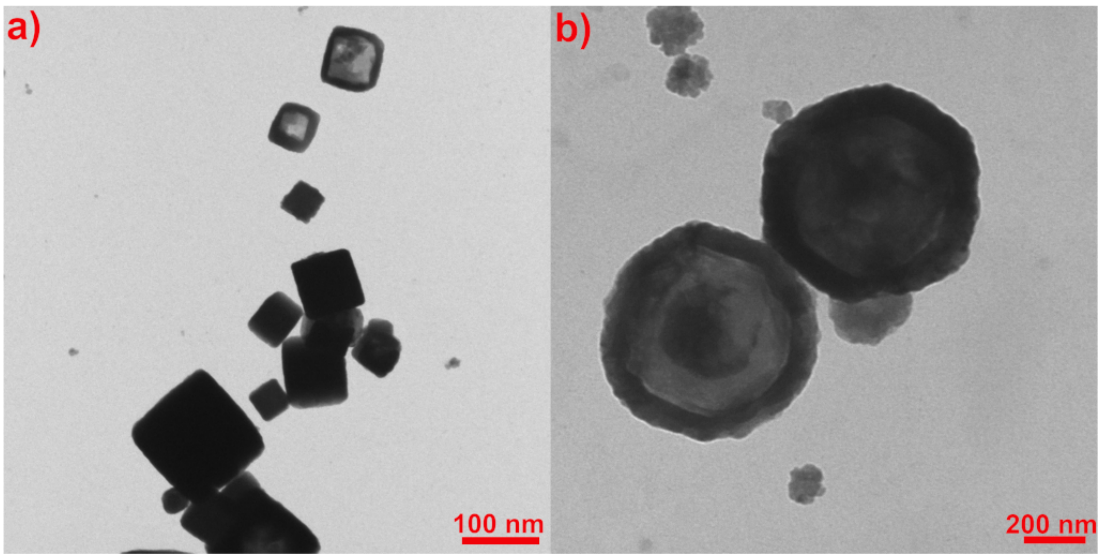

Figure 3.19: TEM images of a 10 mg/mL i-PEGose$_{50}$-*b*-PLLA$_{50}$ solution in a 100 mg/mL NaCl solution showing **a)** cube-shaped and hollow cube-shaped particles (100 nm scale bar) and **b)** hollow hexagonal particles (200 nm scale bar).

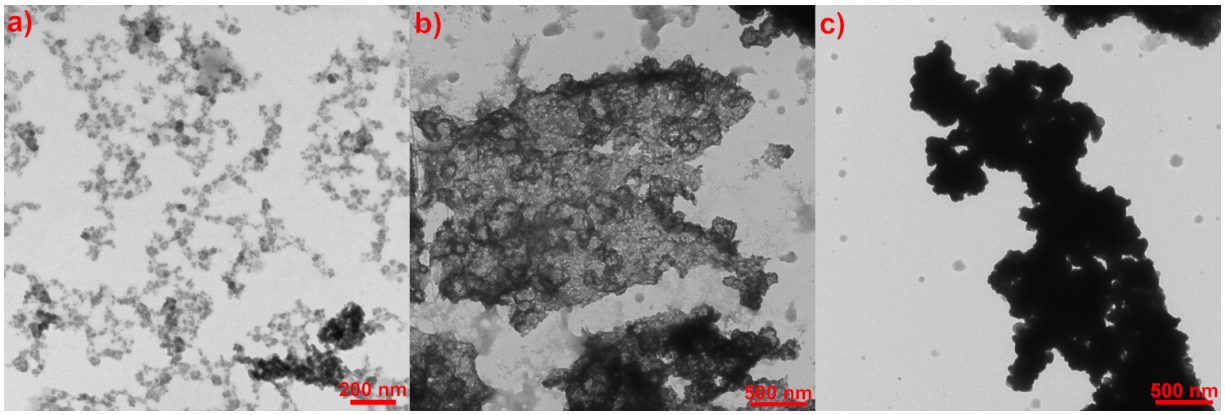

Figure 3.20: TEM images of a 10 mg/mL a-PEGose$_{50}$-*b*-PLLA$_{500}$ solution in a 100 mg/mL NaCl solution showing various disordered aggregate structures. The scale bar represents **a)** 200 nm or **b)** and **c)** 500 nm.

3.3.8 Stability of the particles toward salt removal

To be used in biomedical applications, nanoparticles have to be stable in buffers traditionally used for these types of applications. For this reason, we wanted to investigate the stability of the cube-shaped particles formed towards salt removal. We established that sodium chloride was needed to form the particles but it was still unknown if forming the nanoparticles then removing the salt would alter the morphology of the self-assemblies. We used two methods to remove any salt from the sodium chloride solution: dialysis and centrifugation. The dialysis simply consisted of dialysing the nanoparticle dispersion against deionised water, using a semi-permeable membrane with a molecular weight cut-off of 3.5 kDa. The downside of this method is that the volume of solution inside the dialysis bag tends to increase due to the difference in osmolarity between the bag content and the deionised water, leading to a reduction of the polymer concentration. The second method consisted of forming the nanoparticles in the NaCl solution, centrifugating the nanoparticles, removing the supernatant (NaCl solution) and keeping the precipitate (nanoparticles), then dissolving the precipitate in deionised water, centrifugating and removing the supernatant and repeating this step three times. The nanoparticles prepared in a saline buffer but now in a salt-free solution were then imaged by TEM. Unfortunately, TEM showed no cube-shaped particles after removing the salt from the buffer (See Figure 3.21). However, the morphology of the particles differed from the ones obtained in deionised water, showing spherical aggregates entrapped in a larger network. The dialysis and the centrifugation re-equilibration in water yielded similar results, with spherical particles a bit more defined in the case of the dialysis (See Figure 3.21b). It has to be mentioned that the particles are somewhat resistant to salt removal once they are dried, as after the TEM drying procedure, the nanoparticles are washed with water to remove any excess sodium chloride but X-Ray powder diffraction (XRD) characterisation showed that traces of salt crystals remained (See Figure 7.9).

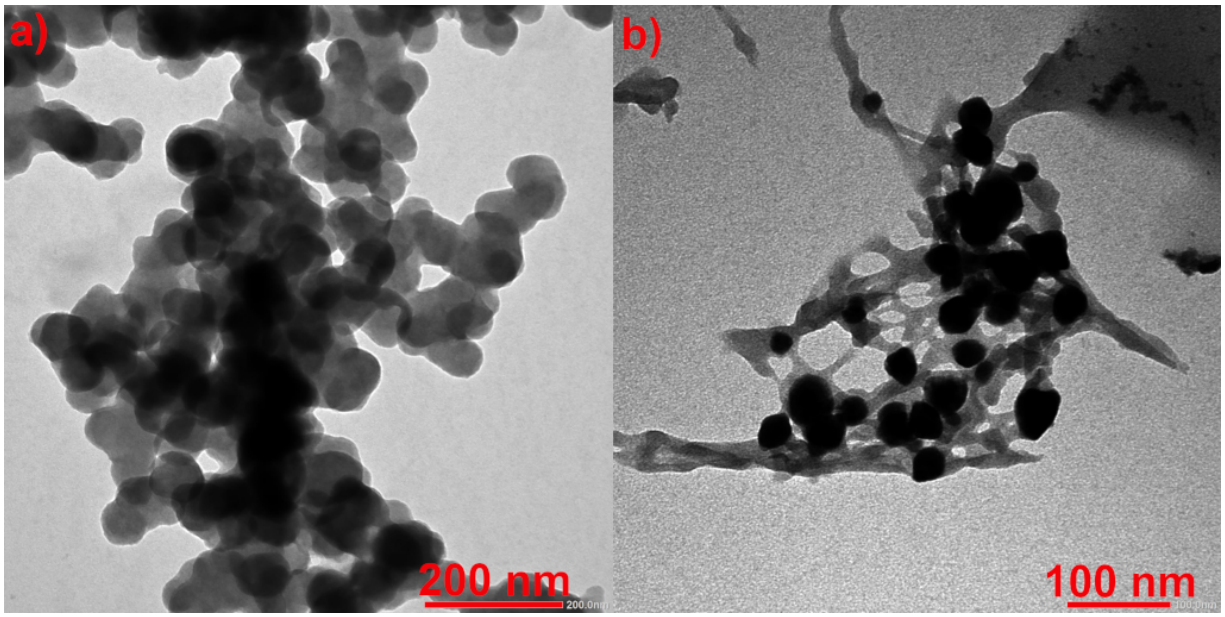

Figure 3.21: TEM images of a 10 mg/mL i-PEGose$_{50}$-*b*-PLLA$_{50}$ solution in a salt-free solution prepared by **a)** centrifugation (200 nm scale bar) or **b)** dialysis (100 nm scale bar).

3.3.9 Influence of the drying effect

So far, the optimal parameters to obtain cube-shaped or anisotropic nanoparticles have been determined to be:

- Isotactic PEGose block
- PLA or PLLA block
- 10 mg/mL block copolymer concentration
- 100 mg/mL saline buffer
- Sodium chloride salt
- Preparing the nanoparticles first then adding the salt
- Drying the solution on the grid then washing the solid with deionised water

One question still remains, which is to know if the anisotropic nanoparticles exist in a solution state or if the TEM drying procedure on the sample grid affects the morphology of the self-assemblies. To solve this question, cryoTEM imaging was performed on four samples: the 85% converted i-PEGose$_{50}$-*b*-PLA$_{50}$ and i-PEGose$_{50}$-*b*-PLA$_{50}$ in a 10 mg/mL or 50 mg/mL sodium chloride solution. Due to cryoTEM limitations, the sodium chloride concentration could not be increased to 100 mg/mL. Similarly, the polymer concentration was recommended to be low, so it was fixed at 0.15 mg/mL which may be too low. Unfortunately, in these conditions,

no cube-shaped particles could be observed. Instead, the 85% converted i-PEGose$_{50}$-*b*-PLA$_{50}$ images were mostly empty, with a few aggregates, and i-PEGose$_{50}$-*b*-PLA$_{500}$ had a few spherical particles (See Figure 3.22).

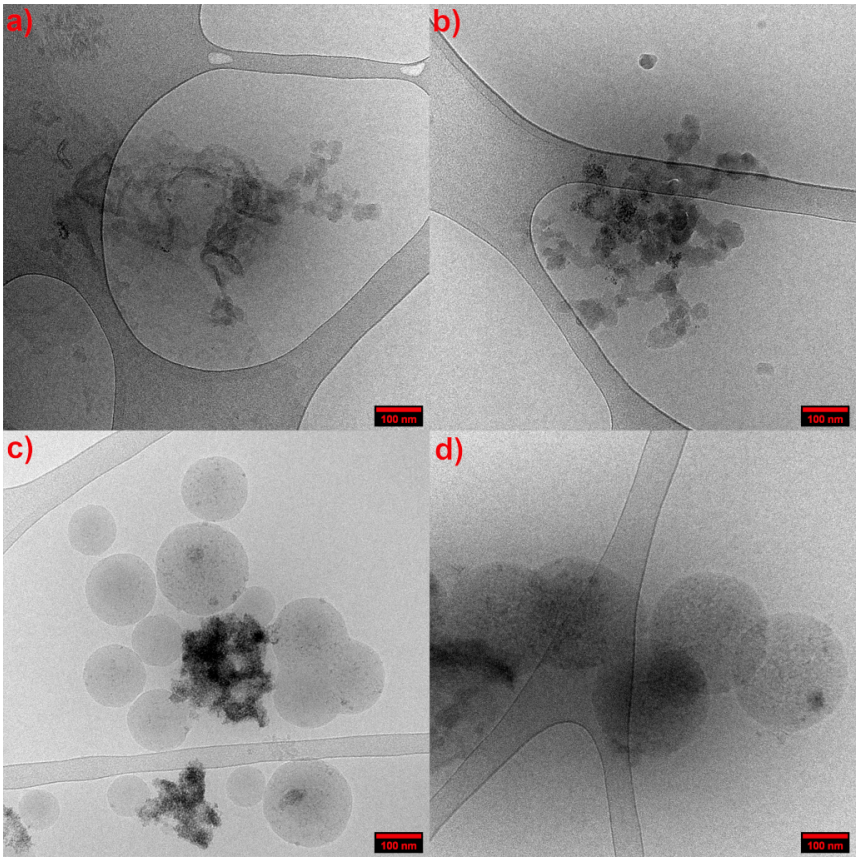

Figure 3.22: cryoTEM images of a 0.15 mg/mL block copolymer solution of an 85% converted i-PEGose$_{50}$-*b*-PLA$_{50}$ in **a)** a 10 mg/mL or **b)** a 50 mg/mL NaCl solution or i-PEGose$_{50}$-*b*-PLA$_{50}$ in **c)** a 10 mg/mL or **d)** a 50 mg/mL NaCl solution.

3.4 Conclusion

In conclusion, i-PEGose-*b*-PLA block copolymers can be added to the limited library of copolymers used for preparation of anisotropic nanoparticles. Moreover, compared to the PEG-*b*-polystyrene polymers that have been reported before,[115] PEGose-PLA has the advantage of being easily functionalisable, thus enabling the preparation of smart cube-shaped nanoparticles. A large number of parameters have been optimised to consistently observe cube-shaped or anisotropic nanoparticles using TEM. However, the lack of clear images of cube-shaped nanoparticles yet using cryoTEM cast doubts on whether these nanoparticles exist in a solution state. The different morphologies obtained using SEM also hint towards a dependency on the drying process to obtain anisotropic nanoparticles. Current investigation seems to suggest that the anisotropic nanoparticles observed are not salt crystals but indeed polymeric particles. However, while morphological changes start to appear in a solution state, it seems like cubes

are only obtained once the solvent is fully evaporated. Future work is then needed to focus on cross-linking the nanoparticles via PEGose hydroxyl groups. This cross-linking would allow the dispersion of the cube-shaped particles in a broader range of buffers to further use them as an efficient drug delivery system.

Chapter 4

Synthesis of PEG-*b*-poly(cycloether), a poloxamer mimic containing a helical block

Parts of this Chapter have been submitted for publication.[2]

4.1 Introduction

Poloxamers were patented in 1973 by Irving Schmolka at BASF.[175] A poloxamer can be described as a triblock copolymer, composed of one block of poly(propylene glycol) (PPG) sandwiched between two blocks of poly(ethylene glycol) (PEG). These materials were originally developed to form aqueous gels with potential uses in biomedical or cosmetic applications.[176–180] Since then, the use of poloxamers has increased dramatically, reaching a total market volume of $225 million in 2021.[181] One major feature of poloxamers is their surface-active properties. Their amphiphilicity, ease-of-production, and biocompatibility led to their extensive use in the cosmetics industry as emulsifiers.[182–185] In recent years, poloxamers have also been used in biomedical applications such as drug delivery, gene therapy, or even bioprocess applications, to protect cell cultures from stressful shear conditions.[186–190] Previously, to tailor poloxamer properties to a specific application, poloxamers were synthesised with various PEG and PPG chain lengths, effectively modifying the amphiphilicity or hydrophilic-lipophilic balance (HLB) of the block copolymer. Poloxamers are generally designed by the letter 'P' followed by three digits, the first two digits multiplied by 100 gives the molecular weight of the hydrophobic middle block, while the last digit multiplied by 10 denotes the % weight content of the hydrophilic PEG block. For example, P407 is a commonly used poloxamer with a 4,000 g/mol PPG block and a 70% PEG content.

In order to produce poloxamers with additional properties, poloxamers can be functionalised with various end-groups.[191,192] For example, Lu and coworkers reported the substitution of the

hydroxy end-group of a P407 poloxamer with an amino group.[193] The amino end-group improved the mucoadhesive properties of the polymer and its subsequent use as an in-situ hydrogel drug delivery system for vaginal administration. Katas and coworkers used P407 end-groups to attach a folic acid targeting ligand to produce a polymeric drug delivery system, which could target cancer cells due to their over-expression of folic acid receptors.[194] The functionalisation of the poloxamer led to an improved cellular uptake and minimal toxicity of the micelles and their cargo. Poloxamers can also be functionalised by adding a reactive linker between each block. For example, Frey and coworkers described the synthesis of a cleavable PEG-*b*-PPG-*b*-PEG copolymer containing two pH-responsive acetal linkers in the polymer backbone.[195] The addition of the acetal linker did not prevent the triblock copolymer from showing good surface-active behaviors. The polymer was used as a surfactant for the miniemulsion polymerisation of styrene, triggering precipitation via a change of pH. Additionally, replacing the PPG block with poly(butylene glycol) has been found advantageous in cases where a more hydrophobic block was needed,[196,197] granting a lower critical micellar concentration (CMC) compared to the corresponding PPG-based block copolymers. In particular, Green and coworkers have developed poly(butylene glycol)-*b*-PEG to form high-internal phase emulsions (HIPE)s and polymerised HIPE foams.[198] The block copolymer was able to stabilise an HIPE at a concentration as low as 0.006 wt%. HIPEs are systems in which the dispersed phase has a fraction volume higher than 0.74. This high volume can lead to a morphology change from spherical droplets to polyhedrons.[199] In addition, HIPEs have unusual properties, like high viscosity and viscoelastic rheological behavior.[200,201] Frequently, HIPEs are used as a polymerisation template to control the microstructure of a material.[202–205] Currently, new poloxamer properties have been obtained by either tuning their hydrophilicity/hydrophobicity ratio (by tuning chain lengths or introducing more hydrophobic blocks) or by adding functional groups.

In this work, the goal was to use the previously described methodology to produce PCEs in order to obtain a poloxamer mimic, consisting of either diblock or triblock copolymers with PEG blocks and a saturated polycycloether block (SPCE), with no additional functional group (See Figure 4.1). The diblock copolymers containing an unsaturated PCE block would be less similar to poloxamers than the corresponding triblock copolymers containing an SPCE block. Nevertheless, these polymers have an identical HLB value to that of the corresponding poloxamers, but a different rigidity. The increase in rigidity moving from PPG/PEG to PCEs can be deduced from persistence lengths, e.g. PEG has a persistence length of 0.38 nm,[206] rigid polysaccharides like Iota-carrageenan and xanthan gum have a high persistence length of 23-26 nm as well as more flexible polysaccharides like locust bean gum and guar gum with random coil conformations still have a persistence length of 3 nm.[207] PCEs with helical or random coil conformations come close to polysaccharides, which leads to increased persistence lengths and higher rigidity than PEG or PPG. Introduction of a rigid block could induce new self-assembly behaviours and good emulsification properties such as high internal phase (See Figure 4.1).

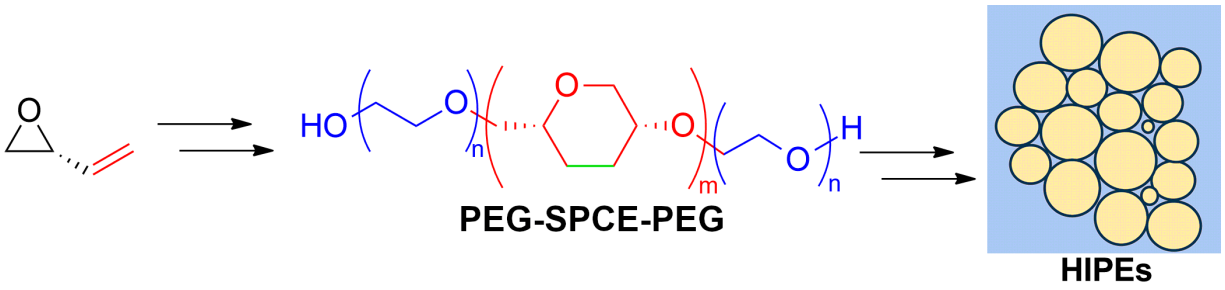

Figure 4.1: Simplified scheme of the work achieved here: the synthesis of PEG-PCE block copolymers and the formation of high-internal phase emulsions (HIPEs).

4.2 Synthesis of the block copolymers

The atactic and isotactic PEB were synthesised according to the procedure described in Chapter 3. End-group modification, ring-closing metathesis, ring-opening polymerisation of ethylene oxide and subsequent hydrogenation yielded the desired block copolymers (See Figure 4.2).

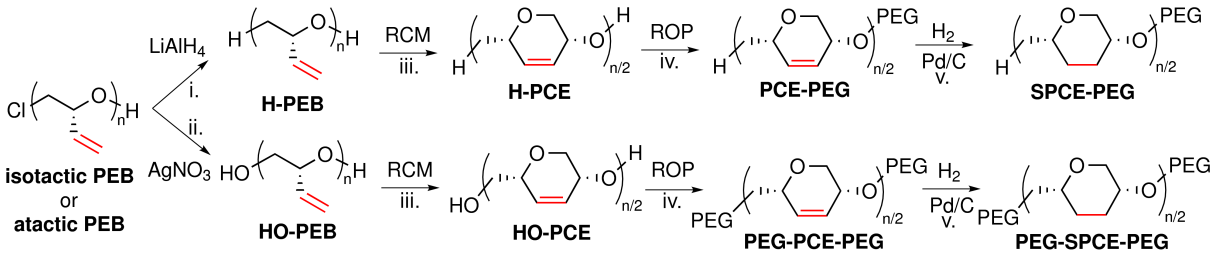

Figure 4.2: Synthesis scheme of PEG-*b*-PCEs. **i.** $LiAlH_4$ in THF (1M), 48h **ii.** $AgNO_3$ in ethanol/water (5:1), reflux for 48h **iii.** Grubbs II catalyst 5 mol% in DCE, reflux for 5 days **iv.** NaH and ethylene oxide in THF (2.5 M), 50 °C for 2 days **v.** Pd/C (10% wt) and H_2 in methanol, 24h.

The number of PEB repeating units (30 repeating units, 2.1 kDa) was chosen to mimic the hydrophobic block in P188 (31 propylene glycol repeating units, 1.8 kDa), one of the commercially most used poloxamers. The polymer molecular weight was estimated by SEC against poly(styrene) calibration and ^{1}H nuclear magnetic resonance (NMR) through end-group peaks integration (See Table 4.1). The polymer structure was confirmed by ^{1}H NMR (See Figure 4.3a).

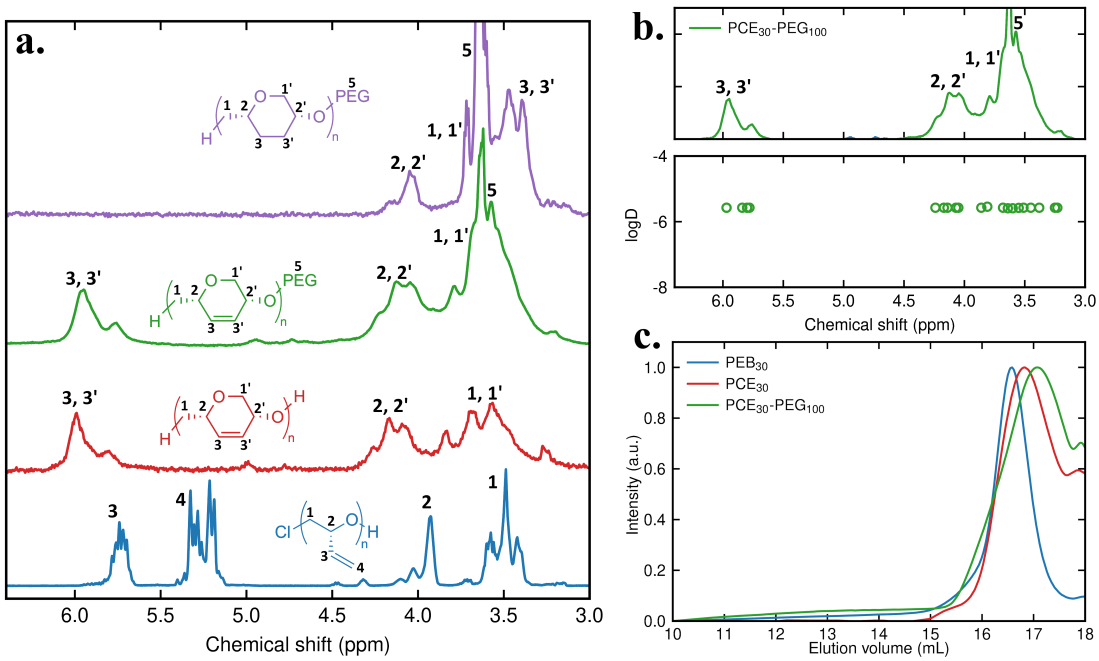

Figure 4.3: **a)** ^{1}H NMR of the synthesised polymers PEB_{30}, PCE_{30}, PEG_{100}-*b*-PCE_{30} and PEG_{100}-*b*-$SPCE_{30}$ in $CDCl_3$, **b)** DOSY ^{1}H NMR of the block copolymer PEG_{100}-*b*-PCE_{30} in $CDCl_3$, **c)** Size-exclusion chromatography traces of PEB_{30}, PCE_{30} and PEG_{100}-*b*-PCE_{30} measured in THF.

A PEB with only 15 repeating units (1.0 kDa) was also synthesised to allow for electrospray-ionisation mass spectrometry (ESI-MS) characterisation. ESI-MS confirmed the structure of PEB repeating units and its chloride and hydroxy end-groups (See Figure 4.4a).

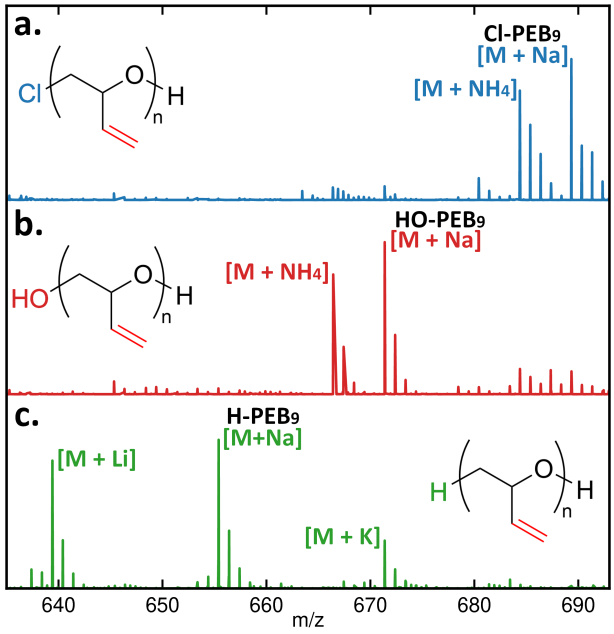

Figure 4.4: ESI-MS spectra of poly(epoxybutene) with a **a)** chloride end-group, **b)** hydroxy end-group and **c)** hydrogen end-group.

Following the ROP of butadiene monoxide, H-PEB or HO-PEB were obtained by modification of the PEB chloride end-group. In order to obtain a triblock copolymer, HO-PEB was synthesised to be used later as a macroinitiator for the ROP of ethylene oxide. While Cl-PEB could have been used, H-PEB was synthesised to prevent any S_N2 side-reaction during the ROP of ethylene oxide, and also because it possesses a similar end-group as those commonly found in PPG based block copolymers. H-PEB was obtained through the reduction of the chloride end-group with 10 equivalents of lithium aluminum hydride ($LiAlH_4$) in THF. The reaction conversion could not be determined by ^{1}H NMR but ESI-MS confirmed both the presence of H-PEB and the absence of any remaining Cl-PEB (See Figure 4.4c). Sodium, lithium and potassium adducts from the use of $LiAlH_4$ and the Rochelle salt solution could be observed in the mass spectrum. HO-PEB was obtained using silver nitrate in a water/ethanol mixture. Similarly, analysis by ^{1}H NMR did not indicate if the reaction had proceeded but ESI-MS confirmed the conversion of the starting polymer and the formation of the HO-PEB structure (See Figure 4.4b). Small peaks corresponding to Cl-PEB were still visible on the HO-PEB mass spectrum which might lead to some diblock copolymer impurities after the ring-opening polymerisation of ethylene oxide. SEC showed that both H-PEB and HO-PEB have a similar molecular weight after the end-group modification, thus confirming the absence of polymer degradation. It is worth noting that the end-group modification could have been performed after the ring-closing metathesis for a more convergent synthesis. However, $LiAlH_4$ reduction of Cl-PCE resulted in a degradation of the polycyclic polymer. The ring-closing metathesis of each PEB polymer was performed in dichloroethane, using Grubbs II catalyst with a 5 mol% catalyst loading, under reflux. Reaction completion was confirmed by ^{1}H NMR after 5 days.The polymers were purified by preparative SEC and characterised by ^{1}H NMR as well as SEC. SEC showed a decrease in polymer molecular weight, confirming the loss of an ethylene molecule for every two vinyl groups (See Figure 4.3c and Table 4.1). The isotactic polymers encompass *cis* 1,4-disubsituted six-membered rings, which induce helicity. Circular dichroism (CD) confirmed the helicity of these isotactic polymers (See Figure 4.5).

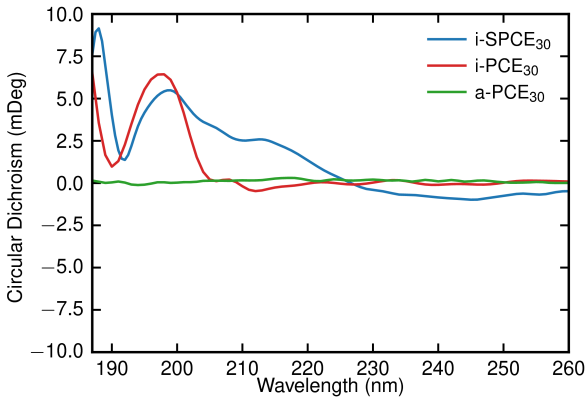

Figure 4.5: Circular dichroism spectra of a-PCE_{30}, i-PCE_{30} and i-$SPCE_{30}$ in a 0.1 mg/mL solution in methanol.

The synthesis of the PEG block was achieved through ROP of ethylene oxide using the previously synthesised PCE as a macroinitiator and sodium hydride as a base (heated at 50°C over two days). A diblock copolymer was obtained when H-PCE was used as macroinitiator for the ROP of ethylene oxide and a triblock copolymer was formed with HO-PCE, due to the protic hydroxy end-group on both ends. The block copolymer, now water-dispersible, was purified by dialysis against water. In the ^{1}H NMR spectrum, the peak at 3.6 ppm confirmed the presence of the PEG block (See Figure 4.3a).

Diffusion-ordered spectroscopy (DOSY) indicated that the diffusion coefficient associated with the PEG peak was the same as diffusion coefficients associated with PCE peaks, thus confirming the presence of a block copolymer structure, with the absence of PEG homopolymers (See Figure 4.3b). SEC did not indicate an increase of the molecular weights, contrary to predicted, but a shift towards lower elution times has been previously reported in cases of block copolymer formation.[208] In the current case, the measured molecular weight was even slightly lower than before the ROP. These results could be explained by various reasons. Firstly, the column is calibrated with poly(styrene) standards, the structure of which differs greatly from the analysed amphiphilic block copolymer. Secondly, block copolymer architectures have been reported to appear with a lower molecular weight than expected due to conformational effects arising from two blocks of different solubilities leading to a smaller hydrodynamic radius than the starting block.[208] In any case, the presence of a monomodal SEC peak, combined with the correct ^{1}H NMR spectrum and a single diffusion coefficient from all DOSY polymer peaks confirm the presence of the desired structure (See Figure 4.3). As previously mentioned, the molecular weight of the PCE homopolymer was estimated by SEC and ^{1}H NMR. The block copolymer molecular weight was then estimated by comparing the integration of PEG peaks and PCE peaks to deduce the PEG block length (See Table 4.1).

Synthesis of SPCEs required one last step involving heterogeneous hydrogenation of the alkene moieties, to obtain a structure that closely mimics the PPG block of a poloxamer. Because of the versatility of the unsaturated PCE structure, that can be functionalised/cross-linked for various applications, we studied the self-assembly and interfacial properties of both unsaturated PCE-PEG and saturated SPCE-PEG. SPCE-PEG were obtained through the hydrogenation of the respective PCE-PEG in methanol over palladium on carbon under a hydrogen atmosphere. The block copolymers were purified by dialysis against deionised water. The reaction conversion was monitored by ^{1}H NMR, and full conversion was confirmed through the disappearance of the alkene peak. CD confirmed that the PCE retained its helicity after the hydrogenation (See Figure 4.5). In total, 9 block copolymers were synthesised, with either diblock or triblock architectures, atactic or isotactic tacticity, saturated or unsaturated 6-membered rings, and varying PEG lengths (100 or 200 repeating units) (See Table 4.1).

Table 4.1: Theoretical polymer molecular weights and experimental polymer molecular weights measured by SEC and ^{1}H NMR. The number of repeating units is based on a single ether linkage. Critical Aggregation Concentrations (CACs) measured by fluorescence spectroscopy and surface tensions measured by droplet shape analysis.

Polymer	M_n Theo[a] (kDa)	M_n SEC[b] (kDa)	M_n NMR[c] (kDa)	Đ[b]	CAC[d] (mg/mL)	Surface tension[e] (mN/m)
$aPEB_{30}$	2.1	2.4	2.7	1.19	-	-
$iPEB_{30}$	2.1	2.3	2.6	1.18	-	-
$aPCE_{30}$	1.7	2.1	-	1.21	-	-
$iPCE_{30}$	1.7	2.0	-	1.22	-	-
$aPCE_{30}$-PEG_{100}	6.1	1.9	6.7	1.14	0.12	32.5
$aPCE_{30}$-PEG_{200}	10.5	2.6	9.6	1.39	0.15	36.6
$iPCE_{30}$-PEG_{100}	6.1	2.9	7.5	1.18	0.04	30.8
$iPCE_{30}$-PEG_{200}	10.5	2.0	13.2	1.31	0.22	37.7
$aSPCE_{30}$-PEG_{100}	6.1	2.9	6.7	1.32	0.05	26.7
$iSPCE_{30}$-PEG_{100}	6.1	2.3	7.5	1.14	0.21	35.1
PEG_{50}-$aPCE_{30}$-PEG_{50}	6.1	2.0	6.2	1.18	0.15	42.0
PEG_{50}-$aSPCE_{30}$-PEG_{50}	6.1	2.5	9.2	1.37	0.04	42.7
PEG_{50}-$iPCE_{30}$-PEG_{50}	6.1	2.0	5.1	1.27	0.11	46.5

a) calculated from starting material equivalents, **b)** measured via SEC in THF with a 1 mL/min flow rate (See Figure 7.20) , **c)** measured via ^{1}H NMR in $CDCl_3$ (See Figure 7.21 and 7.22), **d)** measured via fluorescence spectroscopy using pyrene as a fluorescence probe, **e)** measured at 20°C using a contact angle goniometer and droplet shape analysis.

4.3 Self-assembly properties of PEG-polycycloethers

Poloxamers are amphiphilic polymers that can self-assemble in water. Self-assembly is driven by the minimisation of interactions between the hydrophobic block and water, to reach an equilibrium and reduce the free energy of the system.[209] PEG-PCE block copolymers have the same number of carbon and oxygen atoms per block as a poloxamer. The HLB of a poloxamer should be almost identical to its corresponding PEG-PCE block copolymer when calculated using either Griffin's method or Davies' method.[210] While the main driving force of block copolymer self-assembly is the relative hydrophobicity of each block, the rigidity of a block can have an influence on the conformations it can take, thus affecting the final morphology of the aggregates.[211–217] In that regard, we decided to study the self-assembly properties of PEG-PCE block copolymers in water, to identify any potential divergence from the properties of traditional

poloxamers. We first measured the critical aggregation concentration (CAC) of our polymers by fluorescence spectroscopy using pyrene as a fluorescent probe (See Figure 4.8a).[218] For reference, P188 is a PEG_{38}-*b*-PPG_{29}-*b*-PEG_{38} block copolymer; it has a similar molecular weight and hydrophilic/hydrophobic ratio as PEG_{100}-*b*-PCE_{30} (See Figure 4.10c). The CMC of P188 is published as 4.1 mg/mL at 37°C (it increases as the temperature decreases, with no detectable CMC at 20°C, See Figure 4.6).

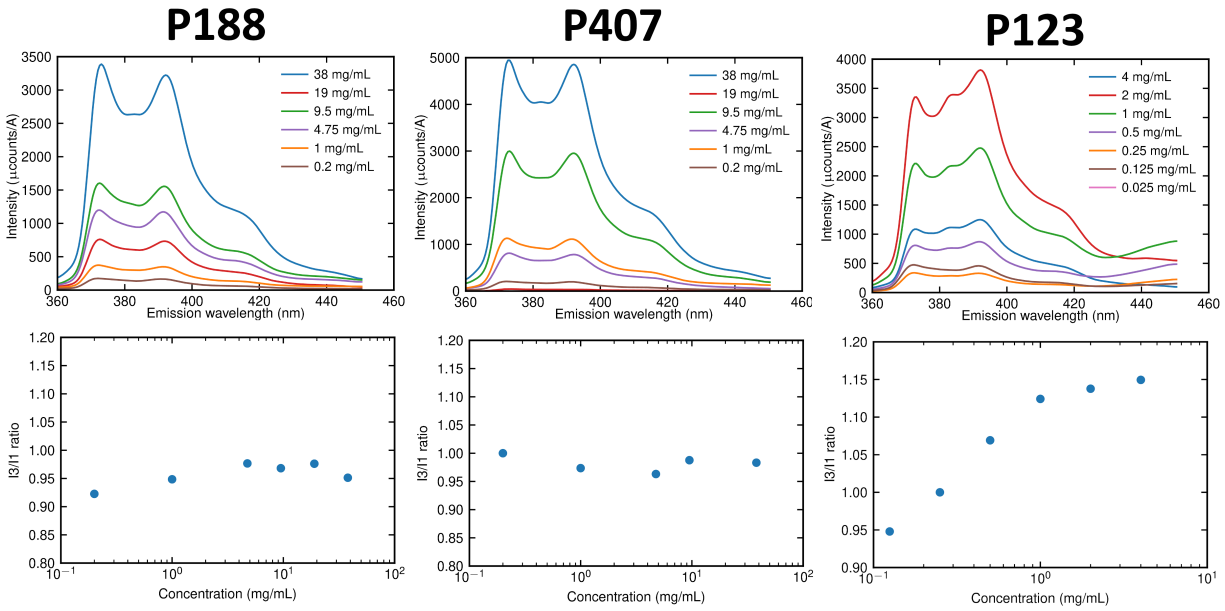

Figure 4.6: Fluorescence intensity trace for poloxamers P188, P407 and P123 at different concentrations, using pyrene as a fluorescence probe, at 20°C. CMC determination by plotting I_3/I_1 ratio (peak intensity was measured at 372 nm I_1 and 384 nm I_3) as a function of concentration. No CMC could be observed for poloxamer P188 and P407 as described in the literature.

By comparison, all PEG-PCE block copolymers had a CAC more than ten times lower at 20°C (See Table 4.1). Therefore, using a polycyclic structure as a hydrophobic block, one can obtain a block copolymer with a much lower CAC while preserving a short hydrophobic block length. The resulting polymer is then both highly hydrophilic and self-assembles at low concentration. A similar result would not be achievable using a poloxamer structure, because the length of the hydrophobic block would have to be increased or the length of the hydrophilic block decreased to lead to a lower CAC (See Figure 4.6).

After exploring the effect of a polycyclic hydrophobic block on the CAC of the block copolymer, we investigated the effect of tacticity. Comparatively, the effect of tacticity (atactic/isotactic), PEG length (100 units or 200 units), architecture (diblock/triblock), and degree of unsaturation had a rather small influence on the value of the block copolymer CAC (See Table 4.1). Yet, some trends can be noticed: a longer PEG length leads to a higher CAC, triblock copolymers tend to have a lower CAC, isotactic PCEs favor slightly higher CACs, and the presence of unsaturated units did not lead to any noticeable effect on the CAC. The size of the aggregates formed by the self-assembly of PEG-PCE block copolymers were measured using dynamic light scattering

(DLS) (See Figure 4.8b). P188 has been reported to form micelles with a 5-10 nm diameter.[219] A P123 5.0 mg/mL solution formed self-assemblies with an average diameter size of 18 nm at 20°C (See Figure 4.7). PEG-PCE block copolymers formed larger aggregates, with a mean diameter ranging from 64 nm to 132 nm (See Table 4.2).

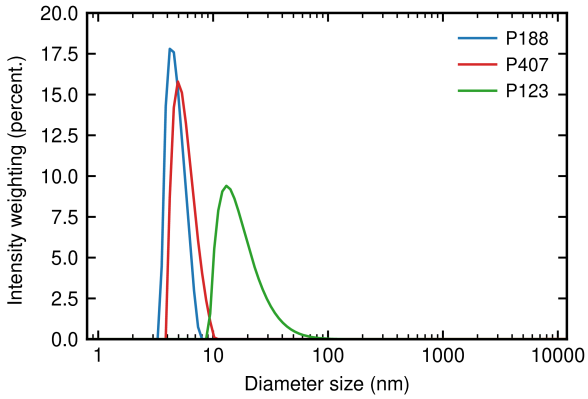

Figure 4.7: Size of poloxamers P188 and P407 polymers, and P123 self-assemblies in water, at 20°C, at a concentration of 5 mg/mL. Measured by dynamic light scattering, using back-scattering (175°) and intensity weighting.

Table 4.2: Nanoparticle diameter size (intensity weighting) of the synthesised PEG-PCE block copolymers in deionised water (1 mg/mL), measured via dynamic light scattering with a 175° scattering angle.

Block copolymer	Nanoparticle diameter size (nm)
$aPCE_{30}$-PEG_{100}	109
$aPCE_{30}$-PEG_{200}	93
$iPCE_{30}$-PEG_{100}	101
$iPCE_{30}$-PEG_{200}	64
$aSPCE_{30}$-PEG_{100}	92
$iSPCE_{30}$-PEG_{100}	85
PEG_{50}-$aPCE_{30}$-PEG_{50}	132
PEG_{50}-$aSPCE_{30}$-PEG_{50}	121
PEG_{50}-$iPCE_{30}$-PEG_{50}	89

Looking at the intensity distribution of the aggregate diameter size plot, two populations of aggregate can sometimes be observed if the sample is analysed shortly after preparation, with one major peak around 100 nm and a smaller peak at 10 nm (See Figure 4.8c). Considering the small molecular weight of the synthesised block copolymer, this result suggests that the polymer can self-assemble into 10 nm micelles but will form larger aggregates over time. Again, previously mentioned parameters (tacticity, PEG length, architecture, degree of unsaturation)

had a relatively low influence on the size of the aggregates. Samples with lower CAC produced slightly larger aggregates (atactic, shorter PEG, triblock).

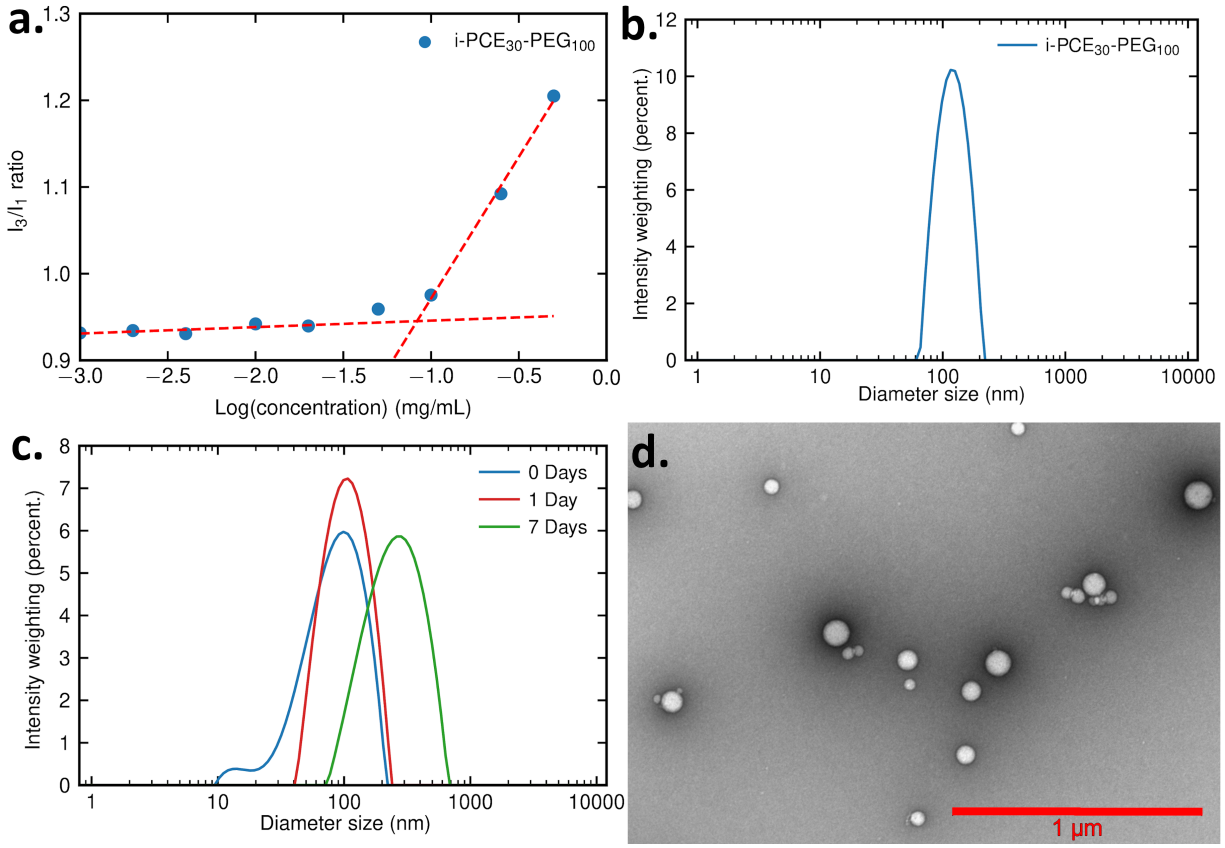

Figure 4.8: a) CAC plot for isotactic PCE_{30}-*b*-PEG_{100} using the intensity of the emission spectrum at 373 nm (I_1) and 384 nm (I_3). Nanoparticle size distribution of **b)** isotactic PCE_{30}-*b)*-PEG_{100} after a day and **c)** isotactic $SPCE_{30}$-*b*-PCE_{30} over 7 days, measured by dynamic light scattering (DLS) using an intensity-weighted distribution, **d)** transmission electron microscopy (TEM) images of unstained isotactic PCE_{30}-*b*-PEG_{100} in deionised water, 1 day after the nanoparticles preparation (1 µm scale bar) (See Figure 7.24 for additional TEM images and size analysis.

The main factor leading to larger aggregates is time: the peak at 10 nm was not noticeable by DLS one week after suspending the polymer in water. The mean diameter size also increased over time (See Figure 4.8c). To confirm the aggregate structure further, the aggregates were imaged using transmission electron microscopy (TEM). The diameter of the aggregates imaged by microscopy correlated with the results from DLS measurements. TEM also indicated the spherical shapes of the aggregates (See Figure 4.8d). Additional DLS characterisation was realised to measure the particle size after 6 months. In intensity weighted distributions a small amount of large particles (500-900 nm) could be observed but the samples consisted mostly of 40-50 nm particles (See Figure 4.9), showcasing the stability of the self-assemblies.

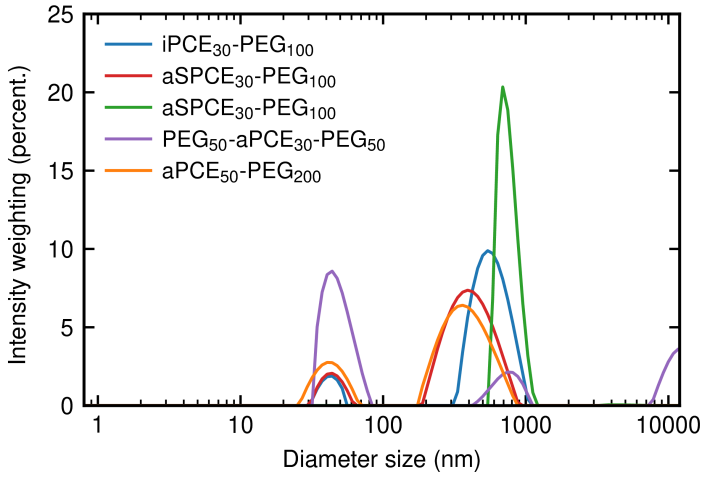

Figure 4.9: Size of PEG-polycycloether self-assemblies in water at a concentration of 5 mg/mL, after 6 months kept at room temperature. Measured by dynamic light scattering, using back-scattering (175°) and intensity weighting.

In conclusion, tweaking the rigidity of the hydrophobic block of a poloxamer by using a PCE led to a block copolymer with a high hydrophilic/hydrophobic ratio, and a high propensity to form aggregates. This could lead to novel drug delivery systems with high encapsulation efficiencies and high loading content.

4.4 Emulsification properties of PEG-*b*-polycycloether block copolymers

Poloxamers are extensively used in the cosmetic industry due to their surfactant properties. For example, poloxamer P184 can be used as an emulsifier for the formulation of various skincare or haircare products like face creams or shampoos. In this regard, the emulsification properties of the synthesised PEG-PCE block copolymers were studied and compared to traditionally used poloxamers. Despite PEG-PCE polymers having a similar HLB value as poloxamers, they were expected to have a different behaviour since it has been previously reported that the rigidity of a surfactant can influence its properties.[220–222] To determine what polymer concentration should be used, a batch of emulsions were prepared with an increasing concentration from 0.01 wt% to 0.5 wt%, and a fixed *n*-dodecane/water ratio of 1:1. The polymer used was an isotactic PCE_{30}-*b*-PEG_{100}. A concentration as low as 0.05% was sufficient to obtain an emulsion but it was only at a concentration of 0.5% that a single emulsion phase was obtained (See Figure 4.10b). Kolliphor® P407 technical information recommends a polymer concentration ranging from 1% to 5% to be used as an emulsifier. Thus, a concentration of 0.5% can be considered advantageously low.

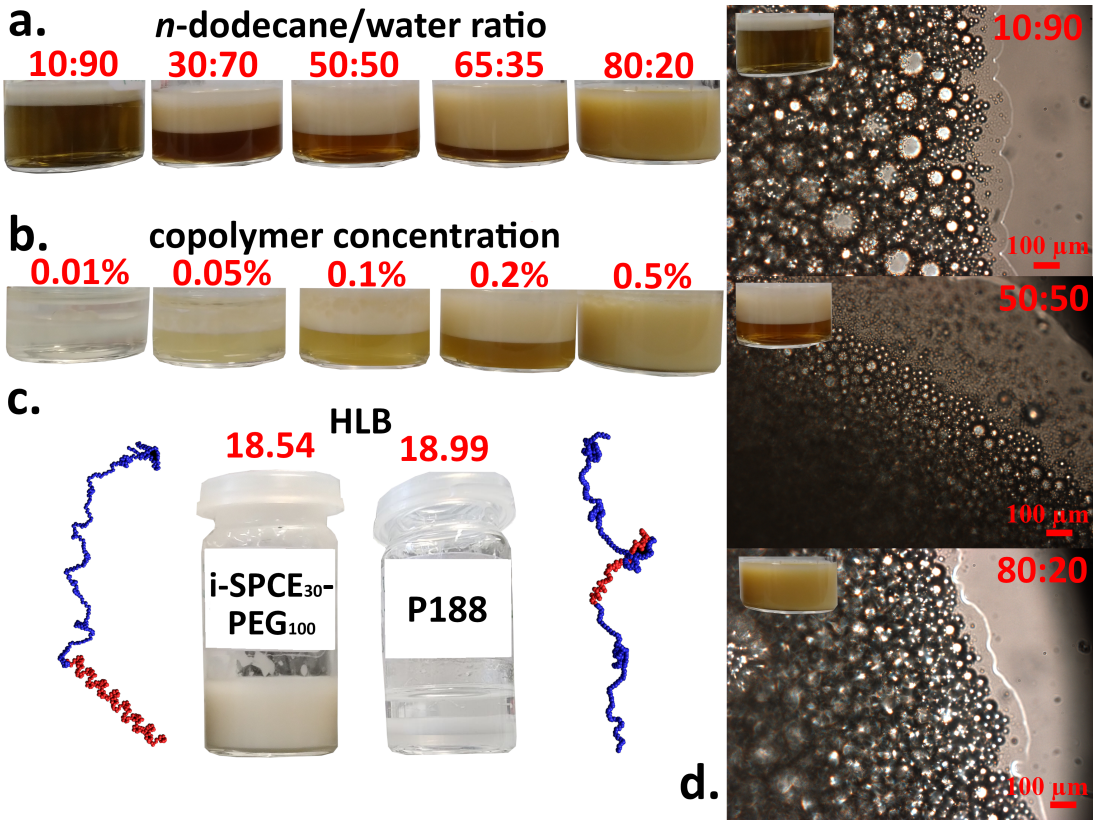

Figure 4.10: Emulsion pictures of isotactic PCE_{30}-*b*-PEG_{100} with **a)** 0.5% block copolymer concentration and a varying oil/water ratio and **b)** fixed 65:35 oil/water ratio and a varying block copolymer concentration. **c)** Emulsion pictures and calculated HLB values of isotactic $SPCE_{30}$-*b)*-PEG_{100} and P188. **d)** Microscopy images of isotactic PCE_{30}-*b*-PEG_{100} with a 0.5% block copolymer concentration a varying oil/water ratio (scale bar 100 µm).

For further studies, all other emulsions were investigated at a fixed polymer concentration of 0.5 wt%. The second parameter studied was the oil/water ratio with an increasing *n*-dodecane content from 10 to 80 vol% (See Figure 4.10a). All emulsions obtained were oil-in-water (O/W) emulsions irrespective of the oil/water ratio. The nature of the emulsion was confirmed by a droplet test, putting a drop of the emulsion in pure *n*-dodecane or water to see in which phase it readily dissolves. The propensity of the block copolymers to form O/W emulsions can be attributed to their high EG content and high HLB value. These O/W emulsions can also be observed using poloxamers with similar molecular weights that have a high EG content like poloxamers P188 or P407. However, using these poloxamers and a high oil content usually leads to an unstable O/W emulsion, with phase separation of both the oil and water phases (See Figure 4.10c). When a PCE and a low oil content were used, a phase separation could be observed over time, with an O/W emulsion phase at the top and a water phase at the bottom. The intensity of this separation decreased with an increasing oil content. The reason seems to be that HIPEs are formed regardless of the oil content used, with excess water forming a separate phase to enable HIPE formation. A single-phase emulsion, stable for at least one week could be obtained using a high oil/water ratio of 80% oil (See Figure 4.10a).

It is worth nothing that replacing *n*-dodecane with toluene, a low viscosity solvent, that is more prone to phase separation, led to the same behavior (See Figure 4.11).

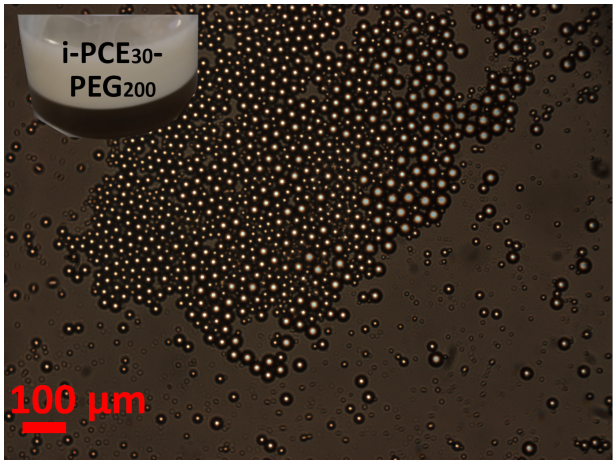

Figure 4.11: Optical microscopy pictures of iPCE$_{30}$-PEG$_{200}$ block copolymer emulsion, with a polymer concentration of 0.5 wt.% and a 65:35 toluene/water ratio (100 µm scale bar).

The HIPE nature of the emulsion was confirmed by the presence of more than 74% oil in the O/W emulsion. Microscopy of the emulsions at different ratios gave similar images of crowded oil droplets, with barely any noticeable continuous phase between them (See Figure 4.10d, 4.12 and 4.13). The diameter of the droplets was similar throughout the samples, averaging at 61 µm with a standard deviation of 15 µm (See Figure 4.14).

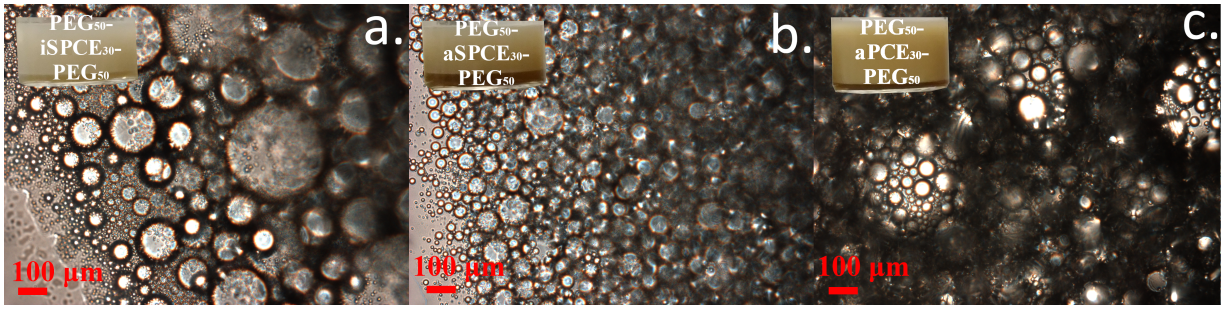

Figure 4.12: Optical microscopy pictures of **a)** PEG$_{50}$-iSPCE$_{30}$-PEG$_{50}$, **b)** PEG$_{50}$-aSPCE$_{30}$-PEG$_{50}$, **c)** PEG$_{50}$-aPCE$_{30}$-PEG$_{50}$ block copolymer emulsions, with a polymer concentration of 0.5 wt.% and a 65:35 *n*-dodecane/water ratio (100 µm scale bar).

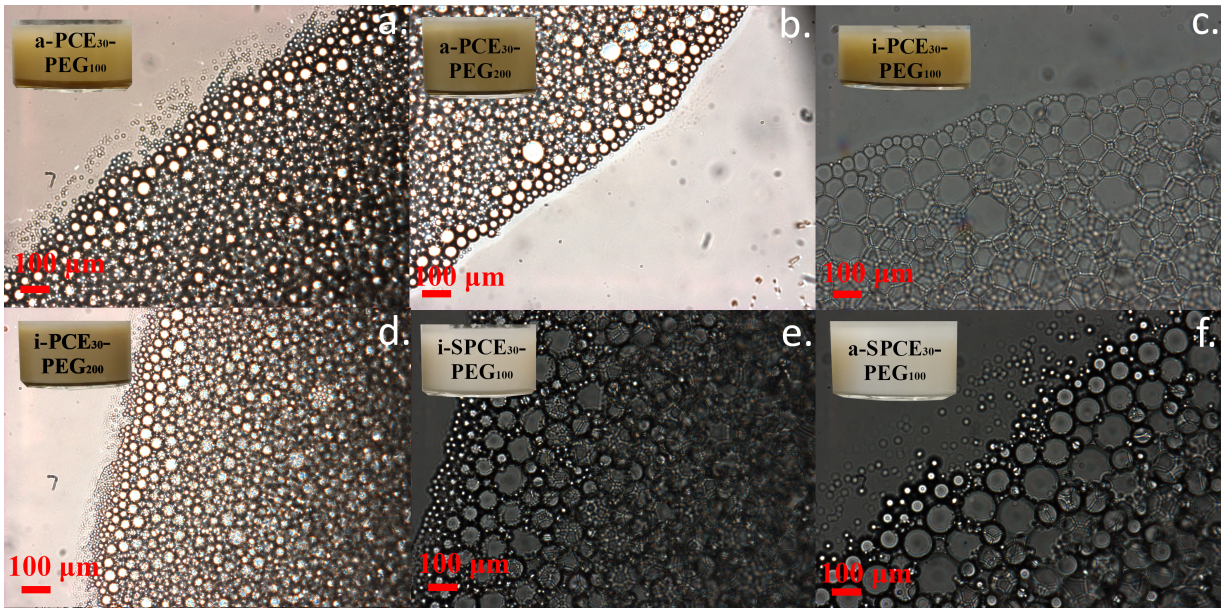

Figure 4.13: Optical microscopy pictures of **a)** aPCE$_{30}$-PEG$_{100}$, **b)** aPCE$_{30}$-PEG$_{200}$, **c)** iPCE$_{30}$-PEG$_{100}$, **d)** aPCE$_{30}$-PEG$_{200}$, **e)** aSPCE$_{30}$-PEG$_{100}$, **f)** aSPCE$_{30}$-PEG$_{100}$ block copolymer emulsions, with a polymer concentration of 0.5 wt.% and a 65:35 *n*-dodecane/water ratio (100 µm scale bar).

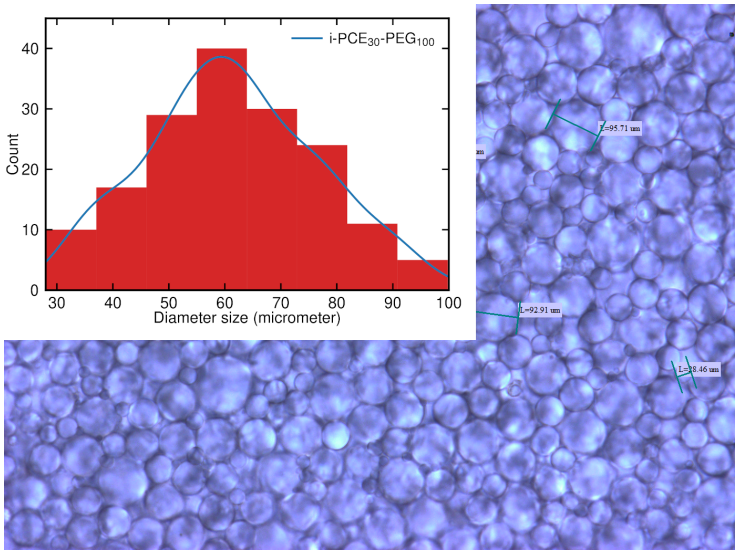

Figure 4.14: Microscope image of an iPCE$_{30}$-*b*-PEG$_{100}$ emulsion with a polymer concentration of 0.5 wt.% and a 50:50 *n*-dodecane/water ratio, along with a size distribution of droplet diameters.

Finally, the influence of the block copolymer structure was studied. In particular, the tacticity (atactic/isotactic), the block architecture (diblock/triblock), the PEG length (100 units or 200 units), and the degree of unsaturation of the PCE backbone. A batch of emulsion was prepared with a fixed block copolymer concentration of 0.5% and a fixed oil/water ratio of 65:35, using all of our block copolymers (See Figure 4.15).

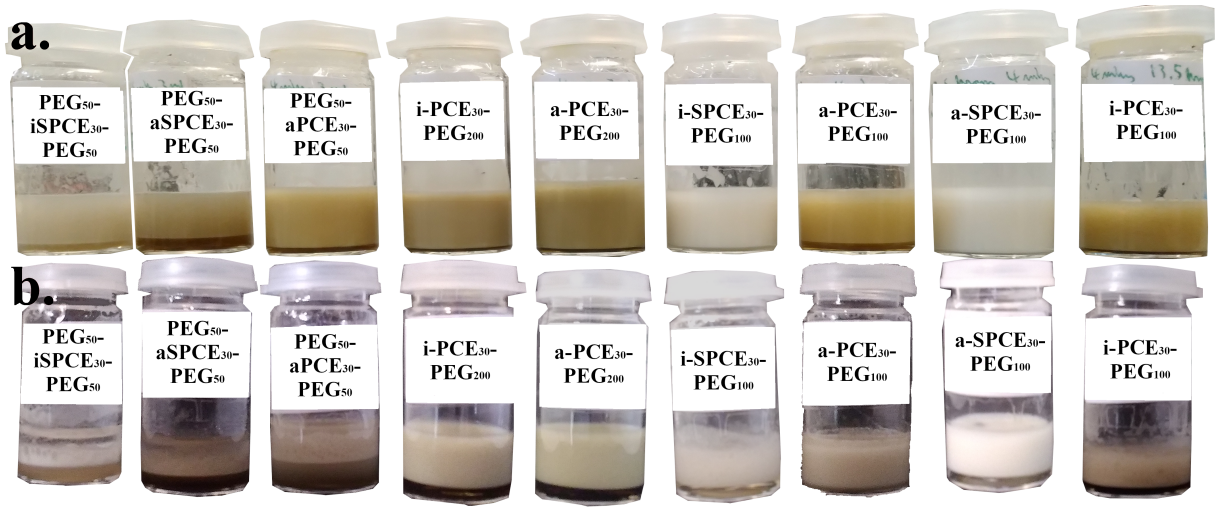

Figure 4.15: Emulsion pictures of different PEG-*b*-PCE block copolymer at 0.5 wt.% concentration and a 65:35 *n*-dodecane/water ratio after **a)** 1 day and **b)** 4 months.

While an oil/water ratio of 80:20 yielded more stable emulsions, an oil/water ratio of 65:35 was chosen to check if a phase separation would happen over time for all samples. As mentioned before, the degree of unsaturation on the PCE did not influence the CAC and the self-assembly of the block copolymer. In a similar fashion, the degree of unsaturation did not seem to have an impact on the emulsification properties of a given PEG-PCE block copolymer: O/W HIPEs were obtained (See Figure 4.12 and 4.13) and $iSPCE_{30}$-*b*-PEG_{100} produced emulsions with the same stability as isotactic PCE_{30}-*b*-PEG_{100} emulsions. The lack of different behavior of both polymer types could be expected due to the only marginal change in polarity between unsaturated and saturated repeating units. The effective stabilisation of emulsions by PCEs with unsaturated units proves itself to be interesting as it might be useful for further design for specific applications, either through functionalisation or cross-linking of the double bond.

Using an isotactic PCE gave a higher CAC, which correlated with less stable emulsions. However, using both an isotactic PCE and a longer PEG chain (200 units) produced stable emulsions. One reason could be that short PEG and isotactic PCE are more prone to self-aggregation; using a longer PEG would reduce the tendency of the block copolymer to self-assemble and promote interfacial assemblies. For atactic PCEs, increasing the number of repeating units of the PEG chain from 100 to 200 decreased the CAC of the block copolymer, but it did not drastically change the nature or stability of the emulsions formed. Emulsions formed with the triblock copolymers were less stable, with a phase separation of both water and *n*-dodecane after a few days. The effect was more pronounced using an isotactic PCE. Overall, the influence of the isotactic block on the emulsification properties was more pronounced for the triblock copolymer (leading to unstable emulsions unless longer PEG chains were used), while for diblock copolymers the effect of tacticity on emulsion behavior was only marginal. A hypothesis could be that the rigidity of the hydrophobic middle block due to helicity would prevent bending of the block copolymer into a curved conformation, which is required for efficient interaction of triblock

copolymers at oil/water interfaces.

The stability of the emulsions formed was assessed by looking at any phase separation or creaming after 4 months (See Figure 4.10 and 4.18) and inspecting the droplet aspect and size by optical microscopy (See Figure 4.16). Atactic PCE_{30}-*b*-PEG_{100} and atactic $SPCE_{30}$-*b*-PEG_{100} showed the best results, with no phase separation and microscopy images still showing HIPEs with a droplet size remaining similar over 6 months. In order to evaluate these poloxamer mimicking polymer systems with respect to their role models P188, P407 and P123, various properties (CAC, particle size, surface tension, HIPE formation) were studied for a direct comparison (See Figure 4.6, 4.7 and 4.17).

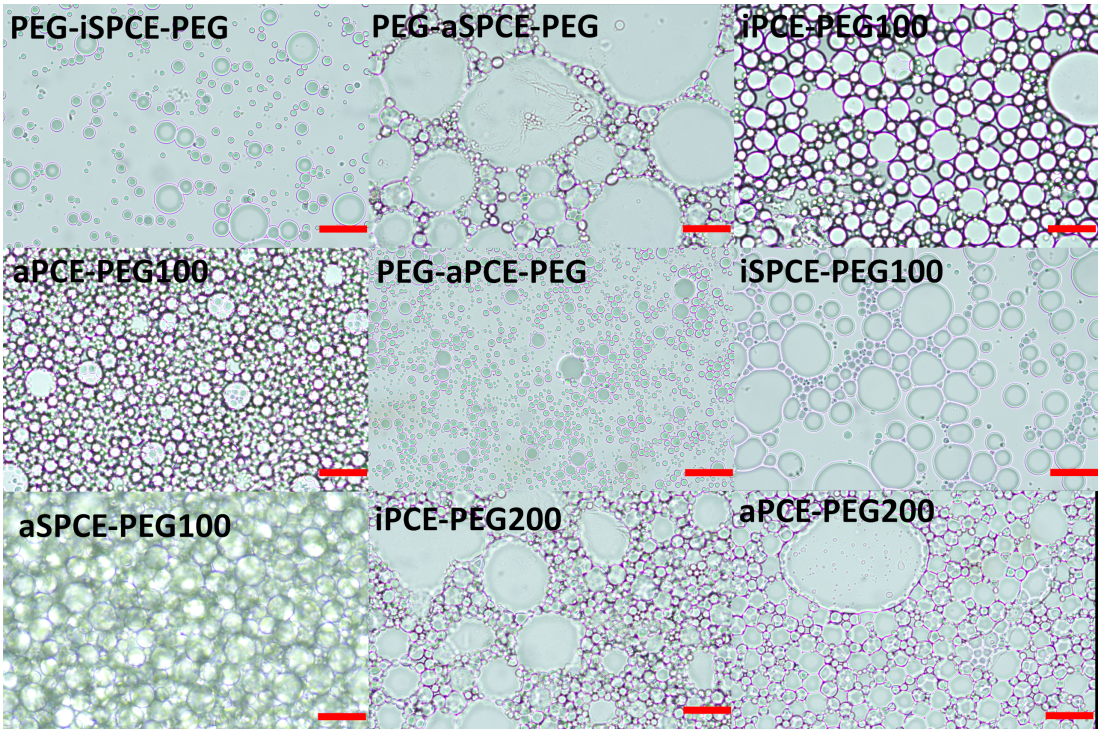

Figure 4.16: Optical microscopy images of *n*-dodecane/water 80:20 vol% emulsions formed by PEG-polycycloethers block copolymer after 6 months. Scale bars are 30 µm.

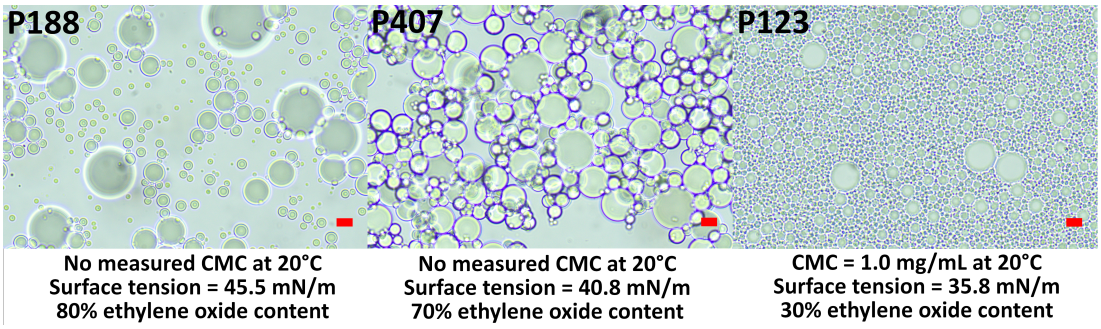

Figure 4.17: Optical microscopy images of *n*-dodecane/water 80:20 vol% emulsions formed by poloxamers P188, P407 and P123 after a day. Scale bars are 10 µm. CMC, surface tension and ethylene oxide content is indicated.

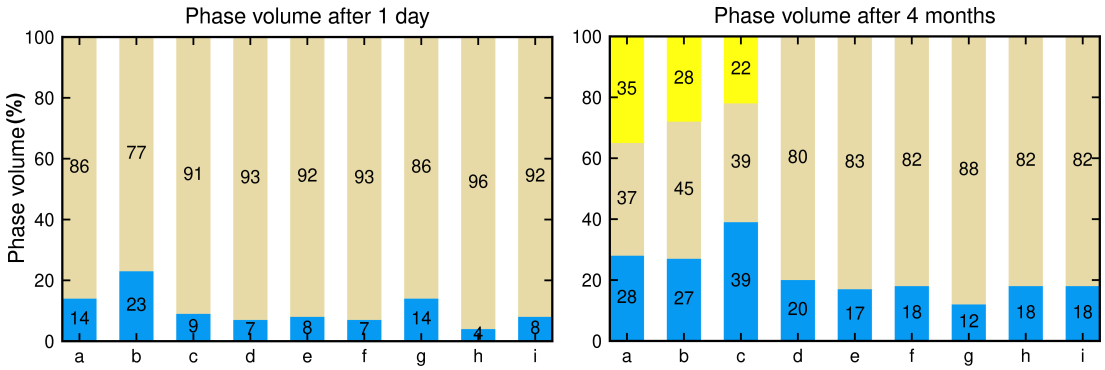

Figure 4.18: Volume of the oil phase (top, yellow), emulsion phase (middle, beige) and water phase (bottom, blue) of emulsions prepared with PEB-*b*-PCE block copolymer at 0.5 wt.% concentration and a 65:35 *n*-dodecane/water ratio after 1 day and 4 months. **a)** PEG_{50}-$iSPCE_{30}$-PEG_{50} **b)** PEG_{50}-$aSPCE_{30}$-PEG_{50} **c)** PEG_{50}-$aPCE_{30}$-PEG_{50} **d)** $iPCE_{30}$-PEG_{200} **e)** $aPCE_{30}$-PEG_{200} **f)** $iSPCE_{30}$-PEG_{100} **g)** $aPCE_{30}$-PEG_{100} **h)** $aSPCE_{30}$-PEG_{100} **i)** $iPCE_{30}$-PEG_{100}.

It was observed that lowering the ethylene oxide content of the block copolymer led to a lower CMC, larger particles, lower surface tensions and a smaller droplet size. It is then interesting to notice that the PEG-PCE synthesised behaved more like a poloxamer with a large hydrophobic block than the poloxamer it is structurally mimicking. Even compared to P123, PEG-PCEs generally showed lower surface tensions, lower CAC, large particle size, and a high propensity to form HIPEs. Overall, while the HLB of a surfactant is often used to predict the nature of the emulsion formed, the current chapter shows that use of a polycyclic hydrophobic block with similar HLB but different rigidity can drastically alter the behavior of a surfactant: lowering its CAC, modifying its self-assembly morphology and promoting the formation of high-internal phase emulsions.

4.5 Conclusion

As the demand for high-performance surfactants increases, the new PEG-polycycloether block copolymers described here stand as potent alternatives to more traditional poloxamers. They exhibit properties that could not be obtained simply by tuning poloxamer block lengths or end-groups, e.g. low CAC with high PEG content, and HIPEs in a broad range of conditions. While additional studies are required to introduce these new polymers into practical applications, these properties could lead to the development of new emulsifiers for use in the food industry, cosmetics, or biomedicine. The impact of a polycyclic middle block highlights the limitations of HLB theory, and further studies are required to understand the explicit relationship between the polycyclic structure and the stereochemistry of the polymers on their conformation in water and at interfaces. The olefin present in the unsaturated polycycloethers allows for functionalisation or cross-linking, paving the way for the preparation of smart surfactants with stimuli-responsive properties.

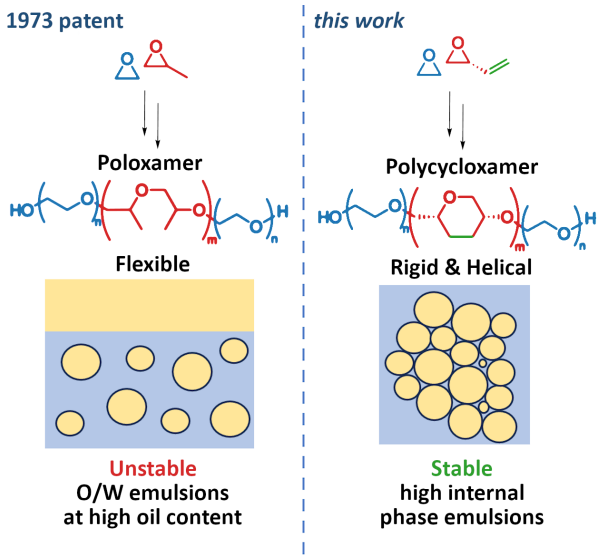

Figure 4.19: Summary of the work achieved in this chapter. Only PEG-*b*-SPCE-*b*-PEG is drawn for simplicity.

4.6 Future work on cell protection

Poloxamers are used for emulsion formulations but they are also increasingly used for the protection of cell membranes, in biomedical or bioengineering applications to reduce cell death.[186] To this end, future work will focus on the potential interactions between the synthesised block copolymers and cells or liposomes. It has already been reported in the literature that replacing the poly(propylene glycol) block with a more hydrophobic poly(butylene glycol) could improve the cell binding.[223] However this improved cell binding did not induce a better cell protection. The polycyclic structure of the PCE block could be advantageous, its high rigidity potentially leading to a reduced membrane destabilisation. Preliminary tests focused on preparing liposomes out of 1-palmitoyl-2-oleoyl-sn-glycero-3-phosphocholine (POPC) as cell mimics. Nile Red was loaded in the liposome membrane; incubation with PEG-*b*-PCE for a week did not induce any decrease of Nile Red fluorescence, confirming the integrity of the liposome membrane (See Figure 4.20). Additionally, pulse-field gradient NMR experiments were performed to show that the block copolymer could effectively bind to the liposome (See Figure 4.21). The intensity of the PEG peak decreased to a lesser extent when the block copolymer was incubated with liposomes, indicating a lower diffusion coefficient and a higher mass. Since the same block copolymer was used with and without incubation with liposomes, it shows that the block copolymer was able to bind to the liposome membrane. Future tests are ongoing to study the cell protection potential of PEG-*b*-PCE.

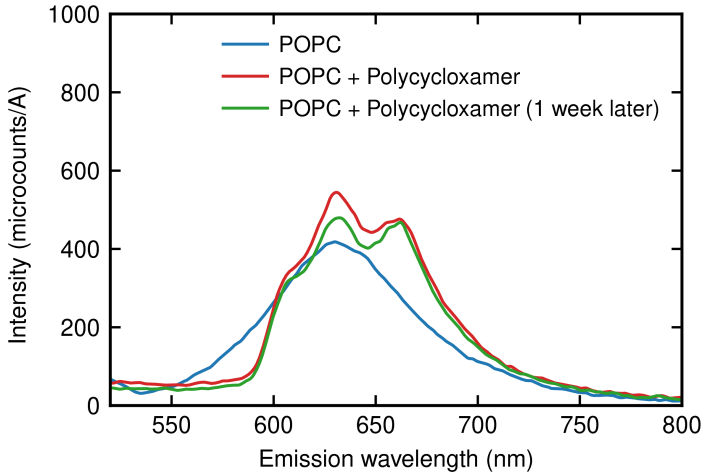

Figure 4.20: Fluorescence spectrum of Nile Red loaded POPC liposomes, after and before incubation with PEG-*b*-PCE block copolymers.

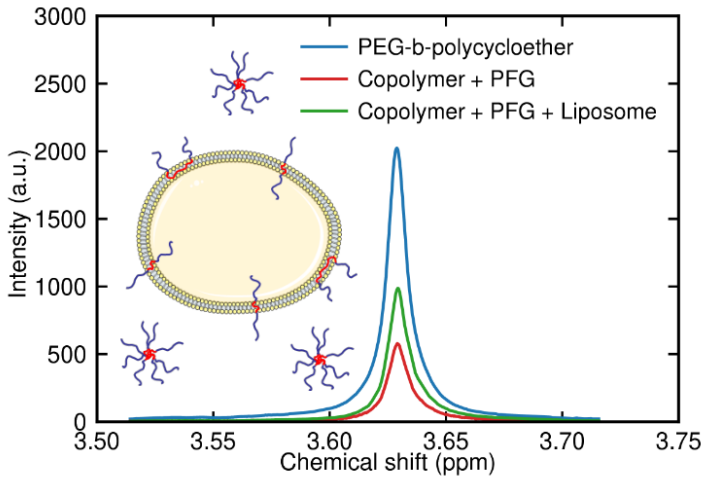

Figure 4.21: ^{1}H NMR spectrum focused on the PEG peak of the PEG-*b*-PCE block copolymer in D_2O, before (blue line, start of the DOSY experiment) and after applying the pulse-field gradient, with (green line, end of the DOSY experiment, decreased intensity proportional to the diffusion coefficient) and without (red line) incubation with liposomes.

Chapter 5

Synthesis of polycyclic cationic polymers

5.1 Introduction

Cationic polymers are a broad class of materials that can be used in a variety of applications, from adhesives to antibacterial agents.[224–228] Recently, a lot of attention has been put into using cationic polymers as a non-viral vector.[16,229,230] Indeed, plasmid DNAs being negatively charged, they can complex with positively charged polymers to form a neutral polyplex. These polyplexes can be used in gene therapy to improve the delivery of these nucleic acid-based therapeutics. The most commonly used cationic polymer is poly(ethylene imine) (PEI).[15] PEI can be synthesised as a linear or branched polymer with varying molecular weights. One issue with PEI is that it is not functionalisable, leading to a fixed number of positive charges per repeating units. This density of positive charges is an important factor for an efficient gene delivery system as it impacts the complexation efficiency of the polymer.[150] It also affects the cell permeation efficiency, as well as the endosomal escape and subsequent release of the gene. Too many positive charges would lead to a cytotoxic polymer, unable to release the complexed DNA. Too little negative charges would lead to complexation issues and a poor endosomal escape.[231] In this chapter, the goal was to use a polycycloether as a platform to access different cationic polymers via post-polymerisation functionalisations (See Figure 5.1). These polymers have a polycyclic structure, which is a structural feature that has not been extensively studied in the past. Additionally, it has been reported that helical transfection agents might improve the cell penetration of a gene delivery system.[232] The synthesised isotactic PCE being helical, we hypothesised that the different cationic polycycloethers we obtain may have unique properties as DNA vectors.

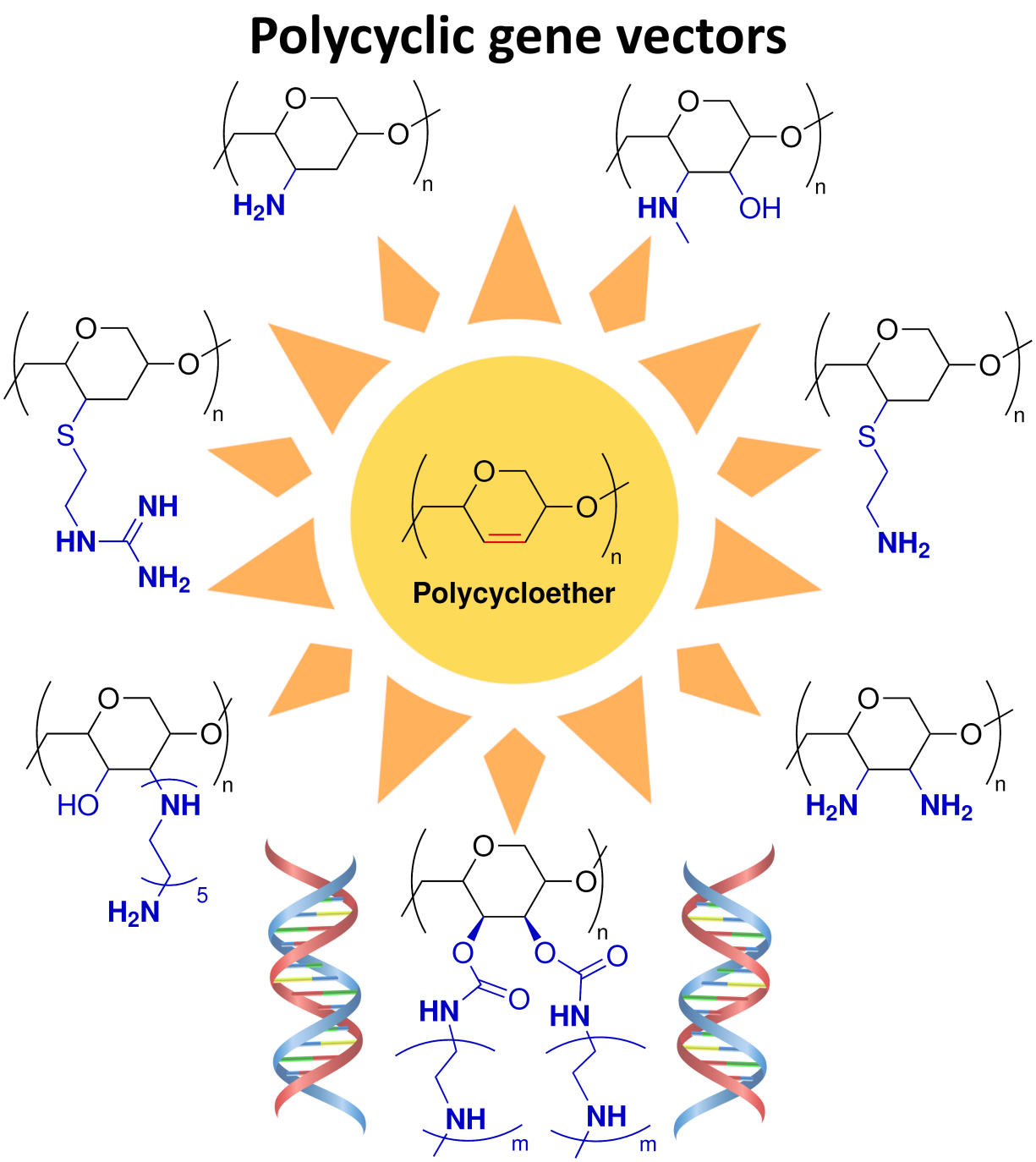

Figure 5.1: Structures of the different cationic polymers synthesised from a functionalisable polycycloether for transfection applications.

5.2 Post-polymerisation functionalisation of a polycycloether

5.2.1 Hydroaminated PCE

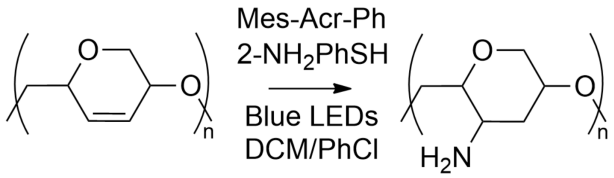

Figure 5.2: Scheme for the synthesis of a hydroaminated PCE.

The first post-polymerisation functionalisation of PCE exploited the reactivity of the internal alkene towards radicals (See Figure 5.2). *N*-phenyl-9-mesityl 2,7-dimethylacridinium tetrafluoroborate was used as a metal-free catalyst along with blue light to catalyse the reaction between PCE, ammonium carbonate and 2-aminothiophenol.[233] The reaction allowed the introduction of primary amines on the main polymer backbone. Characterisation via ^{1}H NMR revealed that full conversion was never achieved, as alkene peaks were still present (See Figure 5.3). The incomplete conversion of the polymer led to the insolubility of the polymer in water. The water solubility was improved by doing the osmium dihydroxylation of the remaining olefins but this led to a low number of cationic charges on the polymer. The theoretical number of amino groups is already low, with a single amino group for every repeating unit, so an incomplete conversion might lead to too little charges for an efficient gene complexation.

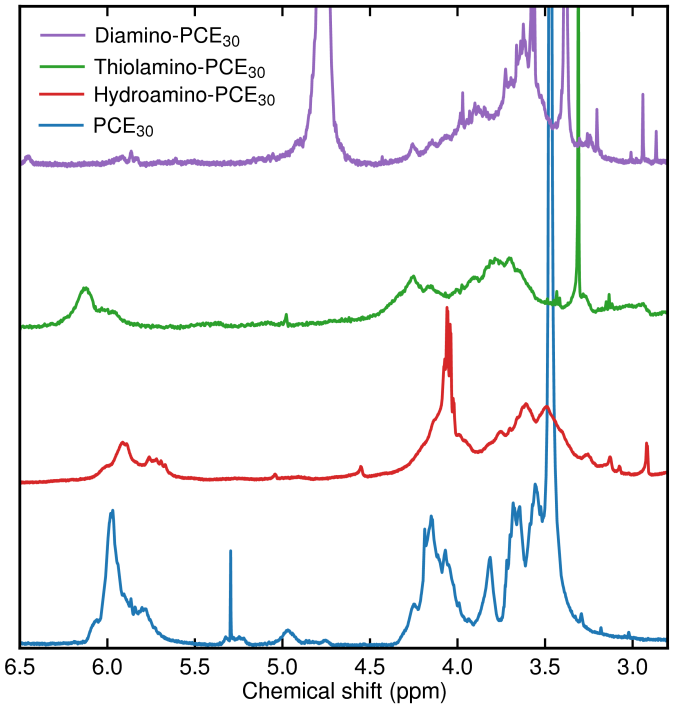

Figure 5.3: ^{1}H NMR of PCE_{30} in $CDCl_3$, Hydroamino PCE in $CDCl_3$, Thiolamino PCE in CD_3OD and Diamino PCE in D_2O.

5.2.2 Thiol-ene functionalisation and guanidinium PCE

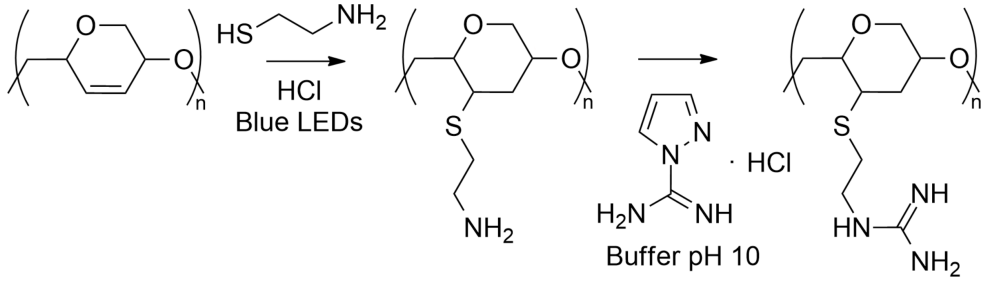

Figure 5.4: Scheme for the synthesis of a thiol or guanidinium-functionalised PCE.

The reactivity of the internal alkene towards radicals was further explored by using thiol-ene reactions (See Figure 5.4). Blue light was used as well as 2-aminoethanethiol but a poor conversion (52%) was again confirmed by ^{1}H NMR (See Figure 5.3). The poor conversion once again resulted in a poor water solubility and a low amount of cationic charges. Two reasons could explain this modest conversion. Blue light catalysed reactions are sometimes dependant on the system used for the irradiation, so the low power output of our system could have impeded the kinetics of the reaction. However, trials were performed using azobisisobutyronitrile (AIBN) as a more traditional radical initiator but the conversion was still low. This leads to the second and most plausible explanation: internal alkenes are not as reactive as external alkenes. This is an issue since the novelty of the synthesised polymer structure lies in its polycyclic structure that implies internal olefins. Radical reactions are then probably not the best way to functionalise a polycycloether. However, in an attempt to increase the water solubility and charge density of the polymer, the free amino group was converted in a guanidinium group. This time the reaction was successful with a good conversion, but the solubility issue remained.

5.2.3 Diamino PCE

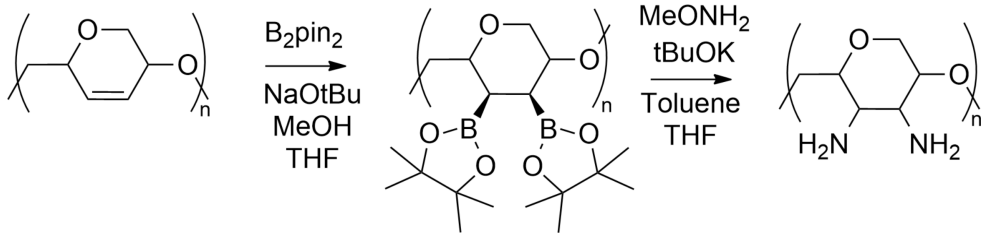

Figure 5.5: Scheme for the diboration of PCE and the synthesis of a diamino PCE.

The insufficient conversion of radical reactions forced us to reconsider our strategy. To this end, the PCE was first submitted to a diboration then it further reacted with methoxyamine and potassium *tert*-butoxide (See Figure 5.5).[234] A diamino PCE was obtained with full conversion (See Figure 5.3). The relatively good water solubility of the polymer led us to believe that it could consequently be tested for transfection tests.

5.3 Biocompatibility and transfection

Before transfection tests were performed, the biocompatibility of the newly synthesised cationic polymers was assessed. Cationic polymers usually run the risk of being cytotoxic. This cytotoxicity is generally due to the cationic charges that can potentially disrupt the integrity of cell membranes, leading to cell death.[225] The biocompatibility of four cationic polymers was then evaluated (See Figure 5.6). Surprisingly, the cell viability remained high even at high concentration (500 µg/mL). Even though it slightly decreased, it remained above 80%. The cell viability reached 120% in the case of the guanidinium functionalised PCE. While this behaviour is peculiar, it has been reported that in some cases a cell population can show increased growth when a polymer is introduced. However, visual inspection of the cells showed that aggregates were formed in the case of the poorly water-soluble cationic polymers (hydroamino PCE, thiolamino PCE and guanidinium PCE). This aggregation might be the reason for the unconventionally high biocompatibility of the synthesised cationic polymers. Nevertheless, as the water-soluble diamino PCE also performed relatively well (88% cell viability at 500 µg/mL), some transfection tests were carried out.

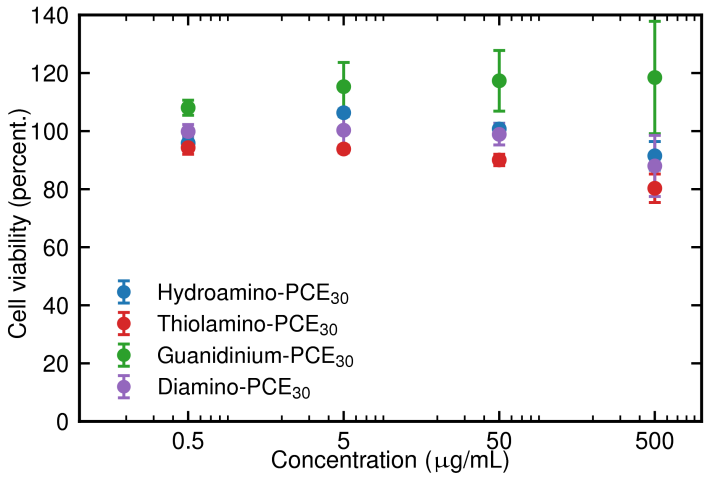

Figure 5.6: Human hepatocellular carcinoma cell viability after incubation with hydroamino-PCE_{30}, thiolamino-PCE_{30}, guanidinium-PCE_{30} and diamino-PCE_{30} with a concentration of 0.5, 5, 50 or 500 µg/mL in a humidified incubator at 37°C under 5% CO_2. Cell studies were performed with the collaboration of Emmanuelle Acs and Jesko Koehnke. Bar plots are available in the appendix, see Figure 7.25.

The nature of the transfection test consisted in mixing one of the four synthesised cationic PCE with a gene that contained the information needed by the cell to produce a fluorescent protein. The cells were then observed using a confocal microscope. If fluorescent cells were visible, it meant that the cationic polymer was able to complexe the gene, cross the cell membrane, perform the endosomal escape and release the gene to the nucleus. A control sample was performed using poly(ethylene imine). The control sample showed fluorescent cells but none of

the PCE showed any photoluminescence at all. At this point, it is hard to tell at which step of the transfection issues arised. Taking into account the poor water solubility of the PCEs and their low cationic charge density, this result is not surprising and orients us towards the synthesis of polymer containing more amino groups.

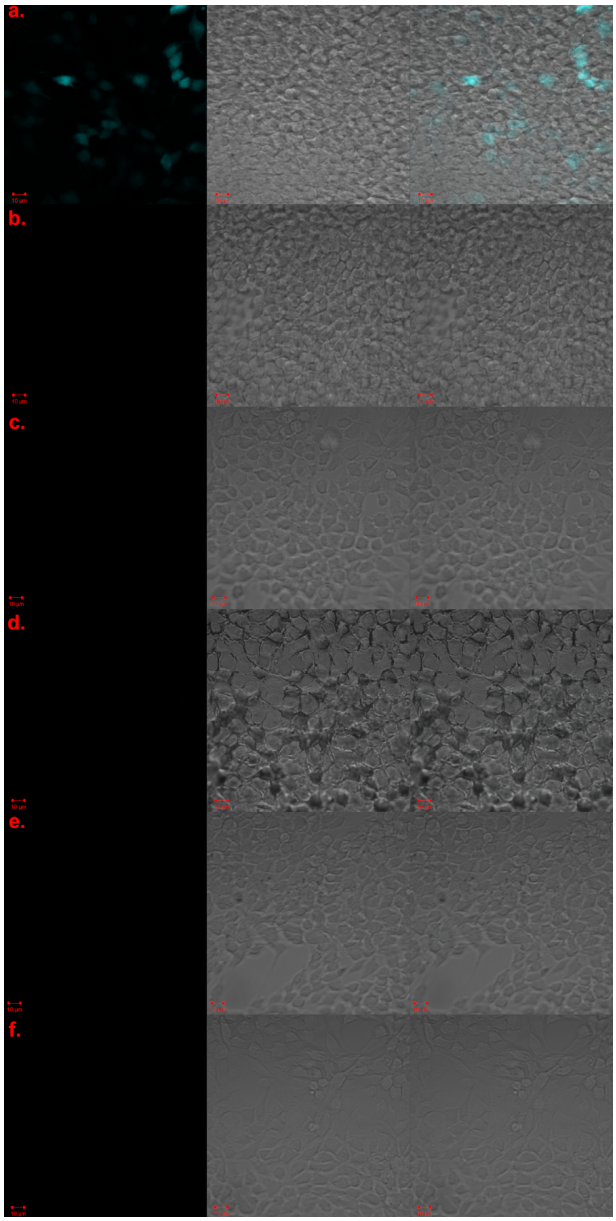

Figure 5.7: Confocal microscope images of **a)** positive control (cells incubated with the fugene transfection agent), **b)** negative control (cells incubated without any polymer, **c)** cells incubated with diamino-PCE_{30}, **d)** thiolamino-PCE_{30}, **e)** guanidinium-PCE_{30} and **f)** hydroamino-PCE_{30}. For each sample, the fluorescence, bright-field and merged images are shown. The images were obtained with the help of Emmanuelle Acs.

5.4 Additional post-polymerisation functionalisations

5.4.1 Epoxidation and subsequent ring-opening

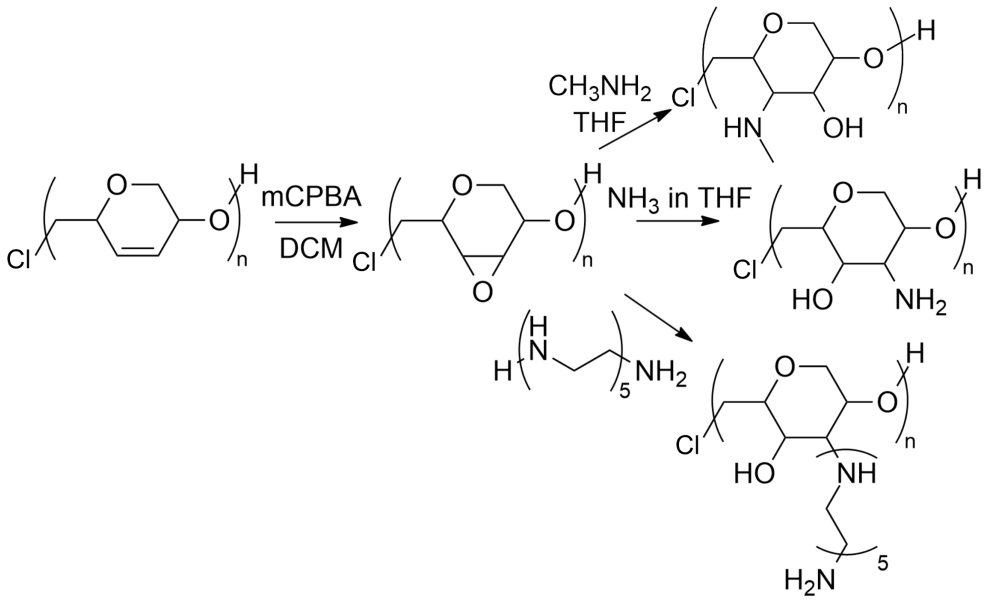

Figure 5.8: Scheme for the epoxidation of PCE and subsequent ring-opening reactions.

In order to add functional groups more easily to polycycloethers, the epoxidation of olefins has been performed using *meta*-chloroperoxybenzoic acid (mCPBA) (See Figure 5.8). A good conversion was obtained but the epoxide was found to be relatively unstable in regards to air and moisture. The polymer solubility shifted from being soluble in organic solvents to water-soluble as it was progressively hydrolysed. The subsequent ring-opening of the epoxide with a nucleophile was then performed in situ. The epoxy PCE is a good platform to access a lot of different functionalities, the epoxide can potentially be opened by a wide range of nucleophiles such as alcohols, thiols or amines. As a first step, methylamine was used to open the epoxy PCE. Compared to the hydroamino PCE, a secondary amine is obtained but a hydroxyl group is also added, which improves the water solubility of the resulting polymer. A good conversion was obtained, with no alkene peak remaining on ^{1}H NMR (See Figure 5.9) and the polymer was water-soluble. Pentaethylene hexamine was also used as a nucleophile to open the epoxy PCE and gave similar results as methylamine, meaning a good conversion (See Figure 5.9) and a water-soluble polymer.

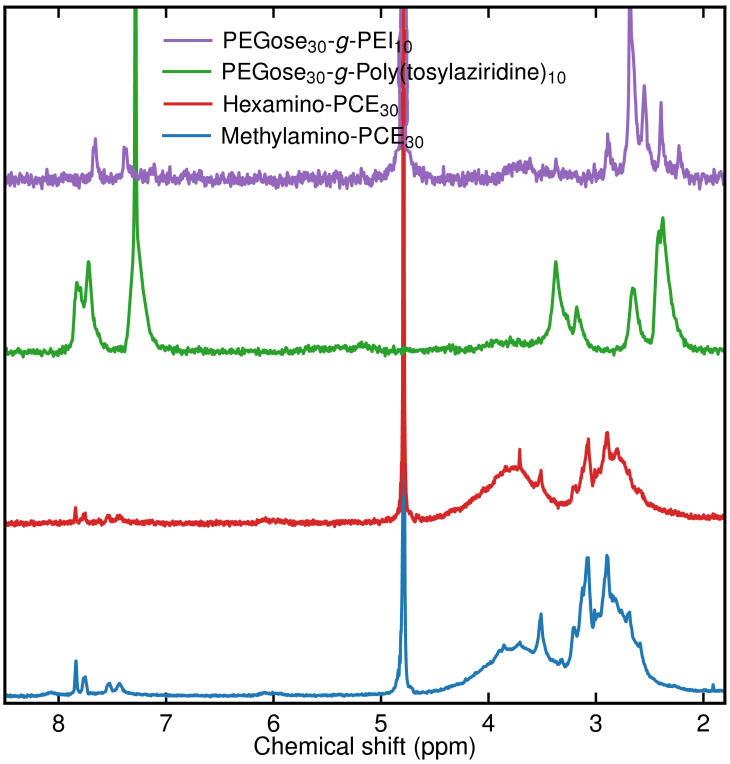

Figure 5.9: ^{1}H NMR of methylamino-PCE$_{30}$, hexamino-PCE$_{30}$ and PEGose$_{30}$-*g*-PEI$_{10}$ in D_2O. ^{1}H NMR of PEGose$_{30}$-*g*-Poly(tosylaziridine)$_{10}$ in $CDCl_3$. Small peaks in the phenyl region between 7 and 8 ppm correspond to traces of tetraphenylporphyrin catalyst impurities.

5.4.2 PEGose-*g*-poly(ethylene imine)

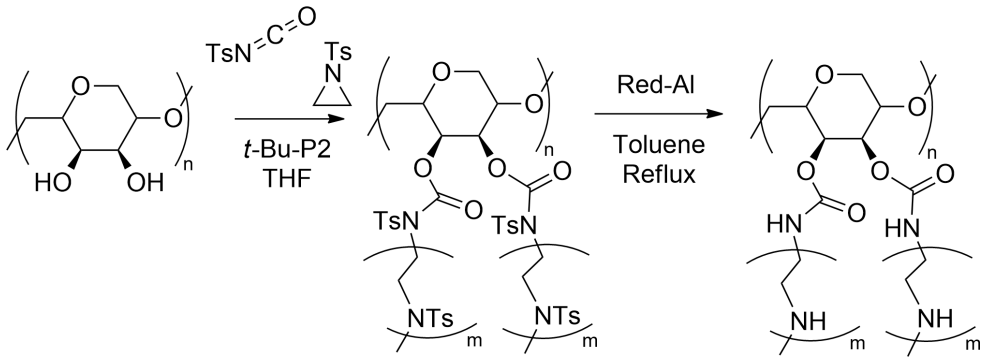

Figure 5.10: Scheme for the synthesis of PEGose-*g*-PEI.

Finally, in order to add even more cationic charges to this polycycloether backbone, the ring-opening polymerisation of a tosyl protected aziridine was undertaken, using PEGose as a macroinitiator (See Figure 5.10). The aziridine was protected with a tosyl group in order to obtain a linear poly(ethylene imine) side-chain, instead of branched one. PEGose was obtained through the osmium dihydroxylation of PCE as described in previous chapters. The base used for this anionic ROP was a phosphazene base P_2-*t*-Bu. *p*-Toluenesulfonyl isocyanate was

used to improve the nucleophilicity of PEGose, as hydroxyl groups are normally not suitable for the ring-opening polymerisation of aziridines. After the reaction, the solubility of the polymer shifted from being water-soluble to soluble in organic solvents, which allowed for mass determination by size-exclusion chromatography in THF (See Figure 5.11).

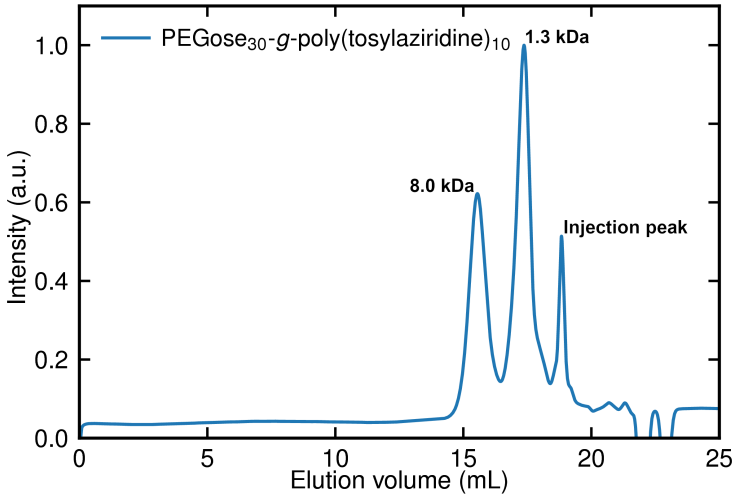

Figure 5.11: SEC trace of PEGose$_{30}$-*g*-poly(tosylaziridine)$_{10}$ measured in THF.

PEGose$_{30}$ homopolymer has a mass of 4.4 kDa. SEC trace of PEGose-*g*-PEI shows two majors peaks, a first peak at 8.0 kDa with a dispersity of 1.12 and a second peak at 1.3 kDa with a dispersity of 1.15. The first peak could correspond to the graft copolymer while the second peak could correspond to poly(tosylaziridine) homopolymers. These homopolymer chains may come from the ring-opening polymerisation of tosylaziridines monomers initiated by traces of water. The mass increase from 4.4 kDa to 8.0 kDa confirms that some of the hydroxyl groups from PEGose were able to initiate the ROP of tosylaziridine monomers. ^{1}H NMR in $CDCl_3$ showed the presence of phenyl protons from the newly added tosyl groups (See Figure 5.9). To obtain a hydrophilic graft copolymer, the tosyl groups were removed using sodium *bis*(2-methoxyethoxy)aluminium hydride (Red-Al) as a hydride reductant. Full deprotection of the tosyl groups could not be achieved but the 85% conversion rate obtained is in agreement with previously reported values in the literature on polytosylaziridine homopolymers.[235] DOSY ^{1}H NMR showed the same diffusion coefficient for PEGose peaks as for PEI peaks, confirming the copolymer structure and potentially the purification of low-mass PEI homopolymers that could have been formed due to traces of water in the reaction mixture. (See Figure 5.12). Despite the incomplete deprotection of poly(tosylaziridine) side-chains, the copolymer was water-dispersible and might be used as a transfection agent.

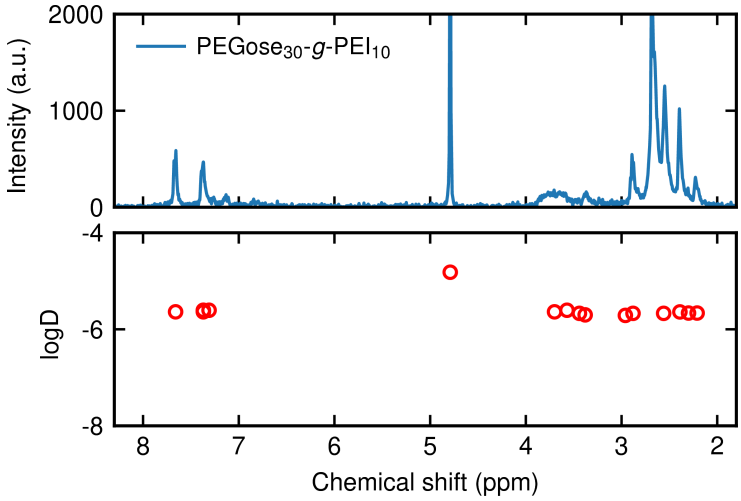

Figure 5.12: DOSY ^{1}H NMR of a-PEGose$_{30}$-*g*-PEI$_{10}$ in D_2O.

5.5 Conclusion and future work

In conclusion, a broad range of polycyclic cationic polymers has been synthesised. These polymers have a varying amount of nitrogen, from 1 to 10 nitrogen atoms per 6-membered rings. They were synthesised via radical reactions, diboration intermediates, ring-opening polymerisation or epoxidation and subsequent ring-opening. Radical reactions yielded unsatisfactory conversion rates while other reactions were more efficient. Increasing the number of nitrogen atoms per repeating units shifted the solubility of the PCE from organic solvents to water. Initial transfection results were negative but the more soluble PCEs with an increased amount of cationic charges still need to be tested. The design of the test may also need to be reworked, with more emphasis on the length and charge density of the polymer used to ensure a good fit between the polymer and the nucleic acids. Additional tests might also be needed to measure quantitatively the number of charges on the polymer in respect to pH. Moreover, dynamic light scattering characterisation of the polyplex might provide some preliminary data to confirm the complexation of the peptide with the cationic polymer. Finally, to increase even more the number of cationic charges on the polymer backbone, the synthesis of a polycyclic aziridine is underway.

Chapter 6

Conclusion

The ring-closing metathesis reaction has been previously reported as a post-polymerisation functionalisation tool to access an unusual polycycloether structure.[74] While this polymer discovery could have been kept at the stage of scientific curiosity, the goal of this research was to leverage this singular structure into materials with unique properties.

Firstly, PEGose-PLA block copolymers were synthesised. The introduction of a polycyclic hydrophilic block allowed the preparation of highly stable nanoparticles, capable of encapsulating and steadily releasing both hydrophilic and hydrophobic cargoes. The developed PEGose-PLA nanoparticles were shown to be an efficient PEG-free drug delivery system. Secondly, controlling the tacticity of the polycyclic block led to polymeric nanoparticles with a rare cubical morphology. Dynamic morphological changes could be obtained in response to different salt concentration stimuli. The reportedly advantageous properties of anisotropic nanoparticles are another argument towards the use of PEGose-PLA systems for biomedical applications. Thirdly, polycycloether-PEG block copolymers were synthesised and used as surfactants. Their structure mimicked the ubiquitously used Poloxamers, but the introduction of a rigid helical block led to unexpected behaviours. While normally hard to achieve, high-internal phase emulsions were obtained at low concentrations, irrespective of the oil/water ratio used. Additionally, liposome membrane binding experiments suggest potential use for cell protection and bioengineering applications, with biological tests currently ongoing. Finally, polycyclic cationic homopolymers were synthesised with a tunable amount of cationic charges. Although more work is underway, this paves the way for the synthesis of novel polymeric gene vectors.

In conclusion, the state of the art on cyclopolymers has been improved, via the expansion of the current library of cyclopolymers but also through the discovery of their unusual properties for various applications. Future work should focus on deepening our understanding of the polymer structure and its relation to self-assembly morphologies. Additional biological tests could be performed, like drug delivery with doxorubicin to kill cancer cells. More cationic polymers could be synthesised, with a focus on polyaziridines and additionnal transfection tests.

Chapter 7

Experimental

7.1 Materials

Benzaldehyde (>99%), calcium hydride, DL-lactide, D-lactide, L-lactide, *n*-dodecane, *N*-methylmorpholine *N*-oxide, phenylboronic acid, potassium osmate, propionic acid, pyrrole (98%) and stannous octoate were obtained from Alfa Aesar. 2-Aminoethanethiol hydrochloride, 2-aminothiophenol, ammonium carbonate, benzylamine, benzyl chloroformate, chlorobenzene, diethylaluminum chloride solution in hexane (1 M), 2,2-dimethoxy-2-phenylacetophenone, ethylene oxide solution in THF (2.5 M), *H*-pyrazole-1-carboxamidine hydrochloride, lithium aluminum hydride solution in THF (1 M), mesyl chloride, methoxyamine (2.0 M in THF), *meta*-chloroperoxybenzoic acid, *N*-phenyl-9-mesityl 2,7-dimethylacridinium tetrafluoroborate, palladium on activated carbon (10% wt), pentaethylene hexamine, phosphazene base P2-*t*-Bu solution (2.0 M in THF), potassium *tert*-butoxide, *p*-toluenesulfonyl chloride, *p*-toluenesulfonyl isocyanate, rhodamine B, sodium *bis*(2-methoxyethoxy)aluminium hydride (Red-Al), sodium hydride (60% dispersion in mineral oil) and silver nitrate (>99%), were obtained from Sigma-Aldrich. Grubbs II catalyst (>97%) was purchased from Carbosynth. (-)-(*R*,*R*)-*N*,*N'*-*bis*(3,5-di-*tert*-Butylsalicylidene)-1,2-cyclohexanediaminocobalt(II) (98%), acetic acid (>99%) and 1,2-dichloroethane (99.8%, extra dry) were obtained from Fisher Scientific. Gibco™Minimum Essential Medium (MEM) medium, Gibco™fetal bovine serum (FBS) and Gibco™0.25% trypsin-EDTA (1x), Gibco™MEM non-essential amino acid solution (100x) (without L-glutamine), Gibco™L-glutamine solution (200 mM), Gibco™penicillin-streptomycin (with 10,000 units penicillin and 10 mg streptomycin/mL), Gibco™Phosphate Buffered Saline (10x) (PBS) solution were purchased from Fisher Scientific. AlamarBlue™Cell Viability Reagent and Prolong™Antifade Glass mountant were purchased from Invitrogen. 4% Formaldehyde in PBS was purchased from ChemCruz. 96-Well cell culture microplates were obtained from Corning. Cell-culture treated Nunc™Lab-Tek™II Chamber Slide™systems for microscopy sample preparation were purchased from Thermo Fisher Scientific. Dry tetrahydrofuran (THF), dry dichloromethane (DCM), and dry toluene were obtained using an

in-house solvent purification system (Pure-SolvTM 500 Solvent Purification System). Other solvents were purchased from Fisher chemicals and were HPLC-grade. Butadiene monoxide (Alfa Aesar, 98%) was dried over calcium hydride for 24 h under reflux and distilled under an atmosphere of argon. DL-lactide, D-lactide and L-lactide were purified by recrystallisation from ethanol followed by another recrystallisation from ethyl acetate. Reactions involving air-sensitive agents and dry solvents were performed in glassware that had been oven-dried (150°C) or flame-dried prior to use. These reactions were carried out with the exclusion of air using an argon atmosphere. Preparative size-exclusion chromatography (SEC) was performed under forced flow conditions using HPLC graded solvents and Sephadex LH-20 (Alfa Aesar) as solid support. Rochelle salt solution (10%) was prepared by dissolving potassium sodium tartrate tetrahydrate (Sigma-Aldrich) in deionised water.

7.2 Characterisations

^{1}H NMR and DOSY spectra were recorded on either a Bruker AVI DPX-400 or a Bruker DPX-400 (400 MHz) instrument. The chemical shifts are expressed in parts per million (ppm) referenced to TMS. $CDCl_3$, D_2O and DMSO-d_6 were used as solvent. Diffusion-Ordered Spectroscopy (DOSY) was performed using the ledbpgp2s pulse sequence. High viscosity solvents such as D_2O and DMSO-d_6 were favored to reduce convection effects. The maximum gradient power used was 50 G/cm, the diffusion delay D20 was 0.08 sec, the diffusion gradient pulse length P30 was 3000 µsec, 16 gradient steps were performed with 64 scans for each.

Size-exclusion chromatography (SEC) was conducted in THF at 35°C using a column system with an Agilent PL Gel Guard Column (5 µm) and an Agilent PL Gel Mixed-D Column (5 µm) as well as an Agilent Infinity1260 II RID and calibration with poly(styrene) standards.

Dynamic light scattering (DLS) measurements on PEGose-*b*-PLA nanoparticles were performed on a ZetaSizer by Malvern with HPLC-grade water as solvent.

Multi-angle dynamic light scattering (MADLS) measurements were performed using an Anton Paar Litesizer 500 using forward scattering (15°), side scattering (90°) and back scattering (175°). The light source was a semiconductor laser diode at 40 mW, 658 nm. All experiments were performed three times and the average size distribution was calculated.

Transmission electron microscopy (TEM) experiments were performed on a JEOL 1200 EX TEM running at 80 kV, tiff images were captured using a Cantega 2K X 2K camera and Olympus ITEM Software. To prepare negative stained samples: suspension droplets (5 µL) were placed on top of the surface of Carbon coated 400 mesh copper grids which were

previously Glow discharged using a Quorum Q150T ES High vacuum system. Samples were left for 5 min to allow attachment, then grids were floated sample side down three times for 30 secs each onto distilled water droplets before negative staining with 2% aqueous uranyl acetate for 5 min then allowed to air dry. To prepare unstained samples, droplets (5 µL) were placed on top the surface of carbon coated 400 mesh copper grids, which were previously Glow discharged using a Quorum Q150T ES High vacuum system. Samples grids were left to air dry before imaging.

Small-Angle X-Ray Scattering (SAXS) scattering curves (See Figure 7.7) were obtained by Daniel McDowall using the beamline B21: high-throughput small-angle X-ray scattering at Diamond Light Source.[236]

Scanning Electron Microscopy (SEM) imaging was performed using a Philips/FEI XL30 ESEM Environmental Scanning Electron Microscope. A drop of nanoparticle solution was evaporated overnight at room temperature then coated with gold using a Polaron SC7640 auto/manual high resolution sputter coater. Chemical composition of the material was done using an Oxford Instruments Energy 250 energy dispersive spectrometer system (EDS) attached to the SEM. Additional SEM images were obtained using a Carl Zeiss Sigma variable pressure analytical SEM with Oxford microanalysis.

Samples for **cryogenic transmission electron microscopy (cryo-TEM)** were prepared by applying a 4 µl droplet of sample suspension to lacey carbon copper grids (200 mesh, Science Services) and plunge frozen into liquid ethane using a Vitrobot Mark IV (FEI, Eindhoven, Netherlands) set at 4°C and 95% humidity. The grids were mounted on a cryo transfer holder (Gatan 914, Gatan, Munich, Germany) and transferred into a JEOL JEM-2100 (JEOL GmbH, Eching, Germany) transmission electron microscope for imaging. The microscope was operated at an acceleration voltage of 200 kV and micrographs were recorded with a bottom-mounted 4 × 4k CMOS camera (TemCam-F416, TVIPS, Gauting, Germany) at a magnification of 50 000×, corresponding to a pixel size of 2.32 Å at the specimen level. Total electron dose for each micrograph was kept below 15 $e^{-}/Å^{-2}$.

High-resolution mass spectrometry (HRMS) was performed on a Bruker microTOFq High Resolution Mass Spectrometer using an Electrospray (ESI) ion source coupled to a time-of-flight (ToF) analyser.

Powder X-Ray diffraction (PXRD) was performed using a Rigaku MiniFlex equipped with a Cu sealed tube X-ray source, a Kβ foil filter and a NaI scintillator.

Inductively coupled plasma mass spectrometry (ICP-MS) experiments were made on an Agilent 7500ce ICP-MS fitted with a self-aspire Teflon nebuliser doing 10 repeats per peak on masses 101, 102 and 104. Concentrations were calculated against Ru standard Alfa Aesar Specpure®.

Emulsion droplets formed with PCE-*b*-PEG block copolymers were analysed using a Leica DM750 binocular **optical microscope** without any dilution. Double hydrophilic block copolymer solutions in water were imaged using a VisiScope IT406 inverted trinocular LED fluorescence microscope by VWR. Size distribution was collected using ImageJ software.

LogP values were calculated using the MolInspiration software.

Enantiopure butadiene monoxide optical rotation was measured using an Autopol III **Polarimeter**, with a mean value obtained through 5 measurements.

Surface tension values were measured by using an Ossila contact angle goniometer. Block copolymer solutions in water were prepared with a fixed concentration of 0.5 wt% and analysed at ambient temperature. For each solution, shape analysis was performed on three drops, using 5 different frames for each drop, the surface tension value was then averaged.

Hydrophilic-Lipophilic Balance (HLB) values were calculated using Chemaxon HLB predictor through the MarvinSketch software, using Griffin's method.

Circular dichroism studies were performed on a Chirascan circular dichroism spectrometer. Temperature was kept at 20°C, spectra were recorded in triplicates from 180 to 260 nm, with an acquisition time of 1.0 s and a wavelength step increase of 1 nm. The sample concentration was kept at 0.1 mg/mL.

Fluorescence spectroscopy studies were made on a Horiba Duetta Bio fluorescence and absorbance spectrometer. A blank was used before each experiment. Both blank and sample absorption spectra were recorded before each experiment to correct the Inner Filter Effect. Nile Red fluorescence was observed with an excitation wavelength of 435 nm and the emission wavelength was recorded from 445 to 800 nm. Integration time was 0.1 s, detector binning was 0.5 nm (1 pixel). Excitation and emission bandpass were 5 nm. The CAC of each PCE-*b*-PEG block copolymer was measured by fluorescence spectroscopy using pyrene as a fluorescence probe as described in the literature.[218] Measurements were made on a Horiba Duetta Bio fluorescence and absorbance spectrometer. A blank consisting of deionised water was used before each experiment. Block copolymer solutions of different concentrations were prepared

in water, before adding 12 µL of a 0.5 M pyrene solution in ethanol. Both blank and sample absorption spectra were recorded before each experiment to account for the Inner Filter Effect. Excitation wavelength was fixed at 334 nm and emission wavelength was recorded from 360 to 450 nm. Integration time was 0.1 s, detector binning was 0.5 nm (1 pixel). Excitation and emission bandpass were 5 nm. Peak intensity was measured at 372 nm (I_1) and 384 nm (I_3). CAC was determined by plotting the I_3/I_1 ratio against the block copolymer concentration and reading the intersection of the regression trendlines at low and high concentrations.

UV-Vis spectroscopy measurements were performed using a Shimadzu UV Mini 1240 UV-vis Spectrophotometer, at ambient temperature. To calculate Rhodamine B encapsulation efficiency, after removing unloaded dye through dialysis, absorbance was measured through a UV-Vis spectrometer, an empty nanoparticle solution was used as a blank. The time needed to remove all unloaded dyes was determined by doing the dialysis of a solution of pure Rhodamine B in water and measuring the time needed to reach a near zero absorbance.

$$Rhodamine\ B\ encapsulation\ efficiency\ (\%) = \frac{sample\ absorbance}{reference\ absorbance} * 100 \qquad (7.1)$$

Rhodamine B release profiles were performed by keeping empty and loaded nanoparticles solution in a 10 kDa MWCO dialysis bag with a 1000-fold excess volume of deionised water, changing the water twice a day. The absorbance was measured and compared with an empty nanoparticle solution as a reference. Nile Red encapsulation efficiency was determined after removing insoluble residues, the water solution was evaporated then solubilised in DMSO and sonicated for 15 minutes then stirred overnight. Fluorescence intensity was then measured and compared to the Nile Red DMSO reference solution.

$$Nile\ Red\ encapsulation\ efficiency\ (\%) = \frac{sample\ fluorescence\ intensity}{reference\ fluorescence\ intensity} * 100 \qquad (7.2)$$

Nile Red release profile was determined by measuring the fluorescence intensity of the samples over time and comparing it to the fluorescence intensity just after removing unloaded Nile Red.

$$Remaining\ Nile\ Red\ content\ (\%) = \frac{fluorescence\ intensity\ t_0}{fluorescence\ intensity\ t} * 100 \qquad (7.3)$$

7.3 Methods

Nanoparticle preparation

Typical procedure to obtain 100-150 nm PEGose-PLA nanoparticles: PEGose-*b*-PLA block copolymer was dissolved in DMSO (0.6 mL) with a concentration of 10 mg/mL then 2 mL of deionised water was added dropwise very slowly under stirring (250 RPM). The drop rate

was kept constant with an addition rate of 1 mL/min. The solution was then dialyzed overnight against an excess of deionised water to remove the DMSO (3.5 kDa MWCO).

Dye loading

Rhodamine B or Nile Red was solubilised in a 5 mg/mL PEGose-*b*-PLA block copolymer solution in DMSO, and 2 mL of deionised water was added dropwise. The Rhodamine B solution was dialyzed against a 1000-fold excess of deionised water for 4 h, the water was changed after 30 min, then every hour. Nile Red was dialyzed against a 1000-fold excess of deionised water for 4 h then filtered to remove insoluble residues.

Nanoparticle stability tests

PEGose-*b*-PLA block copolymer was dissolved in DMSO (0.6 mL) with a concentration of 10 mg/mL then 2 mL of deionised water was added dropwise very slowly under stirring. The drop rate was kept constant with an addition rate of 1 mL/min. The solution was then dialyzed overnight against an excess of deionised water to remove the DMSO (5 kDa MWCO). Buffers, enzyme or salts were added to obtain five different conditions: deionised water at ambient temperature, deionised water at 37°C, 0.1 M Tris with 0.17 mg/mL proteinase K from *Tritirachium album* at 37°C, deionised water with 10 mg/mL sodium cholate hydrate at 37°C, pH 5.5 solution prepared from diluted HCl at 37°C. Nanoparticle size distributions were monitored every day for 4 days using DLS. Additionally, for the proteinase K solution, a qualitative *p*-hydroxydiphenyl test was realised to check the presence of lactic acid or PLA oligomers. One drop of the nanoparticle solution was taken and 1 mL of concentrated sulfuric acid was added. The solution was heated to 85°C then cooled down to ambient temperature and the color of the solution inspected. A purple color would indicate the presence of lactic acid or PLA oligomers.

Biocompatibility

Human hepatocellular carcinoma cell line (HepG2, ECACC No. 85011430) was cultured in MEM medium supplemented with 10% FBS, 100 U/mL penicillin, 100 µg/mL streptomycin, 2 mM L-glutamine and 1% non-essential amino acids. All cells were grown in a humidified incubator at 37°C under 5% CO_2 and passaged in every 3 days. Cells were seeded at a density of 1.10^4 cell/well into 96-well plates and incubated at 37°C in a 5% CO_2 atmosphere. The second day, the cells were treated with the different samples (a-PEGose and PEGose-*b*-PLA) at 0.5 µg/mL, 5 µg/mL, 50 µg/mL, and 500 µg/mL and incubated for 24 h at 37°C in 5% CO_2. After the incubation period, Alamar Blue reagent was added to each well according to the manufacturer's instructions (10% v/v) and cells were incubated at 37°C in 5% CO_2 for additional 4 h. The fluorescence measurements were performed by a CLARIOstar microplate reader (BMG Labtech, Ortenberg, Germany) (λ_{exc} = 560 nm; λ_{em} = 590 nm). The percent cell viability was

calculated in reference to the untreated control cells using the following formula:

$$Cell\ Viability\ (\%) = \frac{sample\ fluorescence\ intensity}{control\ fluorescence\ intensity} * 100 \tag{7.4}$$

Cells without treatment with samples were considered as control. The percent cell viability was calculated comparing the fluorescence intensities of each well to the fluorescence intensity of the untreated cells. This assay was repeated 3 times on different passages of cells. The median value of cell viability was selected for graphical representation.

Cell permeation experiment and Confocal Laser Scanning Microscopy (CLSM)

FITC-labelled (emission wavelength λ = 493 nm) samples (PEGose homopolymer and $PEGose_{50}$-PLA_{50} nanoparticles) were dissolved in water (10 mg/mL). Samples for CLSM were prepared by seeding $2{\cdot}10^4$ cells in each well of the Nunc™Lab-Tek™II Chamber Slide™ as well as treated with polymer samples on the same day (final concentration 50 µL/mL). Cells without treatment with polymer samples were considered as control. Slides were incubated at 37°C in a 5% CO_2 atmosphere for 24 h. The second day, cells were washed with PBS (1%) and then fixed with 4% formaldehyde in PBS for 15 min before being washed twice with PBS (1%). The samples were layered with antifade mountant and a thin cover glass. Slides were left to dry, covered, in a sterile hood overnight before being stored in the dark at 4°C. CLSM and bright-field microscopy were performed on a Zeiss LSM710 confocal microscope (Zeiss, Gottingen, Germany) using software Carl Zeiss ZEN 2011 v7.0.3.286. 0.55 DIC (Carl Zeiss, White Plains, NY, USA), Neofluar 20× and N-Achroplan 10×/0.25 Ph 1 (Carl Zeiss, White Plains, NY, USA) objectives were used. The images were taken with two different channels: one for the fluorescent polymers (FITC, 486-570 nm) and one for a bright-field image of the cells.

Emulsion preparation

To prepare an emulsion, the typical procedure consisted of dissolving the polycycloether/PEG block copolymer in water, adding the oil, keeping a total volume of 4 mL, then using IKA Ultra-Turrax T18 homogeniser for 4 minutes at 13,500 rpm. Toluene and *n*-dodecane were investigated as oil types. Block copolymer concentration ranged from 0.01% to 0.5%. Oil/water ratios ranged from 5% to 90%. The nature of the emulsion (O/W versus W/O) was determined by measuring the conductivity of the emulsion as well as doing a drop test; that is, putting a drop of the emulsion either in pure oil or pure water.

7.4 Chapter 2 - PEGose-*b*-poly(lactic acid) nanoparticles for cargo delivery

Tetraphenylporphyrin - $TPPH_2$

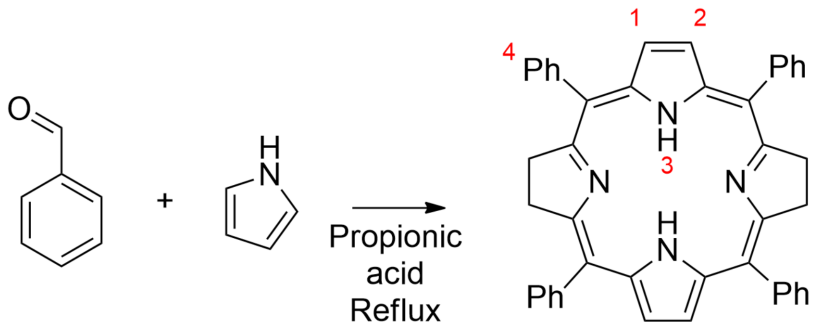

$TPPH_2$ was synthesised from freshly distilled pyrrole (4.6 g, 68 mmol) and benzaldehyde (7.2 g, 68 mmol) in propionic acid (300 mL) under reflux for 4 h. The crude product was precipitated upon standing overnight at ambient temperature, filtered and then washed with water and methanol (20 mL). The obtained crystals were recrystallised from $CHCl_3/CH_3OH$ (1:2 v/v) and dried overnight under vacuum to give $TPPH_2$[74] (2.8 g, 27% yield) as purple crystals.

^{1}H-NMR (400 MHz, $CDCl_3$) δ = 8.84 (s, 8H, H1 H2), 8.22 (s, br, 8H, H4 ortho), 7.76 (s, 12H, H4 meta para), -2.76 (s, 2H, H3).

Tetraphenylporphyrin aluminium chloride - TPPAlCl

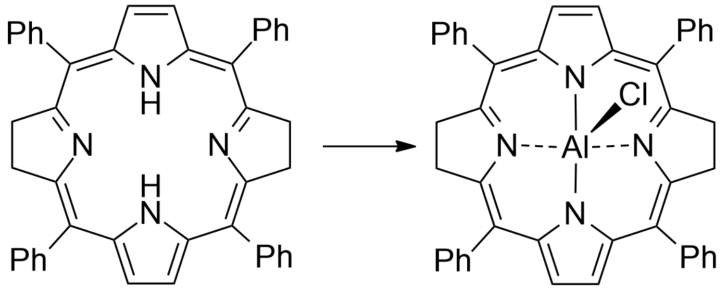

$TPPH_2$ (10 mg, 0.16 mmol) was dissolved in dry DCM (3 mL) and 1 M diethylaluminium chloride solution in hexane (1.8 mL, 1.8 mmol) was added slowly. After 3 h, the volatiles were removed in vacuo, and the product was washed with hexane and dried overnight. Without further purification, the product was used for the synthesis of PEB in the same vessel.

Synthesis of poly(epoxybutene) - PEB_{50}

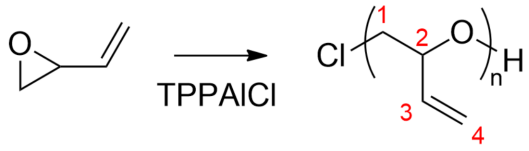

PEB was synthesised by a modified literature procedure.[74] TPPAlCl was prepared in a flame-dried Schlenk tube by dissolving $TPPH_2$ (1.35 g, 2.20 mmol, 1 equiv) in dry DCM (40 mL) and adding slowly a 1 M diethylaluminum chloride solution in hexane (2.20 mL, 1 equiv). After 3 h the volatiles were evaporated using vacuum and a N_2-cooled trap. TPPAlCl was then dried overnight. Racemic 3,4-epoxy-1-butene (14.0 g, 22.0 mmol, 100 equiv) was added the next day to the dried TPPAlCl and the resulting mixture was subsequently stirred at ambient temperature for 2 days. The mixture was quenched with a few drops of 1 M aqueous HCl under stirring. The volatiles were removed in vacuo, and the resulting polymer was dissolved in a 1:1 methanol/DCM mixture for purification by size-exclusion chromatography (Sephadex LH-20, 1:1 methanol/DCM). The fractions were concentrated, and the polymer was dried under vacuum overnight to give a brown oil (11.5 g, 82%).

^{1}H-NMR (400 MHz, $CDCl_3$) δ = 5.77-5.69 (m, br, 1H, H3), 5.33-5.13 (m, br, 2H, H4), 4.02-3.91 (m, br, 1H, H2), 3.60-3.38 (m, br, 2H, H1).
^{13}C-NMR (126 MHz, $CDCl_3$) δ = 136.2 (C3), 117.8 (C4), 80.8 (C2), 72.1 (C1).

Synthesis of polycycloether – PCE_{50}

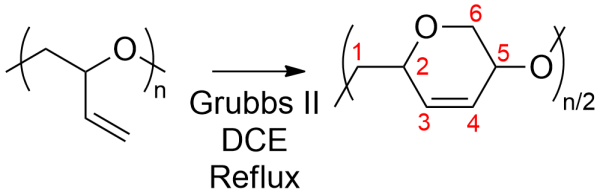

PCE was synthesised by a modified literature procedure.[74] In a large round-bottomed flask, PEB (600 mg, 0.25 M) was stirred for 15 min in 1,2-dichloroethane (38 mL) at reflux. Then, second-generation Grubbs catalyst (178 mg, 210 µmols, 2.5 mol %) in DCE (5 mL) was added slowly under argon. After 5 days, the reaction mixture was cooled to ambient temperature and 1.5 mL (100 equiv) of DMSO was added and the mixture stirred for 1 h. The volatiles were removed in vacuo, and the residue was purified using size-exclusion chromatography (Sephadex LH-20, 3:1 methanol/DCM). The volatiles were removed in vacuo, and 5 mL of DCM was added. Adapted from a literature procedure, the mixture was cooled in an ice-bath, 2.5 mL (100 equiv) of 30% aqueous hydrogen peroxide was added and vigorously stirred for 1 h. The layers were then separated and the organic phase was washed with 50 mL of an aqueous

sodium sulfite solution (100 mg/mL). The oxidative process was repeated one more time, the volatiles were removed in vacuo and the resulting PCE was dried overnight to give a grey solid (198 mg, 52%).

^{1}H-NMR (400 MHz, $CDCl_3$) δ = 6.16–5.64 (2H, H3 H4), 4.37–3.99 (2H, H2 H5), 3.92–3.30 (4H, H1 H6).
^{13}C-NMR (126 MHz, $CDCl_3$) δ = 132.0–124.0 (C3 C4), 74.1–73.2 (C5), 71.2–70.4 (C2), 70.4–69.3 (C6), 68–66.6 (C1).

Synthesis of polycycloether-block-poly(lactic acid) – PCE_{50}-b-PLA_{100}

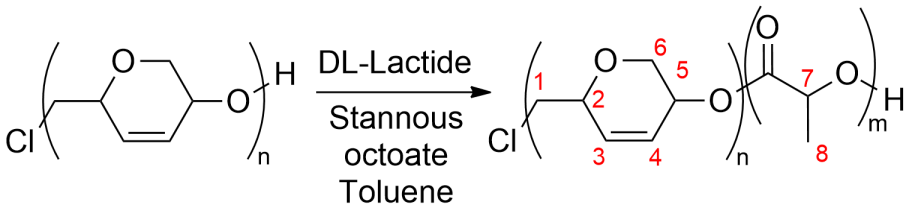

Pure DL-lactide (259 mg, 3.6 mmol, 100 equiv) and PCE (100 mg, 0.036 mmol, 1 equiv) were mixed in anhydrous toluene (5 mL) and the mixture was degassed by the freeze-pump-thaw method. Under an argon atmosphere, stannous 2-ethyl-hexanoate (5 mg, 12 µmols, 0.01 equiv) was added and the reaction mixture was refluxed in an oil bath for 3 h. Subsequently, the toluene was removed under reduced pressure, and the residue was solubilised in THF to perform purification by size-exclusion chromatography (Sephadex LH-20, THF) to give PCE-*b*-PLA as a brown oil (348 mg, 87%).

^{1}H-NMR (400 MHz, $CDCl_3$)
PCE δ = 6.16–5.64 (2H, H3 H4), 4.37–3.99 (2H, H2 H5), 3.92–3.30 (4H, H1 H6).
PLA δ = 5.25-5.10 (4H, H8), 1.70-1.45 (12H, H7).

Synthesis of PEGose-block-poly(lactic acid) – $PEGose_{50}$-b-PLA_{100}

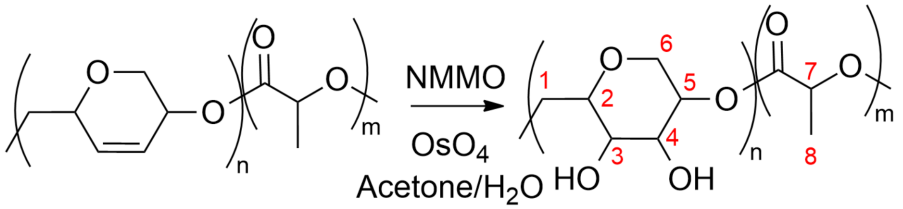

PCE-*b*-PLA (448 mg, 1.0 mmol of the PCE monomer unit) was dissolved in acetone/water (5:1, 20 mL). Dried *N*-methylmorpholine-*N*-oxide was then added to the mixture (129 mg, 1.1 mmol, 1.1 equiv). The reaction mixture was stirred in an ice bath, and then 0.1 mol % of freshly prepared OsO_4 solution (100 µL, 1% in water) was added slowly and the resulting mixture was

stirred for an additional 2 h at 0°C. The reaction mixture was then stirred overnight at ambient temperature. To quench the reaction, 126 mg (1 equiv) of sodium sulfite was added and the resulting mixture was stirred for 1 h. Water was added (20 mL) and the mixture was then dialyzed (3.5 kDa MWCO) against deionised water over 24 h, regularly changing the water. The resulting solution was evaporated to yield PEGose-*b*-PLA as a grey solid (357 mg, 74%).

^{1}H NMR (400 MHz,$(CD_3)_2SO$)
PEGose δ = 4.43–3.61 (8H).
PLA δ = 5.25-5.10 (4H, H8), 1.70-1.45 (12H, H7).

Diborated PCE

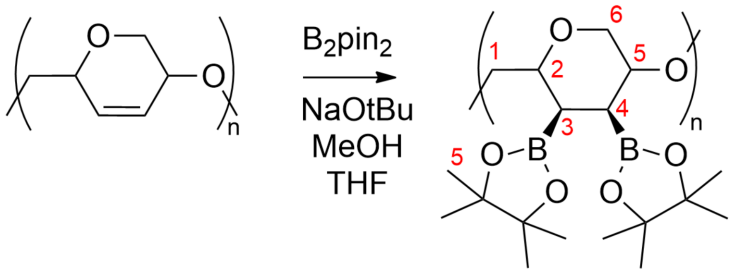

Diborated PCE synthesis was adapted from Nóvoa *et al.*[237] In a flame-dried round-bottomed flask, PCE (112 mg, 0.5 mmol, 1 equiv), B_2pin_2 (254 mg, 1.0 mmol, 2 equiv) and NaOMe (32 mg, 0.3 mmol, 0.6 equiv) were dissolved in a minimum amount of methanol and the resulting solution was refluxed overnight. The mixture was purified by SEC (Sephadex LH-20, methanol) and the volatiles were removed under vacuum to afford the diborated CPE as a brown oil (300 mg, 82%).

^{1}H-NMR (400 MHz, $CDCl_3$) δ = 4.25–3.05 (6H, H1 H2 H5 H6), 2.30-1.25 (2H, H3 H4), 1.23–1.05 (24H, H5).

Osmium-free synthesis of PEGose

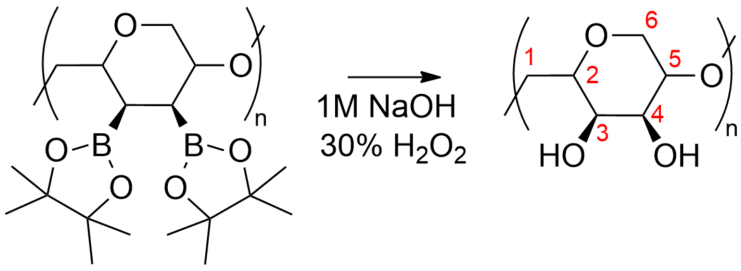

Adapted from a literature procedure.[237] Diborated PCE (100 mg, 0.27 mmol, 1 equiv) and 1 M aqueous NaOH (2.7 mL, 2.7 mmol, 10 equiv) were mixed. Then a 30% aqueous solution

of H_2O_2 (0.3 mL, 5.4 mmol, 20 equiv) was added dropwise. The mixture was stirred overnight at 80°C. The mixture was dialysed (3.5 kDa MWCO) against deionised water overnight. The volatiles were evaporated to give osmium-free PEGose as a grey solid (13 mg, 34%).

^{1}H-NMR (400 MHz, D_2O) δ = 4.43 – 3.61 (8H). ^{13}C-NMR (126 MHz, D_2O) δ = 77.9 (C3), 74.7 (C4), 69.2 (C6), 67.2 (C5), 65.1 (C2), 64.0 (C1).

FITC-labelled PEGose

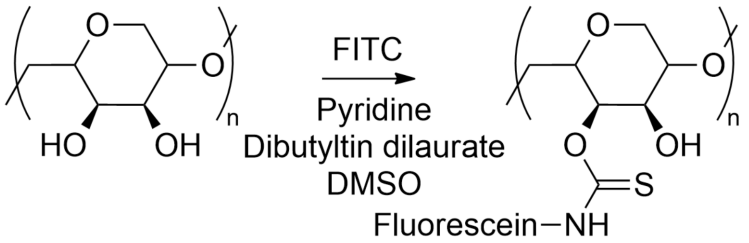

Adapted from de Belder and Granath procedure.[238] FITC-labelled PEGose and PEGose-*b*-PLA were prepared by mixing the polymer (100 mg) in 1 mL of dry DMSO and 50 µL of pyridine. The fluorescent dye isothiocyanate fluorescein was then added (10 mg) followed by dibutyltin dilaurate (2 mg). The reaction mixture was heated to 95°C for 2 h. Subsequently, the labelled polymer was dialyzed (3.5 kDa MWCO) against deionised water over 48 h, regularly changing the water. The water solution was then concentrated and the polymer dried in vacuo (84 mg, 84%, d.s. 0.0005). The degree of substitution was determined by preparing a standard curve with FITC solutions in a Tris buffer, with concentrations ranging from 10^{-6} to 10^{-5} mol/L. The wavelength of absorption was fixed to 493 nm and labelled polymers were dissolved in a Tris buffer.

7.5 Chapter 3 - Self-assembly of i-PEGose-*b*-PLA into polymeric microcubes

Synthesis of enantiopure (R) butadiene monoxide

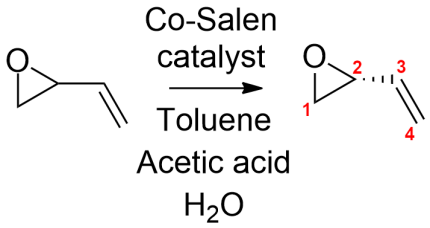

Enantioenriched 3,4-epoxy-butene was obtained by hydrolytic kinetic resolution using a chiral (salen)Co^{III} complex. Commercially available (*R*,*R*) *N*,*N*'-*bis*(3,5-di-*tert*-butylsalicylidene)-1,2-cyclohexanediaminocobalt(II) complex (1.3 g, 2.1 mmol, 0.015 equiv) in toluene (10 mL) was treated with acetic acid (1.5 mL) and stirred under air for 3 h. The crude mixture was left under vacuum overnight. The complex residue obtained was dissolved in racemic 3,4-epoxy-1-butene (10 g, 140 mmol). The solution was cooled to 0°C and H_2O (1.80 mL, 100 mmol, 0.71 equiv) was added dropwise. After 96 h at ambient temperature, (*R*)-3,4-epoxy-1-butene[74] (2.50 g, 35.7 mmol, 32%) was isolated by vacuum transfer into a catch flask cooled with liquid N_2.
$[\alpha]_D^{20}$ +13.6° (*c* 1.0, Et_2O).
$[\alpha]_D^{22}$ +14.8° (*c* 1.18, Et_2O); lit.[26]

^{1}H-NMR (400 MHz, $CDCl_3$)
δ = 5.56-5.46 (2H, H4), 5.30–5.25 (1H, H3), 3.34–3.29 (1H, H2), 2.96-2.92 (1H, H1), 2.64-2.59 (1H, H1').

Synthesis of isotactic poly(epoxybutene) - i-PEB

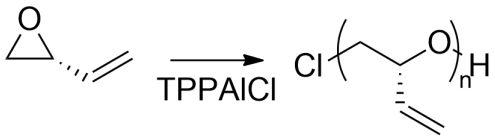

Isotactic PEB was synthesised by the same procedure as for atactic PEB, using enantiopure butadiene monoxide instead. Yield: 2.8 g, 73%.

^{1}H-NMR (400 MHz, $CDCl_3$) δ = 5.73-5.69 (m, br, 1H, H3), 5.28-5.15 (m, br, 2H, H4), 4.01-3.93 (m, br, 1H, H2), 3.57-3.39 (m, br, 2H, H1).
^{13}C-NMR (126 MHz, $CDCl_3$) δ = 136.1 (C3), 117.9 (C4), 80.8 (C2), 72.0 (C1).

Synthesis of isotactic polycycloether - i-PCE

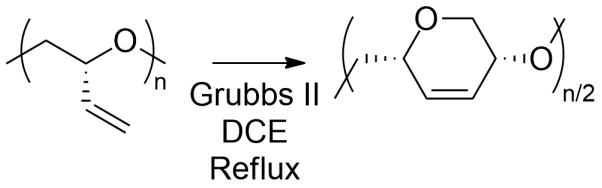

Isotactic PCE was synthesised by by the same procedure as for atactic PCE, using an isotactic PEB instead. Yield: 412 mg, 48%.

Synthesis of isotactic polycycloether-block-poly(DL-lactic acid) - i-PCE$_{50}$-PLA$_{50}$

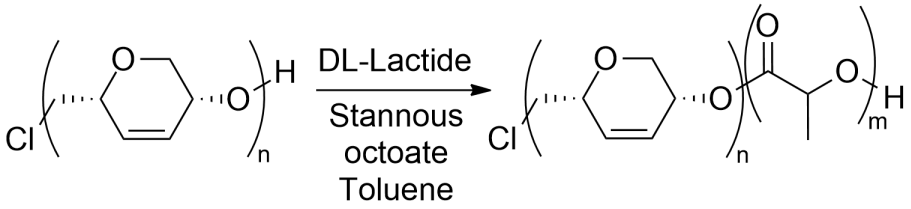

i-PCE$_{50}$-PLA$_{500}$ was synthesised by the same procedure as for a-PCE$_{50}$-PLA$_{100}$. Yield: 312 mg, 82%.

^{1}H-NMR (400 MHz, $CDCl_3$)
PCE δ = 6.04–5.62 (2H, H3 H4), 4.32–3.89 (2H, H2 H5), 3.82–3.28 (4H, H1 H6).
PLA δ = 5.24-5.01 (1H, H8), 1.83-1.72 (3H, H7).

Synthesis of isotactic polycycloether-block-poly(L-lactic acid) - i-PCE$_{50}$-PLLA$_{50}$

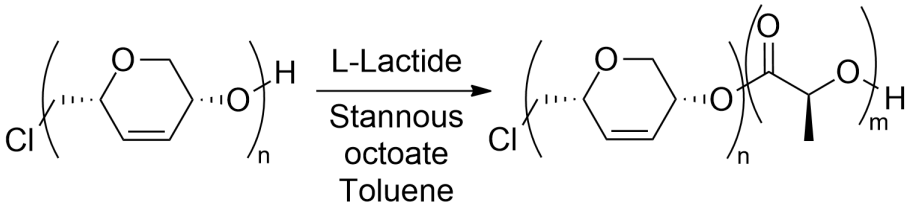

i-PCE$_{50}$-PLLA$_{50}$ was synthesised by the same procedure as for a-PCE$_{50}$-PLA$_{50}$ using an isotactic PCE homopolymer and L-lactide. Yield: 297 mg, 78%.

^{1}H-NMR (400 MHz, $CDCl_3$)
PCE δ = 6.10–5.64 (2H, H3 H4), 4.39–3.95 (2H, H2 H5), 3.90–3.52 (4H, H1 H6).
PLA δ = 5.35-5.08 (1H, H8), 1.71-1.54 (3H, H7).

Synthesis of isotactic PEGose-block-poly(DL-lactic acid) - i-PEGose$_{50}$-PLA$_{50}$

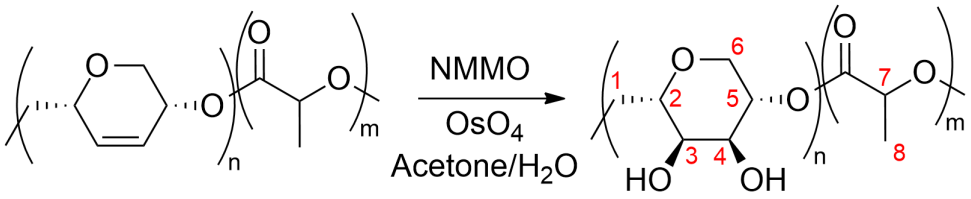

i-PCE-*b*-PLA (448 mg, 1.0 mmol of the PCE monomer unit) was dissolved in acetone/water (5:1, 20 mL). Dried *N*-methylmorpholine-*N*-oxide was then added to the mixture (129 mg, 1.1 mmol, 1.1 equiv). The reaction mixture was stirred in an ice bath, and then 0.1 mol % of freshly prepared OsO_4 solution (100 µL, 1% in water) was added slowly and the resulting mixture was stirred for an additional 2 h. The reaction mixture was stirred overnight at ambient temperature. To quench the reaction, 126 mg (1 equiv) of sodium sulfite was added and the resulting mixture was stirred for 1 h. Water was added (20 mL) and the mixture was then dialyzed (3.5 kDa MWCO) against deionised water over 24 h, regularly changing the water. The resulting solution was freeze-dried to yield i-PEGose-*b*-PLA as a grey solid (357 mg, 74%).

^{1}H NMR (400 MHz,$(CD_3)_2SO$)
PEGose δ = 4.43–3.61 (8H).
PLA δ = 5.25-5.10 (1H, H8), 1.70-1.45 (3H, H7).

Synthesis of isotactic PEGose-block-poly(L-lactic acid) - i-PEGose$_{50}$-PLLA$_{50}$

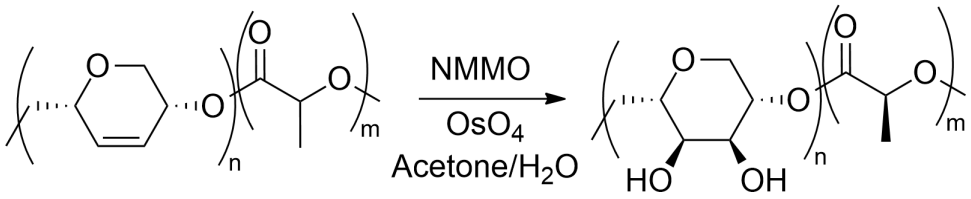

i-PEGose$_{50}$-PLLA$_{50}$ was synthesised by the same procedure as for i-PEGose$_{50}$-PLA$_{50}$ using i-PCE-*b*-PLLA as starting material instead. Yield: 174 mg, 72%.

The product was not soluble in DMSO-d_6 or any other solvent, leading to the absence of a proper NMR characterisation.

7.6 Chapter 4 - Synthesis of PEG-*b*-poly(cycloether), a poloxamer mimic containing a helical block

Atactic and isotactic poly(epoxybutene) were synthesised following the procedure described in the previous chapter.

Reduction of poly(epoxybutene) chloride end-group leading to i-H-PEB$_{30}$

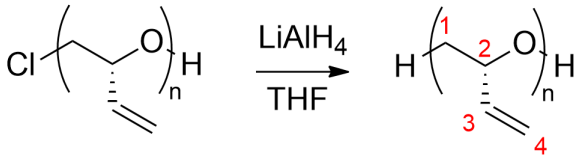

Isotactic H-PEB$_{30}$ was synthesised by dissolving isotactic Cl-PEB$_{30}$ (400 mg, 190 µmol, 1 equiv) in THF (4 mL), then slowly adding a $LiAlH_4$ solution in THF (1 M, 2.0 mL, 2.0 mmol, 10 equiv). The mixture was stirred at ambient temperature for 48 h, quenched with methanol (1 mL) then concentrated under vacuum. DCM (10 mL) and a 10% aqueous Rochelle salt solution (10 mL) were added and the mixture was stirred for 4 h. The organic phase was then separated, washed three times with deionised water, dried over magnesium sulfate, and filtered. The volatiles were removed under vacuum, and the resulting polymer was dissolved in a 1:1 methanol/DCM mixture for purification by preparative SEC (Sephadex LH-20, methanol/DCM 1:1). The fractions were concentrated, and the polymer was dried under vacuum overnight to give a brown oil (isotactic H-PEB$_{30}$: 324 mg, 81%).

^{1}H-NMR (400 MHz, $CDCl_3$) δ = 5.77-5.69 (m, br, 2H, H3), 5.33-5.13 (m, br, 4H, H4), 4.02-3.91 (m, br, 2H, H2), 3.60-3.38 (m, br, 4H, H1).
^{13}C-NMR (126 MHz, $CDCl_3$) δ = 136.2 (C3), 117.8 (C4), 80.8 (C2), 72.1 (C1).

Reduction of poly(epoxybutene) chloride end-group leading to a-H-PEB$_{30}$

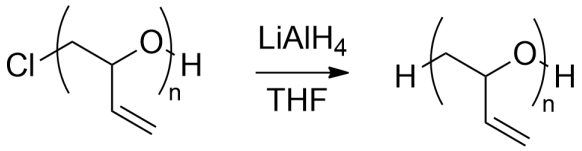

Atactic H-PEB$_{30}$ was synthesised following the previous procedure using atactic Cl-PEB$_{30}$. Yield: 312 mg, 78%.

Hydroxy substitution of poly(epoxybutene) chloride end-group leading to i-HO-PEB$_{30}$

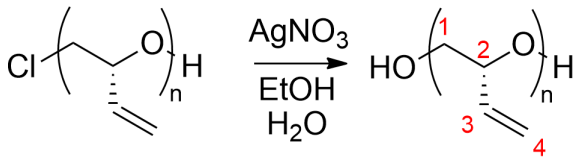

Isotactic HO-PEB$_{30}$ was synthesised by dissolving isotactic Cl-PEB$_{30}$ (500 mg, 240 µmol, 1 equiv) and silver nitrate (210 mg, 2.50 mmol, 10 equiv) in a mixture of ethanol (10 mL) and deionised water (2 mL). The reaction mixture was then refluxed for 48 h and subsequently concentrated under vacuum. The resulting polymer was dissolved in DCM (10 mL), and the resulting solution washed three times with water, dried over magnesium sulfate, and filtered. The volatiles were removed under vacuum, and the resulting polymer was dissolved in a 1:1 methanol/DCM mixture for purification by preparative SEC (Sephadex LH-20, methanol/DCM 1:1). The fractions were concentrated, and the polymer was dried under vacuum overnight to give a brown oil (isotactic HO-PEB$_{30}$: 430 mg, 86%).

^{1}H-NMR (400 MHz, $CDCl_3$) δ = 5.77-5.69 (m, br, 2H, H3), 5.33-5.13 (m, br, 4H, H4), 4.02-3.91 (m, br, 2H, H2), 3.60-3.38 (m, br, 4H, H1).
^{13}C-NMR (126 MHz, $CDCl_3$) δ = 136.2 (C3), 117.8 (C4), 80.8 (C2), 72.1 (C1).

Hydroxy substitution of poly(epoxybutene) chloride end-group leading to a-HO-PEB$_{30}$

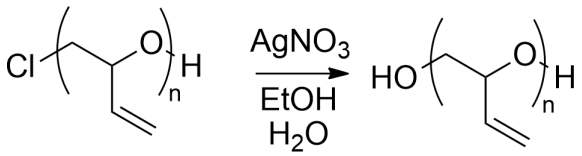

Atactic HO-PEB$_{30}$ was synthesised following the previous procedure using atactic Cl-PEB$_{30}$. Yield: 405 mg, 81%.

Synthesis of atactic polycycloether-block-poly(ethylene glycol) – a-PCE$_{30}$-b-PEG$_{100}$

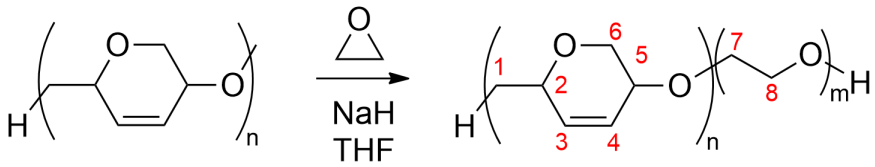

In a flame-dried Schlenk tube, atactic H-PCE$_{30}$ (300 mg, 0.18 mmol, 1 equiv) was added and dried overnight under vacuum. Sodium hydride was added (43 mg, 1.8 mmol, 10 equiv), dry THF was introduced (3 mL), then the mixture was stirred at 50°C for 3 h. The mixture was cooled down to ambient temperature then ethylene oxide in THF (2.5 M, 7.2 mL, 18 mmol,

100 equiv) was added and the mixture was stirred at 50°C for 2 days. An aqueous sodium hydroxide solution was then added (1 M, 1.0 mL) and the mixture was stirred overnight at ambient temperature. The mixture was finally quenched with an aqueous HCl solution (1 M, 1.0 mL) then the volatiles were removed under vacuum. The resulting polymer was dissolved in deionised water and dialyzed (1.0 kDa MWCO) against deionised water over two days. The resulting solution was freeze-dried and i-PCE_{30}-*b*-PEG_{100} was obtained as a viscous brown oil (atactic PCE_{30}-*b*-PEG_{100}: 522 mg, 57% yield).

^{1}H-NMR (400 MHz, $CDCl_3$)
PCE δ = 6.16–5.64 (2H, H3 H4), 4.37–3.99 (2H, H2 H5), 3.92–3.30 (4H, H1 H6).
PEG δ = 3.58-3.62 (27H, H7 H8)
^{13}C-NMR (126 MHz, $CDCl_3$)
PCE δ = 132.0–124.0 (C3 C4), 74.1–73.2 (C5), 71.2–70.4 (C2), 70.4–69.3 (C6), 68–66.6 (C1).
PEG δ = 70.2-70.8 (C7 C8)

Synthesis of isotactic polycycloether-block-poly(ethylene glycol) – i-PCE_{30}-b-PEG_{100}

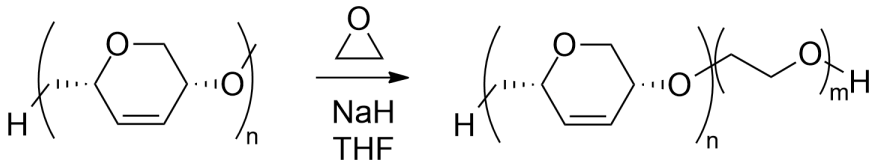

Isotactic i-PCE_{30}-*b*-PEG_{100} was synthesised following the previous procedure using isotactic H-PEB_{30}. Yield: 238 mg, 52%.

Synthesis of isotactic poly(ethylene glycol)-block-polycycloether-block-poly(ethylene glycol) – PEG_{50}-iPCE_{30}-PEG_{50}

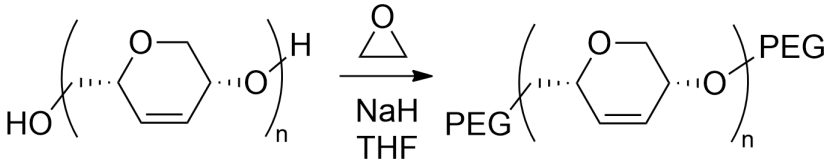

PEG_{50}-*b*-iPCE_{30}-*b*-PEG_{50} was synthesised using the previous procedure, using isotactic HO-PCE_{30} as substrate. Yield: 233 mg, 51%.

Synthesis of atactic poly(ethylene glycol)-block-polycycloether-block-poly(ethylene glycol) – PEG_{50}-aPCE_{30}-PEG_{50}

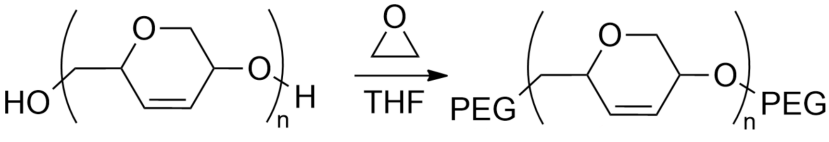

PEG_{50}-*b*-aPCE_{30}-*b*-PEG_{50} was synthesised using the previous procedure, using atactic HO-PCE_{30} as substrate. Yield: 247 mg, 54%.

Synthesis of atactic saturated polycycloether-block-poly(ethylene glycol) – aSPCE$_{30}$-b-PEG$_{100}$

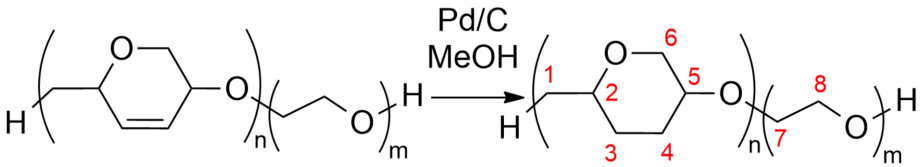

Atactic $SPCE_{30}$-*b*-PEG_{100} was synthesised by adding the corresponding PCE_{30}-*b*-PEG_{100} (58 mg) to a 25 mL round-bottomed flask. Under an argon atmosphere, methanol was added (2 mL) followed by Pd/C (10% wt, 12 mg). The flask was degassed then hydrogen was introduced. The mixture was stirred at ambient temperature for 24 h. The reaction mixture was then filtered, concentrated under vacuum, and the resulting oil solubilised in water, followed by dialysis (1.0 kDa MWCO) against water for 24 h. The aqueous solution was freeze-dried and $SPCE_{30}$-*b*-PEG_{100} was obtained as a viscous yellow oil (atactic $SPCE_{30}$-*b*-PEG_{100}: 42 mg, 76%).

^{1}H-NMR (400 MHz, $CDCl_3$)
PCE δ = 4.35–3.95 (2H, H2 H5), 3.81–3.42 (8H, H1 H6).
PEG δ = 3.58-3.62 (27H, H7 H8)

Synthesis of isotactic poly(ethylene glycol)-block-saturated poly(cycloether)-block-poly(ethylene glycol) – PEG$_{50}$-b-iSPCE$_{30}$-b-PEG$_{50}$

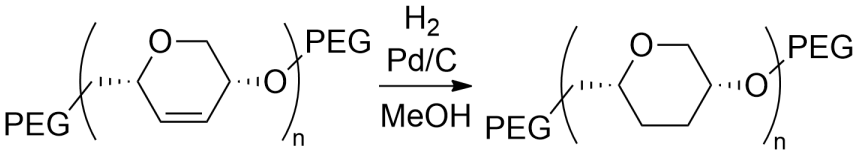

PEG_{50}-*b*-i$SPCE_{30}$-*b*-PEG_{50} was synthesised using the previous procedure, using isotactic PEG_{50}-*b*-iPCE_{30}-*b*-PEG_{50} as substrate. Yield: 41 mg, 74%.

7.7 Chapter 5 - Synthesis of polycyclic cationic polymers

Synthesis of hydroaminated PCE

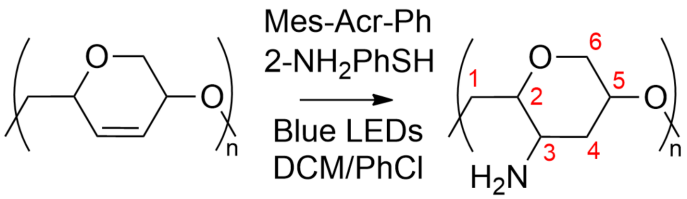

Adapted from the Yi-Dan Du *et al.* procedure,[233] *N*-phenyl-9-mesityl 2,7-dimethylacridinium tetrafluoroborate (14 mg, 28 µmol, 5.0 mol%) was added under argon in a Schlenk-tube. Ammonium carbonate (793 mg, 8.25 mmol, 15 equiv) was then added, followed by DCM (100 mL), PCE (0.55 mmol, 62 mg), 2-aminothiophenol (20.5 mg, 1.65 mmol, 30 mol%) and PhCl (10 mL). The reaction mixture was stirred at RT under irradiation with blue LEDs for 48 h. The conversion was monitored by ^{1}H NMR by integrating the alkene peak. After 2 days, the volatiles were removed in vacuo. The crude mixture was purified by Sephadex LH-20 using methanol as eluent. The volatiles were removed in vacuo to give the desired polymer as a black oil (17 mg, 31% yield).

^{1}H-NMR (400 MHz, CD_3OD) δ = 6.18-5.59 (unconverted alkene protons), 4.52-3.10 (7H, H1 H2 H3 H5 H6), 2.59–1.50 (1H, H4).

Synthesis of thiol-ene PCE

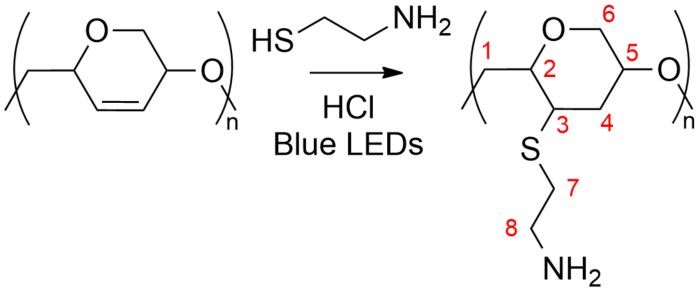

Adapted from the J. Hunt *et al.* procedure,[239] PCE (1.1 mmol, 124 mg) and 2-aminoethanethiol hydrochloride (8.8 mmol, 1.0 g, 8 equiv) were mixed with 20 mL of 1:1 MeOH/water. 2,2-Dimethoxy-2-phenylacetophenone (55 µmol, 14 mg, 0.05 equiv) was added then argon was bubbled through the reaction mixture for 30 min to degas. The solution was irradiated with blue light (maximum emission peak 365 nm) and stirred for 24 h. Volatiles were evaporated and the residue was solubilised in a minimum of methanol then purified by Sephadex LH-20 using methanol as eluent. The volatiles were removed in vacuo to give the desired polymer as a black oil (65 mg, 31% yield).

^{1}H-NMR (400 MHz, CD_3OD) δ = 6.21-5.73 (unconverted alkene protons), 4.25-2.78 (11H, H1 H2 H3 H5 H6 H7 H8), 2.56–2.12 (1H, H4).

Synthesis of guanidinium PCE

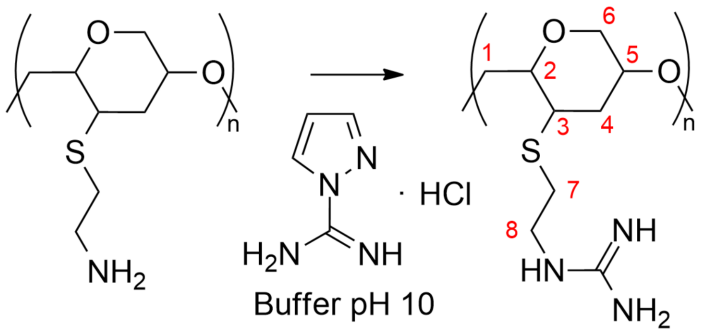

The resulting Thiol-ene PCE (65 mg, 0.34 mmol) was dissolved in a pH 10 buffer. ^{1}H-pyrazole-1-carboxamidine hydrochloride (150 mg, 1.02 mmol) was then added. The reaction mixture was stirred under reflux overnight. The volatiles were evaporated under vaccum then the residue was solubilised in a minimum of methanol then purified by Sephadex LH-20 with methanol as the eluent. After drying under vaccum, the guanidinium-functionalised PCE was obtained as a black oil (35 mg, 45% yield).

^{1}H-NMR (400 MHz, D_2O) δ = 8.52-6.88 (4H, guanidinium protons), 4.51-2.22 (13H, H1 H2 H3 H4 H5 H6 H7 H8).

Synthesis of diamino PCE

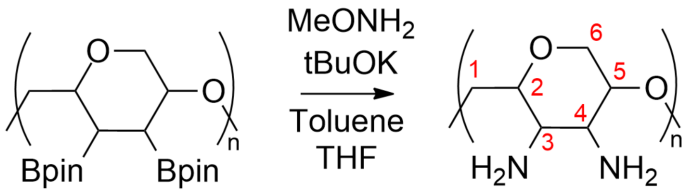

Adapted from the E. Edelstein *et al.* procedure,[234] *t*-BuOK (112 mg, 1 mmol, 5.0 equiv) was cautiously placed in a small Schlenk tube. Methoxyamine (1.96 M in THF, 0.33 mL, 0.66 mmol, 3.0 equiv) was then added. The diborated CPE (75 mg, 0.20 mmol, 1.0 equiv) was added as a solution in toluene (0.66 mL) to achieve a final substrate concentration of 0.2 M. The Schlenk tube was sealed with tape and stirred for 24 h at 80°C. After letting the reaction mixture cool down to ambient temperature, water was added. The mixture was stirred at RT for 1 h then the volatiles were evaporated under vaccum. The residue was solubilised in deionised water then dialyzed over 2 days using a 1.5 kDa MWCO membrane. After removing the water

under vacuum, the polymer was obtained as a black oil (18 mg, 62% yield).

^{1}H-NMR (400 MHz, D_2O) δ = 4.47-3.17 (8H).

Synthesis of epoxyPCE

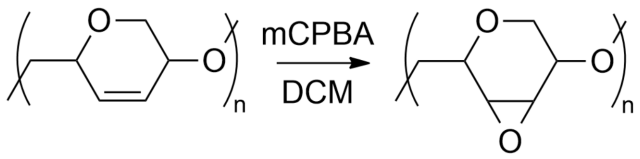

Polycycloether (PCE) (448 mg, 4.0 mmol of the monomer unit) was dissolved in dichloromethane (5 mL). *meta*-Chloroperoxybenzoic acid (mCPBA) (66%, 448 mg, 12.0 mmol) was dissolved in dichloromethane (2 mL) and the resulting solution was added dropwise at 0°C. The crude product was then kept in solution under inert atmosphere and the desired nucleophile was then added *in situ* for the synthesis of hydroxyaminoPCE or hexaminePCE.

Synthesis of methylaminePEGose

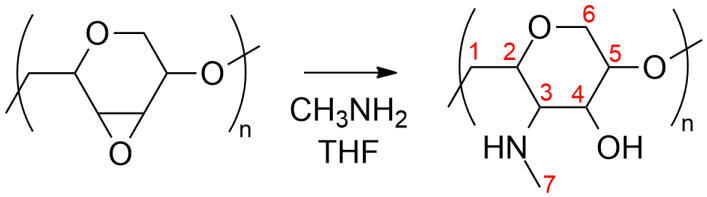

To a solution of epoxyPCE (1.0 mmol of the monomer unit) in dichloromethane (5 mL) was added a solution of methylamine in THF (2.0 M, 5.0 mL, 10 mmol, 10 equiv) at 0°C. The solution was kept stirring for 48 h then concentrated under vacuum. The resulting oil was dissolved in water, purified by dialysis (1.0 kDa MWCO) over 3 days then freeze-dried to obtain methylaminePEGose as a brown oil (58 mg, 36% yield).

^{1}H-NMR (400 MHz, D_2O) δ = 4.31-2.44 (11H).

Synthesis of hexaminePCE

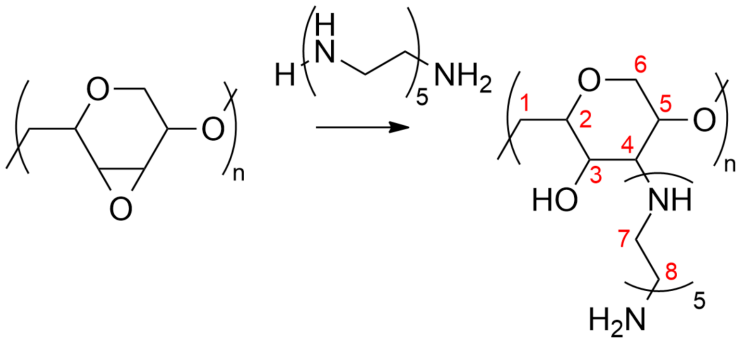

To a solution of epoxyPCE (1.0 mmol of the monomer unit) in dichloromethane (5 mL) was added dry DMSO (5 mL) then pentaethylene hexamine (2.32 mL, 2.32 g, 10 equiv) at 0°C. The solution was kept stirring for 48 h then concentrated under vacuum. The resulting oil was dissolved in water, purified by dialysis (1.0 kDa MWCO) over 3 days then freeze-dried to obtain hexaminePCE as a brown oil (175 mg, 49% yield).

^{1}H-NMR (400 MHz, D_2O) δ = 4.20-2.50 (28H).

Synthesis of PEGose-g-poly(tosylaziridine)

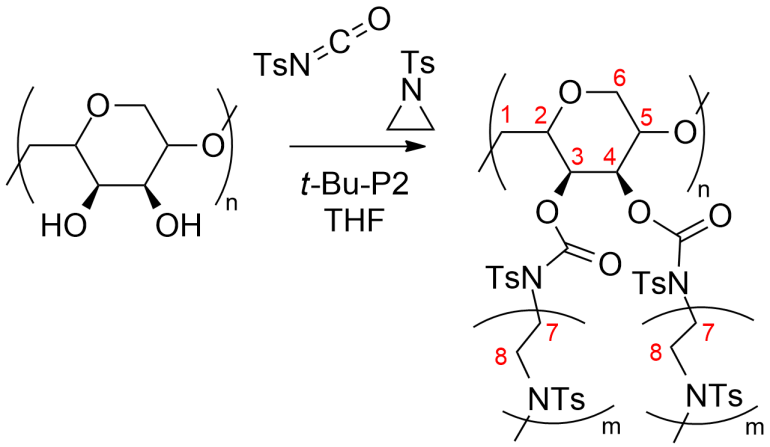

In a flame-dried Schlenk tube, PEGose (100 mg, 1.37 mmol), THF (10 mL), and a t-Bu-P2 solution in THF (2 M, 0.2 mL, 0.3 equiv) were added. A solution of tosylaziridine (2.70 g, 13.7 mmol, 10 equiv) and *p*-toluenesulfonyl isocyanate (0.21 mL, 1.37 mmol, 1 equiv) in THF (2 mL) was then added. The reaction mixture was stirred at 50°C for 24 h. The product was precipitated in methanol, filtered, washed with methanol, then concentrated under vacuum. The polymer was then dissolved in a minimum of dichloromethane then purified by size-exclusion chromatography (Sephadex LH-20, DCM/MeOH 3:1) to afford the desired polymer as a grey solid (246 mg, 6% yield).

^{1}H-NMR (400 MHz, $CDCl_3$) δ = 7.94-7.56 (2H, H-ortho tosyl), 7.39-7.09 (2H, H-meta tosyl), 4.04-3.02 (4H, H7 H8), 4.04-3.02 (0.6H, H1 H2 H3 H4 H5 H6), 2.50-2.13 (3H, tosyl).

Synthesis of PEGose-g-PEI

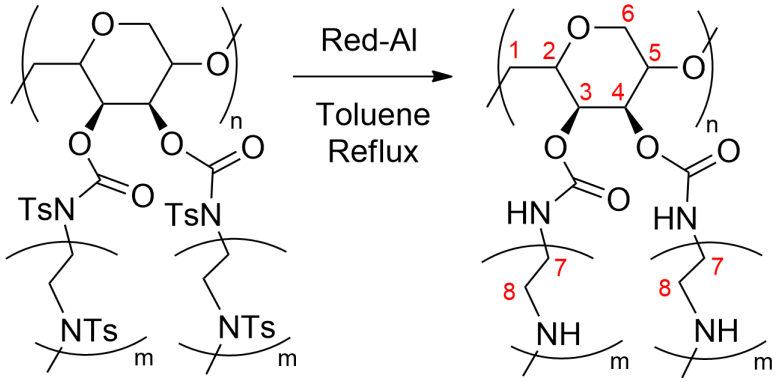

PEGose-*g*-poly(tosylaziridine) (200 mg, 1.02 mmol) was dissolved in toluene (5 mL) then a sodium *bis*(2-methoxyethoxy)aluminium hydride (Red-Al) solution in toluene (70 wt%, 1.16 mL, 4.04 mmol, 4 equiv) was added. The reaction mixture was refluxed overnight then concentrated under vacuum. The resulting product was dissolved in water then purified by dialysis (1.0 kDa MWCO) against water over 3 days. The polymer solution was then freeze-dried to afford PEGose-*g*-PEI as a grey solid (31 mg, 71%).

^{1}H-NMR (400 MHz, D_2O) δ = 3.91-3.18 (0.6H, H1 H2 H3 H4 H5 H6), 2.74-2.49 (4H, H7 H8).

Bibliography

[1] J.-B. Masclef, E. M. N. Acs, J. Koehnke, J. Prunet, B. V. K. J. Schmidt, *Macromolecules* **2024**, *57*, 6013–6023, DOI 10.1021/acs.macromol.4c00528.

[2] J.-B. Masclef, J. Prunet, B. V. K. J. Schmidt, *Adv. Sci.* **2024**, *11*, DOI 10.1002/advs.202310277.

[3] J. Lou, D. J. Mooney, *Nat. Rev. Chem.* **2022**, *6*, 726–744, DOI 10.1038/s41570-022-00420-7.

[4] Y. Liang, J. He, B. Guo, *ACS Nano* **2021**, *15*, 12687–12722, DOI 10.1021/acsnano.1c04206.

[5] M. Hasannia, A. Aliabadi, K. Abnous, S. M. Taghdisi, M. Ramezani, M. Alibolandi, *J. Control. Release* **2022**, *341*, 95–117, DOI 10.1016/j.jconrel.2021.11.010.

[6] K. Kuperkar, D. Patel, L. I. Atanase, P. Bahadur, *Polymers* **2022**, *14*, 4702, DOI 10.3390/polym14214702.

[7] Y. K. Sung, S. W. Kim, *Biomater. Res.* **2020**, *24*, 12, DOI 10.1186/s40824-020-00190-7.

[8] S. Sharma, P. Sudhakara, J. Singh, R. A. Ilyas, M. R. M. Asyraf, M. R. Razman, *Polymers* **2021**, *13*, 2623, DOI 10.3390/polym13162623.

[9] D. Fan, Y. Liu, Y. Wang, Q. Wang, H. Guo, Y. Cai, R. Song, X. Wang, W. Wang, *Front. Pharmacol.* **2022**, *13*, DOI 10.3389/fphar.2022.1044726.

[10] N. Bayliss, B. V. K. J. Schmidt, *Prog. Polym. Sci.* **2023**, *147*, 101753, DOI 10.1016/j.progpolymsci.2023.101753.

[11] D. Shi, D. Beasock, A. Fessler, J. Szebeni, J. Y. Ljubimova, K. A. Afonin, M. A. Dobrovolskaia, *Adv. Drug Deliv. Rev.* **2022**, *180*, 114079, DOI 10.1016/j.addr.2021.114079.

[12] P. Bigini, M. Gobbi, M. Bonati, A. Clavenna, M. Zucchetti, S. Garattini, G. Pasut, *Nat. Nanotechnol.* **2021**, *16*, 1169–1171, DOI 10.1038/s41565-021-01001-3.

[13] A. Blanazs, S. P. Armes, A. J. Ryan, *Macromol. Rapid Commun.* **2009**, *30*, 267–277, DOI 10.1002/marc.200800713.

[14] S. L. Hart, *Curr. Drug Deliv.* **2005**, *2*, 423–428, DOI 10.2174/156720105774370230.

[15] J. Casper, S. H. Schenk, E. Parhizkar, P. Detampel, A. Dehshahri, J. Huwyler, *J. Control. Release* **2023**, *362*, 667–691, DOI 10.1016/j.jconrel.2023.09.001.

[16] L. Zhou, M. Emenuga, S. Kumar, Z. Lamantia, M. Figueiredo, T. Emrick, *Biomacromolecules* **2022**, DOI 10.1021/acs.biomac.2c00767.

[17] M. A. Mintzer, E. E. Simanek, *Chem. Rev.* **2009**, *109*, 259–302, DOI 10.1021/cr800409e.

[18] M. Mohammadi, M. Ramezani, K. Abnous, M. Alibolandi, *Int. J. Pharm.* **2017**, *519*, 287–303, DOI 10.1016/j.ijpharm.2017.01.037.

[19] R. Klein, F. R. Wurm, *Macromol. Rapid Commun.* **2015**, *36*, 1147–1165, DOI 10.1002/marc.201500013.

[20] A. Thomas, S. S. Müller, H. Frey, *Biomacromolecules* **2014**, *15*, 1935–1954, DOI 10.1021/bm5002608.

[21] S. Abbina, A. Parambath in *Engineering of Biomaterials for Drug Delivery Systems*, (Ed.: A. Parambath), Woodhead Publishing Series in Biomaterials, Woodhead Publishing, **2018**, pp. 363–376, DOI 10.1016/B978-0-08-101750-0.00014-3.

[22] M. Barz, R. Luxenhofer, R. Zentel, M. J. Vicent, *Polym. Chem.* **2011**, *2*, 1900, DOI 10.1039/c0py00406e.

[23] K. Knop, R. Hoogenboom, D. Fischer, U. S. Schubert, *Angew. Chem. Int. Ed.* **2010**, *49*, 6288–6308, DOI 10.1002/anie.200902672.

[24] T. T. Hoang Thi, E. H. Pilkington, D. H. Nguyen, J. S. Lee, K. D. Park, N. P. Truong, *Polymers* **2020**, *12*, 298, DOI 10.3390/polym12020298.

[25] J. Herzberger, K. Niederer, H. Pohlit, J. Seiwert, M. Worm, F. R. Wurm, H. Frey, *Chem. Rev.* **2016**, *116*, 2170–2243, DOI 10.1021/acs.chemrev.5b00441.

[26] D. E. White, P. M. Tadross, Z. Lu, E. N. Jacobsen, *Tetrahedron* **2014**, *70*, 4165–4180, DOI 10.1016/j.tet.2014.03.043.

[27] N. Cao, Y. Zhao, H. Chen, J. Huang, M. Yu, Y. Bao, D. Wang, S. Cui, *Macromolecules* **2022**, *55*, 4656–4664, DOI 10.1021/acs.macromol.2c00014.

[28] A. Kolate, D. Baradia, S. Patil, I. Vhora, G. Kore, A. Misra, *J. Control. Release* **2014**, *192*, 67–81, DOI 10.1016/j.jconrel.2014.06.046.

[29] Y. Gao, M. Joshi, Z. Zhao, S. Mitragotri, *Bioeng. Transl. Med.*, DOI 10.1002/btm2.10600.

[30] M. Li, S. Jiang, J. Simon, D. Paßlick, M.-L. Frey, M. Wagner, V. Mailänder, D. Crespy, K. Landfester, *Nano Lett.* **2021**, DOI 10.1021/acs.nanolett.0c03756.

[31] H. Zhao, B. Rubio, P. Sapra, D. Wu, P. Reddy, P. Sai, A. Martinez, Y. Gao, Y. Lozanguiez, C. Longley, L. M. Greenberger, I. D. Horak, *Bioconjugate Chem.* **2008**, *19*, 849–859, DOI 10.1021/bc700333s.

[32] Y. Bavli, B.-M. Chen, G. Gross, A. Hershko, K. Turjeman, S. Roffler, Y. Barenholz, *J. Control. Release* **2023**, *354*, 316–322, DOI 10.1016/j.jconrel.2022.12.039.

[33] Y. Ju, J. M. Carreño, V. Simon, K. Dawson, F. Krammer, S. J. Kent, *Nat. Rev. Immunol.* **2023**, *23*, 135–136, DOI 10.1038/s41577-022-00825-x.

[34] H. Wang, Y. Wang, C. Yuan, X. Xu, W. Zhou, Y. Huang, H. Lu, Y. Zheng, G. Luo, J. Shang, M. Sui, *npj Vaccines* **2023**, *8*, 1–13, DOI 10.1038/s41541-023-00766-z.

[35] M. Ibrahim, E. Ramadan, N. E. Elsadek, S. E. Emam, T. Shimizu, H. Ando, Y. Ishima, O. H. Elgarhy, H. A. Sarhan, A. K. Hussein, T. Ishida, *J. Control. Release* **2022**, *351*, 215–230, DOI 10.1016/j.jconrel.2022.09.031.

[36] M. Estapé Senti, C. A. de Jongh, K. Dijkxhoorn, J. J. F. Verhoef, J. Szebeni, G. Storm, C. E. Hack, R. M. Schiffelers, M. H. Fens, P. Boross, *J. Control. Release* **2022**, *341*, 475–486, DOI 10.1016/j.jconrel.2021.11.042.

[37] C. A. Stone, Y. Liu, M. V. Relling, M. S. Krantz, A. L. Pratt, A. Abreo, J. A. Hemler, E. J. Phillips, *J. Allergy Clin. Immunol. Pract.* **2019**, *7*, 1533–1540.e8, DOI 10.1016/j.jaip.2018.12.003.

[38] M. Kurakula, G. S. N. K. Rao, *J. Drug Deliv. Sci. Technol.* **2020**, *60*, 102046, DOI 10.1016/j.jddst.2020.102046.

[39] A. C. Rönnau, M. Wulferink, E. Gleichmann, E. Unver, T. Ruzicka, J. Krutmann, M. Grewe, *Br. J. Dermatol.* **2000**, *143*, 1055–1058, DOI 10.1046/j.1365-2133.2000.03843.x.

[40] M. Hu, M. Chen, G. Li, Y. Pang, D. Wang, J. Wu, F. Qiu, X. Zhu, J. Sun, *Biomacromolecules* **2012**, *13*, 3552–3561, DOI 10.1021/bm300966d.

[41] M. Imran ul-haq, B. F. L. Lai, R. Chapanian, J. N. Kizhakkedathu, *Biomaterials* **2012**, *33*, 9135–9147, DOI 10.1016/j.biomaterials.2012.09.007.

[42] M. Rahman, M. Alrobaian, W. H. Almalki, M. H. Mahnashi, B. A. Alyami, A. O. Alqarni, Y. S. Alqahtani, K. S. Alharbi, S. Alghamdi, S. K. Panda, A. Fransis, A. Hafeez, S. Beg, *Drug Discov. Today* **2021**, *26*, 1006–1017, DOI 10.1016/j.drudis.2020.11.007.

[43] A. Sunder, R. Hanselmann, H. Frey, R. Mülhaupt, *Macromolecules* **1999**, *32*, 4240–4246, DOI 10.1021/ma990090w.

[44] R. Luxenhofer, S. Huber, J. Hytry, J. Tong, A. V. Kabanov, R. Jordan, *J. Polym. Sci. Part Polym. Chem.* **2013**, *51*, 732–738, DOI 10.1002/pola.26437.

[45] M. A. Mees, R. Hoogenboom, *Polym. Chem.* **2018**, *9*, 4968–4978, DOI 10.1039/C8PY00978C.

[46] B. Guillerm, S. Monge, V. Lapinte, J.-J. Robin, *Macromol. Rapid Commun.* **2012**, *33*, 1600–1612, DOI 10.1002/marc.201200266.

[47] K. Lava, B. Verbraeken, R. Hoogenboom, *Eur. Polym. J.* **2015**, *65*, 98–111, DOI 10.1016/j.eurpolymj.2015.01.014.

[48] J. Ulbricht, R. Jordan, R. Luxenhofer, *Biomaterials* **2014**, *35*, 4848–4861, DOI 10.1016/j.biomaterials.2014.02.029.

[49] E. Vlassi, A. Papagiannopoulos, S. Pispas, *Macromol. Chem. Phys.* **2018**, *219*, 1800047, DOI 10.1002/macp.201800047.

[50] M. Bauer, C. Lautenschlaeger, K. Kempe, L. Tauhardt, U. S. Schubert, D. Fischer, *Macromol. Biosci.* **2012**, *12*, 986–998, DOI 10.1002/mabi.201200017.

[51] R. Hoogenboom, *Angew. Chem. Int. Ed.* **2009**, *48*, 7978–7994, DOI 10.1002/anie.200901607.

[52] N. Adams, U. S. Schubert, *Adv. Drug Deliv. Rev.* **2007**, *59*, 1504–1520, DOI 10.1016/j.addr.2007.08.018.

[53] T. X. Viegas, M. D. Bentley, J. M. Harris, Z. Fang, K. Yoon, B. Dizman, R. Weimer, A. Mero, G. Pasut, F. M. Veronese, *Bioconjugate Chem.* **2011**, *22*, 976–986, DOI 10.1021/bc200049d.

[54] A. Bordat, T. Boissenot, N. Ibrahim, M. Ferrere, M. Levêque, L. Potiron, S. Denis, S. Garcia-Argote, O. Carvalho, J. Abadie, C. Cailleau, G. Pieters, N. Tsapis, J. Nicolas, *J. Am. Chem. Soc.* **2022**, DOI 10.1021/jacs.2c04944.

[55] H. S. Choi, W. Liu, F. Liu, K. Nasr, P. Misra, M. G. Bawendi, J. V. Frangioni, *Nat. Nanotechnol.* **2010**, *5*, 42–47, DOI 10.1038/nnano.2009.314.

[56] H. He, Z. Xiao, Y. Zhou, A. Chen, X. Xuan, Y. Li, X. Guo, J. Zheng, J. Xiao, J. Wu, *J. Mater. Chem. B* **2019**, *7*, 1697–1707, DOI 10.1039/C8TB02590H.

[57] H. Sun, M. Y. Z. Chang, W.-I. Cheng, Q. Wang, A. Commisso, M. Capeling, Y. Wu, C. Cheng, *Acta Biomater.* **2017**, *64*, 290–300, DOI 10.1016/j.actbio.2017.10.016.

[58] D. Nikolova, K. Ruseva, C. Tzachev, L. Christov, E. Vassileva, *Polym. Int.* **2022**, *71*, 662–667, DOI 10.1002/pi.6368.

[59] M. Cai, M. Leng, A. Lu, L. He, X. Xie, L. Huang, Y. Ma, J. Cao, Y. Chen, X. Luo, *Colloids Surf. B* **2015**, *126*, 1–9, DOI 10.1016/j.colsurfb.2014.12.005.

[60] R. Lalani, L. Liu, *Polymer* **2011**, *52*, 5344–5354, DOI 10.1016/j.polymer.2011.09.015.

[61] L. Kisley, K. A. Miller, C. M. Davis, D. Guin, E. A. Murphy, M. Gruebele, D. E. Leckband, *Biomacromolecules* **2018**, *19*, 3894–3901, DOI 10.1021/acs.biomac.8b01120.

[62] S. Zhai, Y. Ma, Y. Chen, D. Li, J. Cao, Y. Liu, M. Cai, X. Xie, Y. Chen, X. Luo, *Polym. Chem.* **2014**, *5*, 1285–1297, DOI 10.1039/C3PY01325A.

[63] J. Pushpamalar, A. K. Veeramachineni, C. Owh, X. J. Loh, *ChemPlusChem* **2016**, *81*, 504–514, DOI 10.1002/cplu.201600112.

[64] A. Plucinski, Z. Lyu, B. V. K. J. Schmidt, *J. Mater. Chem. B* **2021**, *9*, 7030–7062, DOI 10.1039/D1TB00628B.

[65] T. Mehling, I. Smirnova, U. Guenther, R. H. H. Neubert, *J. Non-Cryst. Solids* **2009**, *355*, 2472–2479, DOI 10.1016/j.jnoncrysol.2009.08.038.

[66] N. Zhang, P. Wardwell, R. Bader, *Pharmaceutics* **2013**, *5*, 329–352, DOI 10.3390/pharmaceutics5020329.

[67] C. A. García-González, M. Jin, J. Gerth, C. Alvarez-Lorenzo, I. Smirnova, *Carbohydr. Polym.* **2015**, *117*, 797–806, DOI 10.1016/j.carbpol.2014.10.045.

[68] Y. Wen, J. K. Oh, *Macromol. Rapid Commun.* **2014**, *35*, 1819–1832, DOI 10.1002/marc.201400406.

[69] T. G. Barclay, C. M. Day, N. Petrovsky, S. Garg, *Carbohydr. Polym.* **2019**, *221*, 94–112, DOI 10.1016/j.carbpol.2019.05.067.

[70] D. Bamberger, D. Hobernik, M. Konhäuser, M. Bros, P. R. Wich, *Mol. Pharmaceutics* **2017**, *14*, 4403–4416, DOI 10.1021/acs.molpharmaceut.7b00507.

[71] Y. Liu, L. Yin, *Adv. Drug Deliv. Rev.* **2021**, *171*, 139–163, DOI 10.1016/j.addr.2020.12.007.

[72] J. Yuan, Y. Sun, J. Wang, H. Lu, *Biomacromolecules* **2016**, *17*, 891–896, DOI 10.1021/acs.biomac.5b01588.

[73] S. Biswas, P. Kumari, P. M. Lakhani, B. Ghosh, *Eur. J. Pharm. Sci.* **2016**, *83*, 184–202, DOI 10.1016/j.ejps.2015.12.031.

[74] M. Alkattan, J. Prunet, M. P. Shaver, *Angew. Chem. Int. Ed.* **2018**, *57*, 12835–12839, DOI 10.1002/anie.201805113.

[75] G. Gaucher, M.-H. Dufresne, V. P. Sant, N. Kang, D. Maysinger, J.-C. Leroux, *J. Control. Release* **2005**, *109*, 169–188, DOI 10.1016/j.jconrel.2005.09.034.

[76] J. Lu, B. Han, B. Zhang, B. Zou, M. Hu, H. Liu, C. Zhou, F. Qian, S. Wang, Y. Zhang, Y. Lou, T. Chu, J. Zhou, B. Han, H. Zhong, *J. Control. Release* **2023**, *362*, 197–209, DOI 10.1016/j.jconrel.2023.08.051.

[77] L. Zhang, S. Yang, L. Huang, P. C.-L. Ho, *Int. J. Pharm.* **2020**, *591*, 119981, DOI 10.1016/j.ijpharm.2020.119981.

[78] J. K. Oh, *Soft Matter* **2011**, *7*, 5096, DOI 10.1039/c0sm01539c.

[79] J. Pretula, S. Slomkowski, S. Penczek, *Adv. Drug Deliv. Rev.* **2016**, *107*, 3–16, DOI 10.1016/j.addr.2016.05.002.

[80] R. Z. Xiao, Z. W. Zeng, G. L. Zhou, J. J. Wang, F. Z. Li, A. M. Wang, *Int. J. Nanomedicine* **2010**, *5*, 1057–1065, DOI 10.2147/IJN.S14912.

[81] F. Ebrahimi, H. Ramezani Dana, *Int. J. Polym. Mater. Polym. Biomater.* **2021**, *0*, 1–14, DOI 10.1080/00914037.2021.1944140.

[82] N. F. Zaaba, M. Jaafar, *Polym. Eng. Sci.* **2020**, *60*, 2061–2075, DOI 10.1002/pen.25511.

[83] M. Singhvi, S. Zinjarde, D. Gokhale, *J. Appl. Microbiol.* **2019**, *127*, 1612–1626, DOI 10.1111/jam.14290.

[84] Q. Shuai, Y. Cai, G. Zhao, X. Sun, *Int. J. Mol. Sci.* **2020**, *21*, 1856, DOI 10.3390/ijms21051856.

[85] C. G. Dariva, J. P. H. Figueiredo, C. Ferreira, M. Laranjo, M. F. Botelho, A. C. Fonseca, J. F. J. Coelho, A. C. Serra, *Colloids Surf. B Biointerfaces* **2020**, *196*, 111354, DOI 10.1016/j.colsurfb.2020.111354.

[86] M. Afsharzadeh, M. Hashemi, M. Babaei, K. Abnous, M. Ramezani, *J. Cell. Physiol.* **2020**, *235*, 4618–4630, DOI 10.1002/jcp.29339.

[87] S. Zalba, T. L. M. ten Hagen, C. Burgui, M. J. Garrido, *J. Control. Release* **2022**, *351*, 22–36, DOI 10.1016/j.jconrel.2022.09.002.

[88] S. Salmaso, P. Caliceti, *J. Drug Deliv.* **2013**, *2013*, e374252, DOI 10.1155/2013/374252.

[89] Q. Meng, H. Meng, Y. Pan, J. Liu, J. Li, Y. Qi, Y. Huang, *J. Mater. Chem. B* **2021**, DOI 10.1039/D1TB02015C.

[90] A. Zielińska, F. Carreiró, A. M. Oliveira, A. Neves, B. Pires, D. N. Venkatesh, A. Durazzo, M. Lucarini, P. Eder, A. M. Silva, A. Santini, E. B. Souto, *Molecules* **2020**, *25*, 3731, DOI 10.3390/molecules25163731.

[91] T. Kanamaru, K. Sakurai, S. Fujii, *Biomacromolecules* **2022**, DOI 10.1021/acs.biomac.2c00730.

[92] C. Zhu, Z. Zhang, Y. Wen, X. Song, J. Zhu, Y. Yao, J. Li, *J. Mater. Chem. B* **2023**, 10.1039.D2TB02050E, DOI 10.1039/D2TB02050E.

[93] N. M. Gulati, P. L. Stewart, N. F. Steinmetz, *Mol. Pharmaceutics* **2018**, *15*, 2900–2909, DOI 10.1021/acs.molpharmaceut.8b00292.

[94] X. Fu, L. Hosta-Rigau, R. Chandrawati, J. Cui, *Chem* **2018**, *4*, 2084–2107, DOI 10.1016/j.chempr.2018.07.002.

[95] H. Zhang, H. Xia, J. Wang, Y. Li, *J. Control. Release* **2009**, *139*, 31–39, DOI 10.1016/j.jconrel.2009.05.037.

[96] X. Sun, S. Agate, K. S. Salem, L. Lucia, L. Pal, *ACS Appl. Bio Mater.* **2021**, *4*, 140–162, DOI 10.1021/acsabm.0c01011.

[97] Y. Zhu, B. Yang, S. Chen, J. Du, *Prog. Polym. Sci.* **2017**, *64*, 1–22, DOI 10.1016/j.progpolymsci.2015.05.001.

[98] Z. Hami, M. Amini, M. Ghazi-Khansari, S. M. Rezayat, K. Gilani, *DARU J. Pharm. Sci.* **2014**, *22*, 30, DOI 10.1186/2008-2231-22-30.

[99] A. S. Choi, T. J. Moon, W. Abuhashim, A. Bhalotia, H. Qian, K. E. Paulsen, M. Lorkowski, C. Ndamira, R. Gopalakrishnan, A. Krishnamurthy, W. P. Schiemann, E. Karathanasis, *J. Control. Release* **2023**, DOI 10.1016/j.jconrel.2023.03.054.

[100] J. Siepmann, A. Faham, S.-D. Clas, B. J. Boyd, V. Jannin, A. Bernkop-Schnürch, H. Zhao, S. Lecommandoux, J. C. Evans, C. Allen, O. M. Merkel, G. Costabile, M. R. Alexander, R. D. Wildman, C. J. Roberts, J.-C. Leroux, *Int. J. Pharm.* **2019**, *558*, 128–142, DOI 10.1016/j.ijpharm.2018.12.080.

[101] R. Wehr, J. Gaitzsch, D. Daubian, C. Fodor, W. Meier, *RSC Adv.* **2020**, *10*, 22701–22711, DOI 10.1039/D0RA04274A.

[102] R. Nagarajan, *Langmuir* **2002**, *18*, 31–38, DOI 10.1021/la010831y.

[103] R. A. Khalil, A.-h. A. Zarari, *Appl. Surf. Sci.*, NANOTR9, 9th Nanoscience and Nanotechnology Conference Special Issue **2014**, *318*, 85–89, DOI 10.1016/j.apsusc.2014.01.046.

[104] P. Wei, E. J. Cornel, J. Du, *Macromolecules* **2021**, DOI 10.1021/acs.macromol.1c00060.

[105] D.-f. Li, M.-f. Yang, H.-m. Xu, M.-z. Zhu, Y. Zhang, C.-m. Tian, Y.-q. Nie, J.-y. Wang, Y. Liang, J. Yao, L.-s. Wang, *J. Mater. Chem. B* **2022**, DOI 10.1039/D2TB01190E.

[106] Y. Ogawa, Y. Akimoto, M. Ikemoto, Y. Goto, A. Ishikawa, S. Ohta, Y. Takase, H. Kawakami, M. Tsujimoto, R. Yanoshita, *Biochem. Biophys. Rep.* **2021**, *27*, 101034, DOI 10.1016/j.bbrep.2021.101034.

[107] T. X. Nguyen, L. Huang, M. Gauthier, G. Yang, Q. Wang, *Nanomedicine* **2016**, *11*, 1169–1185, DOI 10.2217/nnm.16.9.

[108] M. A. S. Abourehab, M. J. Ansari, A. Singh, A. Hassan, M. A. Abdelgawad, P. Shrivastav, B. M. Abualsoud, L. S. Amaral, S. Pramanik, *J. Mater. Chem. B* **2022**, *10*, 2781–2819, DOI 10.1039/D2TB00031H.

[109] H. M. G. Barriga, M. N. Holme, M. M. Stevens, *Angew. Chem. Int. Ed.* **2019**, *58*, 2958–2978, DOI 10.1002/anie.201804067.

[110] C. F. Grandes Reyes, S. Ha, K. T. Kim, *J. Polym. Sci.* **2023**, *61*, 1196–1213, DOI 10.1002/pol.20230053.

[111] M. Lindström, H. Ljusberg-Wahren, K. Larsson, B. Borgström, *Lipids* **1981**, *16*, 749–754, DOI 10.1007/BF02535343.

[112] V. Wang, S. Ha, J. Kim, K. T. Kim, *Giant* **2023**, *15*, 100178, DOI 10.1016/j.giant.2023.100178.

[113] H. Chen, M.-H. Li, *Macromol. Rapid Commun.* **2021**, *42*, 2100194, DOI 10.1002/marc.202100194.

[114] S. Rajesh, M. N. Leiske, V. Leitch, J. Zhai, C. J. Drummond, K. Kempe, N. Tran, *J. Colloid Interface Sci.* **2022**, *623*, 1142–1150, DOI 10.1016/j.jcis.2022.04.158.

[115] S. Ha, Y. La, K. T. Kim, *Acc. Chem. Res.* **2020**, *53*, 620–631, DOI 10.1021/acs.accounts.9b00563.

[116] S. D. Allen, S. Bobbala, N. B. Karabin, E. A. Scott, *Nanoscale Horiz.* **2019**, *4*, 258–272, DOI 10.1039/C8NH00300A.

[117] B. V. K. J. Schmidt, *Macromol. Chem. Phys.* **2018**, *219*, 1700494, DOI 10.1002/macp.201700494.

[118] M. Iqbal, Y. Tao, S. Xie, Y. Zhu, D. Chen, X. Wang, L. Huang, D. Peng, A. Sattar, M. A. B. Shabbir, H. I. Hussain, S. Ahmed, Z. Yuan, *Biol. Proced. Online* **2016**, *18*, 18, DOI 10.1186/s12575-016-0048-8.

[119] S. M. Brosnan, H. Schlaad, M. Antonietti, *Angew. Chem. Int. Ed.* **2015**, *54*, 9715–9718, DOI 10.1002/anie.201502100.

[120] A. El Jundi, S. J. Buwalda, Y. Bakkour, X. Garric, B. Nottelet, *Adv. Colloid Interface Sci.* **2020**, *283*, 102213, DOI 10.1016/j.cis.2020.102213.

[121] N. Martin, *ChemBioChem* **2019**, *20*, 2553–2568, DOI 10.1002/cbic.201900183.

[122] J. Willersinn, M. Drechsler, M. Antonietti, B. V. K. J. Schmidt, *Macromolecules* **2016**, *49*, 5331–5341, DOI 10.1021/acs.macromol.6b01355.

[123] H. Park, S. Walta, R. R. Rosencrantz, A. Körner, C. Schulte, L. Elling, W. Richtering, A. Böker, *Polym. Chem.* **2016**, *7*, 878–886, DOI 10.1039/C5PY00797F.

[124] J. Willersinn, B. V. K. J. Schmidt, *Polymers* **2017**, *9*, 293, DOI 10.3390/polym9070293.

[125] O. Casse, A. Shkilnyy, J. Linders, C. Mayer, D. Häussinger, A. Völkel, A. F. Thünemann, R. Dimova, H. Cölfen, W. Meier, H. Schlaad, A. Taubert, *Macromolecules* **2012**, *45*, 4772–4777, DOI 10.1021/ma300621g.

[126] P. Hebbeker, A. A. Steinschulte, S. Schneider, J. Okuda, M. Möller, F. A. Plamper, S. Schneider, *Macromolecules* **2016**, *49*, 8748–8757, DOI 10.1021/acs.macromol.6b01786.

[127] A. Blanazs, N. J. Warren, A. L. Lewis, S. P. Armes, A. J. Ryan, *Soft Matter* **2011**, *7*, 6399–6403, DOI 10.1039/C1SM05771E.

[128] A. Taubert, E. Furrer, W. Meier, *Chem. Commun.* **2004**, 2170, DOI 10.1039/b405610h.

[129] N. Al Nakeeb, J. Willersinn, B. V. K. J. Schmidt, *Biomacromolecules* **2017**, *18*, 3695–3705, DOI 10.1021/acs.biomac.7b01094.

[130] C. W. S. Yeung, M. H. Periayah, J. Y. Q. Teo, E. T. L. Goh, P. L. Chee, W. W. Loh, X. J. Loh, R. Lakshminarayanan, J. Y. C. Lim, *Macromolecules* **2023**, DOI 10.1021/acs.macromol.2c01944.

[131] J. Nicolas, S. Mura, D. Brambilla, N. Mackiewicz, P. Couvreur, *Chem. Soc. Rev.* **2013**, *42*, 1147–1235, DOI 10.1039/C2CS35265F.

[132] Y. Zhong, B. J. Zeberl, X. Wang, J. Luo, *Acta Biomater.* **2018**, *73*, 21–37, DOI 10.1016/j.actbio.2018.04.010.

[133] M. A. Gauthier, M. I. Gibson, H.-A. Klok, *Angew. Chem. Int. Ed.* **2009**, *48*, 48–58, DOI 10.1002/anie.200801951.

[134] H. Muljana, S. Arends, K. Remerie, G. Boven, F. Picchioni, R. K. Bose, *Polymers* **2022**, *14*, 1176, DOI 10.3390/polym14061176.

[135] P.-H. Elchinger, P.-A. Faugeras, B. Boëns, F. Brouillette, D. Montplaisir, R. Zerrouki, R. Lucas, *Polymers* **2011**, *3*, 1607–1651, DOI 10.3390/polym3041607.

[136] J. Rieger, K. V. Butsele, P. Lecomte, C. Detrembleur, R. Jérôme, C. Jérôme, *Chem. Commun.* **2005**, 274–276, DOI 10.1039/B411565A.

[137] A. A. Burkey, N. Ghousifam, A. V. Hillsley, Z. W. Brotherton, M. Rezaeeyazdi, T. A. Hatridge, D. T. Harris, W. W. Sprague, B. E. Sandoval, A. M. Rosales, M. N. Rylander, N. A. Lynd, *Biomacromolecules* **2023**, DOI 10.1021/acs.biomac.2c01488.

[138] S. D. Morrison, R. M. J. Liskamp, J. Prunet, *Org. Lett.* **2018**, *20*, 2253–2256, DOI 10.1021/acs.orglett.8b00595.

[139] G. W. Coates, R. H. Grubbs, *J. Am. Chem. Soc.* **1996**, *118*, 229–230, DOI 10.1021/ja9532603.

[140] W. Kośnik, D. Lichosyt, M. Śnieżek, A. Janaszkiewicz, K. Woźniak, M. Malińska, B. Trzaskowski, A. Kajetanowicz, K. Grela, *Angew. Chem. Int. Ed.* **2022**, *61*, e202201472, DOI 10.1002/anie.202201472.

[141] S. Planer, P. Małecki, B. Trzaskowski, A. Kajetanowicz, K. Grela, *ACS Catal.* **2020**, *10*, 11394–11404, DOI 10.1021/acscatal.0c02770.

[142] E. Tzur, A. Szadkowska, A. Ben-Asuly, A. Makal, I. Goldberg, K. Woźniak, K. Grela, N. G. Lemcoff, *Chem. – Eur. J.* **2010**, *16*, 8726–8737, DOI 10.1002/chem.200903457.

[143] L. C. So, S. Faucher, S. Zhu, *Macromol. React. Eng.* **2013**, *7*, 684–698, DOI 10.1002/mren.201300121.

[144] H. I. Labouta, R. Langer, P. R. Cullis, O. M. Merkel, M. R. Prausnitz, Y. Gomaa, S. S. Nogueira, T. Kumeria, *Drug Deliv. and Transl. Res.* **2022**, DOI 10.1007/s13346-022-01146-1.

[145] J. M. Dang, K. W. Leong, *Adv. Drug Deliv. Rev.* **2006**, *58*, 487–499, DOI 10.1016/j.addr.2006.03.001.

[146] J. L. Coll, P. Chollet, E. Brambilla, D. Desplanques, J. P. Behr, M. Favrot, *Hum. Gene Ther.* **1999**, *10*, 1659–1666, DOI 10.1089/10430349950017662.

[147] J. Dolai, K. Mandal, N. R. Jana, *ACS Appl. Nano Mater.* **2021**, DOI 10.1021/acsanm.1c00987.

[148] S. Mehier-Humbert, R. H. Guy, *Adv. Drug Deliv. Rev.* **2005**, *57*, 733–753, DOI 10.1016/j.addr.2004.12.007.

[149] R. S. Burke, S. H. Pun, *Bioconjug. Chem.* **2008**, *19*, 693–704, DOI 10.1021/bc700388u.

[150] O. Boussif, F. Lezoualc'h, M. A. Zanta, M. D. Mergny, D. Scherman, B. Demeneix, J. P. Behr, *Proc. Natl. Acad. Sci. U. S. A.* **1995**, *92*, 7297–7301, DOI 10.1073/pnas.92.16.7297.

[151] M. Jäger, S. Schubert, S. Ochrimenko, D. Fischer, U. S. Schubert, *Chem. Soc. Rev.* **2012**, *41*, 4755–4767, DOI 10.1039/C2CS35146C.

[152] U. Lächelt, E. Wagner, *Chem. Rev.* **2015**, *115*, 11043–11078, DOI 10.1021/cr5006793.

[153] K. Ita, *Eur. J. Pharm. Sci.* **2020**, *150*, 105358, DOI 10.1016/j.ejps.2020.105358.

[154] Y. Liu, L. Zhou, X. Xu, Z. Cheng, Y. Chen, X.-A. Mei, N. Zheng, C. Zhang, Y. Bai, *Biomacromolecules* **2023**, DOI 10.1021/acs.biomac.3c00682.

[155] Z. Diamantopoulou, M.-E. Gilles, M. Sader, M. Cossutta, B. Vallée, C. Houppe, D. Habert, B. Brissault, E. Leroy, F. Maione, E. Giraudo, D. Destouches, J. Penelle, J. Courty, I. Cascone, *Oncotarget* **2017**, *8*, 90108–90122, DOI 10.18632/oncotarget.21441.

[156] O. Germershaus, S. Mao, J. Sitterberg, U. Bakowsky, T. Kissel, *J. Control. Release* **2008**, *125*, 145–154, DOI 10.1016/j.jconrel.2007.10.013.

[157] W. Fischer, B. Brissault, S. Prévost, M. Kopaczynska, I. Andreou, A. Janosch, M. Gradzielski, R. Haag, *Macromol. Biosci.* **2010**, *10*, 1073–1083, DOI 10.1002/mabi.201000082.

[158] W. B. Liechty, D. R. Kryscio, B. V. Slaughter, N. A. Peppas, *Annu. Rev. Chem. Biomol. Eng.* **2010**, *1*, 149–173, DOI 10.1146/annurev-chembioeng-073009-100847.

[159] M. F. Farona, C. Tsonis, *J. Chem. Soc. Chem. Commun.* **1977**, 363–364, DOI 10.1039/C39770000363.

[160] V. Firetto, M. A. Floriano, A. Z. Panagiotopoulos, *Langmuir* **2006**, *22*, 6514–6522, DOI 10.1021/la060386c.

[161] D. W. Knight, I. R. Morgan, A. J. Proctor, *Tetrahedron Lett.* **2010**, *51*, 638–640, DOI 10.1016/j.tetlet.2009.11.092.

[162] A. Buckinx, M. Rubens, N. R. Cameron, C. Bakkali-Hassani, A. Sokolova, T. Junkers, *Polym. Chem.* **2022**, DOI 10.1039/D2PY00318J.

[163] T. Betancourt, B. Brown, L. Brannon-Peppas, *Nanomed.* **2007**, *2*, 219–232, DOI 10.2217/17435889.2.2.219.

[164] M. Chorny, I. Fishbein, H. D. Danenberg, G. Golomb, *J. Control. Release* **2002**, *83*, 389–400, DOI 10.1016/S0168-3659(02)00211-0.

[165] X. Yan, J. Bernard, F. Ganachaud, *Adv. Colloid Interface Sci.* **2021**, *294*, 102474, DOI 10.1016/j.cis.2021.102474.

[166] E. Lepeltier, C. Bourgaux, P. Couvreur, *Adv. Drug Deliv. Rev.* **2014**, *71*, 86–97, DOI 10.1016/j.addr.2013.12.009.

[167] T. Watanabe, Y. Sakamoto, T. Inooka, Y. Kimura, T. Ono, *Colloids Surf. Physicochem. Eng. Asp.* **2017**, *520*, 764–770, DOI 10.1016/j.colsurfa.2017.02.039.

[168] B. Mui, P. Cullis, E. Evans, T. Madden, *Biophys. J.* **1993**, *64*, 443–453, DOI 10.1016/S0006-3495(93)81385-7.

[169] D. F. Williams, *Eng. Med.* **1981**, *10*, 5–7, DOI 10.1243/EMED_JOUR_1981_010_004_02.

[170] S. Matoori, J.-C. Leroux, *Mater. Horiz.* **2020**, *7*, 1297–1309, DOI 10.1039/C9MH01669D.

[171] N. C. Bell, S. J. Doyle, G. Battistelli, C. L. M. LeGuyader, M. P. Thompson, A. M. Poe, A. Rheingold, C. Moore, M. Montalti, S. Thayumanavan, M. J. Tauber, N. C. Gianneschi, *Langmuir* **2015**, *31*, 9707–9717, DOI 10.1021/acs.langmuir.5b01822.

[172] E. M. Elmowafy, M. Tiboni, M. E. Soliman, *J. Pharm. Investig.* **2019**, *49*, 347–380, DOI 10.1007/s40005-019-00439-x.

[173] A. H. Gröschel, A. Walther, *Angew. Chem. Int. Ed. Engl.* **2017**, *56*, 10992–10994, DOI 10.1002/anie.201703765.

[174] K. Margulis, X. Zhang, L.-M. Joubert, K. Bruening, C. J. Tassone, R. N. Zare, R. M. Waymouth, *Angew. Chem. Int. Ed.* **2017**, *129*, 16575–16580, DOI 10.1002/ange.201709564.

[175] I. Schmolka, US3740421A, **1973**.

[176] E. Russo, C. Villa, *Pharmaceutics* **2019**, *11*, 671, DOI 10.3390/pharmaceutics11120671.

[177] P. Zarrintaj, J. D. Ramsey, A. Samadi, Z. Atoufi, M. K. Yazdi, M. R. Ganjali, L. M. Amirabad, E. Zangene, M. Farokhi, K. Formela, M. R. Saeb, M. Mozafari, S. Thomas, *Acta Biomater.* **2020**, *110*, 37–67, DOI 10.1016/j.actbio.2020.04.028.

[178] G. Niu, F. Du, L. Song, H. Zhang, J. Yang, H. Cao, Y. Zheng, Z. Yang, G. Wang, H. Yang, S. Zhu, *J. Control. Release* **2009**, *138*, 49–56, DOI 10.1016/j.jconrel.2009.04.026.

[179] F. Agnely, A. Djedour, A. Bochot, J. .-. Grossiord, *J. Drug Deliv. Sci. Technol.* **2006**, *16*, 3–10, DOI 10.1016/S1773-2247(06)50001-2.

[180] A. M. Bodratti, P. Alexandridis, *J. Funct. Biomater.* **2018**, *9*, 11, DOI 10 . 3390 / jfb9010011.

[181] Global Poloxamer Market – Industry Reports, https://www.precisionreports.co/global-poloxamer-market-19882483 (Accessed on 01/05/2024).

[182] S. D. Singh-Joy, V. C. McLain, *Int. J. Toxicol.* **2008**, *27 Suppl 2*, 93–128, DOI 10.1080/10915810802244595.

[183] E. H. Gökçe, E. A. Yapar, S. T. Tanrıverdi, Ö. Özer in *Nanobiomaterials in Galenic Formulations and Cosmetics*, (Ed.: A. M. Grumezescu), William Andrew Publishing, **2016**, pp. 363–393, DOI 10.1016/B978-0-323-42868-2.00014-0.

[184] B. Mazumder, S. Ray, P. Pal, Y. Pathak, *Nanotechnology: Therapeutic, Nutraceutical, and Cosmetic Advances*, CRC Press, **2019**.

[185] E. Esposito, M. Drechsler, P. Mariani, E. Sivieri, R. Bozzini, L. Montesi, E. Menegatti, R. Cortesi, *Int. J. Cosmet. Sci.* **2007**, *29*, 39–47, DOI 10.1111/j.1467-2494.2007.00362.x.

[186] O. Šrom, V. Trávníková, L. Bláha, M. Ciofalo, M. Šoóš, *Biochem. Eng. J.* **2022**, *186*, 108549, DOI 10.1016/j.bej.2022.108549.

[187] P. Lemieux, N. Guérin, G. Paradis, R. Proulx, L. Chistyakova, A. Kabanov, V. Alakhov, *Gene Ther.* **2000**, *7*, 986–991, DOI 10.1038/sj.gt.3301189.

[188] H. Madry, L. Gao, A. Rey-Rico, J. K. Venkatesan, K. Müller-Brandt, X. Cai, L. Goebel, G. Schmitt, S. Speicher-Mentges, D. Zurakowski, M. D. Menger, M. W. Laschke, M. Cucchiarini, *Adv. Mater.* **2020**, *32*, 1906508, DOI 10.1002/adma.201906508.

[189] L. J. Feldman, C. J. Pastore, N. Aubailly, M. Kearney, D. Chen, M. Perricaudet, P. G. Steg, J. M. Isner, *Gene Ther.* **1997**, *4*, 189–198, DOI 10.1038/sj.gt.3300382.

[190] H. Peng, K. M. Hall, B. Clayton, K. Wiltberger, W. Hu, E. Hughes, J. Kane, R. Ney, T. Ryll, *Biotechnol. Prog.* **2014**, *30*, 1411–1418, DOI 10.1002/btpr.1967.

[191] T. K. Law, T. L. Whateley, A. T. Florence, *Int. J. Pharm.* **1984**, *21*, 277–287, DOI 10.1016/0378-5173(84)90186-8.

[192] M. A. Abou-Shamat, J. Calvo-Castro, J. L. Stair, M. T. Cook, *Macromol. Chem. Phys.* **2019**, *220*, 1900173, DOI 10.1002/macp.201900173.

[193] L. Ci, Z. Huang, Y. Liu, Z. Liu, G. Wei, W. Lu, *Acta Pharm. Sin. B* **2017**, *7*, 593–602, DOI 10.1016/j.apsb.2017.03.002.

[194] A. M. Butt, M. C. I. Mohd Amin, H. Katas, *Int. J. Nanomedicine* **2015**, *10*, 1321–1334, DOI 10.2147/IJN.S78438.

[195] M. Worm, B. Kang, C. Dingels, F. R. Wurm, H. Frey, *Macromol. Rapid Commun.* **2016**, *37*, 775–780, DOI 10.1002/marc.201600080.

[196] L. Wang, J. Yao, X. Zhang, Y. Zhang, C. Xu, R. J. Lee, G. Yu, B. Yu, L. Teng, *Colloids Surf. B Biointerfaces* **2018**, *161*, 464–470, DOI 10.1016/j.colsurfb.2017.11.013.

[197] C. Yu, Y. Yu, D. Zhao, *Chem. Commun.* **2000**, *0*, 575–576, DOI 10.1039/B000603N.

[198] S. W. Mork, G. D. Rose, D. P. Green, *J. Surfactants Deterg.* **2001**, *4*, 127–134, DOI 10.1007/s11743-001-0165-5.

[199] O. Marin, M. Alesker, S. Guttman, G. Gershinsky, E. Edri, H. Shpaisman, R. E. Guerra, D. Zitoun, M. Deutsch, E. Sloutskin, *J. Colloid Interface Sci.* **2019**, *538*, 541–545, DOI 10.1016/j.jcis.2018.11.111.

[200] C. F. Welch, G. D. Rose, D. Malotky, S. T. Eckersley, *Langmuir* **2006**, *22*, 1544–1550, DOI 10.1021/la052207h.

[201] J. Gao, S. Le, S. Thayumanavan, *Angew. Chem. Int. Ed.* **2021**, *60*, 27189–27194, DOI 10.1002/anie.202109477.

[202] N. R. Cameron, *Polymer* **2005**, *46*, 1439–1449, DOI 10.1016/j.polymer.2004.11.097.

[203] I. Pulko, P. Krajnc, *Macromol. Rapid Commun.* **2012**, *33*, 1731–1746, DOI 10.1002/marc.201200393.

[204] L. L. C. Wong, P. M. Baiz Villafranca, A. Menner, A. Bismarck, *Langmuir* **2013**, *29*, 5952–5961, DOI 10.1021/la3047643.

[205] J. Luo, Z. Huang, L. Liu, H. Wang, G. Ruan, C. Zhao, F. Du, *J. Sep. Sci.* **2021**, *44*, 169–187, DOI 10.1002/jssc.202000612.

[206] G. Settanni, J. Zhou, F. Schmid, *J. Phys.: Conf. Ser.* **2017**, *921*, 012002, DOI 10.1088/1742-6596/921/1/012002.

[207] X. Liu, G. Sala, E. Scholten, *Curr. Res. Food Sci.* **2023**, *7*, 100531, DOI 10.1016/j.crfs.2023.100531.

[208] K. Philipps, T. Junkers, J. Michels, *Polym. Chem.* **2021**, *12*, 2522–2531, DOI 10.1039/D1PY00210D.

[209] J. Szafraniec, A. Antosik, J. Knapik-Kowalczuk, K. Chmiel, M. Kurek, K. Gawlak, J. Odrobińska, M. Paluch, R. Jachowicz, *Pharmaceutics* **2019**, *11*, 130, DOI 10.3390/pharmaceutics11030130.

[210] R. Pasquali, N. Sacco, C. Bregni, *Lat. Am. J. Pharm.* **2009**, *28*, 313–317.

[211] E. C. Davidson, A. M. Rosales, A. L. Patterson, B. Russ, B. Yu, R. N. Zuckermann, R. A. Segalman, *Macromolecules* **2018**, *51*, 2089–2098, DOI 10.1021/acs.macromol.8b00055.

[212] B. D. Olsen, R. A. Segalman, *Mater. Sci. Eng. R Rep.* **2008**, *62*, 37–66, DOI 10.1016/j.mser.2008.04.001.

[213] B. Yu, S. P. O. Danielsen, A. L. Patterson, E. C. Davidson, R. A. Segalman, *Macromolecules* **2019**, *52*, 2560–2568, DOI 10.1021/acs.macromol.9b00211.

[214] R.-M. Ho, C.-K. Chen, Y.-W. Chiang, *Macromol. Rapid Commun.* **2009**, *30*, 1439–1456, DOI 10.1002/marc.200900181.

[215] Y.-W. Chiang, R.-M. Ho, C. Burger, H. Hasegawa, *Soft Matter* **2011**, *7*, 9797–9803, DOI 10.1039/C1SM05921A.

[216] R.-M. Ho, Y.-W. Chiang, S.-C. Lin, C.-K. Chen, *Prog. Polym. Sci.* **2011**, *36*, 376–453, DOI 10.1016/j.progpolymsci.2010.09.001.

[217] A. Halperin, *Macromolecules* **1990**, *23*, 2724–2731, DOI 10.1021/ma00212a023.

[218] H. Li, D. Hu, F. Liang, X. Huang, Q. Zhu, *R. Soc. Open Sci.* **2020**, *7*, 192092, DOI 10.1098/rsos.192092.

[219] P188 Technical Sheet, https://pharma.basf.com/technicalinformation/30631536/kolliphor-p-188-geismar (Accessed on 01/05/2024).

[220] M. A. Schafheutle, H. Finkelmann, *Liq. Cryst.* **1988**, *3*, 1369–1386, DOI 10.1080/02678298808086617.

[221] B. D. Marshall, K. R. Cox, W. G. Chapman, *Soft Matter* **2012**, *8*, 7415–7425, DOI 10.1039/C2SM26019K.

[222] J. A. Hanson, C. B. Chang, S. M. Graves, Z. Li, T. G. Mason, T. J. Deming, *Nature* **2008**, *455*, 85–88, DOI 10.1038/nature07197.

[223] N. J. Van Zee, A. S. Peroutka, M. A. Hillmyer, T. P. Lodge, *Langmuir* **2023**, *39*, 7258–7267, DOI 10.1021/acs.langmuir.2c03443.

[224] Y. Dai, X. Zhang, *Polym. Chem.* **2019**, *10*, 296–305, DOI 10.1039/C8PY01365A.

[225] J. Guo, J. Qin, Y. Ren, B. Wang, H. Cui, Y. Ding, H. Mao, F. Yan, *Polym. Chem.* **2018**, *9*, 4611–4616, DOI 10.1039/C8PY00665B.

[226] D. Rahmat, D. Sakloetsakun, G. Shahnaz, G. Perera, R. Kaindl, A. Bernkop-Schnürch, *Int. J. Pharm.* **2011**, *411*, 10–17, DOI 10.1016/j.ijpharm.2011.02.063.

[227] M. V. de Paz Báñez, K. L. Robinson, M. Vamvakaki, S. F. Lascelles, S. P. Armes, *Polymer* **2000**, *41*, 8501–8511, DOI 10.1016/S0032-3861(00)00217-2.

[228] S. Tomita, S. Ishihara, R. Kurita, *J. Mater. Chem. B* **2022**, *10*, 7581–7590, DOI 10.1039/D2TB00606E.

[229] P. Klemm, J. I. Solomun, M. Rodewald, M. T. Kuchenbrod, V. G. Hänsch, F. Richter, J. Popp, C. Hertweck, S. Hoeppener, C. Bonduelle, S. Lecommandoux, A. Traeger, S. Schubert, *Biomacromolecules* **2022**, *23*, 4718–4733, DOI 10.1021/acs.biomac.2c00919.

[230] A. M. Funhoff, C. F. van Nostrum, M. C. Lok, M. M. Fretz, D. J. A. Crommelin, W. E. Hennink, *Bioconjugate Chem.* **2004**, *15*, 1212–1220, DOI 10.1021/bc049864q.

[231] C. Englert, A.-K. Trützschler, M. Raasch, T. Bus, P. Borchers, A. S. Mosig, A. Traeger, U. S. Schubert, *J. Control. Release* **2016**, *241*, 1–14, DOI 10.1016/j.jconrel.2016.08.039.

[232] Z. Yang, L. Lin, Z. Guo, X. Guo, Z. Tang, H. Tian, X. Chen, *Biomacromolecules* **2022**, *23*, 2867–2877, DOI 10.1021/acs.biomac.2c00331.

[233] Y.-D. Du, B.-H. Chen, W. Shu, *Angew. Chem. Int. Ed.* **2021**, *60*, 9875–9880, DOI 10.1002/anie.202016679.

[234] E. Edelstein, A. Grote, M. Palkowitz, J. Morken, *Synlett* **2018**, *29*, 1749–1752, DOI 10.1055/s-0037-1610172.

[235] E. Rieger, T. Gleede, A. Manhart, M. Lamla, F. R. Wurm, *ACS Macro Lett.* **2018**, *7*, 598–603, DOI 10.1021/acsmacrolett.8b00180.

[236] N. P. Cowieson, C. J. C. Edwards-Gayle, K. Inoue, N. S. Khunti, J. Doutch, E. Williams, S. Daniels, G. Preece, N. A. Krumpa, J. P. Sutter, M. D. Tully, N. J. Terrill, R. P. Rambo, *J. Synchrotron Rad.* **2020**, *27*, 1438–1446, DOI 10.1107/S1600577520009960.

[237] L. Nóvoa, L. Trulli, A. Parra, M. Tortosa, *Angew. Chem. Int. Ed.* **2021**, anie.202101445, DOI 10.1002/anie.202101445.

[238] A. de Belder, K. Granath, *Carbohydr. Res.* **1973**, *30*, 375–378, DOI 10.1016/S0008-6215(00)81824-8.

[239] J. N. Hunt, K. E. Feldman, N. A. Lynd, J. Deek, L. M. Campos, J. M. Spruell, B. M. Hernandez, E. J. Kramer, C. J. Hawker, *Adv. Mater.* **2011**, *23*, 2327–2331, DOI 10.1002/adma.201004230.

Appendix

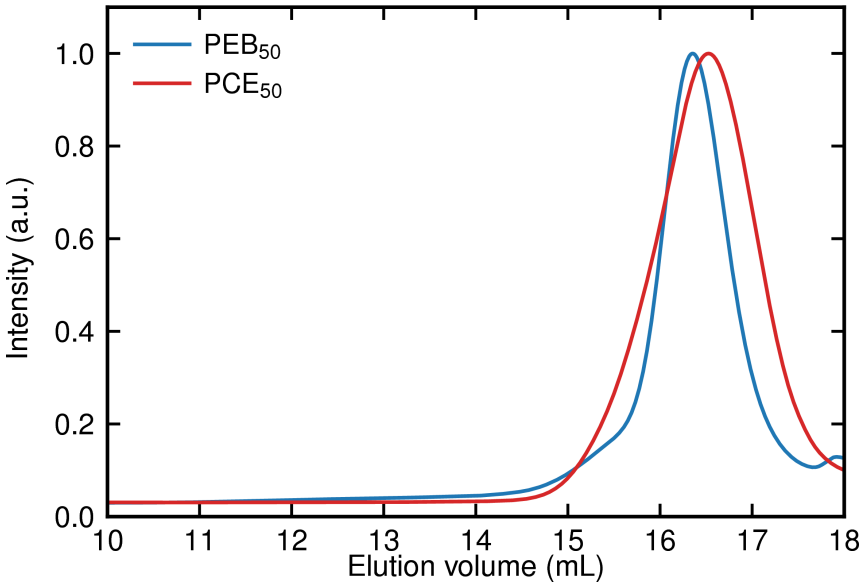

Figure 7.1: SEC traces of atactic PEB_{50} and PCE_{50}, measured in THF with a 1 mL/min flow rate.

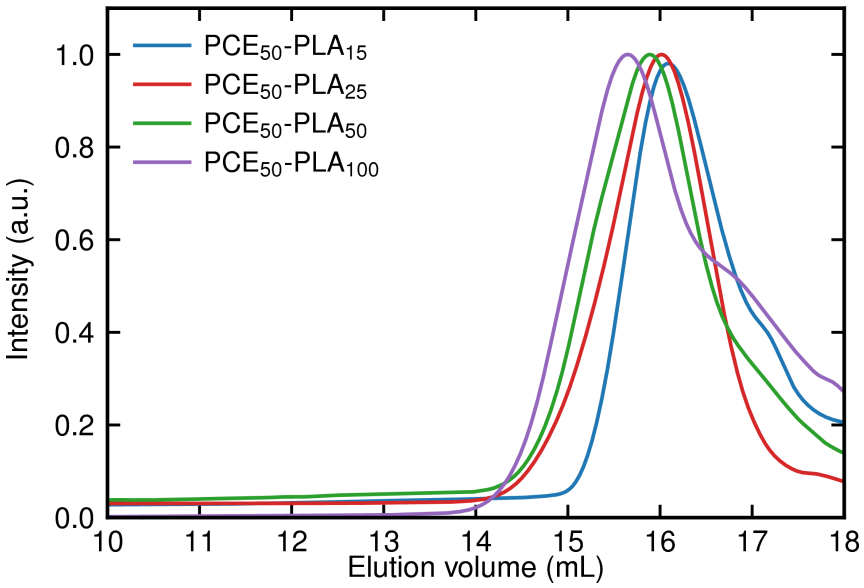

Figure 7.2: SEC traces of PCE_{50}-PLA_{15}, PCE_{50}-PLA_{25}, PCE_{50}-PLA_{50}, PCE_{50}-PLA_{100} measured in THF with a 1 mL/min flow rate.

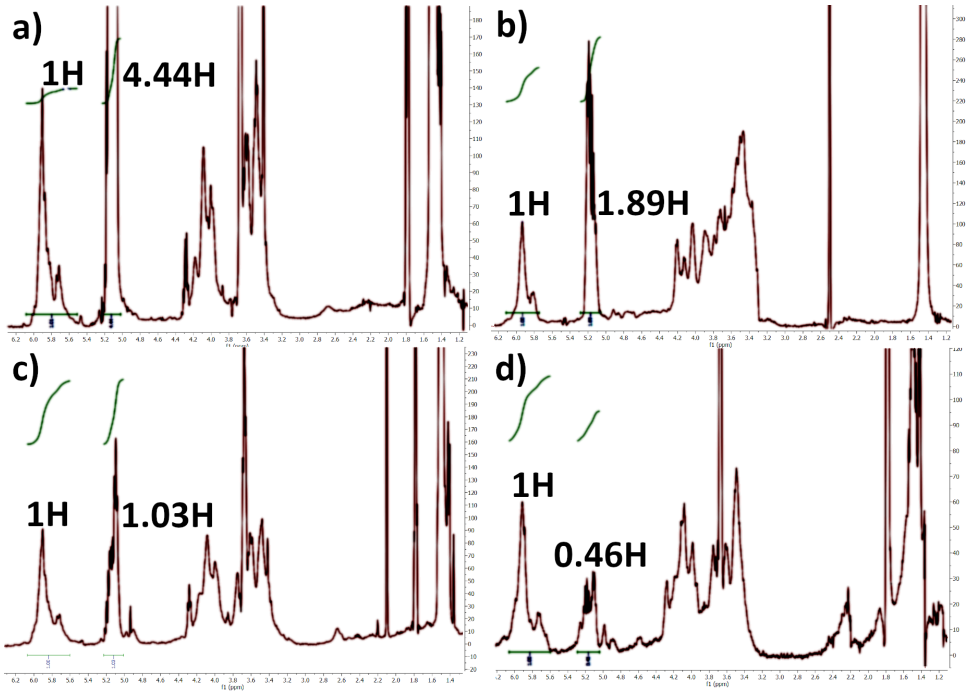

Figure 7.3: ^{1}H NMR spectra of **a)** PCE_{50}-PLA_{100} **b)** PCE_{50}-PLA_{50} **c)** PCE_{50}-PLA_{25} **d)** PCE_{50}-PLA_{15} in $CDCl_3$. Alkene protons from the PCE block were normalised to 2.

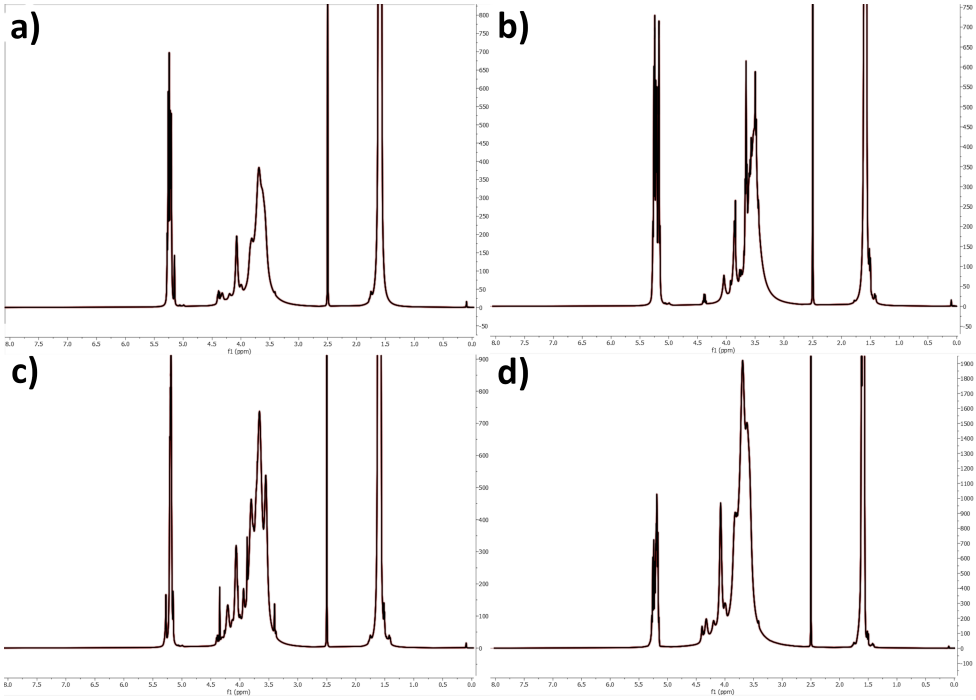

Figure 7.4: ^{1}H NMR spectra of **a)** $PEGose_{50}$-PLA_{100}, **b)** $PEGose_{50}$-PLA_{50}, **c)** $PEGose_{50}$-PLA_{25} and **d)** $PEGose_{50}$-PLA_{15} in DMSO-d_6.

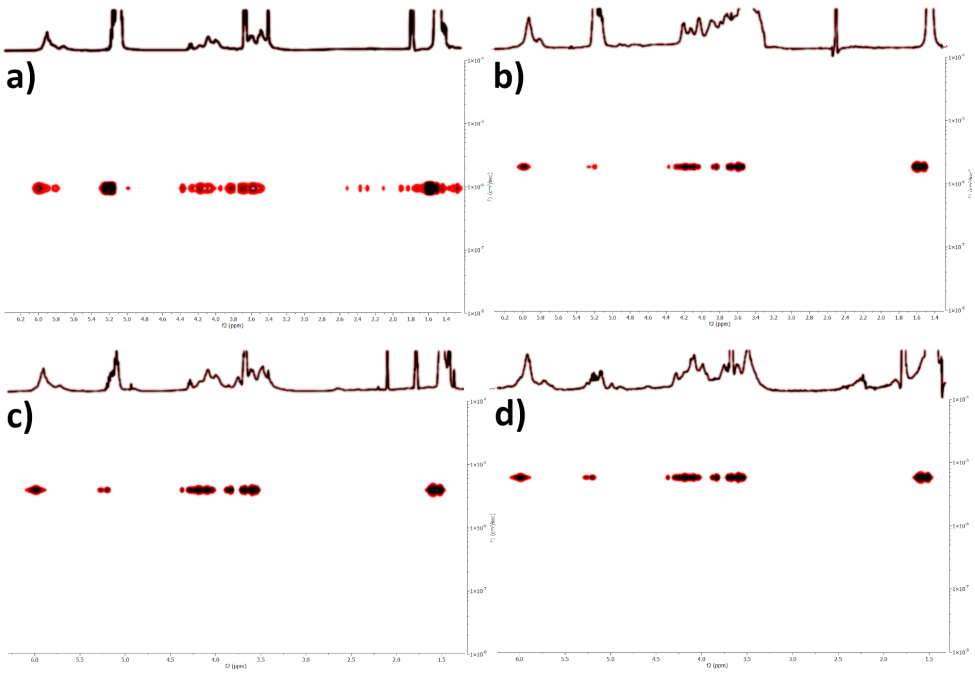

Figure 7.5: ^{1}H NMR DOSY spectra of **a)** PCE_{50}-PLA_{100}, **b)** PCE_{50}-PLA_{50}, **c)** PCE_{50}-PLA_{25} and **d)** PCE_{50}-PLA_{15} in $CDCl_3$.

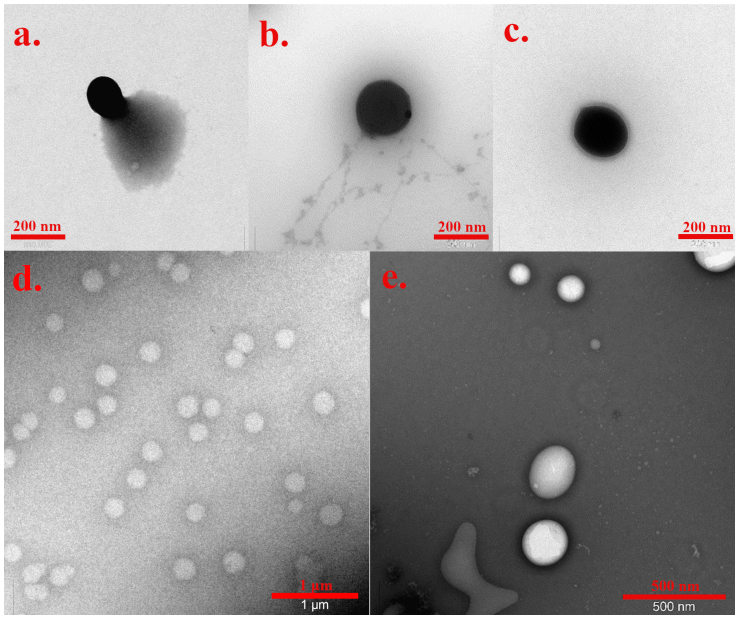

Figure 7.6: TEM images of $PEGose_{50}$-PLA_{50} stained with uranyl acetate **(a. b. and c.)** or without using any stain **(d. and e.)**. The nanoparticles were prepared by dialysing the DMSO block copolymer solution against deionised water. Scale bars are 200 nm.

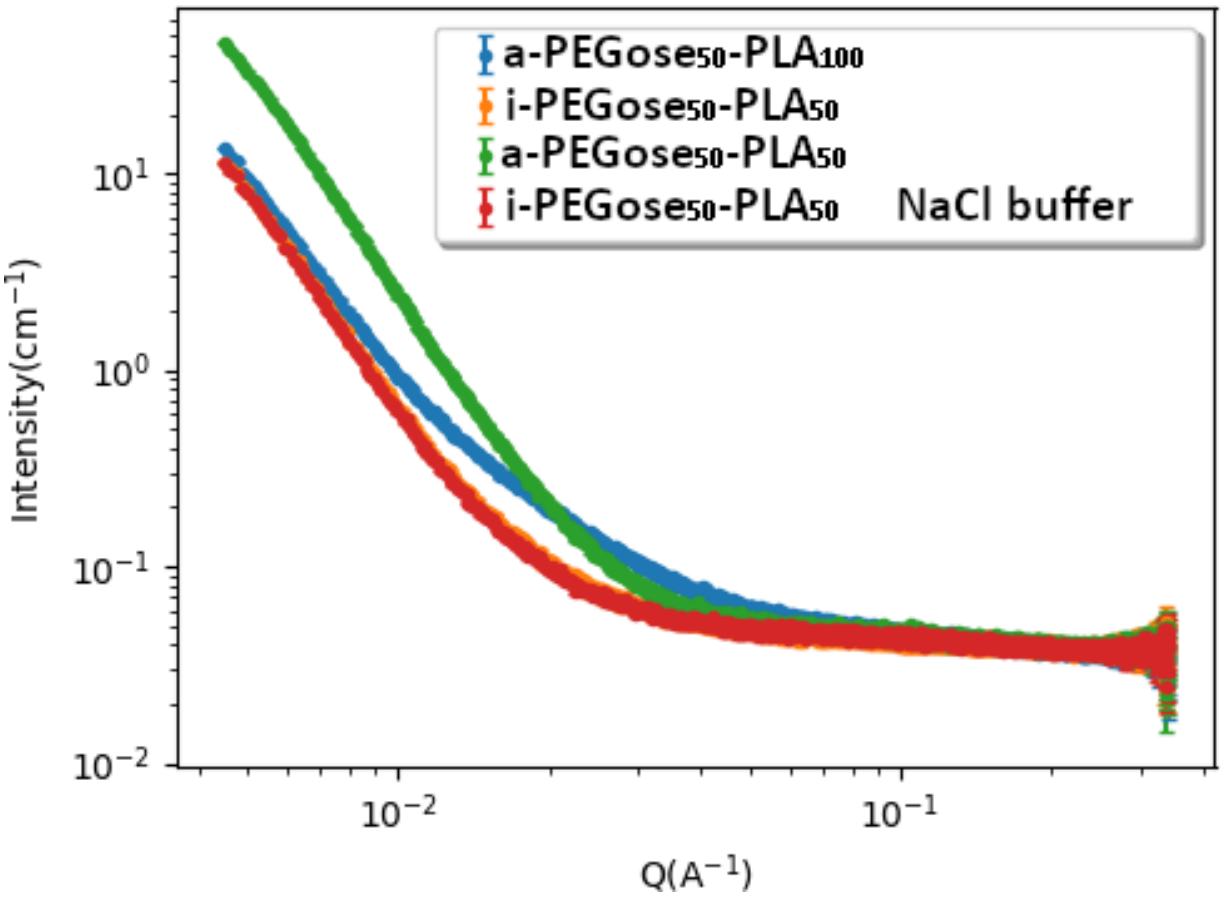

Figure 7.7: SAXS scattering curves for a-PEGose$_{50}$-PLA$_{100}$, i-PEGose$_{50}$-PLA$_{50}$ and a-PEGose$_{50}$-PLA$_{50}$ in deionised water and i-PEGose$_{50}$-PLA$_{50}$ in a 10 mg/mL NaCl solution. The scattering curves were obtained by Daniel McDowall using the beamline B21: high-throughput small-angle X-ray scattering at Diamond Light Source.[236] The data was consequently fitted into a homogeneous sphere with an adsorbed layer model.

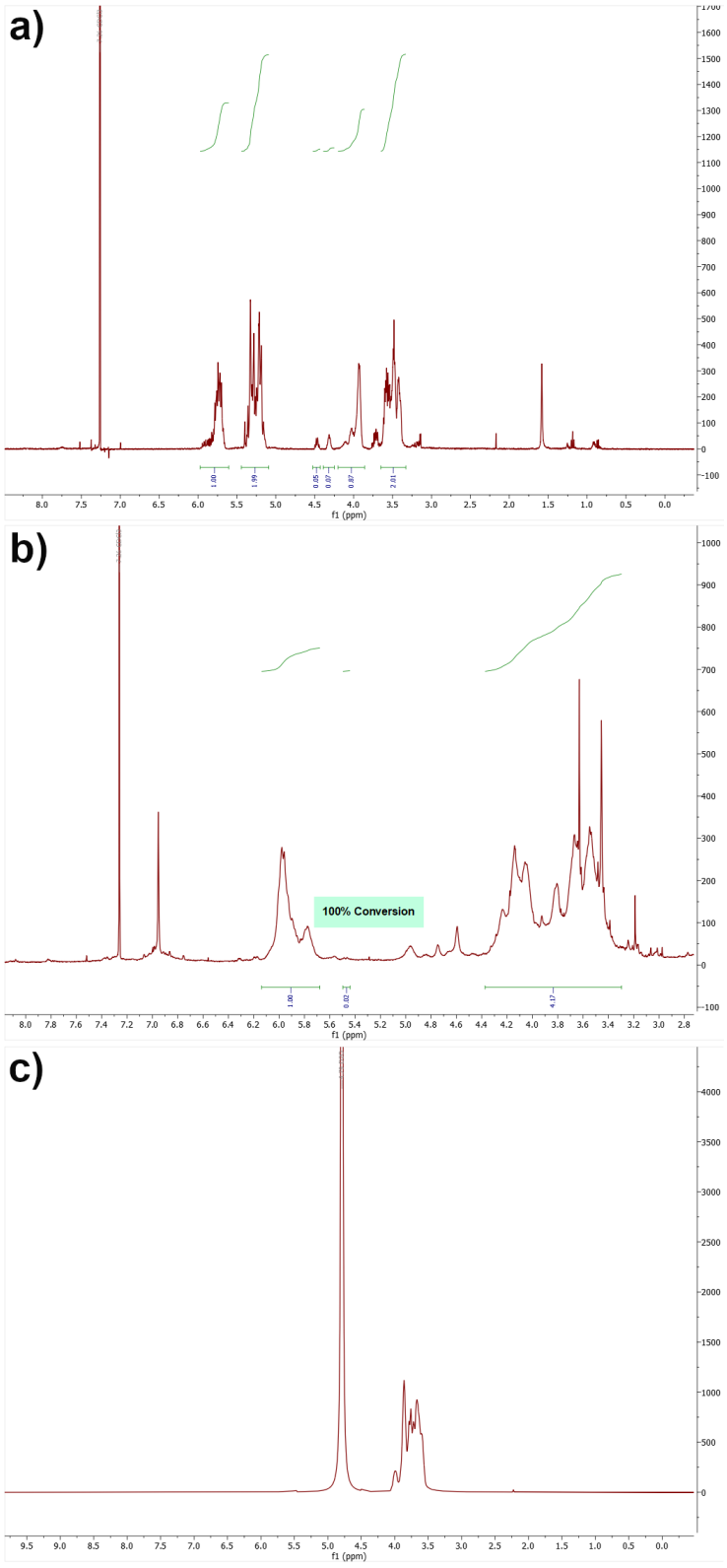

Figure 7.8: ^{1}H NMR spectra of **a)** i-PEB$_{50}$ and **b)** i-PCE$_{50}$ in $CDCl_3$ and **c)** i-PEGose$_{50}$ in D_2O.

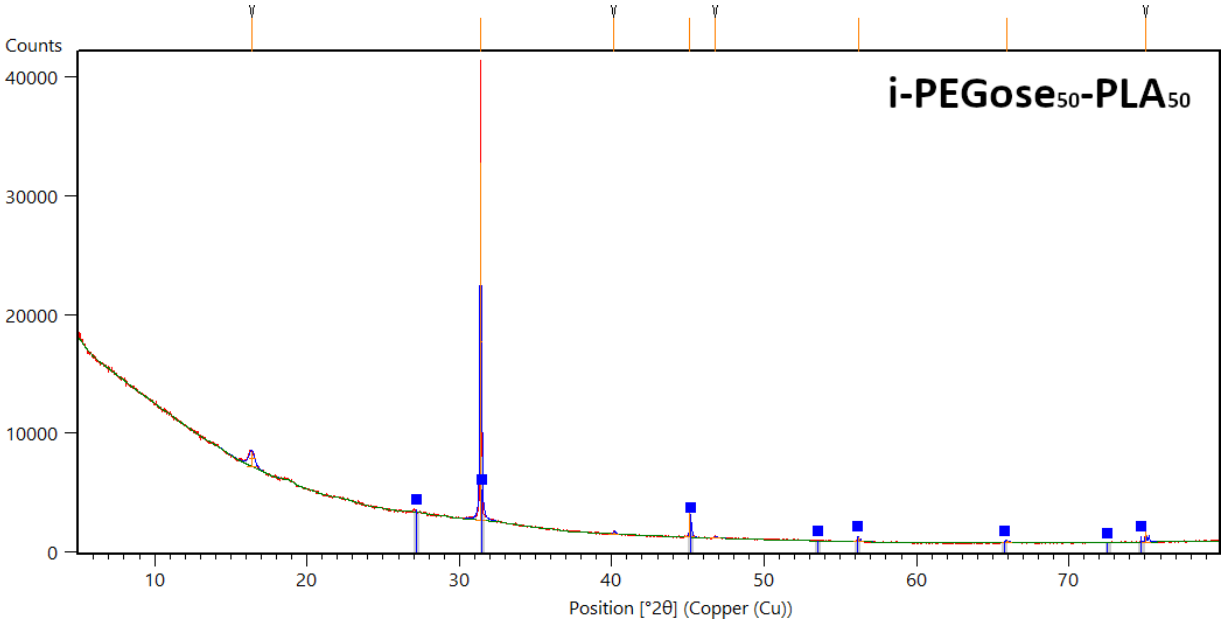

Figure 7.9: Powder X-ray diffraction of one dried drop of a i-PEGose$_{50}$-PLA$_{50}$ 100 mg/mL NaCl solution.

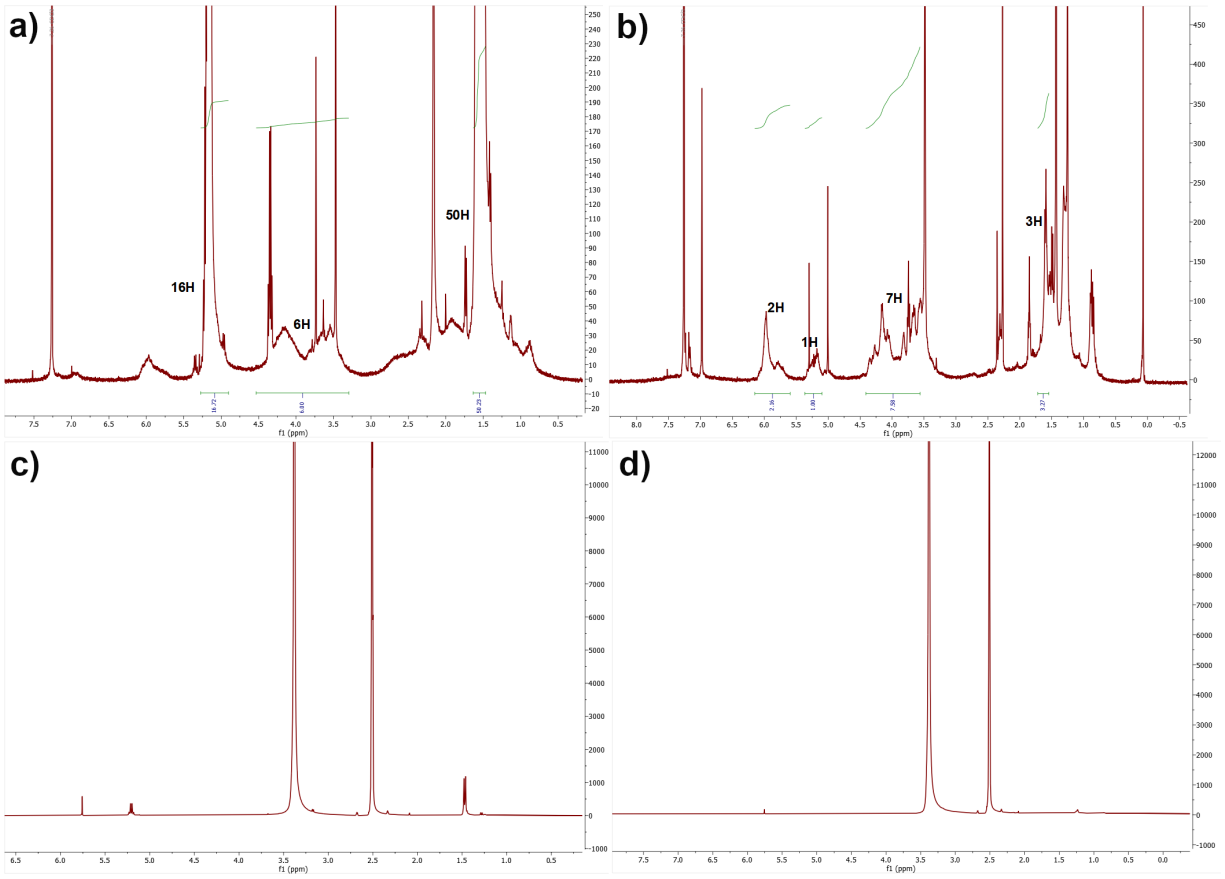

Figure 7.10: ^{1}H NMR spectra of **a)** a-PCE$_{50}$-PLLA$_{500}$ and **b)** i-PCE$_{50}$-PLLA$_{50}$ in $CDCl_3$ and **c)** a-PEGose$_{50}$-PLLA$_{500}$ and **d)** i-PEGose$_{50}$-PLLA$_{50}$ in D_2O.

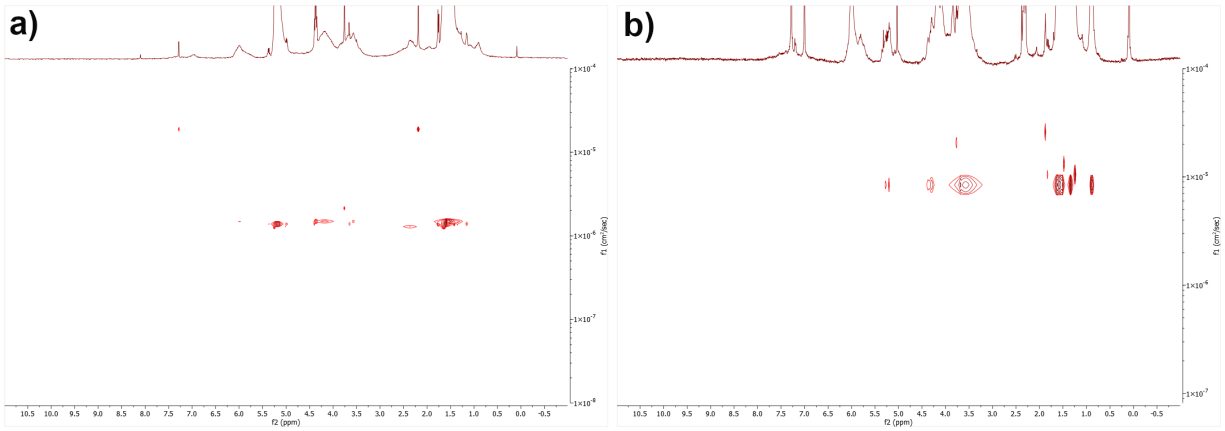

Figure 7.11: ^{1}H NMR DOSY spectra of **a)** a-PCE$_{50}$-PLLA$_{500}$ and **b)** i-PCE$_{50}$-PLLA$_{50}$ in $CDCl_3$.

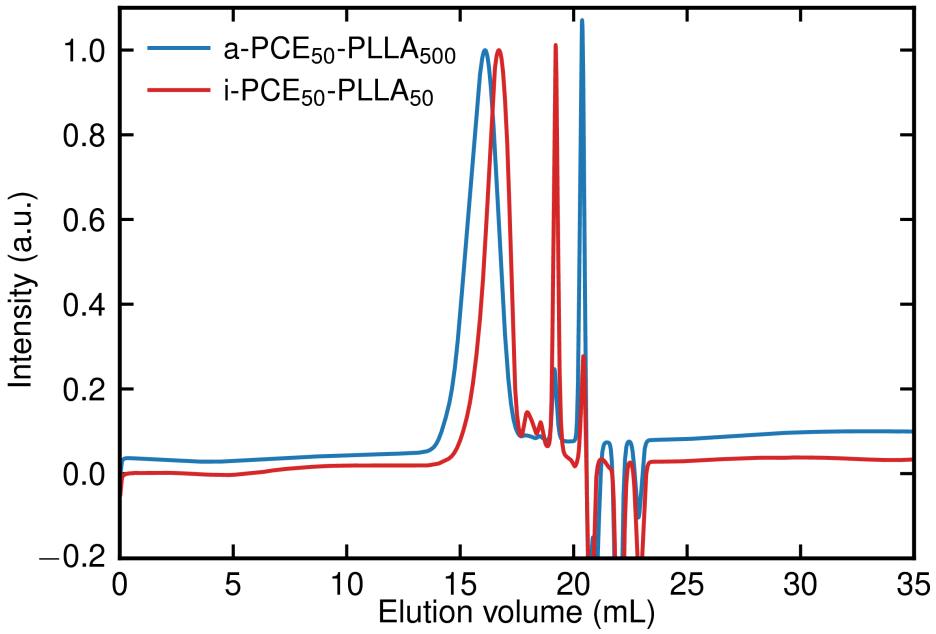

Figure 7.12: SEC traces of a-PCE$_{50}$-PLLA$_{500}$ and i-PCE$_{50}$-PLLA$_{50}$ measured in THF with a 1 mL/min flow rate.

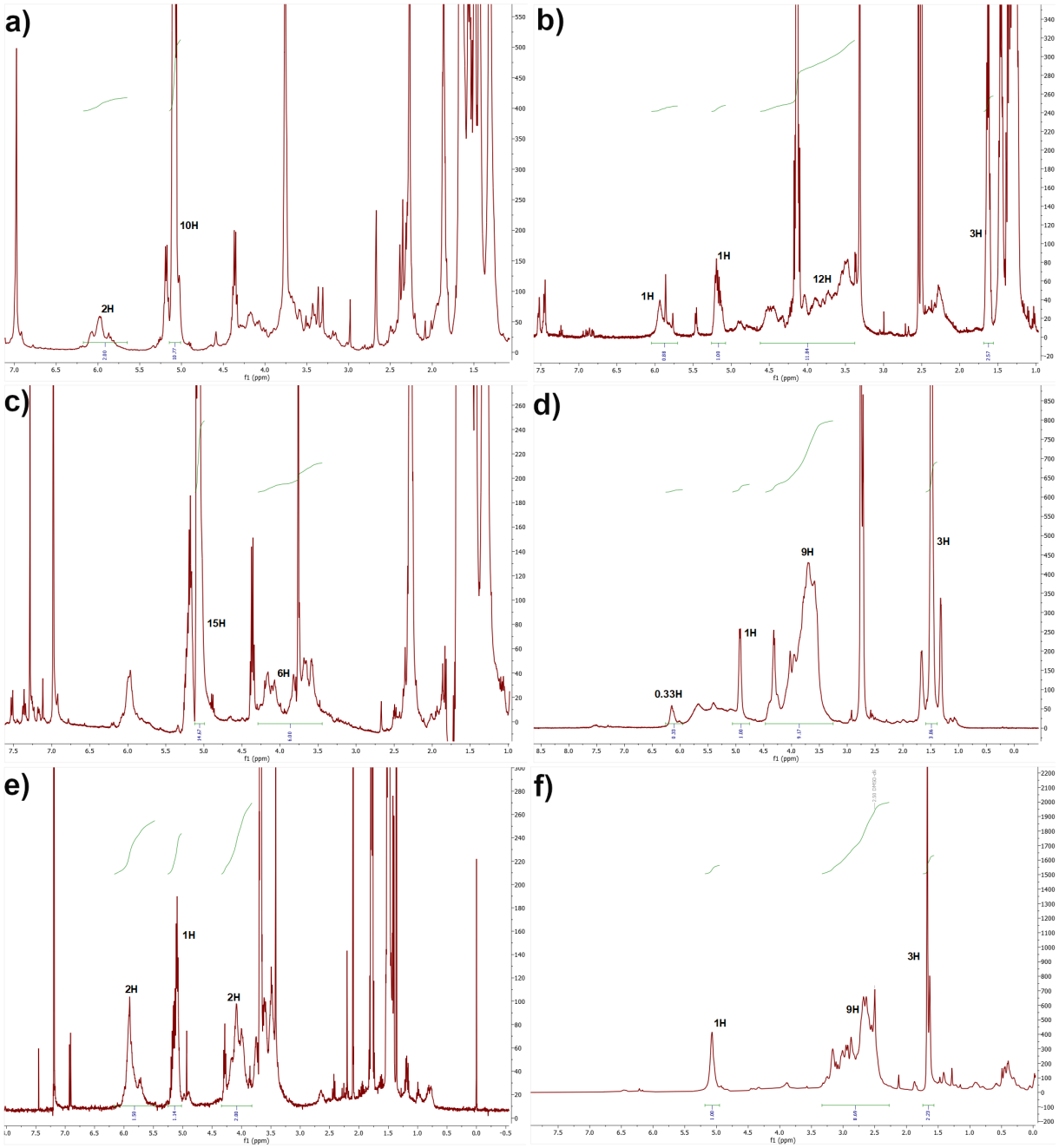

Figure 7.13: ^{1}H NMR spectra of **a)** a-PCE$_{50}$-PLA$_{50}$, **c)** i-PCE$_{50}$-PLA$_{50}$ and **e)** i-PCE$_{50}$-PLA$_{50}$ in $CDCl_3$ and **b)** a-PEGose$_{50}$-PLA$_{50}$, **d)** partly converted a-PEGose$_{50}$-PLA$_{50}$ and **f)** i-PEGose$_{50}$-PLA$_{50}$ in D_2O.

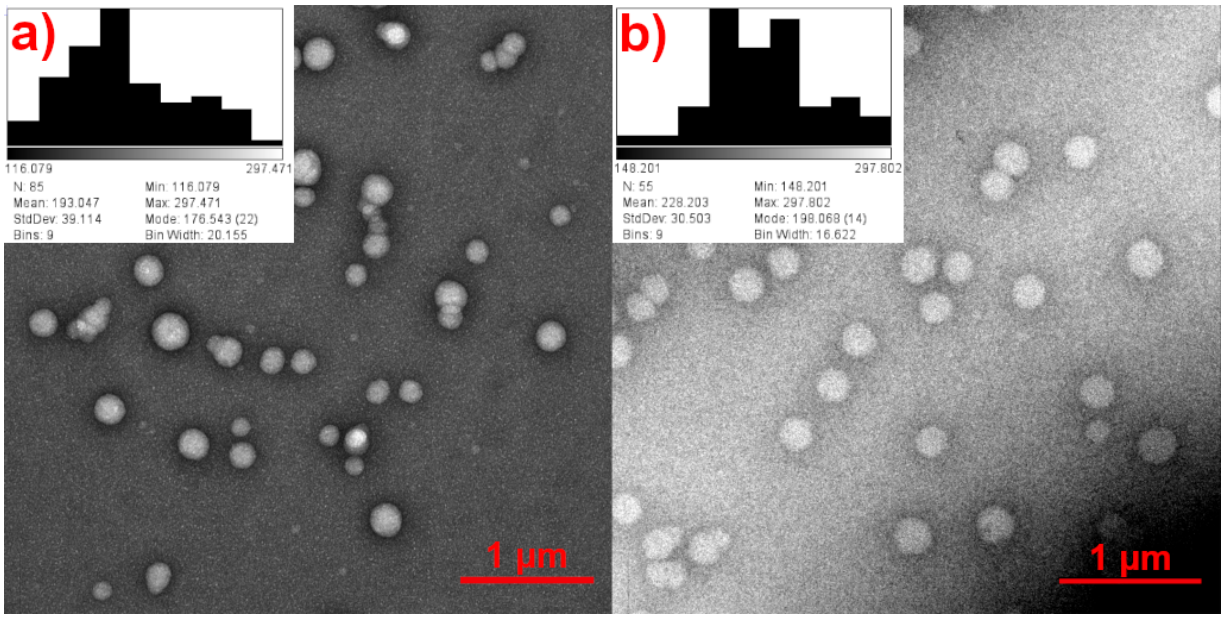

Figure 7.14: Transmission electron microscopy images of unstained **a)** i-PEGose$_{50}$-PLA$_{50}$ and **b)** a-PEGose$_{50}$-PLA$_{50}$ in deionised water with corresponding size analysis (193 nm mean diameter for **a)** and 228 nm for **b)**). Scale bars represent 1 µm.

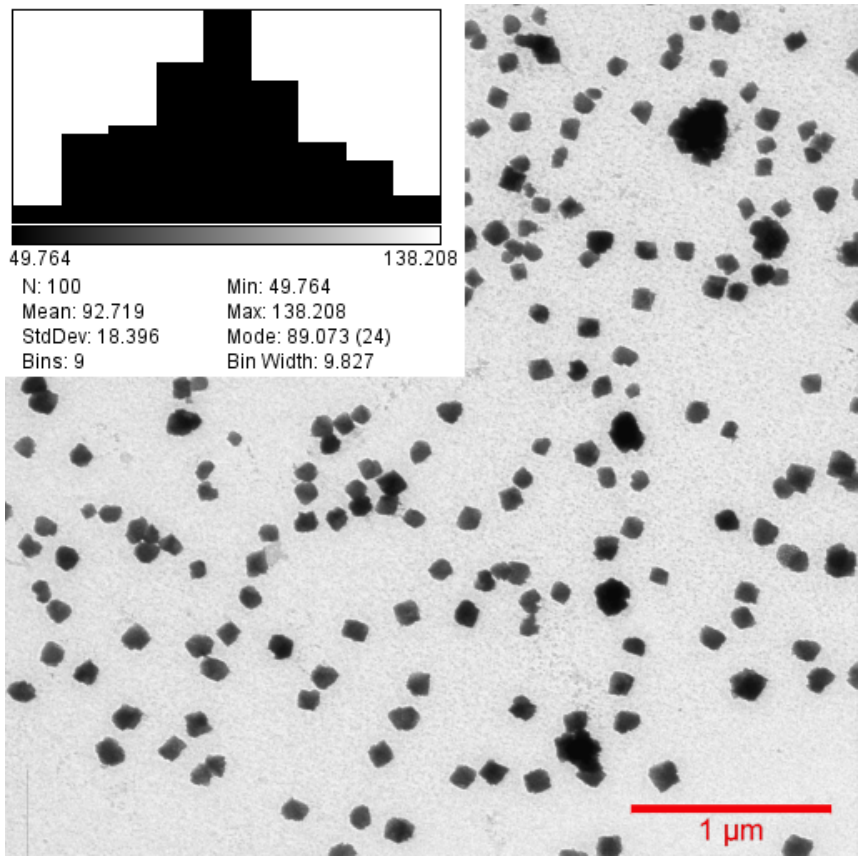

Figure 7.15: TEM images of i-PEGose$_{50}$-*b*-PLA$_{50}$ nanoparticles prepared in deionised water then salt was added to make a 100 mg/mL solution (1 µm scale bar) with corresponding size analysis.

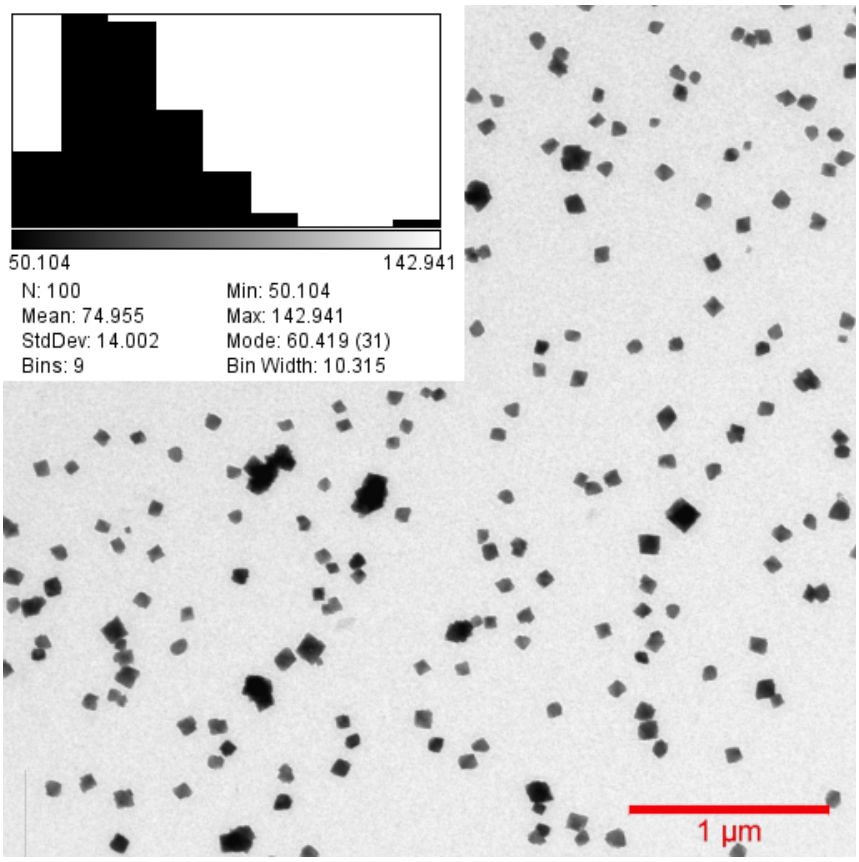

Figure 7.16: TEM images of i-PEGose$_{50}$-*b*-PLA$_{50}$ nanoparticles in a 100 mg/mL NaCl solution at a 10 mg/mL polymer concentration (1 µm scale bar) with corresponding size analysis.

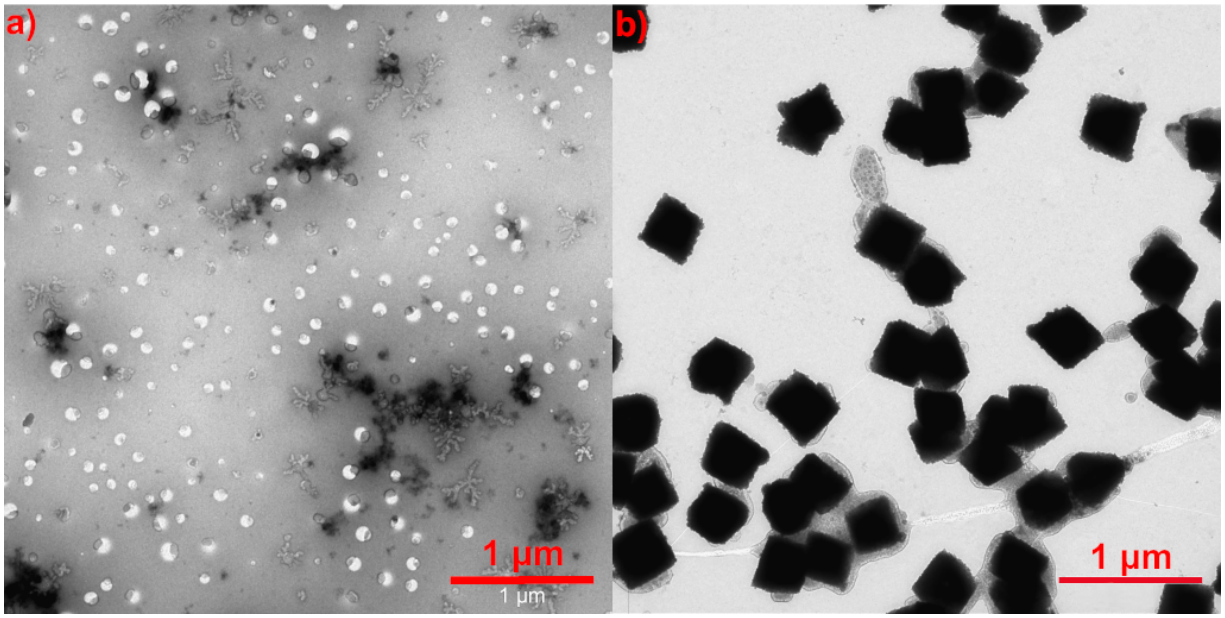

Figure 7.17: Additional unstained TEM images of isotactic PEGose$_{50}$-PLA$_{50}$ in a 100 mg/mL NaCl solution after **a)** 1 hour or **b** 3 days (1 µm scale bar).

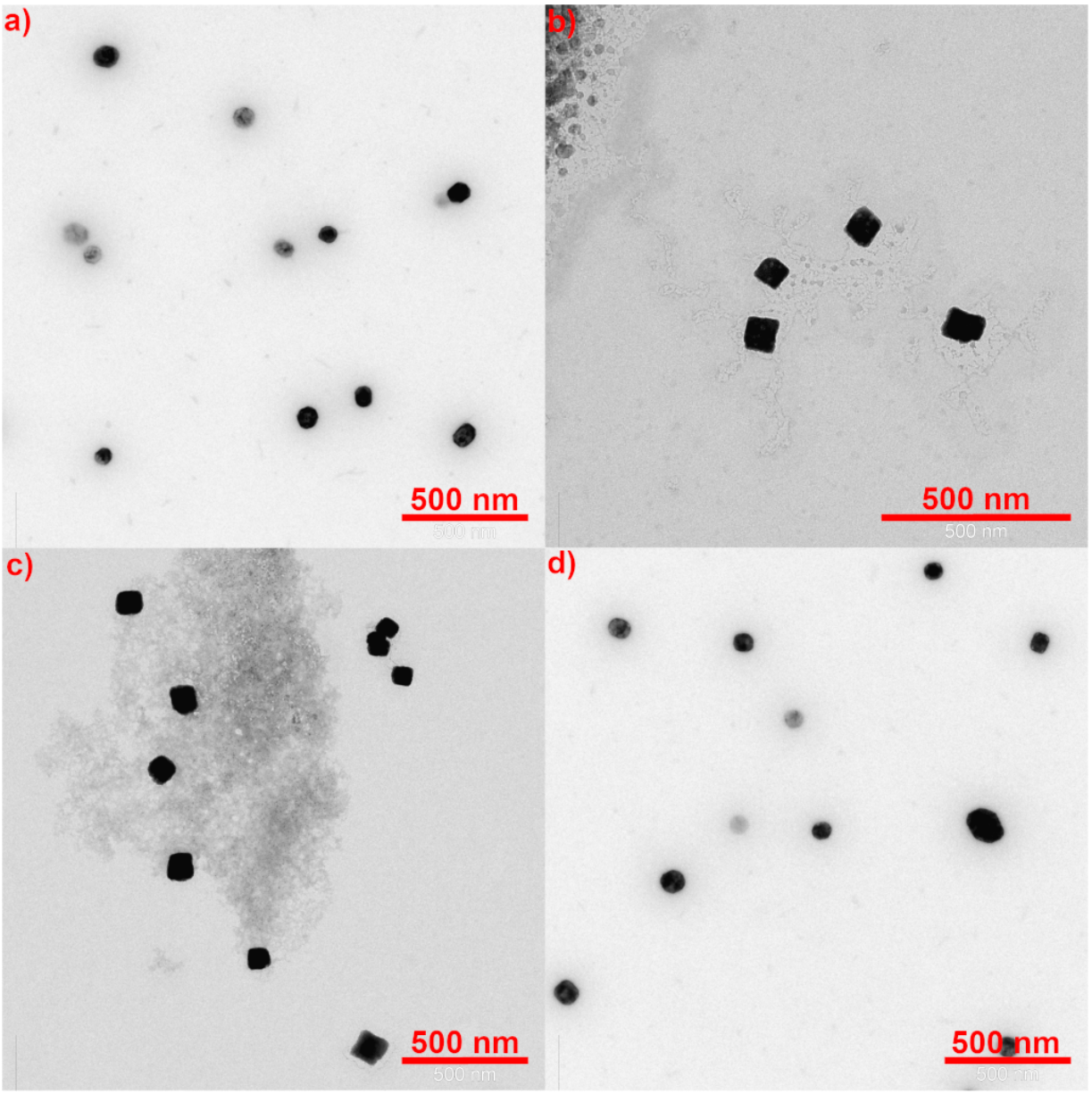

Figure 7.18: Additional TEM images of i-PEGose$_{50}$-*b*-PLA$_{50}$ nanoparticles in a 100 mg/mL NaCl solution at a 1 mg/mL polymer concentration (500 nm scale bars).

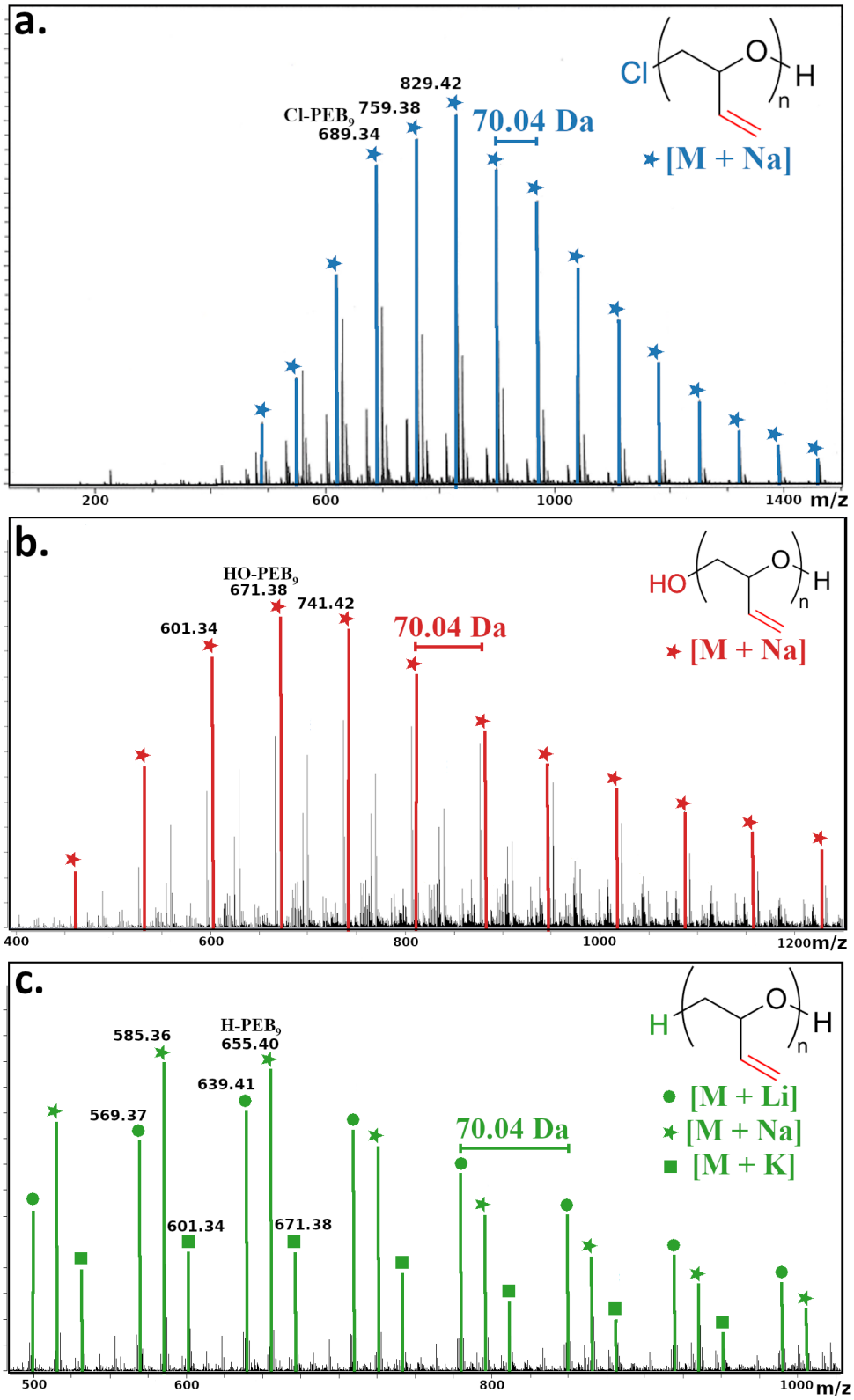

Figure 7.19: Mass spectra of atactic Cl-PEB$_{15}$, atactic HO-PEB$_{15}$, atactic H-PEB$_{15}$ and corresponding adducts. Adducts peaks are separated by 70.04 Da. The polymers with 9 repeating units have been pinpointed in each spectrum.

Table 7.1: m/z values of Cl-PEB$_{15}$, HO-PEB$_{15}$ and H-PEB$_{15}$ adducts. The adducts in bold are shown in Figure 7.19.

Cl-PEB Adducts	**m/z**
[Na + Cl-PEB$_8$]*	619.2969
[Na + Cl-PEB$_9$]*	689.3376
[Na + Cl-PEB$_{10}$]*	759.3787
[Na + Cl-PEB$_{11}$]	829.4189
[Na + Cl-PEB$_{12}$]	899.4596
[Na + Cl-PEB$_{13}$]	969.4997
[Na + Cl-PEB$_{14}$]	1039.5397
[Na + Cl-PEB$_{15}$]	1109.5798
[Na + Cl-PEB$_{16}$]	1179.6174
[Na + Cl-PEB$_{17}$]	1249.6595
[Na + Cl-PEB$_{18}$]	1319.6997
[Na + Cl-PEB$_{19}$]	1389.7387
[Na + Cl-PEB$_{20}$]	1459.7722

HO-PEB Adducts	**m/z**
[Na + HO-PEB$_7$]*	531.2948
[Na + HO-PEB$_8$]*	601.3386
[Na + HO-PEB$_9$]*	671.3822
[Na + HO-PEB$_{10}$]	741.4258
[Na + HO-PEB$_{11}$]	811.4692
[Na + HO-PEB$_{12}$]	881.5127
[Na + HO-PEB$_{13}$]	951.5563
[Na + HO-PEB$_{14}$]	1021.5998

H-PEB Adducts	**m/z**
[Li + H-PEB$_7$]	499.3253
[Na + H-PEB$_7$]	515.3201
[K + H-PEB$_7$]	531.2937
[Li + H-PEB$_8$]*	569.3673
[Na + H-PEB$_8$]*	585.3620
[K + H-PEB$_8$]*	601.3357
[Li + H-PEB$_9$]	639.4093
[Na + H-PEB$_9$]	655.1037
[K + H-PEB$_9$]	671.3776
[Li + H-PEB$_{10}$]	709.4512
[Na + H-PEB$_{10}$]	725.4452
[K + H-PEB$_{10}$]	741.4195
[Li + H-PEB$_{11}$]	779.4931
[Na + H-PEB$_{11}$]	795.4866
[K + H-PEB$_{11}$]	811.4613
[Li + H-PEB$_{12}$]	849.5348
[Na + H-PEB$_{12}$]	865.5273
[K + H-PEB$_{12}$]	881.5031
[Li + H-PEB$_{13}$]	919.5765
[Na + H-PEB$_{13}$]	935.5677
[K + H-PEB$_{13}$]	951.5451

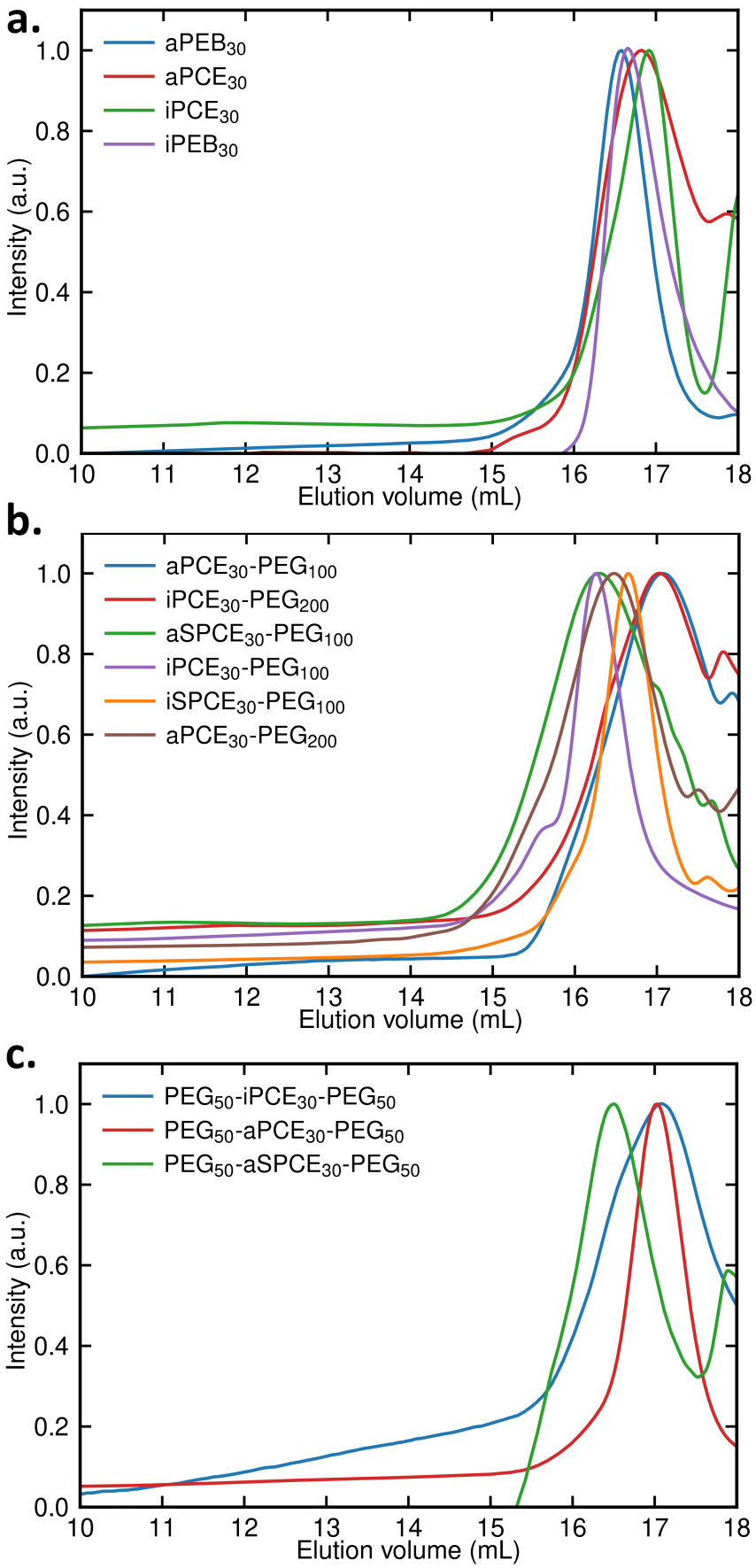

Figure 7.20: Size-exclusion chromatography traces of **a)** the homopolymers, **b)** diblock and **c)** triblock copolymers measured in THF.

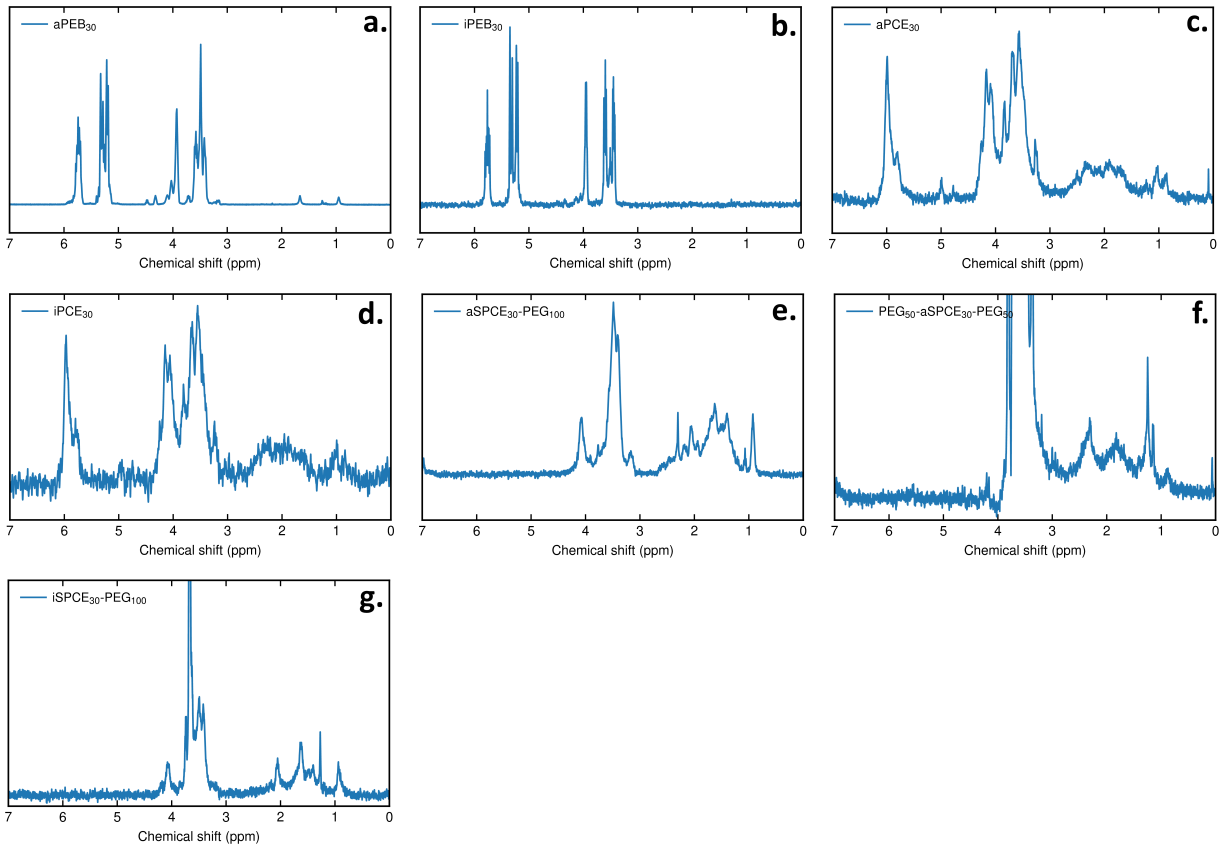

Figure 7.21: ^{1}H NMR of the synthesised polymers in $CDCl_3$: **a)** $aPEB_{30}$, **b)** $iPEB_{30}$, **c)** $aPCE_{30}$, **d)** $iPCE_{30}$, **e)** $aSPCE_{30}$-PEG_{100}, **f)** PEG_{50}-$aSPCE_{30}$-PEG_{30} and **g)** $iSPCE_{30}$-PEG_{100}.

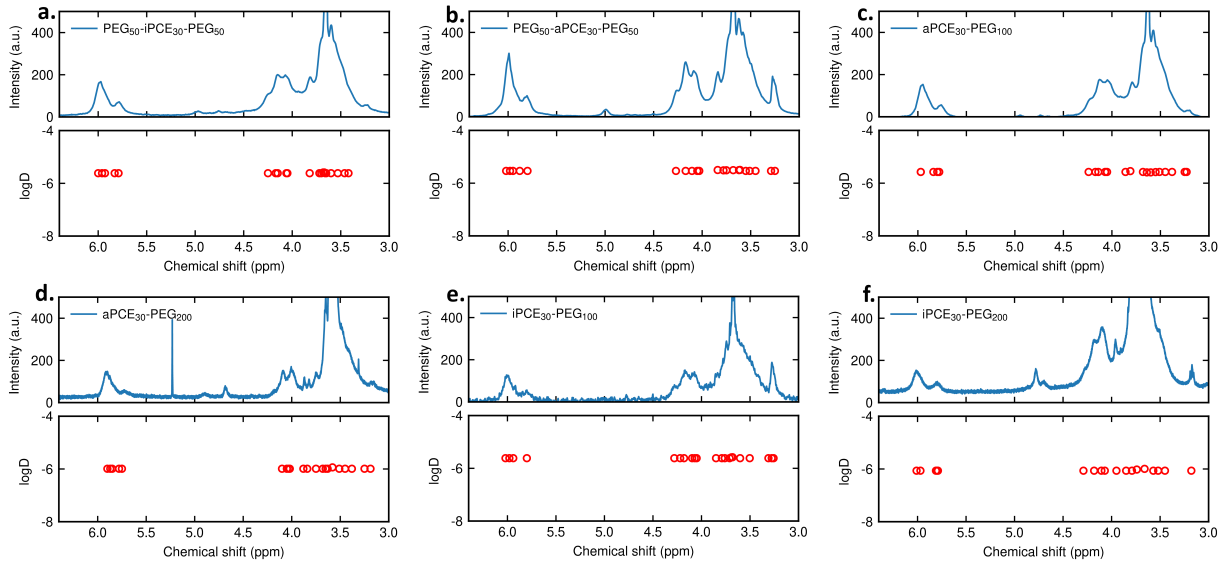

Figure 7.22: Diffusion-Ordered Spectroscopy (DOSY) ^{1}H NMR in $CDCl_3$: **a)** PEG_{50}-$iPCE_{30}$-PEG_{50}, **b)** PEG_{50}-$aPCE_{30}$-PEG_{50}, **c)** $aPCE_{30}$-PEG_{100}, **d)** $aPCE_{30}$-PEG_{200}, **e)** $iPCE_{30}$-PEG_{100} and **f)** $iPCE_{30}$-PEG_{200}.

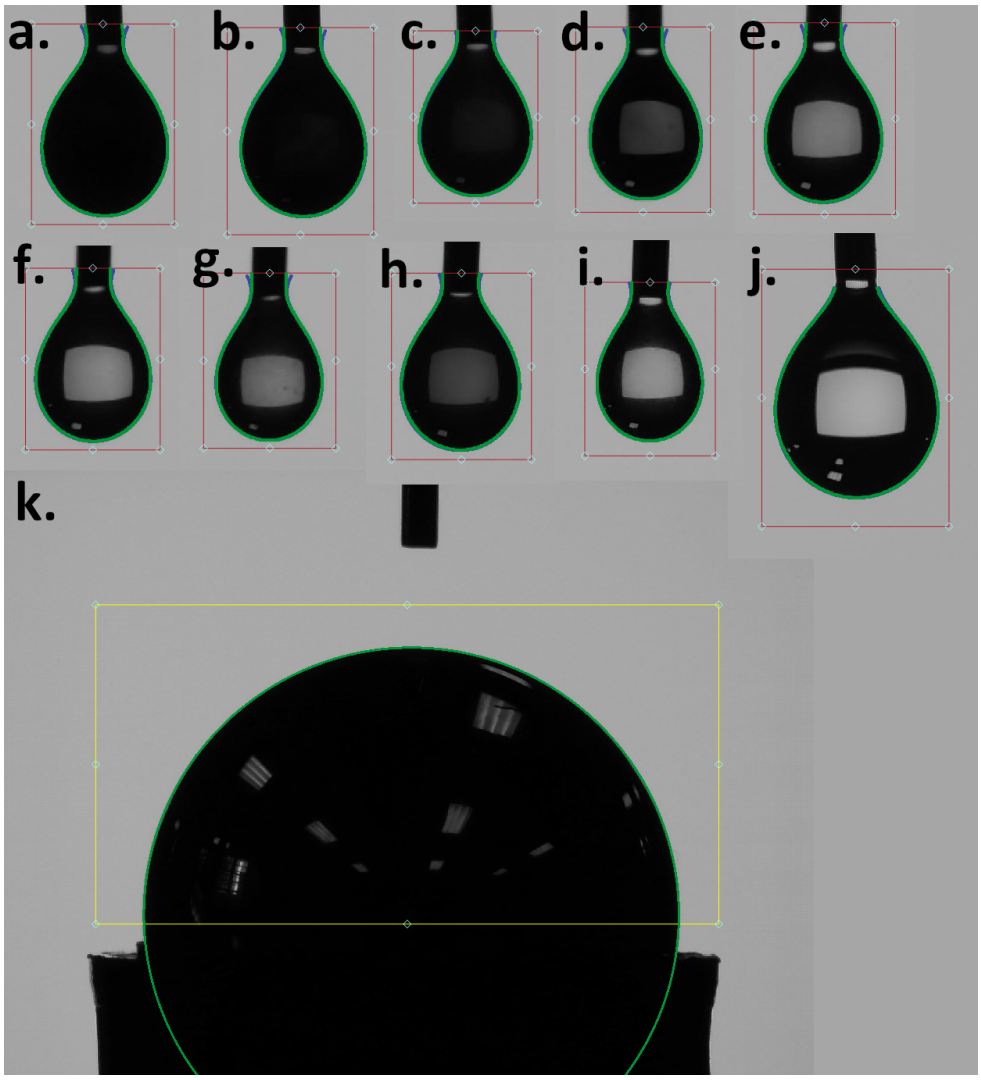

Figure 7.23: Surface tension measurement of **a)** PEG_{50}-$iPCE_{30}$-PEG_{50} **b)** PEG_{50}-$aSPCE_{30}$-PEG_{50} **c)** $aPCE_{30}$-PEG_{100} **d)** $iSPCE_{30}$-PEG_{100} **e)** $iPCE_{30}$-PEG_{200} **f)** $aPCE_{30}$-PEG_{200} **g)** $iPCE_{30}$-PEG_{100} **h)** PEG_{50}-$aPCE_{30}$-PEG_{50} **i)** $aSPCE_{30}$-PEG_{100} and **j)** water. The green line corresponds to the detected edge of the droplet, the blue line corresponds to the simulated fit used to calculate the surface tension. The difference between the simulated edge and the detected edge is the root mean squared error (RMSE). The instrument was calibrated on **k)** a 10.00 mm ball.

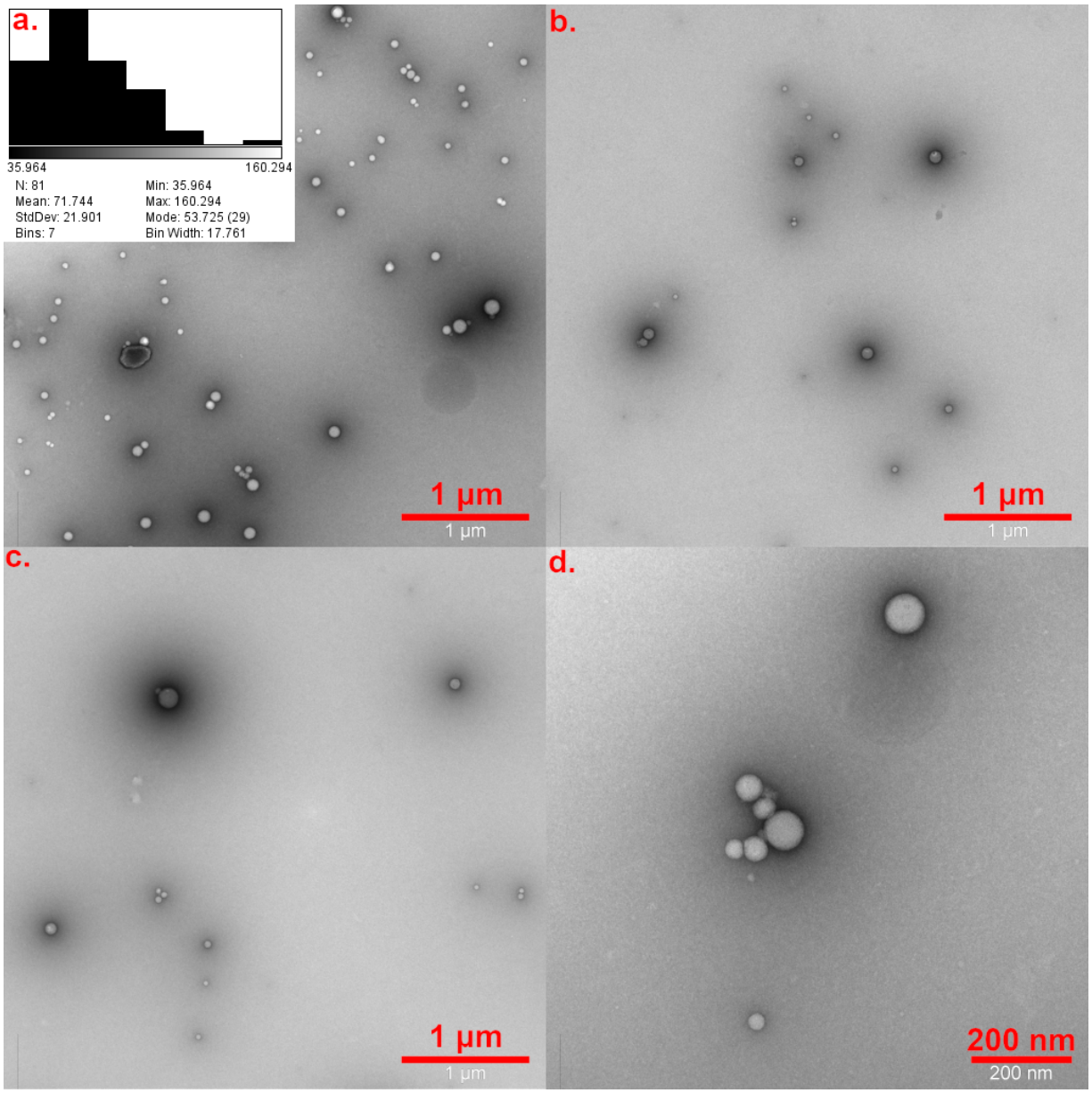

Figure 7.24: Additional transmission electron microscopy (TEM) images of unstained isotactic PCE_{30}-*b*-PEG_{100} in deionised water with size analysis, 1 day after the nanoparticles preparation (1 µm scale bar for **a)**, **b)**, **c)** and 200 nm for **d)**).

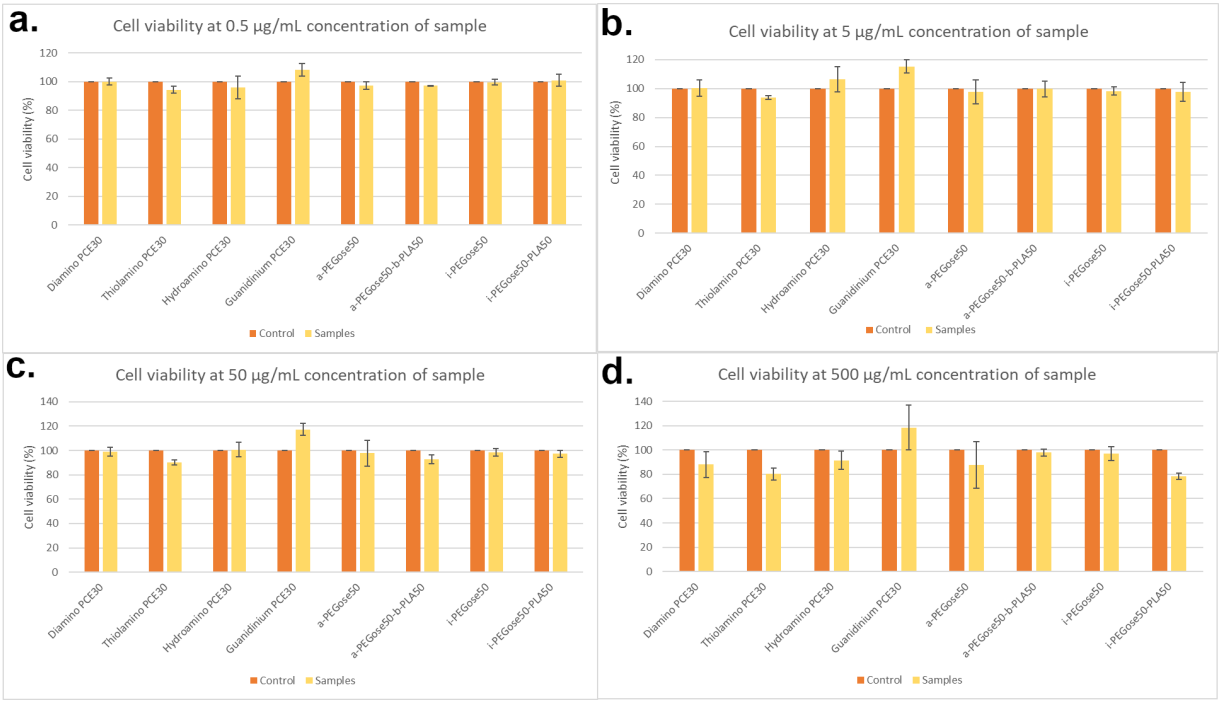

Figure 7.25: Human hepatocellular carcinoma cell viability after incubation with hydroamino-PCE_{30}, thiolamino-PCE_{30}, guanidinium-PCE_{30}, diamino-PCE_{30}, a-$PEGose_{50}$, i-$PEGose_{50}$, a-$PEGose_{50}$-PLA_{50} and i-$PEGose_{50}$-PLA_{50} with a concentration of 0.5, 5, 50 or 500 µg/mL in a humidified incubator at 37°C under 5% CO_2. Cell studies were performed with the collaboration of Emmanuelle Acs and Jesko Koehnke.